UNIVERSITAT DE VIC
UNIVERSITAT CENTRAL
DE CATALUNYA

Assessment of the environmental parameters associated with the production and release of geosmin in a Mediterranean river

PhD Thesis

Doctorate Program in Environmental Sciences and Technology

Carmen Espinosa Angona

June 2020

This study was carried out within the framework of the INTCATCH H2020 project (Grant Agreement No. 689341) and the agreement established with Aigües de Vic S.A. and Aigües d'Osona S.A. and UVic-UCC (2018-2020).

LAIA LLENAS ARGELAGUET, deputy director and project manager of the BETA Technological Center, and MARC ORDEIX i RIGÓ, CERM coordinator (Center for the Study of Mediterranean Rivers),

CERTIFY:

that the PhD student CARMEN ESPINOSA ANGONA has carried out under our direction the work with title "Assessment of the environmental parameters associated with the production and release of geosmin in a Mediterranean river" that is presented in this report and that constitutes her Thesis to apply for a Doctor's Degree from the University of Vic - Central University of Catalonia.

Dra. Laia Llenas Argelaguet

Marc Ordeix i Rigó

Abstract

In recent years, due to natural and anthropogenic causes, there has been an increase in the development of cyanobacterial blooms. These blooms are usually associated with the appearance of undesirable metabolites, either for their toxicity or for altering the organoleptic properties of the water. Among the compounds that generate a bad taste and odor to water is geosmin, one of the most frequent metabolites in freshwater systems. The presence of these compounds is a problem for the managers of the basins since they influence the organoleptic quality of the water and the user's confidence in the drinking water treatment plants.

In this thesis, it has been carried out the study of the physicochemical and biological parameters associated with the production and release of geosmin in a Mediterranean river, and the results generated have been used to develop a predictive model of the geosmin appearance.

From a study carried out with microcosms (aquariums) under controlled conditions, it has been identified that the interaction between a low N:P ratio (4:1) and a high nutrient concentration generates the favorable situation for the development of cyanobacteria. Specifically, this treatment favors the development of the cyanobacterium *Oscillatoria* sp., which begins to produce geosmin, reaching its maximum concentration in biofilm at 16 days. At the end of the experiment (t = 21d), this geosmin is released into the water.

Two factors that have also been identified as determining the geosmin appearance have been the water flow and the light availability. An experiment was carried out with mesocosms (experimental rivers) that received continuous water from the Ter river, a river that in recent years has suffered geosmin episodes. From the results obtained in this experiment, it can be concluded that a lower light availability (20% compared to natural light) and lower water flows favor the development of the *Oscillatoria* sp. cyanobacterium, generating a favorable situation for the geosmin production.

In addition to the experiments carried out in microcosm and mesocosm, for three years, five sampling sites with different ecological status located in the upper part of the Ter river basin have been monitored. The year with higher temperatures and a lower number of precipitations, led to minimum water flows, triggering the largest geosmin episode monitored. In addition to the effect of weather conditions, the geosmin presence varied depending on the sampling site, being higher in those sites with a greater anthropogenic impact.

Finally, with the database generated in the field samplings, a model capable of predicting the geosmin concentration in water has been obtained. The model that has given better results is the *Linear Discriminant Analysis* (MLDA), with a test score value of $r^2 = 0.596$, and capable of predicting the presence - absence of geosmin in 87% of cases.

In addition to the scientific interest of this thesis, the results obtained provide a highly useful tool for companies managing the supply of drinking water. Thanks to the thesis results, it can be concluded that, by slightly changing their water quality monitoring strategy, they can advance and be prepared for possible geosmin episodes, being able to start the geosmin elimination treatment in advance, preventing the geosmin reaches users taps.

Resumen de la tesis

En los últimos años, debido a causas naturales y antropogénicas, se ha producido un incremento en el desarrollo de floraciones de cianobacterias. Estas suelen ir asociadas a la aparición de metabolitos no deseados, bien por su toxicidad o bien por alterar las propiedades organolépticas del agua. Entre los compuestos que generan mal olor y sabor al agua se encuentra la geosmina, uno de los metabolitos más frecuentes en sistemas de agua dulce. La presencia de estos compuestos supone un problema para los gestores de las cuencas ya que influyen en la palatabilidad del agua y en la confianza de los consumidores en las empresas potabilizadoras.

En esta tesis, se ha llevado a cabo el estudio de los parámetros fisicoquímicos y biológicos asociados con la producción y liberación de geosmina en un río mediterráneo, y la aplicación de los resultados obtenidos en el desarrollo de un modelo predictivo de la aparición de geosmina.

A partir de un estudio realizado con microcosmos (acuarios) en condiciones controladas, se ha identificado que la interacción entre una relación N:P baja (4:1) y una concentración de nutrientes elevada genera la situación propicia para el desarrollo de cianobacterias. En concreto, este tratamiento favorece el desarrollo de la cianobacteria *Oscillatoria* sp., que comienza a producir geosmina, alcanzando su máximo de concentración en biofilm a los 16 días. Al final del experimento (t=21d), esta geosmina se libera al medio.

Dos factores que también se han identificado como determinantes de la aparición de geosmina han sido el caudal y la disponibilidad de luz. Se realizó un experimento con mesocosmos (ríos experimentales) que recibían agua en continuo del río Ter, río que en los últimos decenios ha sufrido varios episodios de geosmina. A partir de los resultados obtenidos en este experimento se puede concluir que una menor disponibilidad de luz (20% con respecto a la natural) y caudales menores favorecen el desarrollo de la cianobacteria *Oscillatoria* sp., generando una situación favorable para la producción de geosmina.

Adicionalmente a los experimentos realizados en microcosmos y mesocosmos, durante tres años se han monitoreado cinco puntos con diferentes características ecológicas localizados en la parte alta de la cuenca del río Ter. El año con temperaturas más elevadas y un menor número de precipitaciones dio lugar a caudales mínimos, observándose mayor episodio de geosmina monitoreado en este río. Además del efecto de las condiciones meteorológicas, la presencia de geosmina varió en función del punto de muestreo, siendo más elevada en aquellos puntos con un mayor impacto antropogénico.

Finalmente, con la base de datos generada en los muestreos de campo, se ha obtenido un modelo capaz de predecir la concentración de geosmina en el agua. El modelo que ha dado unos mejores resultados es el *Linear Discriminant Analysis* (MLDA), con un valor de test score de r^2 = 0.596, y capaz de predecir la presencia – ausencia de geosmina en un 87% de los casos.

Además del interés científico de esta tesis, los resultados obtenidos proporcionan una herramienta altamente útil para las empresas de suministro de agua potable. Gracias a los resultados obtenidos, se puede concluir que, cambiando ligeramente su estrategia de monitoreo de la calidad del agua, pueden avanzarse y estar preparadas ante posibles episodios de geosmina, pudiendo iniciar el tratamiento de eliminación de geosmina de manera anticipada, evitando que la geosmina llegue a los grifos de los usuarios.

Resum de la tesis

En els últims anys, tant per causes naturals com antropogèniques, s'ha produït un increment en el desenvolupament de floracions de cianobacteris. Aquestes floracions solen anar associades a l'aparició de metabòlits no desitjats, ja sigui per la seva toxicitat o bé per alterar les propietats organolèptiques de l'aigua. Entre els compostos que generen mala olor i mal gust a l'aigua hi ha la geosmina, un dels metabòlits més freqüents en sistemes d'aigua dolça. La presència d'aquests compostos suposa un problema per als gestors de les conques, perquè influeixen en la qualitat organolèptica de l'aigua i en la confiança dels consumidors en les empreses potabilitzadores.

En aquesta tesi, s'ha dut a terme l'estudi dels paràmetres fisicoquímics i biològics associats amb la producció i alliberament de geosmina en un riu mediterrani, i l'aplicació dels resultats obtinguts en el desenvolupament d'un model predictiu de l'aparició de geosmina.

A partir d'un estudi realitzat amb microcosmos (aquaris) en condicions controlades, s'ha identificat que la interacció entre una relació N:P baixa (4:1) i una concentració de nutrients elevada genera la situació propícia per al desenvolupament de cianobacteris. En concret, aquest tractament afavoreix el desenvolupament del cianobacteri *Oscillatoria* sp., que comença a produir geosmina, aconseguint el seu màxim de concentració al biofilm al cap de 16 dies. En finalitzar l'experiment (t = 21d), aquesta geosmina s'allibera al medi.

Dos factors que també s'han identificat com a determinants de l'aparició de geosmina han estat el cabal i la disponibilitat de llum. Es va fer un experiment amb mesocosmos (rius experimentals) que rebien aigua en continu del riu Ter, riu que els últims anys ha patit diversos episodis de geosmina. A partir dels resultats obtinguts en aquest experiment, es pot concloure que una menor disponibilitat de llum (20% respecte de la natural) i cabals menors afavoreixen el desenvolupament del cianobacteri *Oscillatoria* sp., generant una situació favorable per a la producció de geosmina.

Addicionalment als experiments realitzats en microcosmos i mesocosmos, durant tres anys s'han monitoritzat cinc punts amb diferents estats ecològics localitzats a la part alta de la conca del riu Ter. L'any amb temperatures més elevades i un menor nombre de precipitacions va donar lloc a cabals mínims, donant lloc al major episodi de geosmina monitoritzat. A més de l'efecte de les condicions meteorològiques, la presència de geosmina va variar en funció del punt de mostreig, essent més elevada en aquells punts amb un impacte antropogènic major.

Finalment, amb la base de dades generada als mostreigs de camp, s'ha obtingut un model capaç de predir la concentració de geosmina a l'aigua. El model que ha donat uns resultats millors és el *Linear discriminant Analysis* (MLDA), amb un valor de $r^2 = 0.596$, i capaç de predir la presència - absència de geosmina en un 87% dels casos.

A més de l'interès científic d'aquesta tesi, els resultats obtinguts proporcionen una eina altament útil per a les empreses de subministrament d'aigua potable. Gràcies als resultats obtinguts, es pot concloure que, canviant lleugerament la seva estratègia de monitoratge de la qualitat de l'aigua, poden avançar-se i estar preparats en front de possibles episodis de geosmina, podent iniciar el tractament d'eliminació de geosmina de manera anticipada, evitant que la geosmina arribi a les aixetes dels usuaris.

List of abbreviations

Abbreviation	Definition
2-MIB	2-methylisoborneol
AFDM	Ash Free Dry Mass
AI	Autotrophic Index
AMC	L-Leucine-7-amino-4-methylcoumarin hydrochloride
ANCOVA	Analysis of Covariance
ANN	Artificial Neural Network
ANOVA	Analysis of Variance
Chl *a*	Chlorophyll *a*
DEM	Digital Elevation Model
DIN	Dissolved Inorganic Nitrogen
DO	Dissolved Oxygen
DWTP	Drinking Water Treatment Plant
EC	Electrical conductivity
EEA	Extracellular Enzymatic Activities
EPS	Extracellular Polymeric Substances
F_0	Biomass estimation given by the MINI-PAM
FPP	Farnesyl diphosphate
GC/MS	Gas Chromatography Mass Spectrometry
LASSO	Least Absolute Shrinkage and Selection Operator regression
LDA	Linear Discriminant Analysis
MANN	Artificial Neural Network model
MEP	2-methylerythritol-4-phosphate pathway
MI	Margalef Index
MLDA	Linear Discriminant Analysis model
MPCA	Principal Component Analysis model
MUF	4-methylumbellyferyl-phosphate
MVA	Mevalonate pathway
OTC	Odor Threshold Concentration
PAM	Pulse Amplitude Modulated
PCA	Principal Component Analysis
PDMS/DVB	Polydimethylsiloxane/divinylbenzene
PEP	Leucine-aminopeptidase extracellular enzyme
PHO	Phosphatase extracellular enzyme
QGIS	Quantum Geographic Information System software
ReLU	Rectified Liner Unit activation function
RMSE	Root-Mean Square Errors
SPSS	Statistical Package for the Social Sciences Statistics software
SRP	Soluble Reactive Phosphorus
T&Os	Taste and Odor compounds
TN:TP	Total Nitrogen - Total Phosphorus ratio
WFD	Water Framework Directive
WWTP	Wastewater Treatment Plant
Y	Yield
Y*eff*	Effective PSII quantum yield
Y*max*	Maximum PSII quantum yield

Table of Contents

List of Figures

List of Tables

CHAPTER 1. Introduction

1. Introduction

In recent decades, an increase in the appearance of algal blooms has been observed globally. This increment is related to both natural and anthropogenic factors, among which the increase in the nutrient concentration, the average temperature, and the discharge of pollutants stand out (Vilalta, 2004; Winter et al., 2011). In many cases, these algal blooms generate the appearance of undesirable metabolites, which can be toxic or can affect the organoleptic characteristics of water, influencing both taste and odor (Lee et al., 2017). This last problem has a negative impact in the perception of the population about the quality of drinking water (Ding et al., 2014). Despite numerous episodes have been described in freshwater systems all over the world (Tung et al., 2008), it is unknown why these compounds are produced and under what exact environmental conditions their production is triggered by cyanobacteria in rivers, since most of the studies have focus on lakes and reservoirs or in pure strains evaluated in laboratory conditions. This lack of knowledge is because the companies related to the management of these waters have prioritized developing strategies to eliminate the compounds instead of evaluating the factors associated with their production, information that would allow them to predict their appearance (Jüttner and Watson, 2007).

Throughout this chapter, geosmin, which is one of the main metabolites responsible of bad taste and odor episodes in freshwater ecosystems, is defined. The main environmental factors that have been related to its appearance are also discussed, with special emphasis on nutrients, a factor highly related to the appearance of algal blooms and whose value is greatly affected in rivers with high anthropogenic pressures, like Mediterranean rivers. In freshwater systems such as rivers, the main geosmin producers have been described as benthic, so one section of this chapter is devoted to biofilm. Finally, the main different biological and experimental organizations in ecological studies are described at the end of the Chapter.

1.1. Taste and Odor compounds: Geosmin

1.1.1. Geosmin and associated problems

Some of the metabolites identified as Taste and Odor compounds (T&Os) are geosmin (*trans*-1,10-dimethyl-*trans*-9-decalol – $C_{12}H_{22}O$) and MIB (2-methylisoborneol – $C_{11}H_{20}O$) (Srinivasan and Sorial, 2011). The main problem with the presence of these metabolites in drinking water is associated with the extremely low odor threshold concentration (OTC) (Smith et al., 2009) and their persistence to elimination in a conventional water treatment process such as coagulation,

sedimentation, filtration and chlorination (Bai et al., 2019). Furthermore, there are currently no regulations for these metabolites as their presence has not been described as a risk to human health (Smith et al., 2009).

Between these two T&Os compounds, geosmin has been identified as the main metabolite conferring bad taste and odor to drinking waters (**Figure 1.1**.) (Watson et al., 2016). This metabolite is a volatile bicyclic terpenoid, that exist as (+) and (-) enantiomers, and odor outbreaks are caused by biological production of the naturally occurring (-) enantiomers, which are around 10 times more potent than the (+) molecules (Watson et al., 2007). Geosmin is produced inside cyanobacterial cells during the exponential phase of growth and released into the water as a consequence of death and/or biomass decomposition (Kim et al., 2018; Lee et al., 2017). It can appear in surface waters of freshwater ecosystems exploited for drinking purposes such as lakes, reservoirs or rivers, and it can be perceived by humans at very low concentration (5 – 10 ng/L) resulting in consumers complaints and representing a challenge for drinking water treatment companies.

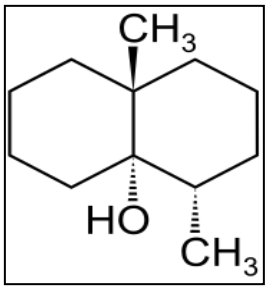

Figure 1.1. Molecular structure of geosmin.

Diverse organisms have been identified as T&Os producers (Li et al.,2012; Jørgensen et al., 2016), including eukaryotes, such as fungi and amoeba, with photoautotrophic cyanobacteria and filamentous heterotrophic bacteria being the main producers (Olsen et al., 2016). In freshwater ecosystems, cyanobacteria are considered the main geosmin producers (Olsen et al., 2016), being the majority benthic or epiphytic (70%) (Jüttner and Watson, 2007). In the group of geosmin-producing cyanobacteria, *Oscillatoria* sp., *Lynghya* sp., *Symploca* sp. and *Anabaena* sp., have been identified as the most commonly genus present in freshwater ecosystems (Smith et al., 2009).

1.1.2. Biosynthesis pathway of geosmin synthesis in bacteria

The geosmin biosynthesis has been resolved via feeding experiments performed with isotope-marked intermediates, and by identifying geosmin synthase and its by-products (Lindholm-Lehto and Vielma, 2018). Different studies performed have demonstrated that there are several biosynthetic pathways of isoprenoid synthesis in microorganisms, one or more of which may lead to the production of geosmin by different taxa (Spiteller et al., 2002; Dickschat et al., 2005). The main biosynthetic pathways described are the 2-methylerythritol-4-phosphate (MEP) pathway and the mevalonate (MVA) pathway, and depending on the organism, one or the other is used. In many bacterial groups, MEP pathway is the major biosynthetic isoprenoid route, although some of them can also use the MVA pathway. Whereas in some myxobacteria, the synthesis of geosmin and other isoprenoids is exclusively via MVA pathway. This biosynthetic pathway also contributes to geosmin production in the stationary growth phase of streptomyces (Dickschat et al., 2005; Jüttner and Watson, 2007).

These metabolic pathways converge in the formation of farnesyl diphosphate (FPP), which is the immediate precursor of cyclic sesquiterpenes (Cane et al., 2006). In the synthesis of geosmin, cyclisation of FPP is achieved by geoA gene encoded geosmin synthase (Giglio et al., 2008; Ludwig et al., 2007). Germacradienol/geosmin synthase is a bifunctional enzyme and catalyze the conversion of FPP into geosmin in a two-step process. First, the H-2 proton of FPP undergoes a 1,2-hydride shift from the B-ring of geosmin. Geosmin is formed via protonation-cyclation of germacradienol with loss of 2-hydroxipropyl moiety, shift of 1,2-hydride and finally, capture of water by sesquiterpene synthase. The germacradienol/geosmin synthase catalyzed the Mg^{2+} dependent conversion of FPP to a mixture of germacradienol, germacrene D, 8,10-dimethyl-1-octalin and geosmin, without involvement of any cosubstrates or redox cofactors (**Figure 1.2.**) (Jiang and Cane, 2008; Lindholm-Lehto and Vielma, 2018).

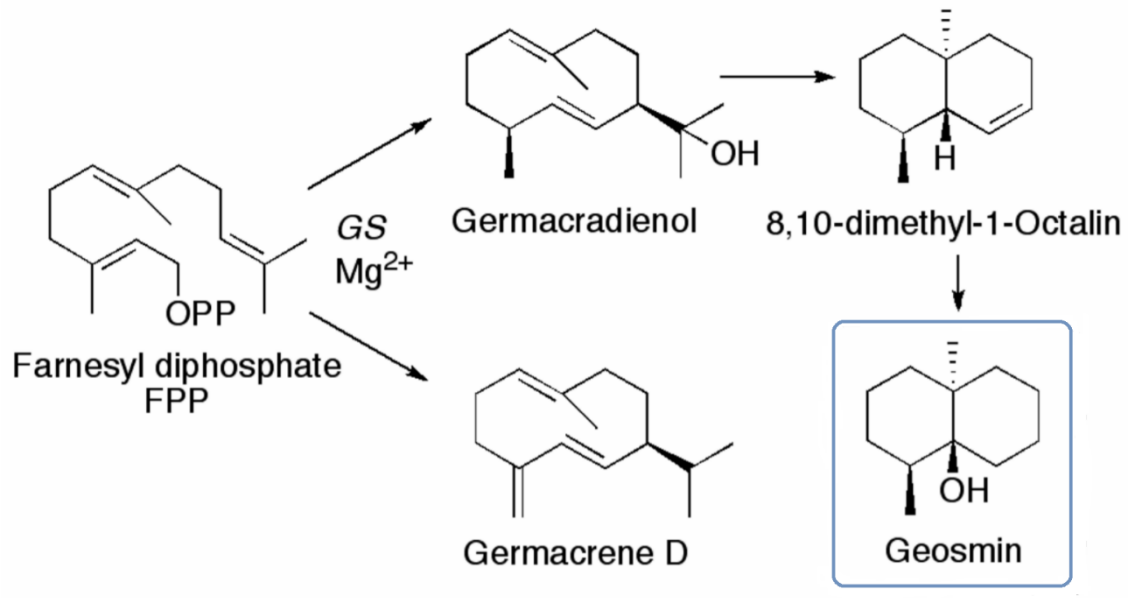

Figure 1.2. Mechanisms of cyclization of FPP to germacradienol, germacrene D, 8,10-dimethyl-1octalin and geosmin. From Giglio et al., 2008.

Despite numerous advances have been made to understand the mechanisms of geosmin production at cellular level, its biological function has not been elucidated yet. A possible hypothesis is that geosmin is a residual metabolite potentially providing energetic benefit to the producing organism. In particular, considering that the energy requirement for chlorophyll *a* production is higher than for geosmin, it has been described that when the organisms do not need high chlorophyll *a* concentration, eventually they start to produce geosmin (Cai et al., 2017). On the other hand, a recent study assesses the possibility that geosmin production serves as a mechanism to attract bugs and thus promote spore dispersal (Becher et al., 2020).

1.1.3. Main environmental factors associated with geosmin appearance

Different environmental factors may influence cyanobacteria growth and microbial production of geosmin (Lee et al., 2017), however, these isolated factors cannot explain the differences in geosmin concentration observed in freshwaters under natural conditions. After a thorough bibliographic search, the most relevant environmental factors that could be related with geosmin formation are described below:

- **Temperature**: Most cyanobacteria species have optimum temperature growth conditions (>20ºC), but many filamentous cyanobacteria have the ability to adapt at lower temperature (Tang et al., 1997).
- **Light availability**: Light affects the production of some volatile organic compounds (VOCs) and the growth of algal species (Lee et al., 2017; Alghanmi et al., 2018). It has

been shown that high light availability can inhibit the formation of gaseous vacuoles in certain cyanobacteria (Li et al., 2012) and several studies have pointed light as a key factor for geosmin production (Wang and Li, 2015; Lee et al., 2017).

- **Water flow**: Water flow may also have a certain effect on microbial production of T&Os, indeed, elevated geosmin concentrations in rivers have been reported in proximity of dams, where the flow was significantly reduced, leaving the water stagnant (Jüttner and Watson, 2007).
- **Nutrients availability**: Another factor promoting geosmin episodes could be the excessive nutrients loading, this high nutrient content often leads to a marked increase in growth of algal communities in aquatic environments, including cyanobacterial algal blooms (Olsen et al., 2016; Harris et al., 2016).

All these factors can be altered by climate change and human activity. As a result of climate change, an increase in cyanobacterial blooms has been predicted, since they have the advantage of adapting to higher temperatures (Lürling et al., 2018). Apart from changes in temperature, it is also expected that there will be more intense extreme events, which would alter the natural flows of rivers and streams (Acuña and Tockner, 2010). Specifically, in Mediterranean climate regions, an acute decrease in average rainfall is expected, associated with less frequent but intense events, and a decrease in annual runoff, which would mean a reduction in river flow (Bangash et al. , 2013; Proia et al., 2013). Furthermore, the hydrological regime of rivers and streams can also be anthropogenically affected by the regulation of the flow as a result of the construction of dams and reservoirs (Rubio-Gracia et al., 2017).

Anthropogenic activities have severely degraded streams and rivers worldwide, since they can alter riverbanks causing riparian forest modification and consequentially altering the quantity and quality of light potentially reaching riverbeds (Dal Sasso et al., 2015). Moreover, one of the major threats to these ecosystems is the excessive nutrient loading that cause eutrophication and leads to substantial alterations in the overall ecosystem functioning and structure (Artigas et al., 2013). These effects have a greater role in rivers that may be affected by water scarcity, such as those found in the Mediterranean, where water flow can significantly decrease, and consequently, its nutrient dilution capacity.

1.2. Nutrients in freshwater ecosystems

1.2.1. Natural concentration of nitrogen and phosphorus

As described in the previous section, a factor highly related to the appearance of algal blooms is the high nutrient concentration present in freshwater systems (Olsen et al., 2016; Harris et al., 2016).

A fundamental characteristic of rivers and streams is that they connect land, freshwater and coastal areas through the water flow. In a river course, from the headwaters to its mouth, different processes are developed, the effects of which could be accumulated and thus, significantly changing material flows. The modifications that may occur in these flows vary depending on the habitats through which the river passes, their connectivity and heterogeneity as well as the biological processes that occur on it (W. M. Wollheim, 2016). A great diversity of interconnected habitats generates a diversity of biogeochemical processes that favor the overall network dynamics (Zarnetske et al., 2012).

The Water Framework Directive (WFD) defines ecological state as the quality of the structure and functioning of aquatic ecosystems, such as rivers and streams, and is determined by the chemical components it presents and its relation to the reference conditions. In these systems, nitrogen (N) and phosphorus (P) have a key role, since they are two essential macronutrients in all organisms and are related to the carbon cycle. This last fact determines both primary production and microbial mineralization of organic matter in aquatic systems (Weigelhofer et al., 2018), also affecting the aquatic ecosystem productivity, water quality and utilization of water resources in the downstream reaches (Pu et al., 2018).

Phosphorus can be found in aquatic ecosystems in four forms: dissolved inorganic phosphorus or soluble reactive phosphorus (SRP), dissolved organic phosphorus (DOP), particulate inorganic phosphorus (PIP) and particulate organic phosphorus (POP). The SRP is bioavailable while organic forms, both soluble and particulate, have to undergo transformations, either chemical or biological, to pass to SRP and thus be biologically available. Nitrogen can be found in freshwater ecosystems in three forms: dissolved inorganic nitrogen (DIN), which includes ammonium, nitrite and nitrate, dissolved organic nitrogen (DON) and particulate organic nitrogen (PON) (Allan and Castillo, 2007). Like the SRP, DIN is bioavailable for both microorganisms and primary producers, with ammonia being the first form to be absorbed due to its lower physiological cost (Weigelhofer et al., 2018).

The concentration of nitrogen and phosphorus in rivers could be influenced by a variety of natural and anthropogenic factors, the relative influences of which vary spatially and temporally (Pu et al., 2018). Among the possible natural sources of P and N, decomposing plant material, the leaching from the soil, erosion of rocks with P, atmospheric deposition of nitrogen and biological fixation of N_2 carried out by cyanobacteria are the main ones (Withers and Jarvie, 2008; Weigelhofer et al., 2018). These contributions usually have very small values, so water currents considered pristine have SRP concentrations <10 ug/L and DIN concentrations around 0.1 mg N-NO_3^-/L, 0.015 mg N-NH_4^+/L and 0.001 mg N-NO_2^-/L (Allan and Castillo, 2007). Although the basin lithology must be taken into account since it can naturally affect the basal nutrients concentration.

1.2.2. Human activities and their relation with nutrient concentration in rivers

Physical, ecological and biogeochemical changes to landscape management impact aquatic ecosystems by altering the flow occurring within streams, the physical condition of the stream channel, stream bed and riparian area, the quality of the water that flows in the stream and, ultimately, the stream ecology (Van Meter, et al., 2016).

The physical impacts of direct channel modification such as reservoirs and dams constructions, affect flow velocities and sediments transport, by decreasing the water flow of the river upstream and acting as a barrier for the sediment (Rubio-Gracia et al., 2017). Other environmental modifications, made for practical needs or economic reasons, such as converting wild lands into agricultural fields or urban areas, also have a significant impact on rivers, mainly because of the changes generated in soil surface properties (De Fraiture et al., 2008).

Urbanization lead to dramatic changes in soil permeability and runoff generation. Greater overland flow also increases erosion and flood peaks. Similar changes can also occur due to the expansion of agricultural land, since the plowing and cultivation cycles remove the layers that protect the soil surface, generating low permeability and thus promoting more surface runoff (Pagliai et al., 2004). In addition, if pollutant concentration is highest near the soil surface, additional surface runoff will also increase the loads of these pollutants being transported to streams and rivers (Van Meter, et al., 2016).

During the twentieth century there was a great industrial development and an intensification of agricultural production, which triggered the eutrophication of aquatic systems, such as rivers and streams, and a consequent deterioration of their ecological status (Grizetti et al., 2011). Depending on the temporal and spatial extent, nutrient contributions to freshwater systems can be differentiated into: (i) point sources (PS), such as industrial effluents and municipal

wastewater, (ii) diffuse or non-point sources (NPS), such as fertilizers used in agriculture, and (iii) intermediate sources, such as runoff from non-permeable surfaces (Weigelhofer et al., 2018).

In the case of point sources, the nutrients present are predominantly in dissolved inorganic form, therefore, they are bioavailable (Withers and Jarvie, 2008). These water discharges mean permanent entries in time and space, so today they are very regulated and controlled. However, there are specific cases in which controls fail, generating an accidental discharge with a high concentration of nutrients in the aquatic environment. In the case of diffuse sources, nutrients come from fertilizers discharged in crop fields and from greater soil runoff and erosion generated by the plowing of the lands. In this situation, nutrient inputs extend much further from the point where they are directly applied, and they are more difficult to control.

Both ammonium and SRP can be easily absorbed by soil particles, then being transported to streams and rivers in events of soil erosion and runoff (Withers and Jarvie, 2008). In the opposite way, nitrate is highly soluble and mobile. When there is an excess of nitrate, a fact mainly related to areas highly exploited by agriculture and livestock, nitrate is leached to groundwater and reaches the rivers through underground flows (Grizetti et al., 2011). In Mediterranean systems, the risk of eutrophication in agricultural basins is greater during spring and summer, since they are the seasons where germination and plant growth occurs, and at the same time conditions of lower water flow occur due to lower rainfall frequency, which generates a lower nutrient dilution potential.

Once nitrogen and phosphorus reach freshwater systems, they begin to undergo different biogeochemical transformations, among them the absorption of nutrients (autotrophic or heterotrophic), the assimilation into biomass and its subsequent release due to excretion or microbial decomposition (Birgand et al., 2007). However, when there is an excess of N and P, situations that worsen the ecological quality of the system can be triggered. For example, higher nutrient concentrations increase both the frequency and intensity of harmful cyanobacterial blooms, generate a lower concentration of dissolved oxygen available, and a loss of habitat and the biodiversity of the ecosystem. Finally, all these situations can affect the human being as a result of the deterioration in the quality of drinking water (Weigelhofer et al., 2018).

Because of the reasons previously described, phosphorus and nitrogen are a concern for the main administrators of the water quality of the basins, especially in basins with a high presence of urban or agricultural land.

1.3. Biofilm

1.3.1. Biofilm as a structural entity

Currently, there are numerous studies on biofilms developed in aquatic systems, the results of which have concluded that depending on the environmental variables and the type of substrate in which they are developed, biofilms have different structural and functional properties (Karatan and Watnick, 2009). In freshwater ecosystems, biofilms are generally known as periphyton, while in marine ecosystems they are called microphytobenthos. All of them present a series of similar properties, being the general characteristic that define biofilm as a set of microorganisms enveloped by a polymeric matrix, which also involves extracellular enzymes and detritus. The substances that make up this matrix (extracellular polymeric substances, EPS), provide the biofilm with mechanical stability, favoring its adhesion to the surface and generating a polymeric network that interconnects the biofilm cells (Wingender and Flemming, 2011). Thanks to this, the organisms found in the biofilm interact with each other, giving rise to a microecosystem (Mora-Gómez et al., 2016).

Depending on the substratum where they develop, biofilm can be highly diverse in aquatic environments. Specifically, biofilms have been described to develop on the surface of rocks and cobbles, on sediment, on dead plant material, on macrophyte plants, as suspended aggregates, and on man-made surfaces.

The biofilm developed on the stone's surfaces of rivers, lakes and marine environments is called epilithic biofilm or epilithon (**Figure 1.3.**). Compared to other biofilms, this one differs because it is more complex at the structural level, standing out for having a higher algal biomass, which can be 60 - 90% of the total biofilm community. However, this proportion may vary in environments with a lower light incidence (such as rivers with a lush riparian forest), where the presence of heterotrophic biomass (bacteria, fungi and protozoa) increases (Romaní, 2010). Depending on the characteristics of the stone, such as the surface texture, its size and its orientation, the development of the biofilm can be influence. It has been described that, at the functional level, an important role played by the epilithic biofilm is the nutrients uptake from the medium. The uptake capacity can be affected depending on the thickness and distribution of the biofilm on the surface, the nutrients concentration in the medium, the diffusion capacity of these in the biofilm, and external factors such as temperature and grazing (Mora-Gómez et al., 2016).

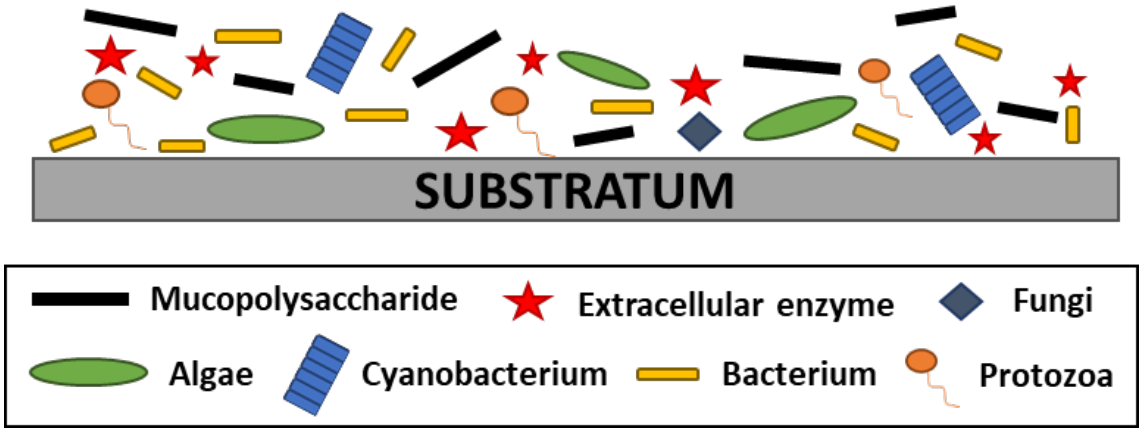

Figure 1.3. Scheme of the river biofilm community structure. Adapted from Ricart, 2010.

Biofilm that develops in sandy sediment is defined as epipsamic, and if it develops in muddy sediment, it is defined as epipelic. The sediment is characterized by being a small, hard and inert substrate, and depending on its size, roughness and grain surface area, it gives rise to differences in microbial community colonization and development. In general, the community present has been described to be more heterotrophic than epilithic biofilm, with an important function in the organic matter decomposition in rivers. Furthermore, nutrients can be adhered to sediment particles thus being available to the community that lives in them. In this sense, sediment acts as a sink of nutrients from the water column through the uptake and deposition (Dodds, 2003).

Epixylic biofilm or epixylon is the one that develops in dead plant material, such as wood and leaves. In this case, the substrate has two functions, on the one hand it is a physical surface on which the biofilm can develop, and on the other, it is a organic matter source for microorganisms. The community of these biofilms stands out for being mainly composed of fungal organisms, which can degrade lignocellulose compounds, the main component of plant tissues (Nikolcheva and Barlocher, 2004). When the biofilm develops in living plants such as macrophytes, it is called epiphytic biofilm. These plants usually present dense microbial growth, however, at the deeper levels, bacteria are favored thanks to a lower light availability, generated by the plant itself (Vadeboncoeur and Steinman, 2002).

In freshwater systems it is also possible to find, although much less frequent, suspended aggregates. These are structures suspended in water, formed by microorganisms, organic and inorganic particles. Their greatest development occurs when the nutrient concentration in the medium is very high, and they play a prominent role in organic matter transport from the water

surface to the benthos. They have been identified as hotspots for carbon remineralization and microbial activity, including enzymatic activities (Grossart et al., 2007). Finally, the biofilm developed on artificial surfaces is known as biofouling, and its formation follows the same sequence as that observed for inert natural substrates. Its presence can pose a major problem, however, it can be avoided through a combination of pretreatments and preventive chemical cleaning (Guo et al., 2012).

Several factors could affect the functioning of biofilms, some are chemical (i.e. nutrients availability) and physical (i.e. light availability, water flow, temperature), while others are biological (i.e. community composition, biomass thickness) (Ricart, 2010; Stevenson, 1996). In freshwater systems where the planktonic community is not predominant, as in the case of small rivers or streams, the first ecosystem compartment which interact with the dissolved substances present (i.e. nutrients, organic matter or pollutants) is the biofilm, and then it could be altered by their presence. Biofilms can respond very quickly to the presence of stressors and also integrate their effects over a long period of time. This is mainly because they are conformed by a wide variety of microorganisms and are small and thin structures, which can have a rapid growth. Because of the abovementioned reasons, biofilms have become a priority tool for the early detection of the effects that possible alterations occurring in the environment may have on aquatic ecosystems (Sabater et al., 2007). For that, biofilm has been considered as an ecosystem compartment to be evaluated to achieve the objectives of this Thesis.

1.3.2. Multi-endpoint approach in biofilm

Biofilm is an ecological compartment that allows to show the effect that environmental variables or chemical factors can have on the aquatic ecosystem through changes in different structural and functional endpoints (Bonnineau et al., 2010).

The capacity that one or other of these endpoints may have to better reflect the stressor effect depends on the potential result and the action mode that this stressor could have. For example, acute effects are detected much better using functional endpoints, such as photosynthetic capacity or extracellular enzymatic activities. On the other hand, chronic or persistent effects can be better evaluated through structural endpoints, such as the evaluation of changes in the community composition or the chlorophyll *a* concentration. Among this two, changes in community composition may better reflect the outcome of being under stress for a long period of time, since the biofilm community tends to change, favoring the presence of those species tolerant or resistant to this particular stressor and decreasing or even disappearing the presence of those sensitive. However, in order to evaluate the cause-effect relationships, the approach

based on changes in the community would not be the most suitable, with complementary studies that assess the short-term effects being necessary (Sabater et al., 2007). Choosing to study one endpoint or another depends on the starting hypothesis and the expected effect of the stressor being evaluated.

A multi-endpoint approach has been used in this Thesis, to cover both functional and structural characteristics of the biofilm communities. The set of endpoints has been classified as:

- Biofilm structure: chlorophyll *a* content (Chl *a*), ash free dry mass (AFDM), autotrophic index (AI) and Margalef index (MI).
- Community composition: phototrophic community composition (cyanobacteria, green algae and diatoms biomass) and algal taxonomic composition.
- Chlorophyll *a* fluorescence measurement: photosynthetic efficiency (*Yeff*), photosynthetic capacity (*Ymax*) and chlorophyll fluorescence (F).
- Nutrient uptake capacity: nitrogen and phosphorus uptake/release rate
- Extracellular enzyme activities: leucine-aminopeptidase and phosphatase.

Biofilm structural endpoints may reflect the long-term effect that a compound can have on a biofilm community. Chlorophyll *a* content has commonly been used as a descriptor of biofilm biomass (Guasch et al., 2007), and its widely known to depend on a number of variables including local and large-scale factors (Urrea-Clos et al., 2014). The accumulation of organic biomass (AFDM) can be affected by factors such as river flow; for example, Ateia et al. (2016) showed that a moderate water flow provides favourable conditions for algal growth and its corresponding biomass accumulation. In addition, high values of AFDM and MI may be related to the accumulation of accessory pigments and reflect a more aged community, as described by Marcarelli et al. (2009) and Ceola et al. (2013). While in high water flow conditions, biofilms are sloughed due to high shear stress, drag and abrasion, leading to low biomass (Ponsatí et al., 2016). Changes in the environmental conditions could lead to a shift in the community composition, usually favouring the most tolerant taxa. For example, the abundance of cyanobacteria is strongly influenced by nutrient availability (Vilalta, 2004) and temperature (Lürling et al., 2018), thus having a competitive advantage under conditions of high nutrient concentration and elevated temperature.

The measurement of *in vivo* chlorophyll *a* fluorescence of biofilm has been found to be one of the most sensitive and non-invasive tools for the rapid detection of compounds and environmental conditions that exhibit harmful effects on photosynthesis (Fai et al., 2007). Standard PAM fluorometers excite chlorophyll fluorescence at a wavelength (665nm, excitation

maximum of the Chlorophyll *a* molecule) and are applied on biofilms to evaluate the global photosynthetic response of the autotrophic compartment (Corcoll et al., 2012). This analyse is based on the principle that light is absorbed by PSII pigments and is able to drive the photochemical conversion at PSII reaction centres (photochemistry), can be dissipated into heat or it can be emitted in the form of light (chlorophyll fluorescence). As these 3 processes are complementary, the fluorescence yield may serve as a convenient indicator of changes in the relative rates of photochemistry and heat dissipation (Corcoll et al., 2012). *Yeff* and *Ymax* indicate the fraction of light that is converted into chemical energy during photosynthesis and then, it can be used as a measure to evaluate functional changes in the algal component of the biofilm after exposure to environmental disturbances (Romero et al., 2019; Argudo et al., 2020).

The biofilm nutrients' uptake capacity can be used as a tool to identify the effect that different stressors could have on the biofilm structure and function, since this capacity can be influenced by biofilm biomass, metabolic activity and advective transport of nutrients to biofilm assemblages (Proia et al., 2017; Doods et al., 2003). Furthermore, nutrients uptake can be time dependent and may reflect the present nutritional state of the biofilm (Sabater et al., 2002).

Extracellular enzymatic activities (EEAs) are used to detect possible effects generated in biofilm communities due to alterations in freshwater systems. It is a very sensitive tool and also has a direct relationship with organic matter, factor that make EEAs ideal for assessing the effects of specific compounds. When the biofilm is exposed to a specific factor, this factor can generate a stress to the community that triggers an increase or decrease in its enzymatic activity, depending on the possible relevance of the stressor as a source of carbon, nitrogen or phosphorus for microbial growth (Ricart, 2010).

The use of biofilm as a tool to detect the consequences caused by changes in aquatic ecosystems cannot remain in simple tests; the overall effect and interaction between different biofilm compartments must also be considered. In addition, to obtain realistic results, it is required to scale up from physiological to structural responses. It has been shown that the combination between functional and structural endpoints may better reflect the adaptation of the community to a specific stressor (Tlili et al., 2008). This approaches combination could allow the detection of factors that affect the "good ecological status" of fluvial systems.

1.4. Biological and experimental organization in ecological studies

In fluvial ecology there are several experimental approaches and, depending on which one is chosen, the ecological relevance degree and the experimental control and replication vary (**Figure 1.4**.).

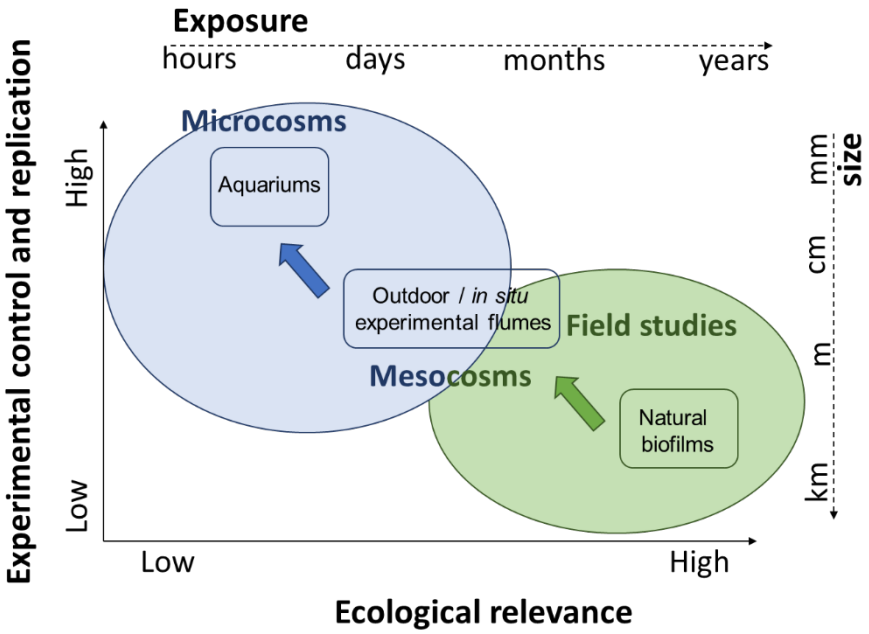

Figure 1.4. Relationship between ecological relevance, experimental control and replication in fluvial ecological experimental approaches. Modified from Clements and Newman, 2002.

1.4.1. Microcosms

In the laboratory it is possible to work at **microcosm** level, either with experiments in single-species cultures, or with more complex communities such as those that form biofilms. In both cases, the experimental conditions are very controlled, so this type of experiments can be easily replicated (**Figure 1.4.**). Culture experiments, mainly with algae, have been widely used as they can grow rapidly in laboratory conditions. However, the conditions must be standardized, since the growth and response of these microorganisms to a stressor can be affected by factors such as temperature, nutrient availability and light intensity.

Although this type of experimental approach generates reliable results, if they are only carried out with a single species, ecological relevance is lost, since obtaining a result in a single species does not allow us to understand the effects produced by the stressor in a community. If the experiment is carried out with biological structures such as biofilms, the response to a stressor of the diverse species that conform the biofilm can be observed, both at the individual level and

at the level of interaction between organisms. Therefore, this approach allows the results to be scaled up at the ecosystem level. They can reflect the sensitivity of all species to a possible risk and allow the detection of direct and indirect effects through the biological community (Mc. Clellan et al., 2008). As an inconvenience, these types of experiments are not as standardized as tests with a single species.

Figure 1.5. Microcosms (aquariums) at BETA Technological Center (Vic, Spain) used in this Thesis to evaluate the effect of nutrient concentration and N:P ratio on biofilm community development and geosmin production. March 18, 2019.

1.4.2. Mesocosms

The intermediate experimental approach in terms of ecological relevance and experimental control are **mesocosms**, both indoor or outdoor (**Figure 1.4.**). One type of mesocosm are the experimental flumes, structures that can range from half a meter to a length of up to 12 m (Kurz et al., 2017), where there is water circulation and where biofilm communities can be developed (**Figure 1.6.**). Although they are smaller and less complex than a real ecosystem, the experimental flumes provide the opportunity to conduct research at ecosystem level allowing replicability and working in conditions that can be managed in terms of cost and logistics (Ricart, 2010). Experimental outdoor flumes are subjected to the atmospheric conditions, what increase its ecological relevance, since the results obtained can be fully scaled at the ecosystem level. However, this same fact supposes a disadvantage, since instability in atmospheric conditions may hinder a future repetition of the experiment. Experiments with biofilms in experimental flumes have been widely used to investigate the effects of toxics substances (Kurz et al., 2017;

Ricart et al., 2010), and their dependence on specific environmental conditions (Romero et al., 2019; Serra et al., 2010; Guasch et al., 2007).

Figure 1.6. Experimental flumes at the Ter River Museum (Manlleu, NE Spain) used in this Thesis to evaluate the effect of water flow and light availability on biofilm community composition and geosmin production. March 19, 2018.

1.4.3. Field studies

Field studies can provide support for a causal relationship between stressors and community responses. Upstream-downstream gradients in biofilm metrics have been detected with field studies due to increases in pollution (Argudo et al., 2020; Montuelle et al., 2010), as well as changes in community composition (Guasch et al., 2009). However, field studies alone cannot be used to establish cause-effect relationship (Clements and Newman, 2002). Compared with experiments with microcosms, they are more realistic, but field studies always have less control.

Figure 1.7. Ter river at Gurb municipality (Osona region), NE Spain. March 2017.

1.4.4. Summary of approaches

In order to evaluate the potential impact of stressors on the biota, the use of controlled exposures provides an excellent basis. Small scale laboratory experiments (microcosms) where algal cultures are exposed for short-time to these stressors have high experimental control and replication but lack of ecological realism. Larger scale laboratory/outdoor experiments (experimental flumes) and field studies have greater ecological relevance but as the system increase in complexity and dimension, the experimental control and replication capacity decreases (**Figure 1.4.**) (Clements and Newman, 2002).

The experiments included in this Thesis have been performed at different levels of experimental organization. Effects of nutrient concentration and N:P ratio on biofilm community development and geosmin production and release, have been evaluated in a microcosm study (aquariums) on biofilm communities (**Figure 1.5.**). The effects related with water flow and light availability on geosmin production was evaluated using mesocosms (outdoor experimental flumes) (**Figure 1.6.**) and a three-years field study that included benthic analysis has been performed in the Ter upper basin (**Figure 1.7.**). This multi-scale approach is appropriate to identify and provide evidences of cause-effects relationships between the environmental variables, nutrient concentration and geosmin episodes.

CHAPTER 2. Objectives and Hypotheses

2. Objectives and hypotheses

The **main objective** of the present Thesis is to investigate the environmental, physicochemical and biological parameters associated with the production and release of geosmin, especially from benthic communities in rivers, and generating useful information that can help relevant stakeholders affected by this problem to prevent and predict geosmin episodes.

To achieve the main objective of this Thesis, a multi-scale approach study has been carried out, from microcosm to field studies. This approach has permitted to obtain information that allows establishing a plausible cause-effect relationship (microcosm and mesocosm studies) and information obtained on a real scale, with greater ecological relevance (mesocosms and in field studies).

Considering the current state of the art and all the information provided in the Introduction, the **specific objectives** foreseen to achieve the main goal of this Thesis are the following:

Microcosm	**Objective**: To asses the impact of nutrient concentration and N:P ratio on biofilm development an in the production and release of geosmin into the water.
Mesocosm	**Objective**: To investigate the direct and indirect effects of water flow and light availability on the main biofilm components and its role in geosmin production by the biofilm
Field study	**Objective**: To explore the relationships between the environmental parameters in fluvial systems and geosmin production by biological communities.
Predictive model	**Objective**: To develop a geosmin model that allows water drinking companies to predict geosmin episodes in freshwater ecosystems.

The described objectives aim to test the following **hypotheses**:

- The increase in the nutrient's concentration present in rivers as the main consequence of anthropogenic pressures will favor the development of cyanobacterial blooms and then will trigger the production of geosmin (addressed in **Chapter 4**).
- The decrease in the water flow of the rivers due to the reduction of rainfalls as a consequence of climate change, together with the channeling of the waters to produce electrical energy and irrigate the adjacent lands, will give rise to structural and functional changes in the biofilm. A lower water flow together with a lower light availability will favor the development of cyanobacterial communities and will lead to the production of geosmin (addressed in **Chapter 5**).
- In rivers with a Mediterranean climate, these factors are not stable, but are affected intra- and interannually. In spring and autumn, it is when a greater abundance of storms has been described, which in rainy years would imply high water flow values. Likewise, spring is the season where plowing and planting take place, which means an increase in the nutrients supply to the rivers, especially phosphorus. In addition, the plants begin to develop, giving rise to thicker and more abundant riparian vegetation. With these premises, it can be hypothesized that the triggering of geosmin episodes will be affected by climatic conditions, being more likely to occur an episode when there is a time with little rainfall, which leads to lower water flows. Likewise, these episodes will take place in sites where the water quality of the river is lower, with a greater presence of anthropogenic pressures that trigger higher nutrient concentrations. And at times when a lower light incidence, due to a more abundant riverside vegetation such as that given in spring, favor the development of geosmin-producing cyanobacteria (addressed in **Chapter 6**).

CHAPTER 3. Methodology

3. Methodology

This chapter presents all the methodology used throughout the Thesis. It is divided into three sections. The first (**3.1.**) explains the different experimental approaches used in the studies carried out throughout this Thesis, the second (**3.2.**) explains the methodology that has been used to analyze water samples and the third (**3.3.**) explains the methodology that has been used to analyze biofilm samples.

3.1. Experimental approaches

This section explains the bench-scale plant that have allowed to perform the microcosms experiment, the pilot plant used to perform the mesocosms experiment and the study site in which the field study of this Thesis has been carried out.

3.1.1. Microcosms

The bench-scale plant used in this Thesis for the microcosms experiment consists in a set of 6 L glass aquariums (26 cm long x 15 cm wide x 17 cm high) located in chamber at controlled temperature (**Figure 3.1.A.**). This chamber presents a control panel from which the temperature and ventilation can be fixed. Each aquarium has a submersible pump (EDEN 105, Eden Water Paradise, Italy) to promote oxygenation and water circulation, and a LED light (LENB 135-lm, LENB/14.97/11.98) connected to a system that allows to configure the photoperiod based on the requirements of the experiment (**Figure 3.1.B.**).

Each microcosm can be filled with stream cobbles and artificial/real water to recreate a freshwater system in which some parameters or conditions can be manipulated. This type of experimental approach allows experiments to be carried out in a controlled and easy to replicate way, and to accurately determine a cause-effect relationship. The experiment performed in this bench plant is explained in the **Chapter 4** of this Thesis.

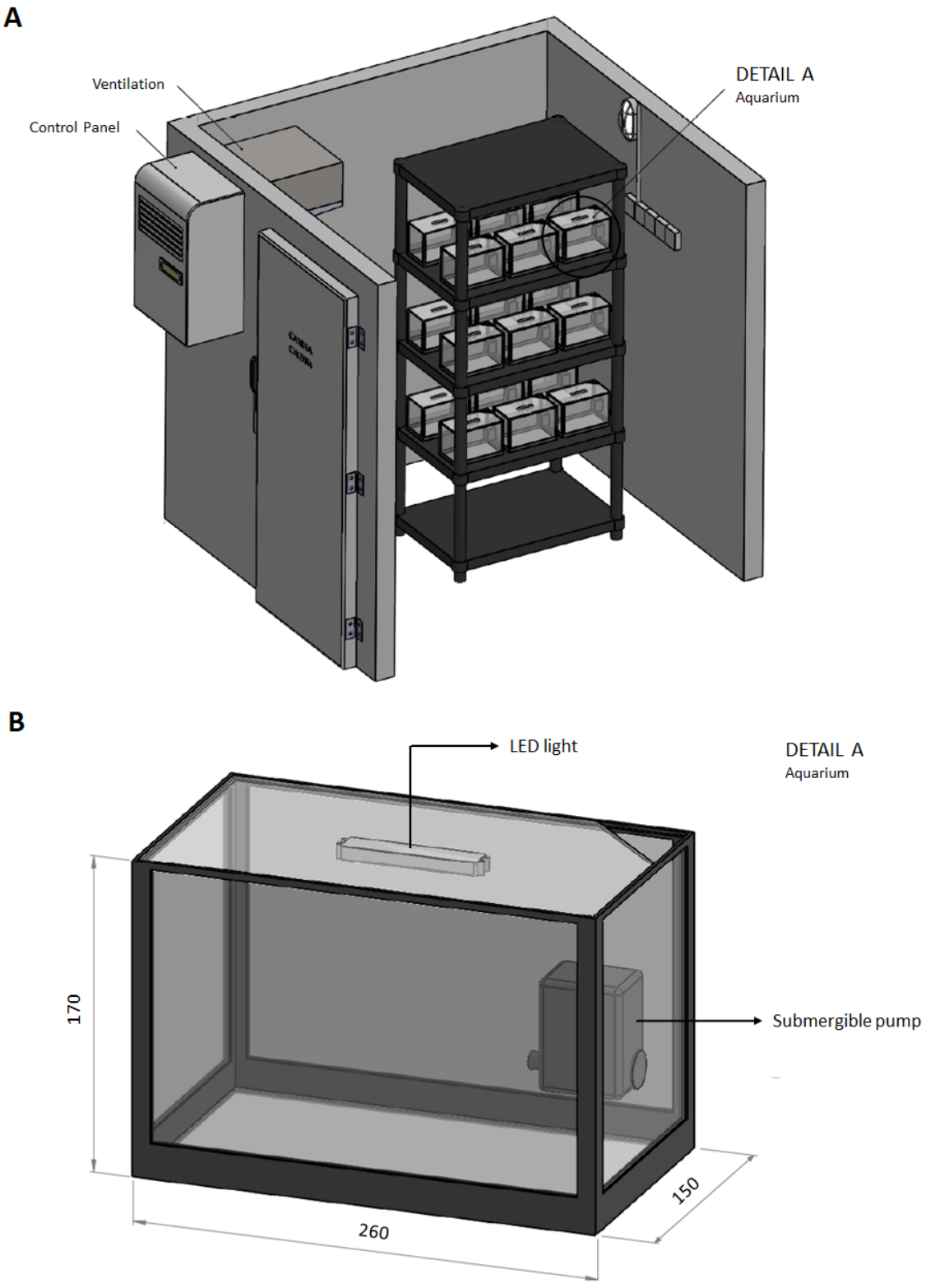

Figure 3.1. A. Three-dimensional representation of the bench-scale plant used in this Thesis. **B.** Three-dimensional representation of the aquariums used for the microcosms experiment performed in this Thesis.

3.1.2. Mesocosms

The pilot plant used in the mesocosms experiment performed in this Thesis is located in Manlleu (Catalonia, NE Spain), close to an industrial channel of the mid-section Ter river, from which can receive water directly.

It consists in 12 outdoor experimental flumes (3.5. m long x 12 cm wide x 8 cm high) made of polyvinyl chloride (PVC) through which water circulates from an initial 1000 L carboy (one for every 3 flumes) to a 500 L carboy located at the end of each 3-flumes set (**Figure 3.2.**). These experimental flumes can be used as an open or closed system. Thanks to four submerged pumps (drainage pump, VXV 1100AS) located in the industrial channel with water from the Ter river, each of the initial carboys receives water continuously, which circulates through the flumes and finally discharges into the same channel downstream of water abstraction. The closed system works thanks to a series of PVC tubes that connect the small carboys with the biggest ones and a series of pumps that allow the water recirculation (**Figure 3.3.**). The experiment performed in this pilot plant is explained in the **Chapter 5** of this Thesis.

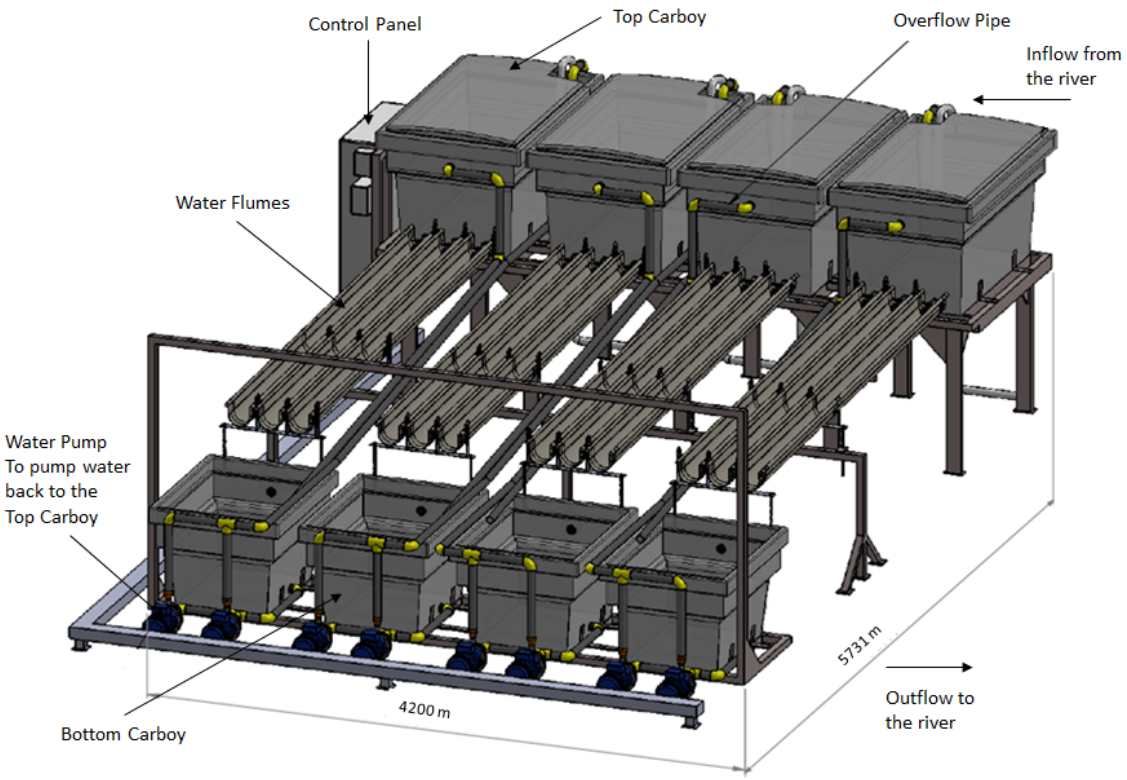

Figure 3.2. Three-dimensional representation of the pilot plant used for the mesocosms experiment performed in this Thesis.

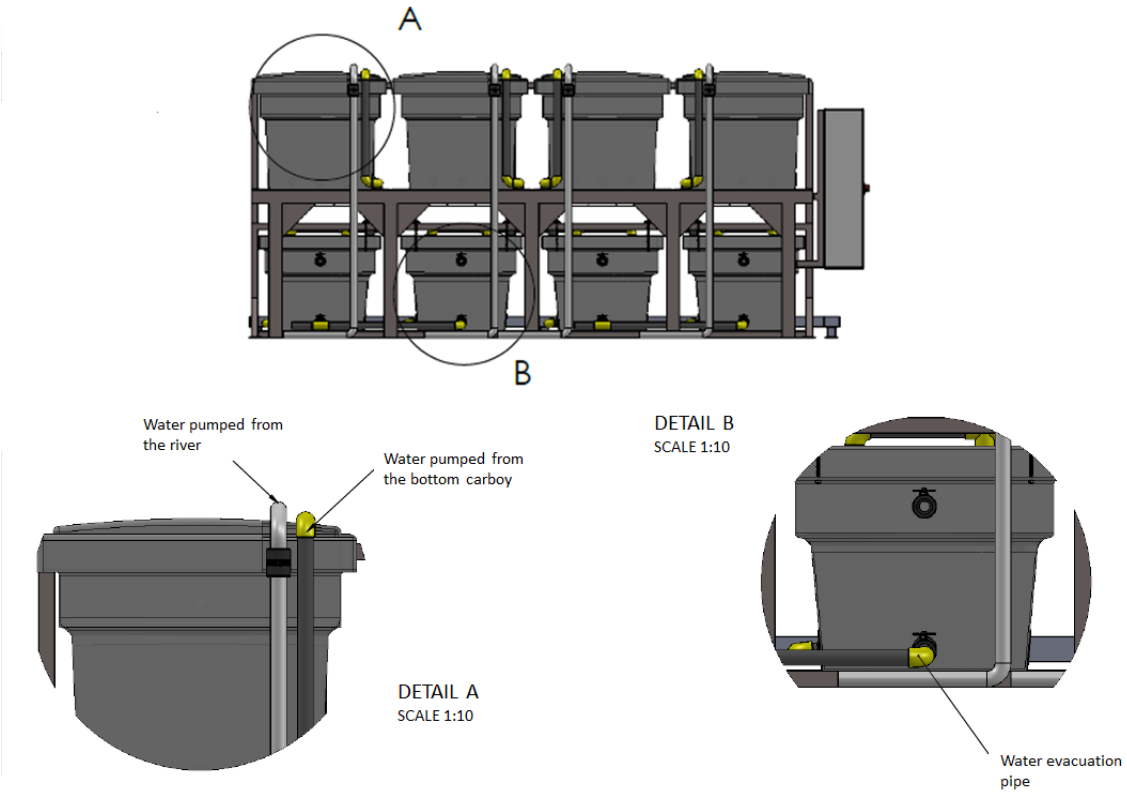

Figure 3.3. Three-dimensional representation of the water connections in the pilot plant.

3.1.3. Field study

3.1.3.1. Ter river

Mediterranean region is one of the most densely and industrially developed areas in Spain. Most of the rivers in this region, including the Ter, reveal many of the anthropogenic disturbances derived from the use of their waters for centuries.

The Ter river is born in the middle of the Catalan Pyrenees (at 2400m high) and flows into the Mediterranean Sea. It has a basin with a surface of 3010 km^2 and a length of 208 km (**Figure 3.4.**). During its course it receives many tributaries. The largest in the upper part is the Freser river and in its middle stretch, there are some small streams and rivers such as Sorreigs, Gurri and Ges. Downstream from these rivers input, the Ter river presents a series of reservoirs: Sau, Susqueda and El Pasteral. The middle and low parts of the river drain calcareous areas; however, the headwaters and some of the tributaries in the middle stretch (Riera Major, Osor and Onyar) flow over siliceous materials.

Figure 3.4. Ter river catchment (Catalonia, NE Spain). From Jordà-Capdevila et al., (2016).

The Mediterranean climate determines the rain patterns over the basin, which is characterized by maximum rainfall occurring during spring and autumn with dry and warm summers. The river annual average discharge is 840 Hm^3, but this value varies considerably between years. The state of the water and the biological communities in the river are obviously affected by this temporary variation (Sabater et al., 1992). Moreover, in its mid-section there are anthropogenic activities such as (i) a high number of dams used to obtain hydraulic energy, (ii) livestock farming and agriculture, leading to an increase in nutrients concentration and (iii) a system of reservoirs (Sau, Susqueda and El Pasteral) with a capacity of 375 Hm^3, which supplies energy and raw water for drinking purposes. All these activities are drastically affecting water flow and water quality downstream of the river (Céspedes et al., 2008). Up to now, the Ter river remains undisturbed only in some of its first and second order tributaries.

The study developed in this Thesis has been carried out in the Ter river as it passes through the El Ripollès and Osona regions.

El Ripollès is characterized by presenting land uses described as coniferous forest, natural grasslands, broad-leaved forest and moors and heathlands (**Figure 3.5.**). The highest population density occurs in the municipality of Ripoll, with a population of 10,686 inhabitants in 2019. The northern part of El Ripollès area is characterized by an Eastern Pyrenean and Pre-Pyrenean Mediterranean climate while the south part is defined as Humid Continental Mediterranean climate (Meteocat, 2018). The mean annual precipitation is 1200 mm in the highest areas and 900 mm in the lowest, and the mean annual temperature is 10°C, with a variation from -3°C to 20°C depending on the season (Meteocat, 2018).

The Osona region presents a high percentage of land used related to non-irrigated arable land, industrial and commercial units, and continuous and discontinuous urban fabric, all this area is

surrounded by coniferous forest (**Figure 3.5.**). In the region there are 26,631 hectares cultivated, about 25% of the total area, of which 26,454 are herbaceous (mostly cereals) destined for animal feed, since in the region there are more than 300 companies related to the meat sector. Its capital is Vic, with an area of 30.92 km^2 and more than 46,000 inhabitants (2019). Close to Vic (at 7 km) is located Manlleu, a city with more than 20,000 inhabitants (2019) and about 17.3 km^2. The Ter river runs between both cities. The Osona region is defined as Humid Continental Mediterranean climate, the mean annual precipitation is around 750 mm, and the temperature is similar to El Ripollès, with an average of 12°C, but with a higher minimum (4°C) (Meteocat, 2018).

Regarding the vegetation of the area evaluated in this Thesis, above 2300 m above sea level (asl), only Alpine vegetation is found, treeless and mainly formed with boreal-like meadows. Between 2300 m asl and 1600 m als Subalpine vegetation occurs, mainly European silver fir (*Abies alba*) and Mountain pine (*Pinus* uncinata) forests. Sub Mediterranean vegetation is found along the Ter river and the slopes from 1600 m to 500 m asl, with different oaks (*Quercus pubescens*, *Q. petraea*, *Q. ilex*) and Scots pine (*Pinus sylvestris*) forests. The forested habitats are mostly on the slopes, while the arable land, population and infrastructures are concentrated in the plain. Alder forests are in regression, with a predominance of willow trees (*Salix alba*).

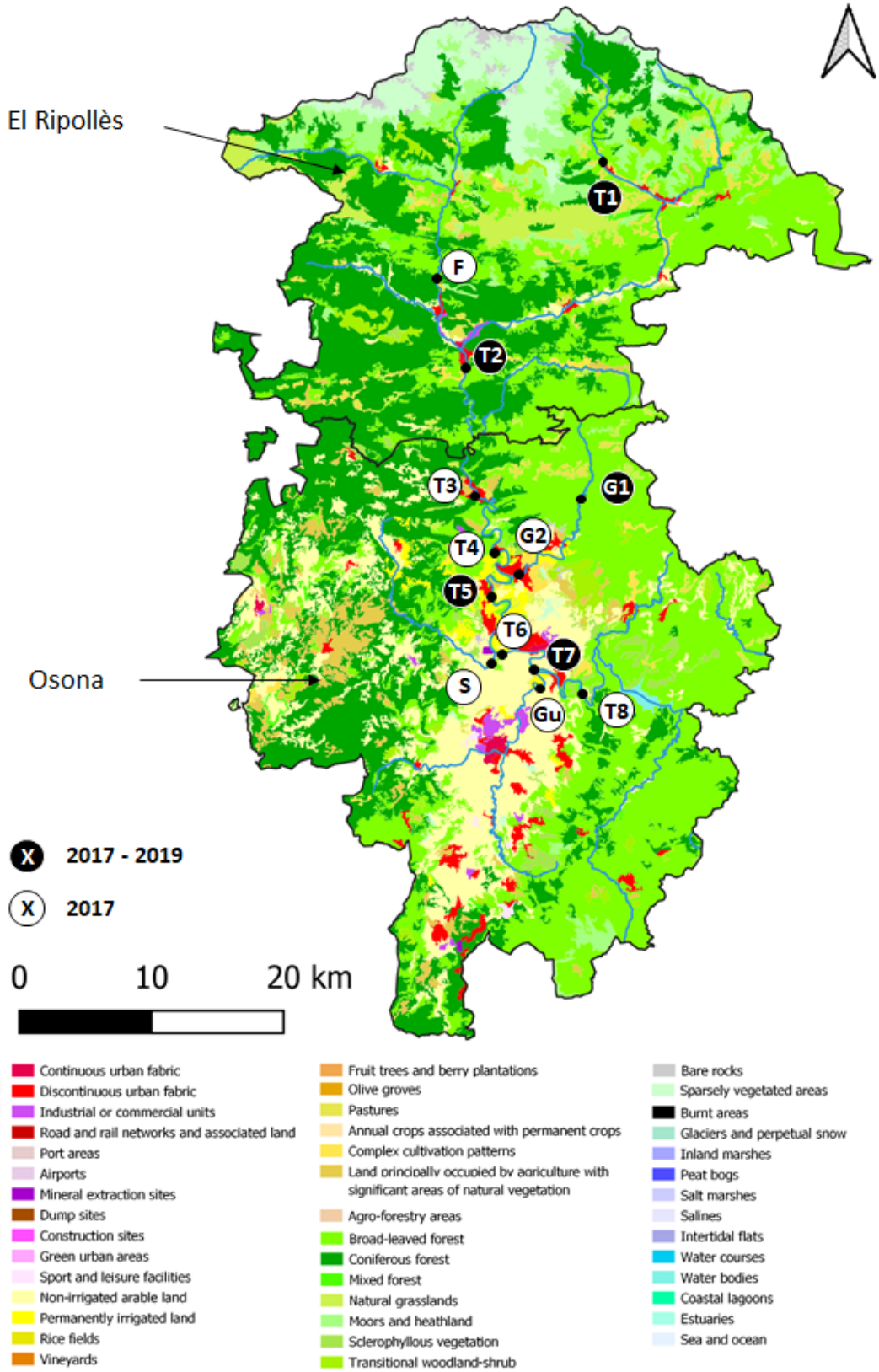

Figure 3.5. Map of land uses catgorized by the CORINE land cover system (2018), of El Ripollès and Osona regions (NE Catalonia, Spain). The white circles referred to the 2017 sampling sites and the black circles referred to the 2017 – 2019 sampling sites.

3.1.3.2. Spatial analysis

Digital elevation model (DEM) data and land use maps interpreted from CORINE land cover system (2018) were used to delineate watershed boundaries and measure the land use composition in the upper Ter river basin using QGIS version 3.10.2. In this study, land use types were classified following the CORINE land-cover classification at level 2 (**Table 3.1.**). Based on the DEM and stream networks of the watershed, 13 sub-watersheds were delineated to compare the relationships between land use and water quality, limiting the sub-basin to 5km around the sampling site to reduce the possible deviation in the land uses percentage that would be generated when considering the whole catchment. The proportions of land use types in the 13 zones were also computed using QGIS.

Table 3.1. CORINE land-cover classification for levels 1 and 2.

LEVEL 1	LEVEL 2
1. Artificial surfaces	1.1. Urban fabric
	1.2. Industrial, commercial and transport units
	1.3. Mine, dump and construction sites
	1.4. Artificial, non-agricultural vegetated areas
2. Agricultural areas	2.1. Arable land
	2.2. Permanent crops
	2.3. Pastures
	2.4. Heterogeneous agricultural areas
3. Forest and semi-natural areas	3.1. Forests
	3.2. Scrub and/or herbaceous associations
	3.3. Open spaces with little or no vegetation

3.2. Water samples analysis

3.2.1. Geosmin

The geosmin concentration present in water samples was determined by gas chromatography mass spectrometry (GC/MS) technique, using the equipment of Thermo Fisher Scientific (ISQ-TRACE GC ULTRA) (**Figure 3.6.**), and following the protocol established by Klausen et al. (2005), with some modifications.

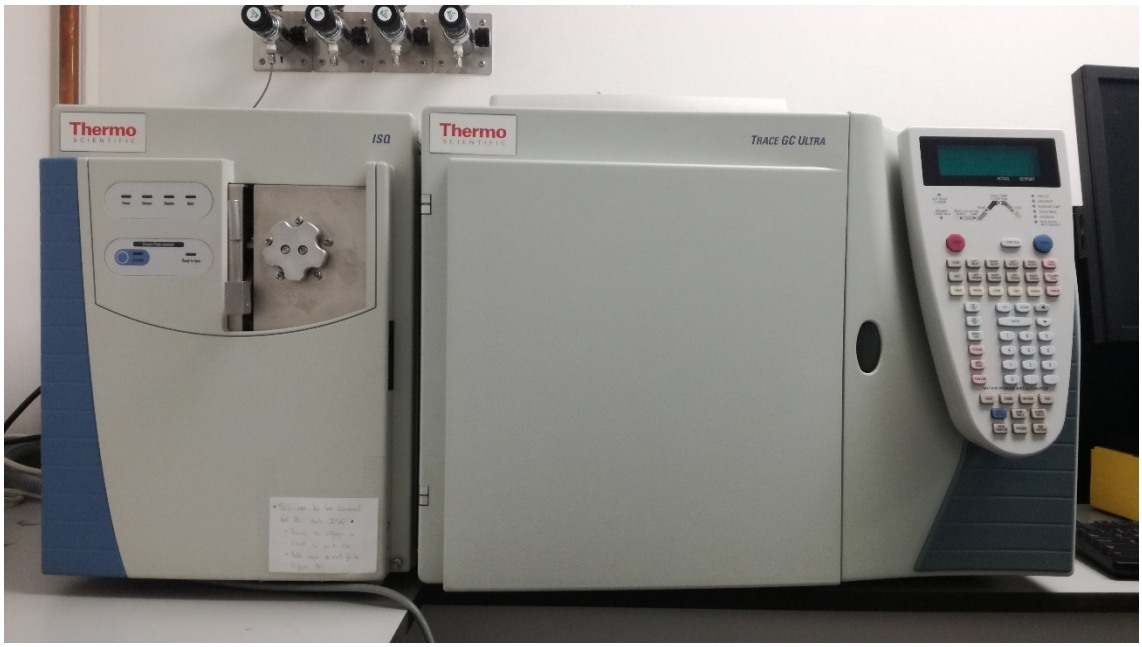

Figure 3.6. Gas chromatograph – Mass spectrometry (GC/MS) ISQ-TRACE GC ULTRA, (Thermo Fisher Scientific) used for the geosmin analysis. BETA Technological Center laboratory, Vic (Spain).

Previous preparation of the material

Preparation of intermediate dilutions. A solution of (±) geosmin and 2 - Methylisoborneol (MIB) (100 µg/L)(>98% purity, Sigma-Aldrich Química SL, Madrid, Spain) in pure methanol was used to prepare dilutions for calibration. Briefly, 200 µL from the stock solution was mixed with 9.8 mL of methanol, to create an intermediate dilution of 2 µg/L. This dilution has to be done in the hood due to the geosmin toxicity at this high concentration.

Preparation of the calibration curve. From the 2 µg/L intermediate dilution, other three intermediate dilutions were prepared, all of them in a final volume of 50 mL of methanol:

200.000, 100.000 and 40.000 ng/L. With these intermediate dilutions eight standard dilutions were prepared in miliQ water for the calibration curve (**Figure 3.7.**).

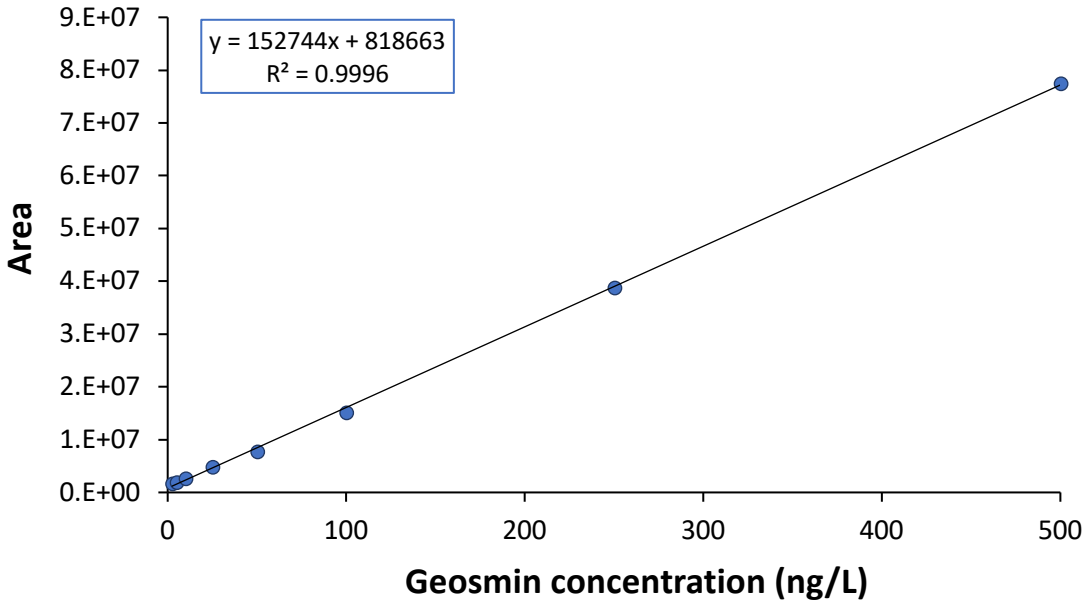

Figure 3.7. Example of a geosmin concentration calibration curve depending on the peak area obtained, and the equation generated (r^2 = 0.9996).

Preparation of samples. Both standard dilutions and water samples were prepared, in triplicate, in a 100 mL opaque reaction vial, that contain 10g of NaCl and a magnetic stir bar.

General procedure for the measurement of geosmin in water

A 65 µm polydimethylsiloxane/divinylbenzene (PDMS/DVB) fibber was injected into the headspace of the sample vial, and the vial was placed on a stirrer, inside an oven at 60°C for 25 min to favour the geosmin volatilization. The magnetic stir bar was rotated to enhance the vaporization, but not so fast that vortex was formed. After the absorption, the fibber was desorbed for 6 min at 250°C in the splitless injector of the GC/MS instrument. The GC column was 30m x 0.25 mm id, 0.25 µm film thickness (Sigma Aldrich), with helium carrier gas at a constant flow of 1 mL/min. The temperature program for the GC oven was an initial isothermal stage at 70°C during 3 minutes, then a first temperature ramp to 200°C at a 10°C/min rate, followed by a second ramp up to 280°C at 30°C/min, with a hold time of 4 min. Temperature of the transfer line and the ion source was 250 and 200°C respectively, and the scan was 111, 112, 125, 164 and 182 m/z fragments. Geosmin was identified by comparing the retention time to

those of the selected analytical standard (**Figure 3.8.**). Quantification was performed using the calibration curve obtained previously (**Figure 3.7**.). The total analysis process lasts 50 minutes.

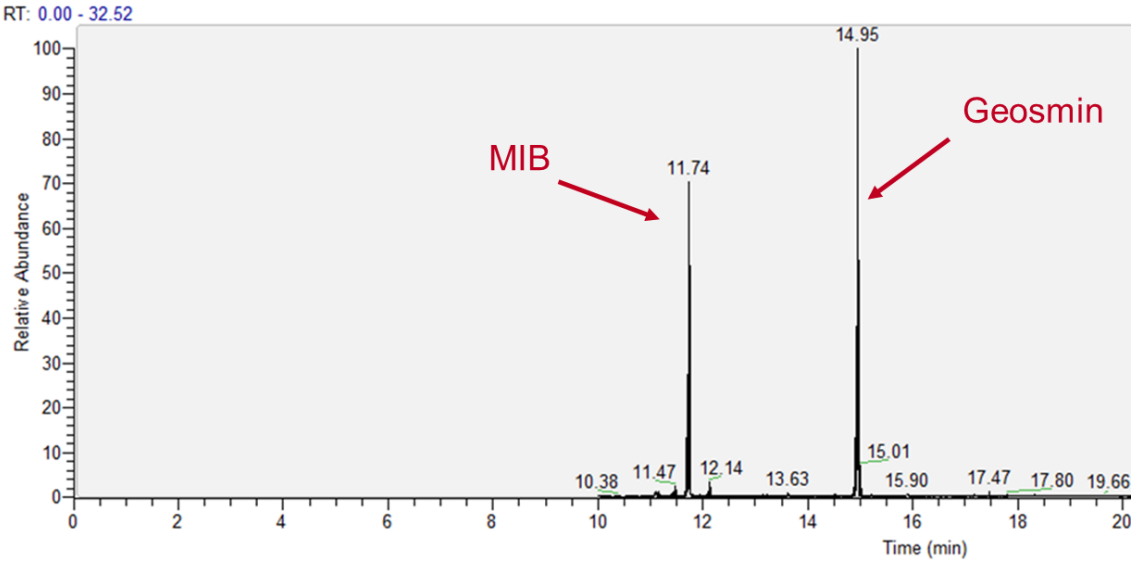

Figure 3.8. Example of a chromatogram obtained for a geosmin and 2-methylisoborneol (MIB) 100 ng/L standard dilution.

3.2.2. Nutrients

3.2.2.1. Soluble Reactive Phosphorus concentration

Soluble Reactive Phosphorus (SRP) concentration in water samples was measured using the protocol described by Murphy and Riley, (1962). All water samples for the SRP analysis were always taken in triplicate.

Previous preparation of the material

Preparation of stock solution and intermediate dilutions. A phosphate stock solution (10000 µM of PO_4-P) (S1) was prepared. For this, 1.3609g of potassium phosphate diacid KH_2PO_4 was weighed and diluted in a flask up to 1L of deionized water (mQ). This solution should be stored in dark conditions in the refrigerator. Intermediate dilutions of 100 µM (S2) and of 10 µM (S3) were prepared from the stock solution.

Preparation of the calibration curve. Whit the intermediate dilutions the following set of concentrations were prepared (**Table 3.2.**):

Table 3.2. Required volumes (in mL) of the intermediate dilutions and miliQ water to obtain the different phosphorus concentrations needed to have a calibration curve.

Standard (µM)	0	0.1	0.2	0.5	1	2	5	10	20
V. S2 (mL)					0.1	0.2	0.5	1	2
V. S3 (mL)	0	0.1	0.2	0.5					
V. mQ Water (mL)	10	9.9	9.8	9.5	9.9	9.8	9.5	9	8

Preparation of mixed reagent. To obtain the mixed reagent the following reagents were needed:

- Ammonium molybdate: 11.2g tetrahydrate ammonium molybdate [$(NH_4)_6Mo_7O_{24}{\cdot}4H_2O$] was weighed and diluted in 500mL of miliQ water.
- Sulfuric acid: 900 mL miliQ water placed in a 1 L flask and 140 mL of H_2SO_4 was added.
- Ascorbic acid: 27g of ascorbic acid was dissolved in 500mL of mQ water.
- Antimony potassium tartrate: 0.34g of antimony potassium tartrate ($C_4H_4O_7SbK$) was dissolved in 250mL of miliQ water.

The mixed reagent is not stable, so it had to be prepared every time. Depending on the total mixed reagent volume needed, the amount of each reagent varied. For example, for a total volume of 100 mL, 20 mL of ammonium molybdate, 50 mL of sulfuric acid, 20 mL of ascorbic acid and 10 mL of antimony potassium tartrate were needed.

Preparation of samples. The sample was filtered using a 0.2 µm nylon membrane filters (Merck Millipore), obtaining a final sample volume of 10 mL.

General procedure for the measurement of SRP

1 mL of mixed reagent was added to both the standard dilutions and the samples and mixed with the vortex. They were placed in the dark between 1 and 12 hours and finally, the color intensity of them were measured using a spectrophotometer (NanoPhotometer™ P-360, INTEM) at 890 nm.

3.2.2.2. Ammonium concentration

The ammonium concentration was analyzed following the protocol described in Reardon et al. (1966). All samples for ammonium analysis were always taken in triplicate.

Previous preparation of the material

Preparation of intermediate dilutions. Intermediate and standard dilutions were obtained from an ammonium stock solution (1 g/L PanReac-AppliChem) (S1). From this, intermediate dilutions of 10 mg/L (S2) and 1 mg/L (S3) were prepared.

Preparation of the calibration curve. With the intermediate dilutions the following set of concentrations were prepared (**Table 3.3.**):

Table 3.3. Required volumes (in mL) of the intermediate dilutions and miliQ water to obtain the different ammonium concentrations needed to have a calibration curve.

Standard (mg/L)	**0**	**0.01**	**0.02**	**0.03**	**0.04**	**0.05**	**0.1**	**0.2**	**0.5**	**1**	**2**	**5**	**10**
V. S2 (mL)										1	2	5	10
V. S3 (mL)		0.1	0.2	0.3	0.4	0.5	1	2	5				
V. mQ Water (mL)	10	9.9	9.8	9.7	9.6	9.5	9	8	5	9	8	5	0

The **Figure 3.9.** shows an example of a calibration curve performed for the colorimetric ammonium analysis. The color of the samples varies from yellow, for samples with little concentration, to dark blue, when the ammonium concentration is high.

Preparation of reagent 1 and reagent 2. Reagent 1 was stable for 1 month and must be prepared as follows:

- 8.5g sodium salicylate and 10g of sodium citrate were added in 200mL mQ water.
- 0.1g sodium nitroprusside was added and mQ water was added until made up to 250mL

Reagent 2 is stable and must be prepared as follows:

- 5g sodium hydroxide was added in 250mL mQ water.
- 0.4g sodium dichloroisocianurate was added and the final mQ water was 500 mL.

Preparation of samples. 10 mL of sample was filtered through 0.2 µm nylon membrane filter (Merck Millipore).

General procedure for the measurement of ammonium

1 mL of reagent 1 was added to each sample and to each standard dilution. After that, 1 mL of reagent 2 was added to each sample and to each standard dilution. Both standard dilutions and samples were mixed well by vortexing and stored in a dark place at room temperature between 1 and 12 hours. Finally, the absorbance in the spectrophotometer (NanoPhotometer™ P-360, INTEM) was measured at 690 nm.

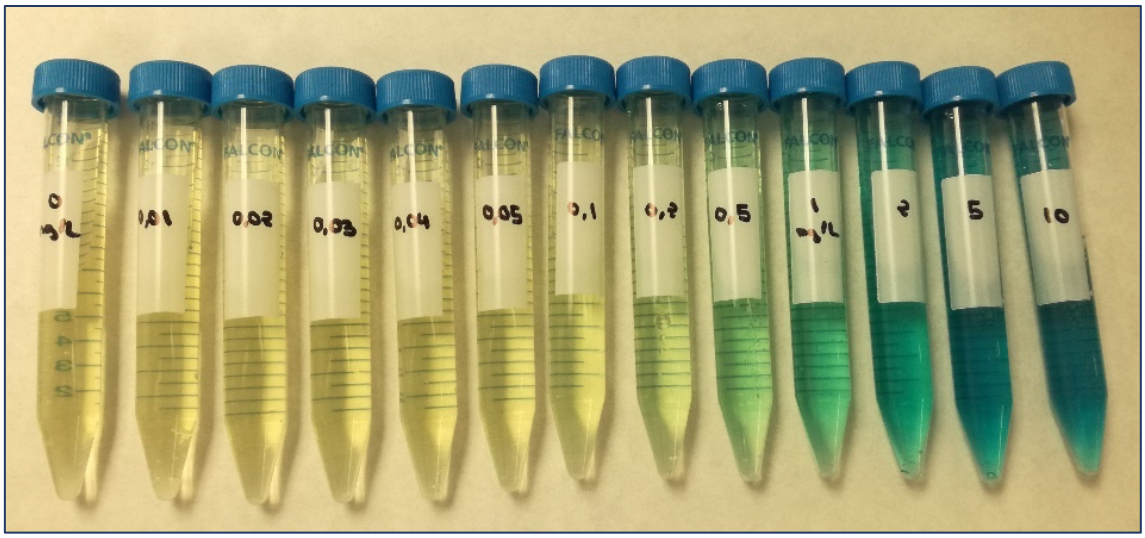

Figure 3.9. Example of a calibration curve performed for the colorimetric ammonium analysis.

3.2.2.3. Nitrite concentration

Nitrite concentration was determined following the method described in Rand et al. (1976). All samples for nitrite analysis were always taken in triplicate.

Previous preparation of the material

Preparation of the intermediate dilutions. Intermediate dilutions were obtained from a nitrite stock solution (1g/L PanReac-AppliChem) (S1). The concentration of this intermediate dilutions was 100 mg/L (S2) and 10 mg/L (S3).

Preparation of the calibration curve. With the intermediate dilutions, the following set of standard dilutions was prepared (**Table 3.4.**):

Table 3.4. Required volumes (in mL) of the intermediate dilutions and miliQ water to obtain the different nitrite concentrations needed to have a calibration curve.

Standard (mg/L)	0.1	0.2	0.4	0.6	0.8	1
V. S3 (mL)	0.45	0.9	1.8	2.7	3.6	4.5
V. mQ water (mL)	44.55	44.1	43.2	42.3	41.4	40.5

The **Figure 3.10.** shows an example of a calibration curve performed for the colorimetric nitrite analysis. The samples color varies from transparent, for samples with little concentration, to bright pink, when the nitrite concentration is high.

Preparation of color reagent. 100 mL of 85% phosphoric acid and 10 g of sulfanilamide were measured in 800 mL of miliQ water. When dissolved, 1 g of N-(1-naphthyl) ethylenediamine

dihydrochloride was added and completed up to 1 L in miliQ water. This solution was stable for one month if stored in the refrigerator in an opaque flask.

Preparation of samples. The sample was filtered using a 0.2 µm nylon membrane filter (Merck Millipore) to obtain a final volume of 45 mL. The pH of the sample should be between 5 and 9. If necessary, it has to be adjusted using HCl 1N or NH_4OH.

General procedure for the measurement of nitrite

2 mL of color reagent was added to both the standard dilutions and the samples, and they were read at 543 nm using a spectrophotometer (NanoPhotometer™ P-360, INTEM) between 10 minutes and 2 hours after the color reagent addition.

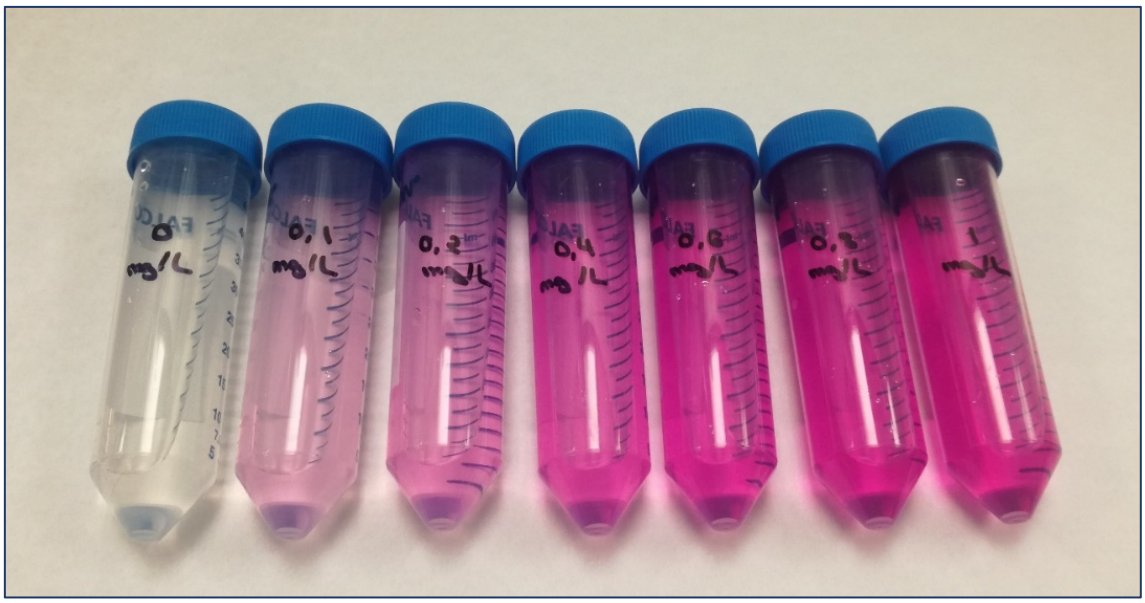

Figure 3.10. Example of a calibration curve performed for the colorimetric nitrite analysis.

3.2.2.4. Nitrate concentration

Nitrate concentration was determined following the method described in Rand et al. (1976). All samples for nitrate analysis were always taken in triplicate.

Previous preparation of the material

Preparation of the intermediate dilutions. Intermediate dilutions were obtained from a nitrate stock solution (1g/L PanReac-AppliChem) (S1). The intermediate dilutions concentration were of 100 mg/L (S2) and 10 mg/L (S3)

Preparation of the calibration curve. With the intermediate dilutions, the following set of standard dilutions was prepared (**Table 3.5.**):

Table 3.5. Required volumes (in mL) of the intermediate dilutions and miliQ water to obtain the different nitrate concentrations needed to have a calibration curve.

Standard (mg/L)	1	2	4	6	10	15	18
V. S2 (mL)			1.8	2.7	4.5	6.75	8.1
V. S3 (mL)	4.5	9					
V. mQ water (mL)	40.5	36	43.2	42.3	40.5	38.25	36.9

Preparation of samples. The sample was filtered using a 0.2 µm nylon membrane filter (Merck Millipore) to obtain a final volume of 45 mL.

General procedure for the measurement of nitrate

Both to the standard dilutions and to the samples, 1 mL of HCl 1N was added and mixed. The absorbance was measured in the spectrophotometer (NanoPhotometer™ P-360, INTEM) at 220 nm and 275 nm. To obtain the final absorbance, the following equation must be used (**Eq. 3.1.**):

$$\boldsymbol{Final\ absorbance = Abs.220\ nm - 2 \cdot Abs.275nm} \qquad \boldsymbol{Eq.3.1.}$$

where, Abs. 220 nm = absorbance value read at 220 nm wavelength, and Abs. = 275 nm = absorbance value read at 275 nm wavelength.

3.2.3. Suspended solids

First, the 47-mm GF/F glass-fiber filters (0.7 µm pore size, Whatman) were muffled for at least 1 hour at 500°C. After that, the filters were left in the desiccator at room temperature and, once they had cooled, the filters were weighed (*weight 1)*. 500 mL of water sample was filtered through the pre-weighed filters. Then, the filters were drying up 72h at 60°C (Forced air oven, MEMMERT IFE500) and they were weighed again (*weight* 2) in order to calculate the suspended solids (SS) present in the water sample (**Eq. 3.2.**).

$$\boldsymbol{SS\ (g) = weight\ 2\ (g) - weight\ 1\ (g)} \qquad \boldsymbol{Eq.3.2.}$$

where, weight 1 = weight value without the sample and weight 2 = weight value after 72 h in the oven.

3.2.4. Turbidity

The turbidity of the water samples was measured using a turbidimeter (HI 98713, HANNA Instruments). For that, 10 mL of sample was taken and placed in the quartz cuvette. After 10 seconds, the instrument gave the results in UNF.

3.2.5. Organic Matter

The organic matter present in the samples was estimated using the spectrophotometer (NanoPhotometer™ P-360, INTEM) and reading the absorbance at 254 nm at room temperature. The Autozero was set with miliQ water.

3.2.6. Chlorides

Chlorides were determined by volumetric precipitation, reacting them with silver nitrate in the presence of potassium chromate, following the protocol described in Standard Methods 4500 ClB.

Previous preparation of the material

Preparation of silver nitrate 0.0282N. 4.7909 g of silver nitrate were dissolved up to 1000 mL in distilled water. It was stored in an opaque bottle to protect it from light.

Preparation of potassium chromate at 10%. 10 g of potassium chromate were dissolved in 100 ml of distilled water.

Preparation of sample. Before performing the analysis, the sample must be adjusted to a pH between 7 and 10, with sulfuric acid or sodium hydroxide, as appropriate.

General procedure for the measurement of chlorides

100 ml of the water sample or a dilution was taken, 3 drops of the 10% potassium chromate reagent were added and it was titrated, stirring vigorously, with 0.0282N silver nitrate solution until a reddish color appeared. It was necessary to make a control with chlorine-free water.

Chlorides calculation. To obtain the chloride concentration, the following equation (**Eq. 3.3.**) must be used:

$$\boldsymbol{Chlorides\ (mg/L) = (V - V') \cdot 10} \qquad \boldsymbol{Eq.3.3.}$$

where, V = ml of silver nitrate used in the evaluation of the sample and V' = ml of silver nitrate used in the evaluation of the control.

3.2.7. Sulfates

The principle of this analysis was based on the sulfate ion precipitates with the barium ion forming crystals of barium sulfate. The absorbance of the barium sulfate suspension was measured with a spectrophotometer and the sulfate concentration was determined. The method established for this analysis is that described in Standard Methods 4500 SO_4^{2-}E.

Previous preparation of the material

Preparation of buffer solution A. 30 g of magnesium chloride hexahydrate, 5 g of sodium acetate trihydrate, 1 g of potassium nitrate and 20 mL of acetic acid (99%) were dissolved in 500 ml of distilled water and completed to make 1 liter.

Preparation of buffer solution B. This solution was for when the sulfate concentration in the sample was less than 10 mg/L. 30 g of magnesium chloride, 5 g of sodium acetate, 1 g of potassium nitrate, 0.111 g of sodium sulfate and 20 ml of acetic acid were dissolved in 500 ml of water and completed to 1 liter.

Preparation of the sulfate stock solution. 0.1479 g of anhydrous sodium sulfate were dissolved in distilled water and diluted to 1000 mL. 1 mL of this solution contains 100 ug of sulfate.

General procedure for the measurement of sulfates

Preparation of the calibration curve. Standard solutions of 0 to 40 mg/L were prepared at intervals of 5 mg/L. Above 40 mg/L the accuracy decreases, and barium sulfate suspensions lose stability. Two curves were prepared: one for buffer solution A (curve A) and one for standard solution B (curve B).

- Curve A: from 0 to 40 mg/L in a total sample volume of 100mL.
- Curve B: from 0 to 10 ng/L in a total sample volume of 100mL.

Absorbance measure. 100 mL of sample or a solution was taken in a 250 mL Erlenmeyer. 20 mL of buffer solution (A or B according to the expected sulfate concentration) was added and mixed with a magnetic stirrer. A teaspoon of barium chloride was added (0.2 to 0.3 mL) and 60 seconds had to be waited while the sample was mixing at a constant speed. After this time, the solution was transferred to a spectrophotometer cuvette and after 5 minutes the absorbance at 420 nm was read.

Sulfates calculation. The sulfate concentration was obtained from the calibration curve. If buffer A was used, the absorbance of the control was subtracted before comparing with the calibration curve. If standard B was used, the concentration of the control was subtracted, once compared to the calibration curve. The results are expressed in mg of sulfate/liter.

3.2.8. pH, electrical conductivity, temperature and dissolved oxygen

Both in the field campaign and in the experiments carried out in the microcosm and mesocosm, portable probes were used to measure the temperature, dissolved oxygen concentration and

saturation (YSI professional plus, YSI Incorporated, USA), pH (XS pH7+ DHS) and electrical conductivity (XS COND 7+) (**Figure 3.11.**).

To ensure a reliable measurement, these probes have to be calibrated every day. For this, commercial reagents are used. In the case of pH, a series of buffers are used at pH 4, 7 and 10; for the electrical conductivity, a buffer at 1413 µS/cm is used; and the oxygen (both the concentration in mg/L and the percentage of saturation) is calibrated in the probe cover itself, after having thoroughly cleaned it with distilled water. Once the probes are calibrated, they are introduced into the water and wait until the provided value stabilizes.

Figure 3.11. From the left to the right, portable probe for pH, oxygen and temperature and electrical conductivity.

3.3. Biofilm samples analysis

3.3.1. Geosmin

The concentration of geosmin in biofilm was quantified following the protocol described by Wang and Li, (2015). All biofilm samples for geosmin analysis were always taken in triplicate.

Previous preparation of the material

Preparation of samples. The cobble surface was scrapped in a known volume of water to obtain a biofilm suspension and the area of the scraped cobble was obtained by drawing the surface on aluminum foil and recalculating depending on the weight. An aliquot of 5 mL of this suspension was frozen (-80°C) and used to analyze geosmin concentration in biofilm. For this analytic, samples were frozen (-80°C) and thawed five times to facilitate cell breakage and geosmin release in the aquatic phase. Afterwards, the sample was decanted in a 100 mL opaque

reaction vial, that contained 10 g of NaCl and 45 mL of sterile dH_2O, to obtain 50 mL of total volume, and a magnetic stir bar.

General procedure for the measurement of geosmin in biofilm

A 65 µm PDMS/DVB fibber was injected into the headspace of the sample vial. Separation and analysis of extracted volatile compound was performed in GC/MS instrument (ISQ – TRACE GC ULTRA) as described in the geosmin concentration in water section (**3.2.1.**).

The geosmin concentration in biofilm, in ng/mg, was calculated as follows (**Eq. 3.4.**):

$$\boldsymbol{Geosmin\ (ng/mg) = \frac{G_w \cdot V}{AFDM}} \qquad \boldsymbol{Eq.\ 3.4.}$$

where G_w = geosmin concentration in ng/L, V = biofilm sample volume analysed (in L) and AFDM = organic matter present in the biofilm sample (in mg).

3.3.2. Chlorophyll *a*

Algal biomass was estimated from the analysis of Chlorophyll *a (*Chl *a*) concentration in biofilms. This analysis was performed using the protocol described by Artigas et al. (2015). The cobble surface was scrapped in a known volume of water to obtain a biofilm suspension and the area of the scraped cobble was obtained by drawing the surface on aluminum foil and recalculating depending on the weight. An aliquot of 10 mL of this suspension was used to analyze Chlorophyll *a*. All biofilm samples for Chlorophyll *a* analysis were always taken in triplicate. During all the procedure, samples were covered with aluminum foil to avoid the degradation of chlorophyll due to light.

Previous preparation of the material

Preparation of sample. If the sample contained water, it was filtered before to eliminate it (GF/C filters, Whatman). Once the sample was filtered, it was placed in a glass vial.

General procedure for the measurement of Chlorophyll *a*

Incubation. 10 mL of 90% acetone was added to the glass vial, enough to cover the sample, and the vial was wrapped in aluminum foil to protect the sample from light. The sample was left overnight in the fridge at 4°C.

Absorbance measure. After the night the sample was filtered (GF/C filters, Whatman), but this time the filtrate was collected, which was what is used to read on the spectrophotometer (NanoPhotometer™ P-360, INTEM). 5 mL of 90% acetone were added to the vial, to finish

extracting the chlorophyll that may have remained and the sample was filter again, without changing collector or filter.

The Autozero was done in the spectrophotometer (NanoPhotometer™ P-360, INTEM) with the cuvette filled with 90% acetone.

The filtrate was placed in the spectrophotometer cuvette and read at three wavelengths:

- 430 nm (carotenoid peak), 665 nm (chlorophyll peak) and 750 nm (turbidity peak). The cuvette must be 1 cm.
- If the 430 nm peak was greater than 2, the sample was diluted (acetone was added to the filtrate).
- If the 750 nm peak was greater than 0.02 it was necessary to re-filter the sample until it adjusts to the value.

Chlorophyll a calculation. The chlorophyll *a* concentration was calculated following the method described by Jeffrey and Humphrey (1975), using the **Equation 3.5**.

$$\boldsymbol{Chlorophyll\ a\ (\mu g/cm^2) = \frac{(Abs.665\ nm - Abs.750\ nm) \cdot 11.4 \cdot AV}{SS}} \qquad \boldsymbol{Eq.3.5.}$$

where, Abs. 665nm = absorbance value read at 665 nm wavelength, Abs. 750 nm = absorbance value read at 750 nm wavelength, AV = acetone volume (in mL) and SS = scratched surface (in cm^2).

Margalef Index calculation. The Margalef Index (MI) was calculated as the quotient between the carotenoid /Chlorophyll *a* ratio (**Eq. 3.6.**):

$$\boldsymbol{MI = Abs.430\ nm / Abs.665\ nm} \qquad \boldsymbol{Eq.3.6.}$$

where, Abs. 430 nm = absorbance value read at 430 nm wavelength and Abs. 665 nm = absorbance value read at 665 nm wavelength.

This index is based on the fact that Chlorophyll *a* is the pigment that is synthesized and degraded more quickly, while other pigments accumulate and are more resistant to degradation than Chlorophyll *a*. Thus, all populations that have low productivity, are characterized by lower concentrations of pigments and, therefore, the relationship of Chlorophyll *a* with the rest of the pigments is lower or higher depending on the age of the populations. Therefore, with this index, low values are obtained in population that grow rapidly and increase when the population is more mature and with a low renewal rate (Margalef, 1960).

3.3.3. Ash Free Dry Mass

Total biofilm biomass was measured as ash free dry mass (AFDM). The cobble surface was scrapped in a known volume of water to obtain a biofilm suspension and the area of the scraped cobble was obtained by drawing the surface on aluminum foil and recalculating depending on the weight. An aliquot of 10 mL of this suspension was used to analyze AFDM. All biofilm samples for the AFDM analysis were always taken in triplicate.

Previous preparation of the material

Preparation of filters. First, the 47-mm GF/F glass-fiber filters (0.7 µm pore size, Whatman) were muffled for at least 1 hour at 500°C. After that, they were left in the desiccator at room temperature until they had cooled, and then weighed (*weight 1)*.

General procedure for the measurement of AFDM

Obtaining the dry weight value. The samples were filtered through the pre-weighed filters. The filters were drying up 72h at 60°C (Forced air oven, MEMMERT IFE500) and they were weighed again (*weight* 2) in order to calculate dry matter (DM) (**Eq. 3.7.**).

$$\boldsymbol{DM(g) = weight\ 2\ (g) - weight\ 1\ (g)} \qquad \boldsymbol{Eq.\ 3.7.}$$

where, weight 1 = weight value without the sample and weight 2 = weight value after 72h in the oven.

Obtaining the ash free dry mass value. Samples were combusted at 500°C (Carbolite muffle ELF 11/14B) for 4h. After that time, they were placed in the desiccator at room temperature and weighed (*weight 3*). The difference in filter mass before and after drying for DM (72h at 60°C) and after combustion (4h at 500°C) subtracted from DM was calculated to obtain AFDM (**Eq. 3.8.**).

$$\boldsymbol{AFDM\ (g) = weight\ 3\ (g) - weight\ 2(g)} \qquad \boldsymbol{Eq.\ 3.8.}$$

where, weight 2 = weight value after 72h in the oven and weight 3 = weight value after 4h in the muffle.

Results were standardized by the scratched biofilm surface of the cobbles (**Eq. 3.9.**).

$$\boldsymbol{AFDM\ (g/m^2) = \frac{weight\ 3\ (g) - weight\ 2(g)}{scratched\ surface\ (m^2)}} \qquad \boldsymbol{Eq.\ 3.9.}$$

Autotrophic Index calculation. The Autotrophy Index (AI) was also calculated (**Eq. 3.10.**):

$$\boldsymbol{AI = AFDM/Chl - a} \qquad \boldsymbol{Eq.\ 3.10.}$$

where, AFDM = ash free dry mass value (in g/m^2) and Chl-*a* = chlorophyll *a* concentration (in g/m^2).

This index represents the theoretical limit of 200, therefore, values above 200 indicate a predominance of heterotrophs, and lower values of autotrophs (Weber, 1973).

3.3.4. Biofilm community

Biofilm samples for algal taxonomic identification were collected and evaluated under the optical microscope (Nikon Eclipse 600Q). The cobble surface was scrapped in a known volume of water to obtain a biofilm suspension and the area of the scraped cobble was obtained by drawing the surface on aluminum foil and recalculating depending on the weight. An aliquot of 9 mL of this suspension was used to perform the algal taxonomic identification.

Previous preparation of the material

Preparation of the samples. Samples were always taken in triplicate and fixed with 4% formaldehyde, adding a volume corresponding to 10% of the sample volume (9 mL of sample + 1 mL formaldehyde). Before the analyses, the sample was homogenized and diluted as needed. Then, 1 mL of sample was removed from the glass vial and placed in a falcon tube. Being samples with formalin, its manipulation was always carried out under hood. Using a Pasteur pipette, a drop (20 µL) of the sample was placed on a slide holder, which was covered with a coverslip to squash and press the sample, preventing cells from remaining in different planes, which would make the microscope count difficult.

General procedure for algal taxonomic identification

An identification was made using phase-contrast and Nomarski differential interference contrast optics at a magnification of 400 increments (**Figure 3.12.**). A minimum of 400 cells were counted and at least 6 vision fields were measured per sample. Algal identification was done following Krammer and Lange-Bertalot (1991 – 1997) and Large Bertalot (2001). At least ten randomly selected individuals of each taxon were measured and their biovolume was calculated following the procedure described in Hillebrand et al. (1999). Values were transformed as described in Ricart et al. (2009) using the surface area of the sample, the dilutions needed and the number of cells counted, and were expressed as µm^3/cm^2. The equation bellow (**Eq. 3.11.**) shows the conversion factors used to do the calculation:

$$\frac{TB}{nº\ Vf} \cdot \frac{1\ Vf \cdot 400}{0.002\ cm^2} \cdot \frac{4.84\ cm^2\ coverslip}{20\ \mu L\ S} \cdot \frac{10\ ml\ TS}{\pi \cdot 1^2\ cm^2} \cdot \frac{1000\ \mu L}{1\ mL} \qquad Eq.\ 3.11.$$

where, TB = total biovolume (in µm^3), Vf = vision field, S = sample and TS = total sample.

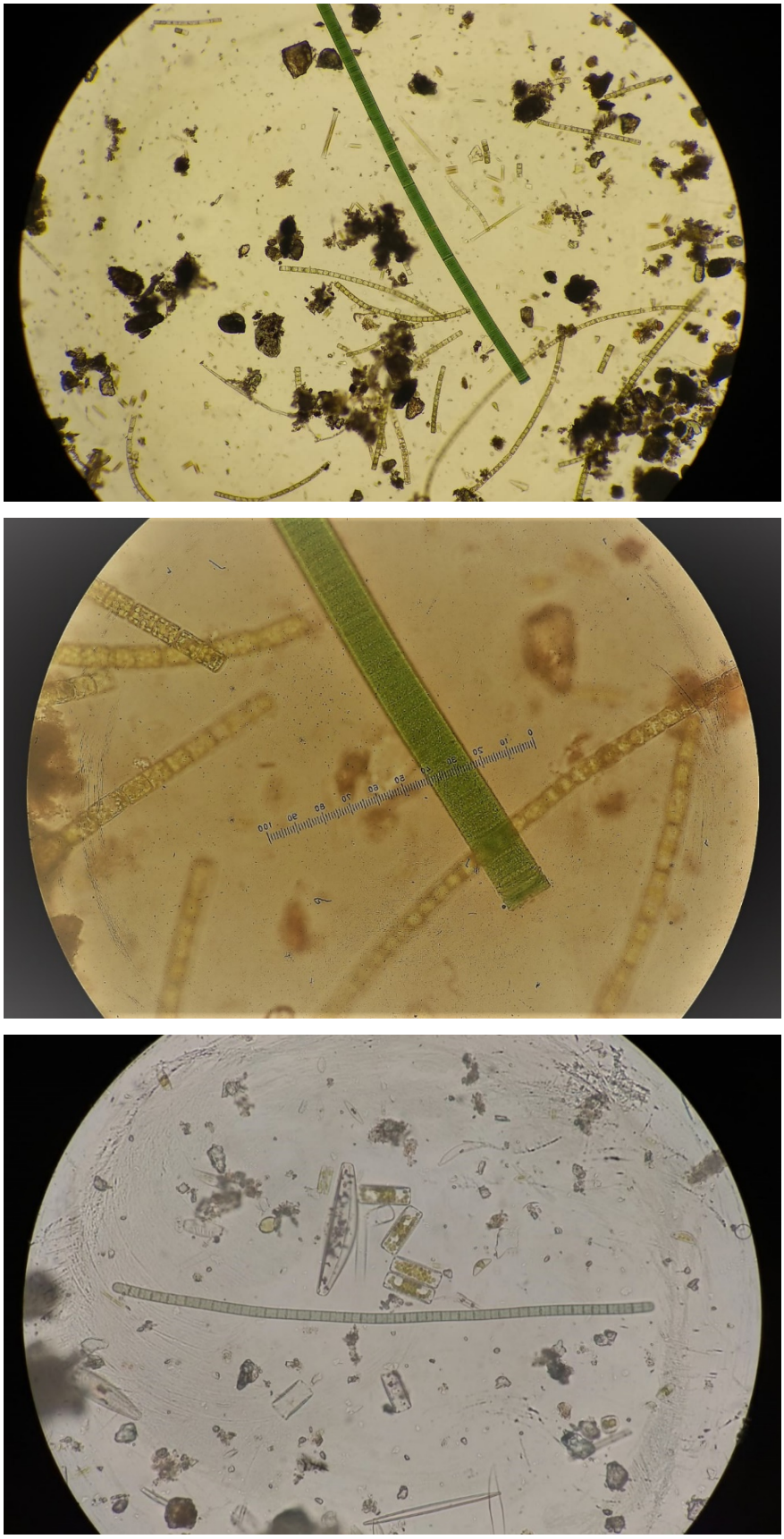

Figure 3.12. Some examples of the biofilm community observed in the samples evaluated using the optical microscope (Nikon Eclipse 600Q).

3.3.5. Biofilm yield

In situ, in vivo florescence analysis was performed using a portable pulse amplitude modulated (PAM) fluorometer (Mini-PAM, HeinzWalz, Effeltrich, Germany) (**Figure 3.13.**) from a constant distance between the light-emitting diode and the samples (1mm). The Mini-PAM could give information about the minimum fluorescence yield (F_0), that can be used as an estimation of algal biomass, and the yield (Y), which can be measured in the dark, obtaining the maximum PSII quantum yield (*Ymax*), or in the natural light, obtaining the effective PSII quantum yield (*Yeff*). The *Ymax* is defined as a measurement of the photosynthetic capacity of the community, whereas the *Yeff* is a measurement of the community photosynthetic efficiency (Barral-Fraga et al., 2018).

Briefly, we verified that the Mini-PAM settings set were correct and we maintained them during all the samplings. The settings established were: Damp = 3, Gain = 7 and Meas-int = 8. Then, a zero to calibrate the Mini-PAM was performed using a clean surface.

A cobble from the water system evaluated was taken and before the biofilm dried, three readings were made with the Mini-PAM of the surface of the cobble. To ensure the reliability of the Mini-PAM reading, the value of F must be greater than 130. If not, we would be in a situation where there is not enough biomass to perform a correct yield reading.

If the work was done in natural light conditions, the value of Y provided by the Mini-PAM was the *Yeff*. To obtain the value of *Ymax*, the sample was acclimatized to lack of light conditions. To do this, the cobble was covered for 10-15 minutes and thus the reading performed, always preventing light reaching the cobble.

Figure 3.13. Mini-PAM (HeinzWalz, Effeltrich, Germany) used in the different experiments performed in this Thesis.

3.3.6. Phototrophic community composition

The BenthoTorch portable fluorimeter probe (bbe Moldaenke, Schwentinenta, DK) (**Figure 3.14.**), gives information about the phototrophic community composition. The fluorescence excitation is undertaken by seven diodes (LEDs) that emitted light at three wavelengths (470, 525 and 610nm). An additional LED of 700nm is used to compensate the effects of background reflection. The BenthoTorch measures the resulting fluorescence of Chlorophyll *a* emitted at 680nm. The calculation of the respective biomass of the photosynthetic groups is via algorithm based on the fluorescence response to all different excitation wavelengths. The calculation algorithms are based on characteristic spectral fingerprints (fluorescence spectral signature) for each photosynthetic group (Echenique-Subiabre et al., 2016).

Briefly, a cobble from the water system evaluated was taken. The BenthoTorch was applied directly to the surface of biofilms, ensuring that the foam pad around the diodes shadowed the biofilms from extern light.

Results of the measurements were displayed in a lateral screen after 10s and the data produced were given for three photosynthetic groups: cyanobacteria, diatoms and green algae. Biomasses of each group were expressed as a Chlorophyll *a* equivalent per unit of surface, in µg chl*a*/cm^2 and the pre-programmed factor settings of the BenthoTorch were used for all measurements.

Figure 3.14. BenthoTorch (bbe Moldaenke, Schwentinenta, DK) using in the *in situ* biofilm community measurements performed in the different experiments done in this Thesis.

3.3.7. Extracellular Enzymatic Activities

The extracellular enzyme activities of leucine-aminopeptidase and phosphatase were measured by using fluorescent-linked substrates (L-leucine-7-amino-4-methylcoumarin hydrochloride [AMC] used for peptidase and 4-methylumbellyferyl-phosphate [MUF] for phosphatase) following the protocol described in Romaní and Marxsen (2002). The leucine-aminopeptidase is related with the peptides decomposition and the phosphatase is related with the decomposition of phosphate esters.

Previous preparation of the material

Preparation of artificial fluorescent substrates. The artificial fluorescent substrates (100 mg) were diluted with the necessary volume of distilled and autoclaved water and in amber vials (or protected from light) to obtain a concentration of 10 mM (S1). This solution (20 - 40 mL depending on the molecular weight of each substrate) was stored in the freezer (-20°C) and defrosted and refrozen immediately every time it was used.

Preparation of MUF and AMC stock solutions. MUF (ref. M1381, Sigma) and AMC solutions (ref. A9891, Sigma) were dissolved in distilled and autoclaved water at a 10.000 µM concentration and were stored in the freezer. They were thawed each time the standard dilutions were prepared.

Preparation of the glycine buffer solution 0.05M, pH 10.4. For 1000 mL:

- 196.5 mL glycine (G7126, Sigma) 0.2M (18.765g in 250 mL miliQ water).
- 803.5 mL NaOH 0.2M (8g in 1000 mL)

Preparation of the calibration curve. From the 10 mM intermediate dilution, a 100 µM intermediate dilution (S2) was prepared in 10 mL.

Whit these intermediate dilutions the following set of concentrations was prepared in a final volume of 5mL (**Table 3.6.**):

Table 3.6. Required volumes of the intermediate dilutions (in µL) and miliQ water (in mL) to obtain the different extracellular enzymatic activities concentrations needed to have a calibration curve.

Standard (µM)	**0**	**0.2**	**0.4**	**0.6**	**0.8**	**1**	**3**	**5**	**7**	**10**	**50**	**100**
V. S1 (µL)											25	100
V. S2 (µL)	0	10	20	30	40	50	150	250	350	500		
V. mQ Water (mL)	0	4.99	4.98	4.97	4.96	4.95	4.85	4.75	4.65	4.50	4.975	9.90

General incubation procedure for the measurement of enzymatic activities

Start of incubation. A volume (µL) of the artificial substrate (MUF-P, AMC-Leu) was added to each sample to have the final saturation concentration obtained with the previous saturation curves. Together with the samples, a blank was added for each activity in which the artificial substrate was added as well as the samples to take into account the possible fluorescence of the substrate we add (abiotic degradation of the artificial substrate). In the control and/or water samples it was not necessary to add artificial substrate for the activity since it helped us to determine the natural fluorescence of the sample and of the water. Together with the samples, blanks and substrate control we added the MUF and AMC standards (**Figure 3.15.**).

Incubation. 1h incubation in the dark and with stirring at room temperature (20°C). The incubation time was about 1 hour. The linearity of the enzymatic activity is maintained during the first 90 minutes; therefore, it is not appropriate to carry out longer incubations of this time. It is important to calculate the incubation time accurately to have a good measure of the activity and it is appropriate to use always the same incubation time for samples from the same system.

Incubation ends. To stop the incubation, a glycine buffer 0.05M, 10.4 pH, was added to denature the proteins. At the same time this buffer converted MUF and AMC into its most fluorescent anionic forms (Chróst and Krambeck, 1986). The buffer was added to all samples, controls, targets and standards with a ratio of 1/2 v/v buffer/sample.

Fluorescence measure. The fluorescence was measured at 380/460 nm excitation/emission for MUF and at 380/460 nm excitation/ emission for AMC using the Spark® multimode microplate reader (TECAN). The quantification of the fluorescence was performed with the standard solutions of MUF and AMC and calculating the calibration line. The fluorescence intensity of the substrate and water blank were subtracted from all samples to correct the possible non-enzymatic hydrolysis of the substrate and the presence of fluorescent compounds in the water.

Values were expressed as µmol MUF·$cm^{-2}h^{-1}$ and µmol AMC·$cm^{-2}h^{-1}$.

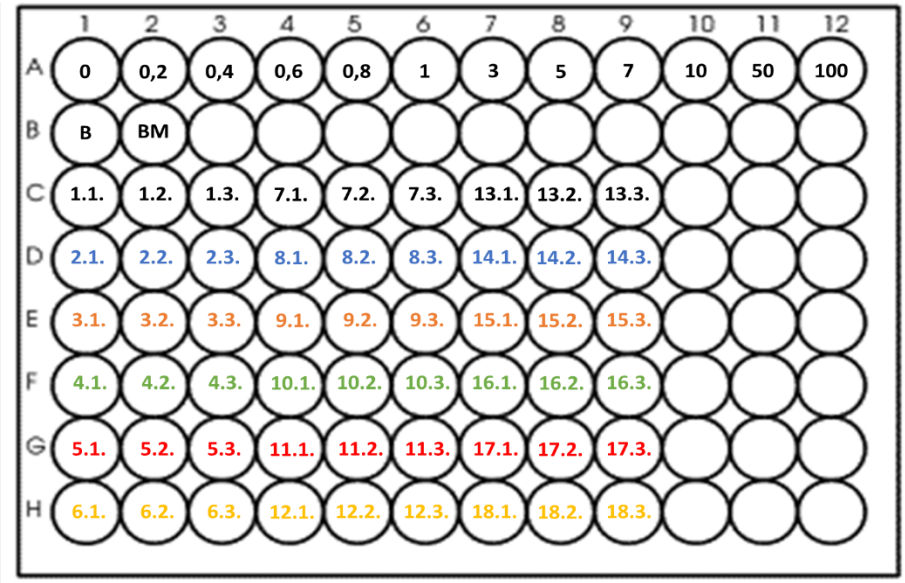

Figure 3.15. Schematic representation of the black 98-well plate used to read extracellular enzymatic activities. The first row corresponds to the calibration curve, the second with the blank (B) and the blank of the sample (BM), and from row C to H, are the wells where the microcosms biofilm samples were evaluated, each row being a different treatment (for three aquariums, for three replicas per aquarium).

3.3.8. Nutrients Uptake

The determination of the nutrient uptake/release capacity by the biofilm was different depending on the experiment performed. In the experiment with mesocosms (experimental flumes) it was calculated as a mass balance, without addition of nutrients, while in the experiment with microcosm (aquariums) an addition of nutrients was made and the results were normalized by the nutrients basal concentration of each treatment .

Briefly, the nutrients uptake capacity of biofilms in the experimental flumes experiment was estimated considering the difference in nutrients concentrations between the input and the outflow of each flume taking into account the area colonized by biofilms (Proia et al., 2017). The uptake capacity (U, mg m^{-2}) (**Eq. 3.12.**) was calculated as:

$$\boldsymbol{U = \frac{(C_i \cdot V_i) - (C_f \cdot V_f)}{A}} \qquad \boldsymbol{Eq.\,3.12.}$$

where C_i = the initial nutrient concentration; V_i = the initial volume; C_f = the final nutrient concentration; V_f = the final volume and A = the area colonized by the biofilm.

The uptake capacity of biofilms in the microcosms experiment was calculated by measuring nutrient temporal decay after a controlled spike in the aquariums. The basal nutrients concentration was previously determined, and each microcosm was later spiked with appropriate volume of phosphate (KH_2PO_4, PanReac-AppliChem) and ammonium (1 g/L

standard solution, PanReac-AppliChem) stock solution in order to quadruple the background concentration of nutrients (Merbt et al., 2017). The biofilms were incubated for 240 minutes under controlled temperature and light conditions. Aliquots of water were taken in triplicate at 1, 5, 30, 60, 120, 180 and 240 minutes after spiking, immediately filtered through 0.2 µm nylon membrane filters (Merk Millipore) and stored at -20°C until analyses. The uptake rate (U, mg/m^2·min) was calculated as (**Eq. 3.13.**).

$$\boldsymbol{U = \frac{\frac{[(C_i \cdot V_i) - (C_f \cdot V_f)]}{C_i \cdot V_i}}{A \cdot T_f}} \qquad \boldsymbol{Eq.\,3.13.}$$

where C_i = the initial nutrient concentration; V_i = the initial volume; C_f = the final nutrient concentration; V_f = the final volume; A = the area colonized by the biofilm and T_f = the residence time.

CHAPTER 4. Effects of the interaction between nutrient concentration and N:P ratio on geosmin production by freshwater biofilms

These results have been submitted to Science of the Total Environment: ***Espinosa, C****., Abril, M., Ricart, M., Vendrell-Puigmitja, L., Ordeix, M., Llenas, L. & Proia, L. (2020). Effects of the interaction between nutrient concentration and N:P ratio on geosmin production by freshwater biofilms.*

4. Effects of the interaction between nutrient concentration and N:P ratio on geosmin production by freshwater biofilms

4.1. Introduction

In recent decades, anthropogenic activities have severely degraded streams and rivers worldwide. Excessive nutrient loading is one of the major threats to these ecosystems (Dodds and Smith, 2016), causing eutrophication and leading to substantial alterations in the overall ecosystem functioning and structure. These effects are of greater importance in rivers affected by situations of water scarcity (i.e. Mediterranean streams), where water flow can be extremely reduced, thus generating a greater increase in nutrient concentration (Karaouzas et al., 2018). The effects of nutrient concentration on the biofilm community of running waters have been widely documented, describing that depending on the nutrient concentrations present in water the benthic nutrient stoichiometry can differ, together with the nutrient uptake rates (due to changes in nutrient demand) modifying the microbial interactions between the autotrophic and heterotrophic biofilm compartments (Price and Carrick, 2016; Bechtold et al., 2012). In fact, in a study analyzing data from 620 stations of the United States National Stream Water-Quality Monitoring Networks, the 40% of algal biomass variance in biofilms was explained by differences in the total N and P concentration (Doods et al., 2002).

The variations in nutrient export due to anthropogenic activities can also modify ratios between dissolved inorganic nitrogen (DIN) and soluble reactive phosphorus (SRP), ranging from 6:1 to 171:1 in perennial Mediterranean streams (von Schiller et al., 2008). Thus, microbial communities in Mediterranean freshwaters, have to face variations in both water nutrient concentration and N:P supply (Artigas et al., 2015). Deviation from Redfield ratio (C106:N16:P1) has been used as an indication of which nutrient is limiting for algal growth (Redfield et al., 1963). Specifically, the N:P ratio of 16:1 is used as a reference to differentiate P-limitation (N:P>16) from N-limitation (N:P<16) although this value may differ between algal and cyanobacterial groups (Geider and La Roche, 2002; Sabater et al., 2016). Therefore, water N:P ratios may control population dynamics and species coexistence in river biofilms.

When an imbalance in the N:P ratios is generated, important physiological changes may occur. When there is a lower phosphorus concentration in relation to N supply (high N:P ratio), there is a decrease in algal growth as a consequence of a reduction of RNA molecules and a greater storage of carbohydrates (Cai et al., 2013). Whereas hen the phosphate concentration in water

exceed a characteristic threshold value (low water N:P), phosphorus is stored in the form of polyphosphates granules (Sabater et al., 2016). Fast-growing species (i.e. diatoms) have higher N-requirements per unit of biomass and unit of time than slow-growing taxa (i.e. cyanobacteria). Consequently, fast-growing species are more sensitive to nutrient than slow-growing algae (Sabater et al., 2016).

The main described effect of eutrophication is that often leads to a marked increase of algal communities' growth, including cyanobacterial algal blooms. Abundant growth of cyanobacteria in freshwaters has been correlated with the appearance of secondary metabolites, such as geosmin and 2 – methylisoborneol (MIB) (Espinosa et al., 2020; Lee et al., 2017). These metabolites affect the organoleptic characteristics of water, influencing both odor and taste, which have a negative impact in the perception of the population about the quality of drinking water (Ding et al., 2014). Among the existing T&Os, geosmin has been identified as the main metabolite conferring bad taste and odor to drinking waters (Watson et al., 2016). Despite some heterotrophic bacteria have been identified as potential geosmin producers, cyanobacteria are considered the main producers in freshwater ecosystems (Olsen et al., 2016).

High nutrient concentrations and low nitrogen to phosphorus ratio (TN:TP), have been described as important factors promoting cyanobacteria growth and dominance in freshwater ecosystems (Olsen et al., 2016; Harris et al., 2016). However, under eutrophic conditions where nutrients are not limiting, the TN:TP ratio is not as predictive of the domain of cyanobacteria, thus both the nutrient supply ratios and the absolute nutrient concentrations are determining factors in the structure of the community (Harris et al., 2016). Most of these studies have focused on phytoplanktonic organisms, whereas very few investigate on benthic producers. A study performed in the Llobregat river (Spain) pointed out that unbalanced proportion between nitrogen and phosphorus (TN:TP = 10) could have favored geosmin production by biofilms (Vilalta et al., 2003), but there is still a lack of information about the effects induced by high nutrient concentrations and its joint effect with N:P ratio on triggering geosmin production by benthic cyanobacteria.

Previous studies indicated that environmental factors such as temperature, light and nutrient availability influence geosmin production (Alghanmi et al., 2018; Lee et al., 2017). However, most of these were carried out on cultures of a single species under controlled laboratory conditions (Parinet et al., 2010; Li et al., 2012; Suurnäkki et al., 2015), and very few studies have deal with the identification of geosmin production drivers of natural benthic communities. Fluvial biofilms are complex microbial communities formed by different groups of organisms,

that together with extracellular enzymes and detritus are enclosed within a polymeric matrix. One of the organisms that conform the biofilm are the cyanobacteria, the main responsible for geosmin episodes in river systems. Therefore, the drivers behind cyanobacteria growth, which are able to produce geosmin in freshwater ecosystems have to be evaluated in order of generate useful information to understand and predict the occurrence of geosmin episodes in rivers.

4.2. Objective

This study was designed to explore the effect of N:P ratio (as DIN:SRP ratio) under low and high nutrient concentration on biofilm structure and functioning, and its relationship with the geosmin concentration in biofilm and water. To test this, an experiment was carried out in controlled laboratory microcosms exposing natural biofilm communities to three different N:P ratios; low (4:1), optimal (Redfield, 16:1) and high ratio (64:1) under two nutrient concentration levels (low and high) in water. To the best of our knowledge, this is the first study evaluating the joint effect of N:P ratio and nutrient concentration on geosmin production by a complex microbial community. The main outcomes of this study could be very useful for catchment managers and water utilities, helping them to predict under which nutrient conditions they have to expect geosmin in water used for drinking purposes, improving their response time in geosmin treatment and reducing consumer discomfort and complaints.

4.3. Material and Methods

4.3.1. Experimental design and sampling procedure

Eighteen microcosms consisting of 6L glass aquariums (length x width x height 26 x 15 x 17 cm) were used to evaluate the biofilm functional and structural response under different nutrient concentration and N:P ratio in water. Each microcosm, containing 16 scraped and autoclaved stream cobbles, was filled with 3L of artificial water. Artificial water was prepared to simulate a pristine stream as described in Ylla et al. (2009) and was obtained by dissolving pure salts in distilled water creating a chemical composition of 14.96 mg/L Na^{+}, 10.81 mg/L Ca^{2+}, 0.52 mg/L K^{+}, 0.40 mg/L Mg^{2+}, 9.71 mg/L SO_4^{2-}, 12.45 mg/L SiO_3^{2-}, 19.67 mg/L Cl^{2-} and 14.52 mg/L HCO_3^{-}. To maintain these conditions, microcosms water renewal was done every 2 – 3 days. Each aquarium had a submersible pump (EDEN 105, Eden Water Paradise, Italy) to promote oxygenation and water circulation. The photoperiod was set at 12h light: 12h dark using LEDs (LENB 135-lm, LENB/14.97/11.98) and the room temperature was fixed at 16°C.

Figure 4.1. Microcosms (aquariums) used in this experiment to evaluate the effect of N:P ratio and nutrient concentration on biofilm community development and geosmin production and release. Laboratory of BETA Technological Center, Vic (Spain).

The experiment was carried out during a geosmin episode occurred in May 2019 in the Ter river (NE Spain), coinciding with the presence of benthic *Oscillatoria* mats (authors, personal observation). From this river, a natural biofilm suspension was obtained by scrapping 3 cobbles randomly selected along a 50m river stretch located at the water collection point of the water drinking company Aigües de Vic (2 16 53.2479 E*;* 41 59 16.9003 N), and it was inoculated in each

microcosm to promote biofilm colonization. During the colonization period (three weeks), new inoculum was added after each water renewal to favor biofilm settlement in the microcosms.

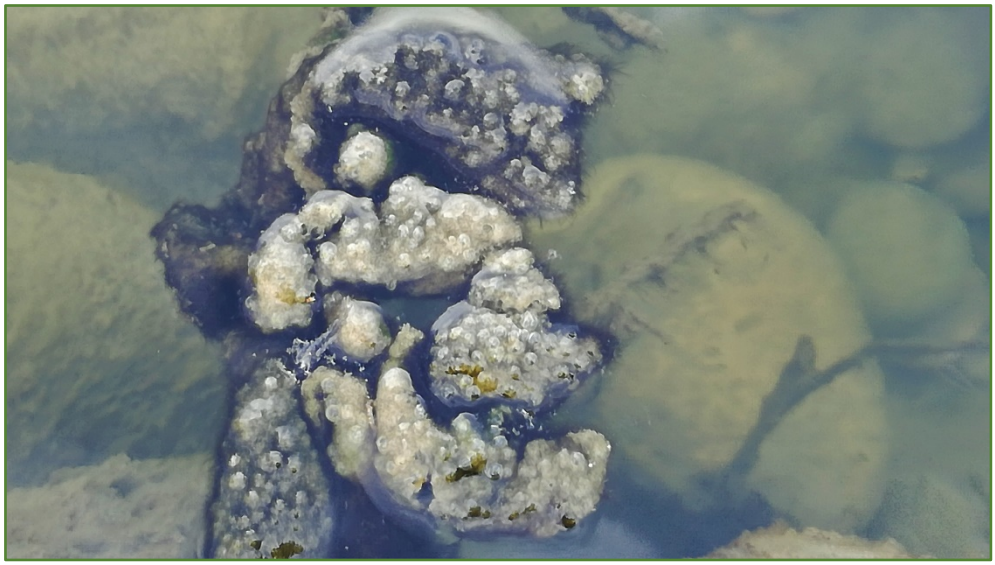

Figure 4.2. *Oscillatoria* sp. floc observed at Ter river in Gurb (Catalonia, Spain) (2 16 53.2479 E; 41 59 16.9003 N) where the biofilm samples that were inoculated in this experiment were taken.

After the colonization period, six treatments were set by crossing three N:P ratios (Low = 4:1 (A), Optimal = 16:1 (B) and High = 64:1 (C)) with two nutrient concentrations (Low and High); each treatment had 3 replicates (**Table 4.1.**). Specifically, these treatments were low nutrient concentration and low N:P ratio (LN-A), low nutrient concentration and optimal N:P ratio (LN-B), low nutrient concentration and high N:P ratio (LN-C), high nutrient concentration and low N:P ratio (HN-A), high nutrient concentration and optimal N:P ratio (HN-B) and high nutrient concentration and high N:P ratio (HN-C). N:P ratios were determined as DIN (Dissolved Inorganic Nitrogen) divided by Soluble Reactive Phosphorus (SRP) in molar quantities. DIN concentration was determined as the sum of ammonium ($N\text{-}NH_4^+$) and nitrate ($N\text{-}NO_3^-$) concentration. Nutrient concentration and N:P ratios were chosen to cover a range representative of Ter river basin variation, whose nutrient concentration ranges between 12 – 300 µg $N\text{-}NH_4^+$/L, 100 – 2000 µg $N\text{-}NO_3^-$/L and 10 – 950 µg $P\text{-}PO_4^{3-}$/L . During the exposure period, which lasted for 21 days, nutrient concentration in each aquarium was maintained at each water renewal, which were done every 2 – 3 days. Nitrogen concentration was adjusted using nitrate and ammonium standard solutions (1 g/L PanReac-AppliChem), and the phosphorus concentration was adjusted

using a concentrated stock solution (10000 µM $P\text{-}PO_4^{3-}$) obtained by dissolving pure salts (KH_2PO_4, PanReac-AppliChem) into deionized water.

Table 4.1. Average and SD values (n=27) for the ammonium ($N\text{-}NH_4^+$ µg/L), nitrates ($N\text{-}NO_3^-$ µg/L), SRP ($P\text{-}PO_4^{3-}$ µg/L), and the DIN:SRP ratio for the different treatments: low nutrient (LN) and high nutrient (HN); low ratio (A = 4:1), optimal ratio (B = 16:1) and high ratio (C = 64:1).

	Treatment					
	LN			**HN**		
	A	**B**	**C**	**A**	**B**	**C**
$N\text{-}NH_4^+$ (µg/L)	12.7 ± 2.7	12.6 ± 0.6	11.7 ± 1.7	110 ± 7	110 ± 6	106 ± 5
$N\text{-}NO_3^-$ (µg/L)	107 ± 15	108 ± 18	112 ± 5	1175 ± 112	1174 ± 90	1142 ± 24
$P\text{-}PO_4^{3-}$ (µg/L)	61.0 ± 4.8	18.2 ± 3.8	4.0 ± 0.6	682 ± 49	164 ± 9	42.0 ± 6.6
DIN:SRP	4.2 ± 0.2	14.9 ± 1.4	69.8 ± 7.2	4.4 ± 0.5	16.5 ± 1.1	64.8 ± 5.2

Before and after each water renewal during both colonization and exposure periods, physic-chemical parameters were measured with portable probes: temperature, dissolved oxygen concentration and saturation (YSI professional plus, YSI Incorporated, USA), pH (XS pH7+ DHS) and conductivity (XS COND 7+). From each microcosm, water samples were taken and filtered through 0.2 µm nylon membrane filters (Merck Millipore) before the analysis of SRP and DIN forms (ammonium and nitrate). All samples were stored at -20°C until analysis.

Biofilms were sampled before the beginning of the nutrients manipulation (t0) and after 2, 7, 16 and 21 days. Three cobbles were randomly sampled from each microcosm at each sampling day. The photosynthetic efficiency and the phototrophic community composition were measured directly with an amplitude modulated fluorimeter (Mini-PAM fluorometer, Walz, Effeltrich, Germany) and a BenthoTorch portable fluorimeter probe (bbe Moldaenke, Schwentinenta, DK) respectively. After that, each cobble was scrapped in 45 mL of water from the same microcosm to obtain a biofilm suspension. Aliquots of this suspension were used to analyze geosmin concentration in biofilm, Chlorophyll *a* (Chl *a*), ash free dry mass (AFDM), algal taxonomic composition and extracellular enzymatic activities (AEE). AEE samples were analyzed the same day and the rest were stored frozen (-20°C) until analyses, except aliquots for geosmin concentration that were stored at -80°C and aliquots for algal taxonomic identification, which were fixed with formalin (2%) and stored at 4°C. The area of the scraped cobbles was obtained by drawing the surface on aluminum foil and recalculating depending on the weight (Graham et al., 1988).

Additionally, water samples were also taken to analyze nutrients and geosmin concentrations in water. Samples for geosmin quantification in water were stored at 4°C in dark conditions until

the analysis, that was performed within the 48 hours after collection to avoid degradation. Water samples for nutrient analyses were filtered through 0.2 µm nylon membrane filters (Merck Millipore) and frozen at -20°C until analyses. All the protocols used are described in the **Chapter 3** of this Thesis.

4.3.2. Data treatment

Before statistical analysis, the Kolmogorov – Smirnov test was performed to verify that the variables fulfilled the conditions of normal distribution. Physicochemical and biological data were evaluated using the two-way repeated measures analysis of variance (ANOVA) in SPSS Statistics version 21, with nutrient concentration and N:P ratio as factors and sampling date (time) as repeated measure. This program was also used for the two-way ANOVA analysis, being the N:P ratio, nutrient concentration and its interaction the factors evaluated in each sampling day. The Post-hoc test performed was Bonferroni test. Pearson correlation coefficient tests were performed to explore the relationship between the variables. Statistical significance was set at $p < 0.05$ for all tests performed. The distribution of the variables according to the treatments was evaluated using a principal component analysis (PCA) performed with RStudio software (version 3.6.0).

4.4. Results

4.4.1. Physicochemical parameters

The physicochemical conditions in the microcosms remained stable throughout the experiment, with water temperature varying insignificantly around 16°C, slight alkaline pH and low conductivity (**Table 4.2.**), and without significant differences among them despite the treatments (repeated measures ANOVA).

Table 4.2. Mean value and standard deviation of the physicochemical variables evaluated in the microcosms throughout the experiment (n = 30): pH, water temperature (ºC), electrical conductivity (EC) (µS/cm), dissolved oxygen (DO) (mg/L), and oxygen saturation (%) for the different treatments: low nutrient (LN) and high nutrient (HN); low ratio (A = 4:1), normal ratio (B = 16:1) and high ratio (C = 64:1).

	Treatment					
	LN			**HN**		
	A	**B**	**C**	**A**	**B**	**C**
pH	8.1 ± 0.2	8.1 ± 0.2	8.1 ± 0.2	8.0 ± 0.3	8.0 ± 0.2	8.1 ± 0.2
Temperature (ºC)	16.8 ± 0.4	16.9 ± 0.3	16.8 ± 0.3	16.7 ± 0.3	16.8 ± 0.3	16.9 ± 0.3
EC (µS/cm)	164 ± 17	163 ± 14	158 ± 33	166 ± 13	164 ± 14	170 ± 12
DO (mg/L)	8.3 ± 0.5	8.0 ± 0.6	8.2 ± 0.5	8.2 ± 0.5	8.4 ± 0.5	8.0 ± 0.4
Saturation (%)	85 ± 5	84 ± 7	85 ± 5	84 ± 5	86 ± 5	83 ± 4

4.4.2. Geosmin concentration

4.4.2.1. Geosmin in biofilm

Geosmin concentration in biofilm (**Figure 4.3. A., Table 4.3.**) varied significantly over time among microcosms depending on the N:P ratio, nutrient concentration and its interaction (**Table 4.4.**).

From day 7 to the end of the experiment, geosmin concentration in biofilm was significantly the highest in the HN-A treatment (**Table 4.3.**). Under these conditions, geosmin concentration increased gradually reaching its maximum (3.8 ± 0.9 ng/mg) at t=16d and decreasing thereafter to 2.0 ± 0.7 ng/mg (t=21d, **Figure 4.3.A.**). Under HN-B conditions, the biofilm did not produce geosmin during the whole experiment.

4.4.2.2. Geosmin in water

The concentration of geosmin in water (**Table 4.3.**) varied significantly over time among microcosms depending on the N:P ratio, nutrient concentration and its interaction (**Figure 4.3.B., Table 4.4.**).

At the beginning of the experiment (t=0d), geosmin was detected in all treatments at low concentrations (27.4 ± 6.7 ng/L), without any significant difference among microcosms (**Table 4.3.**). After 7 days of treatment, geosmin concentration in water was significantly higher at lower N:P ratio (Bonferroni test: $p < 0.005$) independently from nutrient concentration. However, from then on, the interaction between the two factors had a significant effect on geosmin concentration. At the end of the experiment (day 21), both nutrient concentration, N:P ratio and its interaction showed a significant effect on geosmin concentration in water. Particularly, the microcosms developed under the lowest N:P conditions showed higher geosmin concentration compared to the other ratios (Bonferroni test: $p < 0.001$) and the highest concentration (136 ± 6 ng/L) was found under HN conditions (**Figure 4.3.B.**). The only treatment where geosmin was not detected at the end of the experiment was HN-B.

Table 4.3. Mean value and standard deviation for geosmin in water (ng/L), geosmin in biofilm (ng/mg), cyanobacteria and diatoms biomass (µg chl*a*/cm^2), Chlorophyll a (µg/cm^2), photosynthetic efficiency (Yeff) and PHO (µmol MUF/cm^2·h) at the beginning of the experiment (not significant differences between treatments), and for the treatments: low nutrient (LN) and high nutrient (HN); low ratio (A = 4:1), optimal ratio (B = 16:1) and high ratio (C = 64:1), at times 7, 16 and 21 days.

	Treatment																		
		LN									**HN**								
		A			**B**			**C**			**A**			**B**			**C**		
	0d	**7d**	**16d**	**21d**	**7d**	**16d**	**21d**	**7d**	**16d**	**21d**	**7d**	**16d**	**21d**	**7d**	**16d**	**21d**	**7d**	**16d**	**21d**
Geosmin in water (ng/L)	27.4 ± 6.7	21.2 ± 2.9	18.7 ± 2.8	20.9 ± 13.6	12.8 ± 3.4	7.0 ± 2.8	23.3 ± 5.4	14.8 ± 2.9	7.2 ± 2.1	18.4 ± 8.7	26.6 ± 2.2	32.0 ± 3.9	135.8 ± 6.1	7.5 ± 3.1	4.8 ± 0.0	< 2.5	11.6 ± 1.9	7.5 ± 3.5	21.5 ± 4.2
Geosmin in biofilm (ng/mg)	0.10 ± 0.05	0.03 ± 0.01	0.26 ± 0.19	0.08 ± 0.04	0.16 ± 0.08	0.17 ± 0.07	0.10 ± 0.03	0.13 ± 0.1	0.38 ± 0.12	0.04 ± 0.03	1.39 ± 0.35	3.76 ± 0.96	2.03 ± 0.74	0.08 ± 0.00	0.09 ± 0.00	0.00 ± 0.00	0.04 ± 0.03	0.20 ± 0.07	0.03 ± 0.00
Cyanobacteria (µg chl*a*/cm^2)	0.43 ± 0.06	1.23 ± 0.71	0.61 ± 0.27	0.55 ± 0.06	0.28 ± 0.22	0.38 ± 0.21	0.48 ± 0.20	0.52 ± 0.30	0.52 ± 0.10	0.39 ± 0.20	1.95 ± 0.36	1.63 ± 0.36	0.87 ± 0.38	0.28 ± 0.16	0.57 ± 0.15	0.46 ± 0.05	0.66 ± 0.23	0.34 ± 0.31	0.59 ± 0.14
Diatoms (µg chl*a*/cm^2)	2.10 ± 0.60	2.68 ± 0.42	1.55 ± 0.82	1.61 ± 0.45	2.37 ± 0.99	1.62 ± 0.63	1.63 ± 0.35	3.00 ± 2.31	2.66 ± 1.29	1.61 ± 0.51	3.49 ± 0.40	2.14 ± 1.12	2.33 ± 1.90	1.65 ± 1.02	4.35 ± 1.05	2.99 ± 2.52	2.00 ± 0.51	1.66 ± 1.69	3.38 ± 0.75
Chlorophyll *a* (µg/cm^2)	3.90 ± 0.64	3.50 ± 1.31	3.10 ± 1.89	6.51 ± 0.51	2.63 ± 0.48	3.82 ± 1.19	4.20 ± 0.92	7.87 ± 0.88	4.14 ± 1.38	2.80 ± 0.70	2.87 ± 0.81	3.68 ± 0.32	8.68 ± 1.73	5.12 ± 2.45	7.99 ± 1.32	18.32 ± 0.97	5.10 ± 0.28	11.72 ± 2.31	10.00 ± 3.37
Yeff	0.589 ± 0.029	0.646 ± 0.064	0.581 ± 0.083	0.640 ± 0.053	0.614 ± 0.036	0.635 ± 0.068	0.680 ± 0.040	0.639 ± 0.047	0.555 ± 0.056	0.645 ± 0.033	0.630 ± 0.084	0.545 ± 0.042	0.529 ± 0.046	0.607 ± 0.083	0.657 ± 0.025	0.672 ± 0.031	0.633 ± 0.031	0.615 ± 0.036	0.631 ± 0.068
PHO (MUF/ cm^2·h)	19.7 ± 1.9	16.8 ± 7.7	16.5 ± 9.4	24.2 ± 4.2	13.0 ± 1.6	23.6 ± 12.9	29.3 ± 11.6	33.2 ± 8.5	42.0 ± 20.1	31.6 ± 11.7	17.4 ± 9.6	25.6 ± 9.2	35.9 ± 11.7	24.2 ± 8.3	17.5 ± 7.9	36.1 ± 6.5	26.9 ± 14.2	54.4 ± 28.8	72.0 ± 18.4

Table 4.4. Statistical F value for the repeated measures ANOVA and the Two-Way ANOVA tests. Times t=0d and t=2d have not been included since there were not statistical differences for any of the variables evaluated. The factors evaluated were nutrient concentration (N), nutrient ratio (R) and their interaction (NxR) as independent variables, and geosmin in water (ng/L), geosmin in biofilm (ng/mg), cyanobacteria and diatoms biomass (µg/cm^2), Chlorophyll a (µg/cm^2), photosynthetic efficiency (Yeff) and PHO (µmol MUF/cm^2·h) as dependent variables. Significant results ($p < 0.05$) are marked in bold.

		Repeated	ANOVA		
		Measures ANOVA	**t = 7d**	**t = 16d**	**t = 21d**
Geosmin in Water (ng/L)	**N**	**9.218**	0.339	4.217	**21.647**
	R	**37.028**	**22.538**	**50.416**	**126.284**
	NxR	**15.300**	3.438	**7.466**	**50.045**
Geosmin in Biofilm (ng/mg)	**N**	**26.344**	**22.400**	**30.634**	**6.903**
	R	**21.997**	**25.138**	**39.069**	**9.642**
	NxR	**24.887**	**35.325**	**39.945**	**9.666**
Cyanobacteria (µg chl*a*/cm^2)	**N**	**2.797**	0.813	**5.082**	0.118
	R	**6.445**	**5.275**	**33.674**	3.436
	NxR	1.534	0.090	**7.754**	0.551
Diatoms (µg chl*a*/cm^2)	**N**	0.976	0.927	1.748	0.731
	R	**3.156**	**4.392**	**28.453**	3.441
	NxR	1.759	0.129	**12.003**	1.175
Chlorophyll *a* (µg/cm^2)	**N**	**41.036**	0.280	**14.819**	**110.164**
	R	**13.744**	**12.083**	**6.335**	**14.530**
	NxR	**13.737**	**6.565**	3.737	**22.191**
Yeff	**N**	**3.722**	0.778	4.591	2.058
	R	**4.860**	0.298	**6.004**	**5.239**
	NxR	**2.229**	0.018	0.989	3.156
PHO (µmol MUF/ cm^2·h)	**N**	1.821	0.171	0.380	**11.171**
	R	0.734	3.476	**4.956**	**5.769**
	NxR	1.138	1.224	0.430	3.290
PEP (µmol AMC/ cm^2·h)	**N**	2.125	**8.495**	0.002	3.371
	R	0.944	**13.478**	3.270	0.503
	NxR	0.882	3.925	0.402	0.513

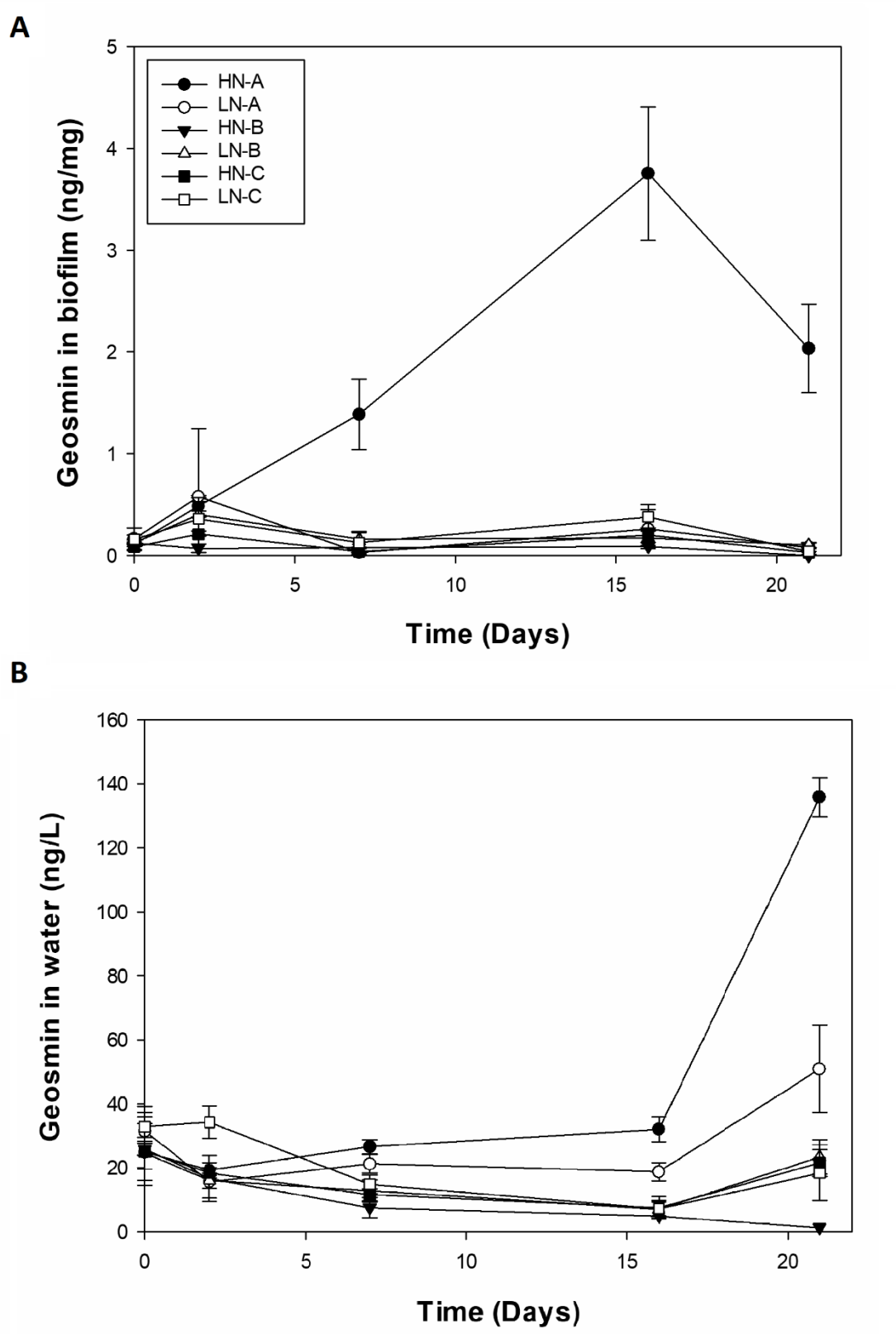

Figure 4.3. Mean values and standard deviation on sampling days for the different treatments: HN-A, LN-A, HN-B, LN-B, HN-C, LN-C, being HN = High nutrient, LN = low nutrient and A = 4:1, B = 16:1 and C = 64:1 DIN:SRP ratio, for the **(A)** geosmin concentration in biofilm (ng/mg) and **(B)** geosmin concentration in water (ng/L).

4.4.3. Biofilm attributes

4.4.3.1. Structural parameters

- Community composition

During the experiment, the phototrophic community composition of the biofilm (cyanobacteria, green algae and diatoms) varied over time (**Table 4.3.**). Specifically, the N:P ratio influenced significantly the cyanobacteria biomass and the relative diatoms and cyanobacteria abundances over time (**Table 4.4.**) The diatoms biomass was affected by the nutrient concentration and its interaction with the N:P ratio (**Table 4.4.**).

One week after the beginning of nutrients manipulation (t=7d), the cyanobacteria biomass was statistically different depending on the N:P ratio, being significantly higher under low N:P treatments (Bonferroni test: $p < 0.01$). At day 16, nutrient concentration and its interaction with N:P ratio had also a significant effect on cyanobacteria biomass, being significantly higher under low N:P treatments (Bonferroni test: $p < 0.01$) and resulting the highest in HN-A treatment (1.63 ± 0.36 µg chl*a*/cm^2). A similar trend was observed for the cyanobacteria relative abundance. The highest value of abundance was found in the HN-A treatment at t=16d (48 ± 2%), nevertheless, at the end of the experiment, this value decreased to 31 ± 7% (**Figure 4.4.**). The opposite pattern was observed for the diatoms relative abundance.

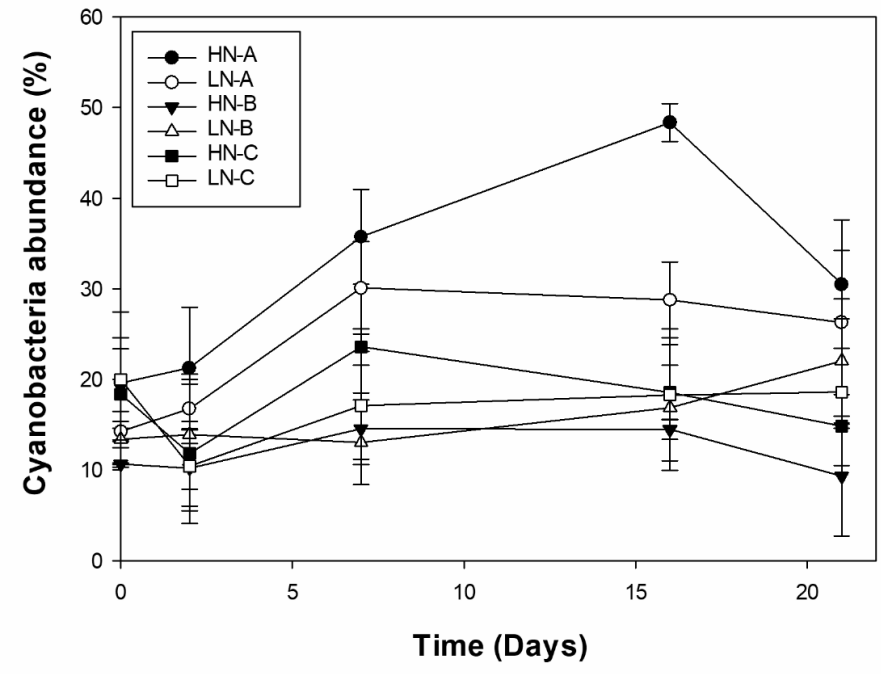

Figure 4.4. Mean values and standard deviation of the cyanobacteria biovolume (in %) for the different sampling days and for the different treatments: HN-A, LN-A, HN-B, LN-B, HN-C, LN-C, being HN = High nutrient, LN = low nutrient and A = 4:1, B = 16:1 and C = 64:1 DIN:SRP ratio.

At the end of the experiment (t=21d) the algal taxonomic community was evaluated (**Figure 4.5.**). The relative abundance of *Oscillatoria* sp. was higher under low N:P ratio conditions compared with the other ratios (Bonferroni test: p =0.001), reaching the highest value (45 ± 10%) under the HN-A treatment. The cyanobacterium *Oscillatoria* sp. and the diatom *Melosira* sp. biovolume varied among microcosms depending on the N:P ratio ($F = 18.9$; $p < 0.001$ for *Oscillatoria* sp., $F = 17.5$; $p < 0.001$ for *Melosira* sp.) and its interaction with nutrient concentration ($F = 5.0$; $p < 0.05$ for *Oscillatoria* sp., $F = 5.0$; $p < 0.05$ for *Melosira* sp.). In addition, a strong negative correlation was found between *Oscillatoria* sp. and *Melosira* sp. biovolume (Pearson's correlation: $r = -0.914$; $p < 0.001$). The *Oscillatoria* sp. biovolume was also positively correlated with geosmin concentration in water and biofilm (Pearson's correlation: $r = 0.886$; $p < 0.001$ and $r = 0.888$; $p < 0.001$, respectively).

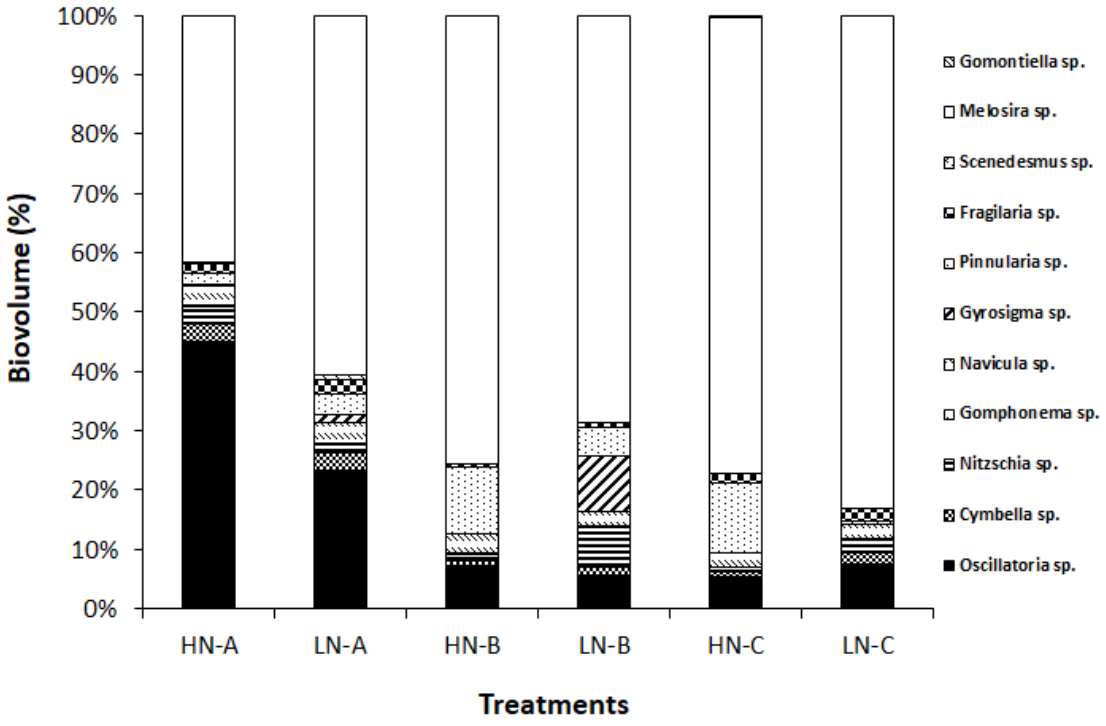

Figure 4.5. Relative taxa expressed as biovolume (in %) present in the biofilm of each treatment: HN-A, LN-A, HN-B, LN-B, HN-C, LN-C, being HN = High nutrient, LN = low nutrient and A = 4:1, B = 16:1 and C = 64:1 DIN:SRP ratio.

- Chlorophyll *a*

Chlorophyll *a* varied significantly throughout the experiment depending on the nutrient concentration, N:P ratio and its interaction (**Table 4.3.** and **4.4.**).

At the end of the experiment (t=21d) both factors and its interaction showed a significant effect on the biofilm Chlorophyll *a* content (**Figure 4.6.**), with higher concentration under the optimal N:P ratio conditions compared with high N:P ratio treatment (Bonferroni test: $p < 0.005$). It was

also observed that under HN conditions the biofilm had a higher production of Chlorophyll *a*, being the HN-B treatment the one showing the highest concentration (18.3 ± 0.9 µg/cm^2) (**Table 4.4.**).

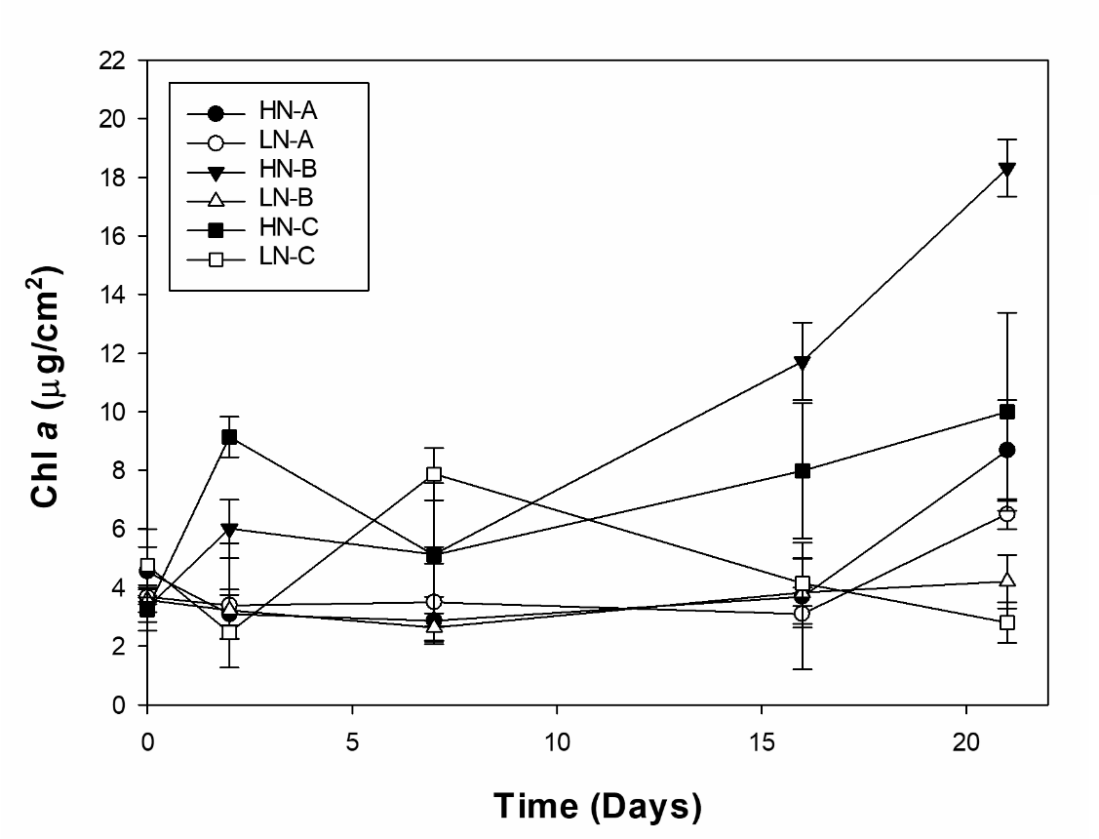

Figure 4.6. Results obtained in the different treatments (HN-A, LN-A, HN-B, LN-B, HN-C and LN-C, being HN = High nutrient, LN = low nutrient and A = 4:1, B = 16:1 and C = 64: 1 DIN:SRP ratio) for the different sampling days for the Chlorophyll a µg/cm^2.

4.4.3.2. Functional parameters

- Photosynthetic capacity

The photosynthetic capacity of the biofilm (expressed as Yeff) (**Table 4.3.**) differed over time among microcosms depending on the N:P ratio, nutrient concentration and its interaction (**Table 4.4.**). At t=16d, the N:P ratio had a significant effect on the Yeff, being the low N:P treatment (0.563 ± 0.025) significantly lower than the optimal N:P ratio (0.646 ± 0.016) (Bonferroni test: $p < 0.05$). At the end of the experiment (t=21d) this pattern become more obvious reaching the lowest value of Yeff in the HN-A treatment (0.529 ± 0.046).

- Nutrient uptake capacity

Phosphate uptake (or release) capacity was significantly affected by nutrient concentration ($F = 5.4$, $p < 0.05$) and its interaction with N:P ratio ($F = 25.4$, $p < 0.001$). In general, the uptake rate

was higher in LN conditions (0.20 ± 0.06 mg/m^2·min) than under HN conditions (0.09 ± 0.04 mg/m^2·min), except for the high N:P ratio that showed the opposite trend. The ammonium uptake capacity was significantly affected by nutrient concentration ($F = 25.2$, $p < 0.001$), with higher uptake capacity under LN conditions (0.37 ± 0.07 mg/m^2·min) compared with HN (0.13 ± 0.004 mg/m^2·min). Nitrate uptake capacity did not differ among microcosms.

- Extracellular Enzymatic Activities

The phosphatase activity (PHO) of biofilms varied throughout the experiment (**Table 4.4.**). Specifically, at t=16d, biofilms under the high N:P ratio conditions showed higher PHO that those of the optimal N:P ratio treatment (Bonferroni test: $p < 0.05$) (**Table 4.3.**). At the end of the experiment, the PHO values were different depending on the nutrient concentration and N:P ratio, being the high N:P ratio treatment significantly different from the others (Bonferroni test: $p < 0.05$), and higher under HN conditions (72.0 ± 18.4 µmol MUF/cm^2·h). For the peptidase activity, no significant differences were observed among microcosms over time.

Both nutrients uptake/release capacities and enzymatic activities, showed differences depending on the nutrient concentration under which the biofilm community developed, not relating these variables with the production and release of geosmin. These results can be observed in the **Figure 4.7**. The PCA shows how the parameters evaluated are distributed according to the different treatments. It emphasizes that the X axis (explaining the 49.8% of variance) separates the HN-A treatment from the rest, being the one with the highest concentration of geosmin in water and in biofilm, greater cyanobacteria biomass, and higher presence of *Oscillatoria* sp. The Y axis (17.8% of variance) separates the optimal (B) and high (C) N:P ratio treatments according to the concentration of nutrients (LN or HN), since these conditions affected the enzymatic activities and the nutrients uptake/release capacities of the biofilms.

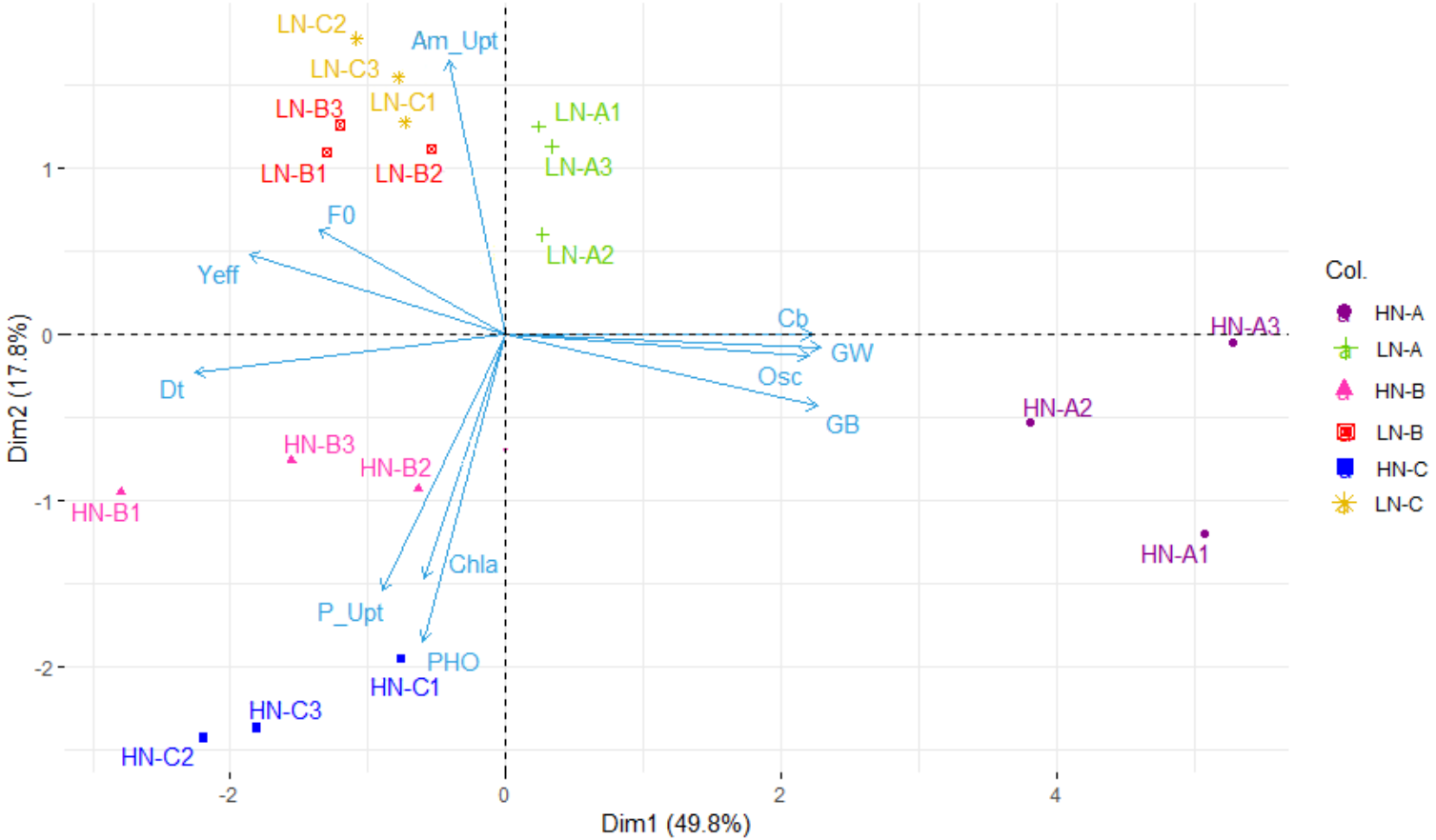

Figure 4.7. Principal Component Analysis showing treatments distribution based on the variables evaluated. Axes 1 and 2 combined explain 67.6% of the variance. Treatments: LN-A, LN-B, LN-C, HN-A, HN-B and HN-C, being HN = High nutrient, LN = low nutrient and A = 4:1, B = 16:1 and C = 64: 1 DIN:SRP ratio. Variables: geosmin in biofilm (GB), geosmin in water (GW), cyanobacteria biomass (Cb), diatoms biomass (Dt), Oscillatoria sp. (Osc), photosynthetic efficiency (Yeff), Chlorophyll a (Chla), SRP uptake (P-Upt), ammonium uptake (Am_Upt) and phosphatase activity (PHO).

4.5. Discussion

This study demonstrates that, both nutrient concentration and N:P ratio are important drivers of geosmin occurrence in freshwaters by favoring the growth of geosmin producing organisms in biofilm communities and promoting the intracellular geosmin formation and its subsequent release to the water column.

The biofilm community structure begun to change 7 days after the nutrient manipulation started, mainly because of the different N:P ratios. In particular, cyanobacteria increased its relative abundance becoming predominant in the biofilms exposed to low N:P ratio conditions, specially under high nutrient concentration (HN-A) (**Figure 4.4.**). These results agree with recent studies describing how the phosphorus availability excess may stimulate the magnitude of cyanobacteria blooms (Jankowiak et al., 2019). Moreover, it has been described that cyanobacteria can store essential metabolic nutrients in the cytoplasm, especially under eutrophic conditions (Felisberto et al., 2011). For example, phosphorus can be accumulated in intracellular polyphosphate granules, whereas under nitrogen-limited conditions cyanobacteria have also shown a high capacity to fix it (Felisberto et al., 2011). Different studies, performed mainly in lakes, have pointed out some nutrient thresholds to control the growth of cyanobacteria, as the TP value, which had to be between 20 – 100 µg TP/L (Li et al., 2018; Sharma et al., 2011). Stroom and Kardinaal (2016) reported that below 0.03 mg TP/L, the risk of cyanobacteria dominance is 10%, increasing to 40% at 0.07 mg TP/L, whereas another study indicated that the N levels can be also important, being the 0.8 mg TN/L threshold to limit the growth rate of *Microcystis* dominated blooms (Xu et al., 2014). The results obtained in this study pointed out that similar values can be fixed as nutrient thresholds for cyanobacteria growth in rivers, together with the N:P ratio. Since the N:P ratio value should be maintained at a level of at least 10, but preferably above 50 – 64, thereby reducing the likelihood for N-limiting situation which may favor cyanobacteria dominating blooms (Li et al., 2018). It should be noted that in our study we have evaluated the N:P ratio as DIN:SRP, while in the studies of lakes and reservoirs the ratio is calculated from TN and TP.

At the end of the experiment (d21), cyanobacteria abundance in the HN-A treatment decreased, arguably because of cells degradation. It has been demonstrated that the growth phase of different cyanobacterial strains could last from 8 to 24 days before entering in stationary or degradation phase (Kruskopf and Du Plessis, 2006; Jindal et al., 2011). Nevertheless, the conditions were still optimal for the cyanobacteria community, which were present in this treatment, being *Oscillatoria* sp. almost 45% of the total biofilm biovolume, a value pretty higher

compared to its presence in other treatments (**Figure 4.5.**).The growth phase of the Oscillatoria genus varies depending on the species. Kruskopf and Du Plessis (2006) observed that *Oscillatoria simplicissima* reached the fast growth phase after 8 days, whereas *Oscillatoria formosa*, could grow exponentially for 24 days and before starting the stationary phase (Jindal et al., 2011).

Changes at structural level were reflected on functional parameters being photosynthetic efficiency /Yeff) significantly lower under low N:P ratio. This could be explained by the highest presence of cyanobacteria in these treatments, since some studies have found that cyanobacteria usually show low photosynthetic efficiency values compared with the rest of the algal community (Espinosa et al., 2020; Luimstra et al., 2018).

In this study, the highest geosmin concentration in both biofilm and water was registered under low N:P ratio combined with high nutrient concentration (HN-A). In this treatment, at t=16d, the geosmin production per cyanobacteria biomass was between 6 – 20 times higher than in the other treatments, thus confirming the important role of these variables as main drivers of the biofilm geosmin production and release. Moreover, our results indicate that cyanobacteria, and more specifically *Oscillatoria* sp., could be the main responsible of geosmin production in freshwater biofilm communities. In fact, the linear regression analyses performed between cyanobacteria biomass (µg chl*a*/cm^2) and geosmin occurrence in biofilm and water shows a significantly high relationship (**Figure 4.8.**). Geosmin occurs in freshwater ecosystems as intracellular (cell-bound) and/or dissolved fractions (Jüttner and Watson, 2007). In our study, geosmin concentration pattern differed between the two compartments evaluated (water and biofilm) over time (**Figure 4.3.**). In HN-A treatment, geosmin in biofilm, increased earlier than in water (**Figure 4.3.A.**), and reached its maximum at t = 16d when resulted the 99.1 ± 0.6% of the total geosmin detected (both water and geosmin). This was the maximum intracellular geosmin concentration observed and coincided with the greater cyanobacteria abundance in the biofilm (**Figure 4.4.**). In the same treatment, the geosmin concentration in biofilm decreased substantially at the end of the experiment resulting the 86.6 ± 5.1% of total geosmin detected. This was reflected in a marked increase of dissolved geosmin concentration in water (**Figure 4.3.B.**).The decoupling observed between the presence of intracellular geosmin and its release to the water could explain the lower R^2 obtained in the linear regression analysis between cyanobacteria biomass and geosmin in water. This pattern could be related with cyanobacteria life cycle, and more specifically to their optimal geosmin production (associated to growth phase) and release time (linked to biomass decomposition and/or cell lysis), since it has been described that many cyanobacteria species can produce geosmin, although they may not actively release it until cell lysis occurs (Kim et al., 2018). Furthermore, the relative amounts of

intra and extracellular portions of geosmin may also vary considerably with cell age, environmental conditions and among different species (Alghanmi et al., 2018). Results obtained in our study agreed with other studies, carried out with cyanobacterial cultures, which indicated that the highest intracellular production of geosmin occurred in late exponential growth phase, with release starting during stationary phase and full release occurring with cells death and lysis (Saadoun et al., 2001). Another study performed with *Anabaena* sp. cultures found that about 85 – 95% of the total geosmin was concentrated in the cell rather than released in the cultivation medium (Alghanmi et al. 2018). A similar trend was observed by Ho et al. (2012), who found that >98% of the total geosmin was intracellular in untreated *Anabaena circinalis* rich waters. Nevertheless, all these studies were carried out with mono specific cyanobacterial cultures, whereas our work is the first one demonstrating the role of nutrient concentration and N:P ratio as main drivers of the geosmin intracellular production and release to the water from producing organisms that are part of a complex benthic microbial community.

At structural level, Chlorophyll *a* concentration was affected by both factors and its interaction, with higher Chlorophyll *a* concentration under HN-B conditions. There was a negative correlation between geosmin and Chlorophyll *a* concentration's in biofilm (Pearson's correlation: r = -0.535; p = 0.049). This trend could be observed at the end of the experiment (t=21d), when the highest concentration of Chlorophyll *a* (0.38 ± 0.01 ng/mg) was measured in the treatment in which there was no geosmin production (HN-B) (**Figure 4.9.**). Geosmin and Chlorophyll *a* have the same metabolic pathway and it has been described that when cyanobacteria start synthetizing geosmin the production of Chlorophyll *a* decreases or even stops (Cai et al., 2017). Other studies have shown that under elevated nitrate concentrations, a greater amount of Chlorophyll *a* is synthesized, with a correspondent decrease of geosmin synthesis (Saadoun et al., 2001). This partially agrees with our results, since under elevated nitrogen conditions, we found the highest Chlorophyll *a* concentration, but when phosphorus concentration also increased (lower N:P ratio), Chlorophyll *a* concentration was lower and geosmin levels increased (**Figure 4.6.**). This evidence would confirm the fundamental role of phosphorus concentration in the geosmin production process.

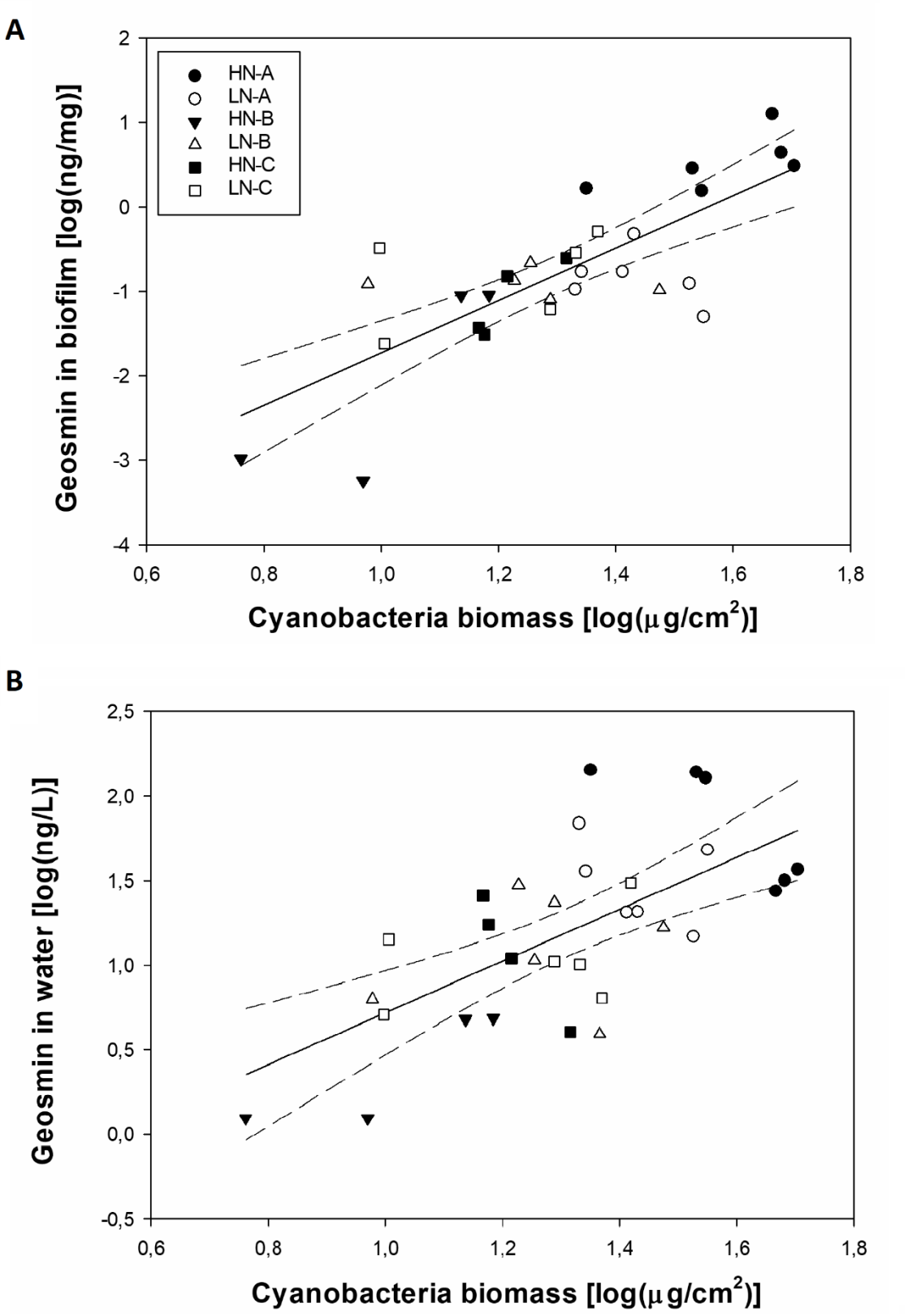

Figure 4.8. The relationship between **(A)** log geosmin in biofilm (ng/mg) and log cyanobacteria biomass (µg chl*a*/cm^2) (R^2 = 0.59, F = 40.35, p < 0.0001) and **(B)** log geosmin in water (ng/L) and log cyanobacteria biomass (µg chl*a*/cm^2) (R^2 = 0.43, F = 22.76, p < 0.0001), at t =16d and t =21d.

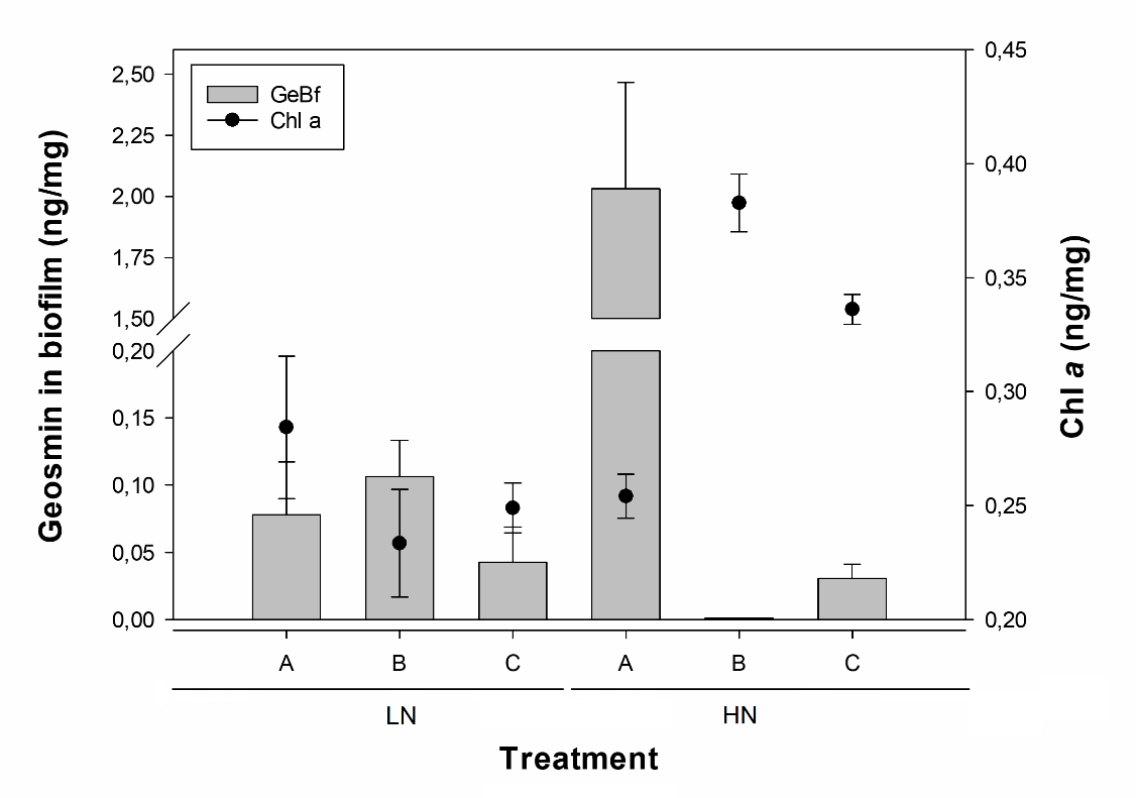

Figure 4.9. Mean values and standard deviation at t=21d for the different treatments (HN-A, LN-A, HN-B, LN-B, HN-C, LN-C, being HN = High nutrient, LN = low nutrient and A = 4:1, B = 16:1 and C = 64:1 DIN:SRP ratio) of the geosmin concentration in biofilm (ng/mg) vs. Chl a concentration in biofilm (ng/mg).

Results of this study indicated that the interaction between the N:P ratio and nutrient concentration in water, has a key role in the geosmin production and release by cyanobacteria in biofilm. Therefore, freshwater systems affected by high nutrient concentration, and with an imbalance of phosphorus over nitrogen are of special concern because they are susceptible to experience geosmin episodes. These episodes could lead to bad odor and taste situations on surface waters, potentially affecting the costumers trust and being a huge problem for waters utilities in those rivers exploited for drinking purposes.

4.6. Conclusions

Overall, this experimental study showed that both, nutrient concentration and N:P ratio, had a clear effect on the biofilm community structure and function and consequently on the geosmin formation in biofilm and its consequent release into water. Low N:P ratio and high nutrient concentration favored the *Oscillatoria* genus appearance, generating the optimal conditions for geosmin production. However, it should be noted that the conclusions of this study are limited

to the nutrient levels evaluated, not knowing whether the increase in cyanobacterial biomass as a function of the N:P ratio and the nutrients concentration is linear, exponential or follows some other type of trend. Therefore, further investigation on this topic should evaluate higher levels of these factors to establish the trend of these behaviors with greater precision.

Our results could help drinking water companies in the forecasting and management of geosmin episodes since, noting the need to include the analysis of nitrates and phosphorus in water samples from the collection point in their laboratory monitoring routine, and to carry out the N:P ratio calculation. Furthermore, including in this routine the study of biofilm community's development, drinking water companies could detect if there is an increase in the presence of cyanobacteria which, in a situation of high nutrient concentration and low N:P ratio, could trigger the appearance of geosmin in water.

The need to predict and manage these geosmin episodes is especially important in Mediterranean areas under the current climate change context, which it is expected to drastically reduce river flows. Under this context, our results strongly suggest a potential increase of geosmin episodes, due to the appearance of cyanobacteria, such as *Oscillatoria* sp., which will be favored by the decrease in the dilution capacity of nutrients and the increase in the final nutrient concentration in water.

CHAPTER 5. Water flow and light availability influence on intracellular geosmin formation in river biofilms

These results have been published in: ***Espinosa, C****., Abril, M., Guasch, H., Pou, N., Proia, L., Ricart, M., Ordeix, M. & Llenas, L. (2020). Water flow and light availability influence on intracellular geosmin production in river biofilms. Front. Microbiol. 10:30002. https://doi.org/10.3389/fmicb.2019.03002*

5. Water flow and light availability influence on intracellular geosmin formation in freshwater biofilms

5.1. Introduction

Due to several natural and anthropogenic factors such as nutrient enrichment, temperature increase and pollutant loading, cyanobacterial blooms are increasing worldwide (Winter et al., 2011; Vahtera et al., 2007; Vilalta, 2004), usually associated with the appearance of Taste and Odor compounds (T&Os). The presence of these compounds are becoming a problem in waterbodies management, because the influence the aesthetic water quality and consumer trust in drinking water companies (Ding et al., 2014). These compounds are perceived from humans at very low concentration (Smith et al., 2009), resulting in consumer complaints. Odor episodes in drinking water have become an universal water issue reported worldwide (Tung et al., 2008). Exact causes and conditions under which cyanobacteria begin to produce these compounds have not been completely defined, since companies have prioritized the definition of strategies to treat and eliminate these compounds instead of evaluating the factors associated with their production in the ecosystem (Jüttner and Watson, 2007).

Among the existing T&Os, geosmin has been identified as the main metabolite conferring bad taste and odor to drinking water (Watson et al., 2016). This metabolite is a volatile bicyclic terpenoid, produced inside cyanobacterial cells during the exponential phase of growth and released into the water as a consequence of cell death and/or biomass decomposition (Kim et al., 2018). Despite some heterotrophic bacteria have been described as potential geosmin producers, cyanobacteria are considered the main relevant in freshwater ecosystems (Olsen, Chislock, and Wilson, 2016). The majority are benthic or epiphytic (70%), while the rest are planktonic (Jüttner and Watson, 2007). In the group of geosmin-producing cyanobacteria, *Oscillatoria* sp., *Lynghya* sp., *Symploca* sp. and *Anabaena* sp. have been identified as the most commonly found in freshwater ecosystems (Smith et al., 2009).

Different environmental factors may influence cyanobacteria growth and geosmin production (Lee et al., 2017). For example, most cyanobacteria species are known to have optimum temperature growth conditions (>20°C), but many others have the ability to adapt to lower temperature by controlling its pigments levels (Tang et al., 1997). High light availability has also been described to inhibit the formation of gaseous vacuoles in certain cyanobacteria (Blevins et al., 1995; Li et al., 2012), pointing light as a key factor for geosmin production (Saadoun et al., 2001; Wang and Li, 2015; Lee et al., 2017). Water flow may also have a certain effect on microbial

production of T&Os, indeed, elevated geosmin concentration have been reported in proximity to dams of several rivers, where the flow is significantly reduced (Jüttner and Watson, 2007). Light availability and water flow are factors that can be altered both by human activity and climate change (Elosegi and Sabater, 2013).

Global climate models predict changes that will generate more frequent and intense extreme events in next decades (Acuña and Tockner, 2010), altering natural flow regimes of rivers. Specific predictions for Mediterranean climate regions indicate a strong reduction in the mean precipitation and a probable decrease in annual runoff that will lead to reduced river flows (Bangash et al., 2013). In addition, hydrological regime of running waters can be affected by flow regulation through dams and impoundments building (Rubio-Gracia et al., 2017). Moreover, anthropogenic activities can alter river banks causing riparian forest modifications and consequentially altering the quantity and quality of light potentially reaching riverbeds (Dal Sasso et al., 2015). Variation of light and/or water flow regimes accounts for much of the variation in the structure and functioning of benthic microbial communities (von Schiller et al., 2008), and therefore, they could represent indirect drivers of geosmin production in rivers.

The Ter river born in the middle of the Catalan Pyrenees (at 2400m high) flows into the Mediterranean Sea. The Mediterranean climate determines the rain patterns over the basin, which is characterized by maximum rainfall in spring and autumn and dry and warm summers. Moreover, in its mid-section there are some anthropogenic activities such as dams used to obtain hydraulic energy, and livestock farming and agriculture, leading to an increase in nutrients concentration. All these activities are drastically affecting water flow and water quality downstream of the river (Céspedes et al., 2008). In addition, geosmin episodes in the Ter river basin have increased in the last decades (personal communication). This is a concern for drinking water treatment companies in the area, as they are not able to predict the presence of geosmin in the river and, therefore, apply the specific treatment when needed.

Although it has been described that geosmin production depends on environmental conditions, most of the studies were carried out with single specie cultures under controlled conditions (Li et al., 2012; Suurnäkki et al., 2015; Wang and Li, 2015), with very few studies dealing with the identification of geosmin production drivers in natural benthic microbial communities. It is therefore essential to understand how the variation of multiple environmental variables can affect biofilm community structure and subsequently geosmin formation.

5.2. Objective

This study was designed to explore the combined effects of light availability and water flow on biofilm structure and functioning, and its relationship with intracellular geosmin formation. To test this, an experiment was carried out with outdoor mesocosms that received water from the Ter river (Catalonia, NE Spain).

5.3. Material and Methods

5.3.1. Experimental design and sampling procedure

In this experiment, 10 outdoor experimental flumes (3.5 m long x 12 cm wide x 8 cm high), which receive water directly from an industrial channel of the mid-section Ter river in Manlleu (NE Catalonia, Spain), have been used (**Figure 5.1.**). The experiment was conducted from late March till April in 2018, since it is known that in the Ter river this is the period in which a greater production of geosmin is expected.

The river water was pumped from the river channel by four submerged pumps (drainage pump, VXV 1100AS) into four 1000 L carboys, each of them feeding three experimental flumes that discharge into the same channel downstream of water abstraction.

Figure 5.1. Outdoor experimental flumes located in Manlleu, close to the Ter river, which water was used in the experiment. Ter River Museum (NE Catalonia, Spain). March 19, 2018.

The two parameters manipulated in this study were light intensity and water flow. Particularly, two light and five water flow conditions were set for the experiment. Five flumes were left under natural light conditions (High Light treatment, HL = 515 ± 57 µmol photons/m^2·s) whereas the rest were covered with a greenhouse net to achieve an 80% reduction of the light reaching the flumes (Low light treatment, LL =107 ± 38 µmol photons/m^2·s). This light availability reduction was chosen according to the light availability common for streams in a well-develop riparian forest (Bowes et al., 2012; Hill and Fanta, 2009). Light intensity was monitored continuously during the experiment using HOBO Data Loggers (Hobo® Pendant, Onset Computer Corp., MA, USA). By manipulating the independent tap of each flume, five levels of water flow were set: F1 = 0.09 L/s; F2 = 0.18 L/s; F3 = 0.36 L/s; F4 = 0.72 L/s; and F5 = 1.10 L/s, in both HL and LL flumes. Water flow was regularly quantified by measuring the volume of water per minute outflowing from each flume. Both, light and water flow conditions, were randomly distributed across the experimental flumes (**Figure 5.2.**).

Figure 5.2. Experimental flumes used to evaluate the light availability (left photo) and water flow (right photo) effect on biofilm community development and geosmin production.

Thirty river cobbles, previously scraped and autoclaved, were placed in each flume to allow biofilm colonization using inflowing river water as natural inoculum. Biofilm development and physicochemical parameters were monitored once per week throughout the experiment and a sampling was carried out at the end of the experiment, after 41 days, to evaluate the overall response of the biofilms to the treatments.

Physicochemical parameters were measured in situ with specific probes: temperature, dissolved oxygen concentration and oxygen saturation (YSI professional plus, YSI Incorporated, USA), pH (XS pH7+ DHS) and conductivity (XS COND 7+). At the inlet and outflow of each flume, three water samples were taken per sampling day. Samples were filtered through 0.45 µm cellulose filters before the analysis of Soluble Reactive Phosphorus (SRP), $N\text{-}NH_4^+$, $N\text{-}NO_2^-$ and $N\text{-}NO_3^-$. All samples were stored at -20°C until analysis, which were performed as described in **Chapter 3**. With the data obtained, the nutrients uptake capacity of biofilm was estimated, considering the difference in nutrient concentration between the input and the outflow of each flume, taking into account the area colonized by biofilm, as described in **Chapter 3**.

The last day of the experiment, 3 cobbles from each flume were randomly collected and scraped in 30ml of water from the same flume to obtain a biofilm suspension (**Figure 5.3.**). Aliquots of these suspensions were used to analyze geosmin concentration, Chlorophyll *a* (Chl *a*), ash free dry mass (AFDM), algal taxonomic composition and photosynthetic efficiency. The photosynthetic efficiency was measured in situ with an amplitude modulated fluorimetry (Mini-PAM fluorometer Walz, Effeltrich, Germany). Samples were stored frozen at -20°C until analyses, except aliquots for geosmin concentration that were frozen at -80°C and taxonomic samples, which were fixed with formalin (2%) and stored at 4°C. All the samples were analyzed following the protocols described in **Chapter 3**.

Figure 5.3. Cobbles with biofilm from one of the flumes used in this experiment at time 41 days.

5.3.2. Data treatment

Physicochemical and biological data were evaluated using an Analysis of Covariance (ANCOVA) in SPSS Statistics version 21, with water flow being the independent variable and light availability the covariate. The distribution of the phototrophic community of the biofilm according to the treatments was evaluated using a Principal Component Analysis (PCA), and Pearson correlation coefficient test were performed to explore the relationship between intracellular geosmin concentration and the biological and the physicochemical variables. Statistical significance was set at $p < 0.05$ for all test performed.

5.4. Results

5.4.1. Physicochemical parameters

The experimental conditions of the carboys and flumes remained stable throughout the experiment, with low water temperature, high oxygen water levels, slight alkaline pH and medium mineralization (**Table 5.1**). There were not significant statistically differences among the carboys along the experiment (ANCOVA, $p = 0.781$). Nutrient concentrations in the carboys varied throughout the time as a consequence of the variations naturally occurring in Ter river, which supplied the water to the mesocosms. This variation was the same for all the flumes.

Table 5.1. Mean value and standard deviation of the physicochemical variables evaluated in the flumes throughout the experiment (n = 84), under low light (LL) and high light (HL) conditions for the different flow treatments (F): pH, water temperature (ºC), electrical conductivity (EC) (µS/cm), dissolved oxygen (DO) (mg/L), oxygen saturation (%), water flow (L/s), light irradiance (µmol photons/m^2·s), ammonium (µg N-NH_4^+/L), nitrite (µg N-NO_2^+/L), nitrate (mg N-$N0_3^+$/L) and phosphate concentration (µg P-PO_4^{3-}/L).

	Low Light (LL)					High Light (HL)				
	F1	**F2**	**F3**	**F4**	**F5**	**F1**	**F2**	**F3**	**F4**	**F5**
pH	8.3 ± 0.3	8.4 ± 0.2	8.4 ± 0.2	8.4 ± 0.2	8.4 ± 0.2	8.4 ± 0.2	8.3 ± 0.3	8.4 ± 0.2	8.4 ± 0.2	8.4 ± 0.2
Water temperature (ºC)	10 ± 3	10 ± 3	9 ± 3	10 ± 3	10 ± 3	10 ± 3	10 ± 3	10 ± 3	10 ± 3	10 ± 3
EC (µS/cm)	332 ± 58	339 ± 50	337 ± 55	335 ± 54	333 ± 56	333 ± 50	336 ± 52	336 ± 53	334 ± 59	340 ± 55
DO (mg/L)	10.8 ± 1.5	11.4 ± 0.9	11.3 ± 0.8	11.3 ± 0.9	11.3 ± 0.9	11.1 ± 1.1	11.3 ± 0.8	11.4 ± 0.8	11.3 ± 0.7	11.4 ± 0.7
Saturation (%)	95 ± 13	100 ± 6	99 ± 6	99 ± 8	99 ± 6	98 ± 9	100 ± 6	100 ± 6	99 ± 5	99 ± 7
Water flow (L/s)	0.09 ± 0.00	0.18 ± 0.00	0.31 ± 0.02	0.61 ± 0.04	1.20 ± 0.09	0.09 ± 0.01	0.17 ± 0.01	0.33 ± 0.03	0.60 ± 0.07	1.14 ± 0.02
Light irradiance (µmol photons/m^2·s)	110 ± 15	118 ± 13	114 ± 16	109 ± 21	112 ± 15	509 ± 32	516 ± 18	519 ± 22	512 ± 17	511 ± 28
N-NH_4^+ (µg/L)	74 ± 62	74 ± 62	75 ± 60	78 ± 70	76 ± 59	78 ± 70	73 ± 59	78 ± 70	74 ± 62	75 ± 60
N-NO_2^- (µg/L)	8 ± 5	6 ± 4	9 ± 7	7 ± 4	7 ± 6	8 ± 7	6 ± 4	6 ± 4	6 ± 3	7 ± 5
N-NO_3^- (mg/L)	0.9 ± 0.3	0.9 ± 0.3	0.9 ± 0.3	0.8 ± 0.3	0.9 ± 0.3	0.9 ± 0.2	0.9 ± 0.2	0.8 ± 0.2	0.9 ± 0.2	0.9 ± 0.3
P-PO_4^{3-} (µg/L)	19 ± 6	10 ± 2	14 ± 4	13 ± 5	10 ± 3	12 ± 4	12 ± 2	13 ± 6	12 ± 5	14 2

5.4.2. Biofilm attributes

5.4.2.1. Structural parameters

Biofilm biomass measured as AFDM (g/cm^2) showed a different pattern as response to light availability (ANCOVA, F = 4.560, p < 0.05) (**Figure 5.4.A.**). In particular, biofilms developed under lower flow and light conditions (F1LL, F2LL) showed significantly higher values of AFDM (60 ± 8 g/m^2 and 56 ± 7 g/m^2, respectively) with respect to the biofilms from higher flow and light treatments (**Figure 5.4.A.**). The Chlorophyll *a* (µg/cm^2) did not present differences depending on the light (ANCOVA, F = 1.503, p =0.230) (**Figure 5.4.B.**). The lowest values were found at the extreme water flows, F1 and F5, both with a Chlorophyll *a* concentration around 5 ± 1 µg/cm^2. The Autotrophic Index (AI) was significantly affected by light (ANCOVA, F = 5.351, p < 0.05) (**Figure 5.4.C.**),with the flumes with low flow and low light (F1LL and F2LL) being the ones with the highest values, 837 ± 150 for F1LL and 976 ± 255 for F2LL. Similar results were observed for Margalef Index (MI) (ANCOVA, F = 4.528, p < 0.05) (**Figure 5.4.D.**), with biofilms developed in flumes with lower flows (F1 and F2) showing higher values than the others. In particular, under low light conditions biofilms showed greater values of MI, being F1LL the highest (3.2 ± 0.2).

In LL conditions, water flow was negatively correlated with AFDM (Pearson's correlation, r = -0.829, p < 0.001), AI (r = -0.735, p < 0.01), and MI (r = -0.718, p < 0.01); in HL conditions, no correlations were found between these structural parameters and water flow.

Phototrophic community structure was different among flumes (**Figure 5.5.**), particularly, changes were detected on the relative abundances (expressed as biovolume) of *Oscillatoria* sp. (ANCOVA, F = 0.175, p < 0.001), *Melosira* sp. (ANCOVA, F = 1.268, p < 0.05) and *Pinnularia* sp. (ANCOVA, F = 4.358, p < 0.05). Precisely, the principal component analysis (PCA) evidenced that the biofilms developed under lower flow conditions (F1) were different in terms of relative abundances of the taxa (**Figure 5.6**.). Light availability influenced the community structure. Indeed, F1LL biofilms were separated from the rest mainly driven by the higher relative abundance of *Oscillatoria* sp., among others (**Figures 5.5. and 5.6.**). On other hand, the biofilm in F1HL flume was also differentiated from the rest by the presence of *Fragilaria* sp., *Gomontiella* sp. and *Achnantes* sp. The relative abundance of the genera *Oscillatoria* sp. was affected by the interaction of light and water flow, being dominant in biofilms developed under lower flow and low light availability (F1LL).

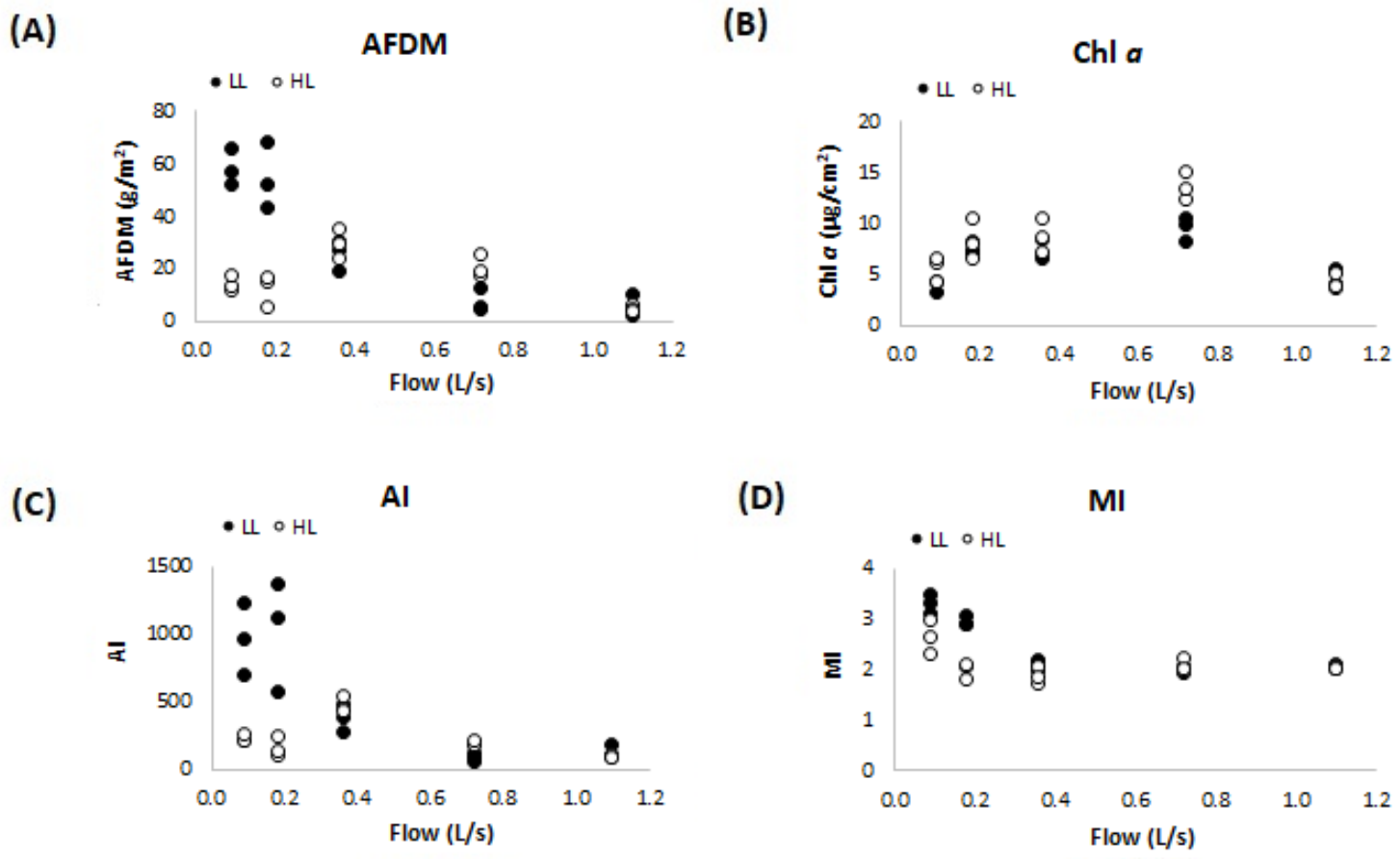

Figure 5.4. Results obtained in the different treatments for the different structural biofilm descriptors measured at the end of the experiment (t = 41 days): **(A)** Ash Free Dry Mass (AFDM) (g/m^2), **(B)** Chlorophyll a (µg/cm^2), **(C)** Autotrophic Index (AI) (AFDM/Chl a), and **(D)** Margalef Index (MI) (Abs. 430 nm/Abs. 665 nm).

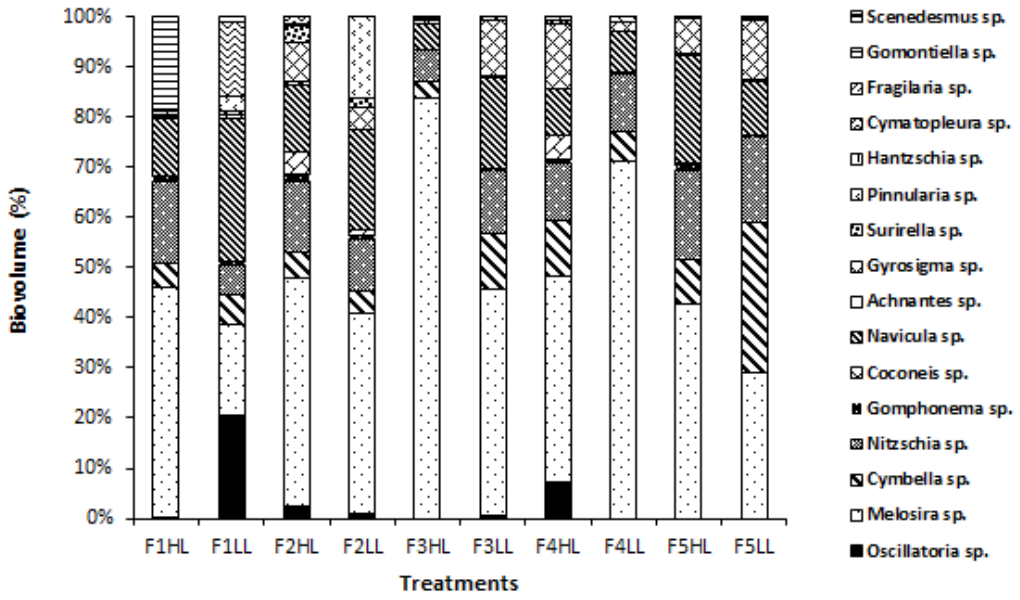

Figure 5.5. Biovolume (in %) of algae, diatoms and cyanobacteria present in the biofilm of each treatment, from the lowest flow (F1) to the highest (F5), under conditions of natural light (HL) and reduced (LL).

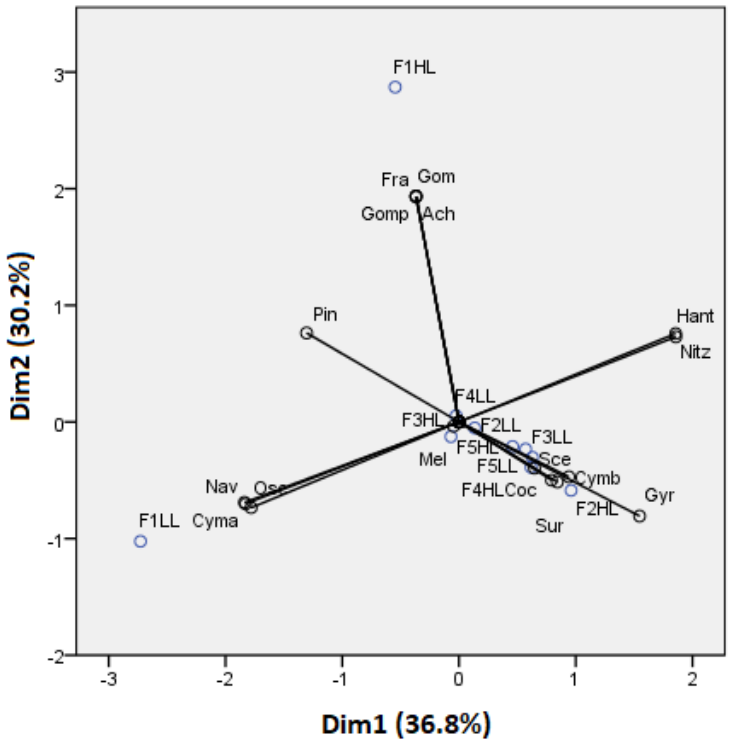

Figure 5.6. Principal component analysis showing flumes distribution based on biofilm algal species. Axes 1 and 2 combined explain 66.98% of the variance. Cyanobacteria: Osc = *Oscillatoria* sp. and Gom = *Gomontiella* sp.; diatoms: Mel = Melosira sp.; Cmb = *Cymbella* sp.; Nit = *Nitzschia* sp.; Gomp = *Gomphonema* sp.; Coc = *Coconeis* sp.; Nav = *Navicula* sp.; Ach = *Achnantes* sp.; Gyr = *Gyrosigma* sp.; Sur = *Surirella* sp.; Pin = *Pinnularia* sp.; Han = *Hantzschia* sp.; Cym = *Cymatopleura* sp.; Fra = *Fragilaria* sp. and green algae: Sce = *Scenedesmus* sp.

5.4.2.2. Functional parameters

- Photosynthetic capacity

The biofilm photosynthetic capacity (expressed as Ymax) showed significant differences depending on light (ANCOVA, $F = 1.607$, $p < 0.05$), being slightly superior under LL conditions. There was a positive correlation between the water flow and Ymax ($p < 0.05$), where the biofilms growing under lower flow conditions (F1) exhibited the lowest values (0.347 ± 0.085 for F1LL and 0.278 ± 0.005 for F1HL).

- Nutrient Uptake Capacity

Nutrient uptake (or release) capacity of ammonium (**Figure 5.7.A.**), nitrate (**Figure 5.7.B.)** and phosphate (**Figure 5.7.C.**), were significantly affected by light conditions (ANCOVA, $F = 12.153$, $p < 0.001$ for the ammonium; $F = 416.361$, $p < 0.001$ for the nitrate, and $F = 119.28$, $p < 0.001$ for the phosphate). The ammonium uptake capacity tended to increase at higher flows, reaching, under LL conditions, the values of 1.05 mg $N\text{-}NH_4^+/m^2$ (F5LL). Nitrate was normally not consumed but released by biofilms along the flumes, as a probable consequence of nitrification activity within the communities. The nitrate release capacity showed the opposite trend with respect to ammonium uptake capacity pattern. Indeed, the highest release value (4.68 mg $N\text{-}NO_3^-/ m^2$) was found in flumes with higher flow and light availability (F5HL). Phosphate uptake capacity had the same pattern as ammonium uptake capacity; being higher in biofilms grown under higher flow and lower light availability conditions when the uptake values were higher (4.50 mg $P\text{-}PO_4^{3-}/ m^2$). If the DIN:SRP ratio is calculated; being DIN the sum of the dissolved inorganic nitrogen, it is observed that the differences in nutrient uptake dynamics were reflected in the water DIN:SRP ratio which showed differences depending on the treatment, being lower at low flows (11:1) and increasing notably in the highest flow flumes (417:1).

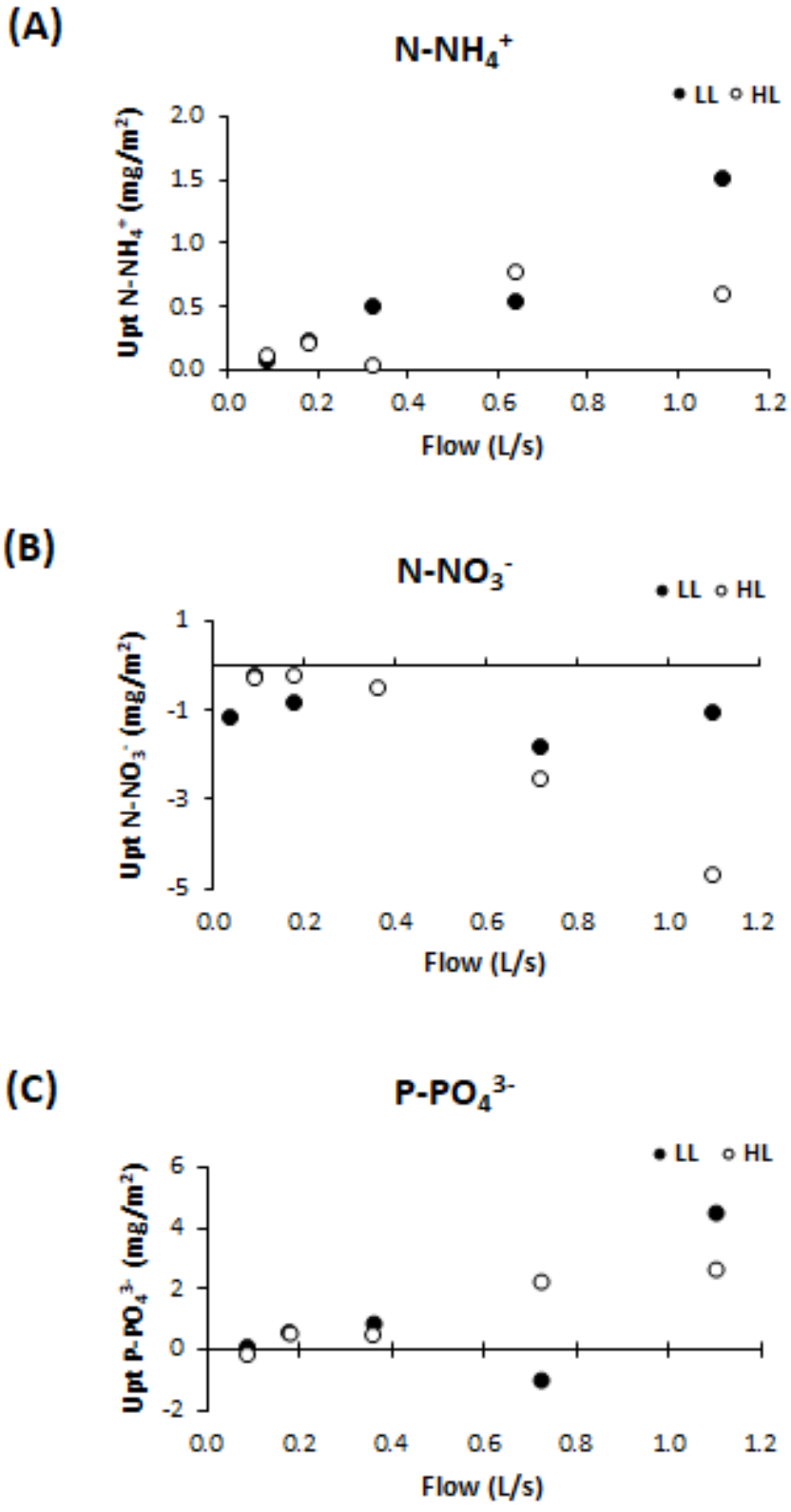

Figure 5.7. Uptake/release capacity values for different treatments: **(A)** ammonium (mg $N\text{-}NH_4^+/m^2$), **(B)** nitrate (mg $N\text{-}NO_3^-/ m^2$), and **(C)** phosphate (mg $P\text{-}PO_4^{3-}/ m^2$).

5.4.3. Geosmin concentration in biofilm

Light availability had a significant effect on the concentration of intracellular geosmin (ANCOVA, $F = 72.641$, $p < 0.001$), which also presented a negative correlation with water flow (Pearson's correlation, $r = 0.918$, $p < 0.01$). Geosmin was detected above the quantification limit in the biofilms of four treatments: F1LL, F2LL, F2HL and F4HL. The highest concentrations were measured in biofilm developed under lower flow and light conditions reaching 2118 ± 460 ng/g at F1LL and 710 ± 326 ng/g at F2LL, respectively (**Figure 5.8**.).

The geosmin concentration in biofilm correlated positively with different variables: *Oscillatoria* sp. biovolume (Pearson's correlation, $r = 0.776$; $p < 0.01$), *Oscillatoria* sp. relative abundance (Pearson's correlation, $r = 0.924$, $p < 0.0001$), AFDM (Pearson's correlation, $r = 0.817$, $p < 0.01$), Margalef Index (Pearson's correlation, $r = 0.857$, $p < 0.01$), and Autotrophic Index (Pearson's correlation, $r = 0.769$, $p < 0.01$). Regarding the physicochemical variables, geosmin concentration in biofilm correlated positively with phosphate concentration (Pearson's correlation, $r = 0.963$, $p < 0.001$), and temperature (Pearson's correlation, $r = 0.761$, $p < 0.05$), and negatively with nitrite concentration (Pearson's correlation, $r = -0.887$, $p = 0.001$).

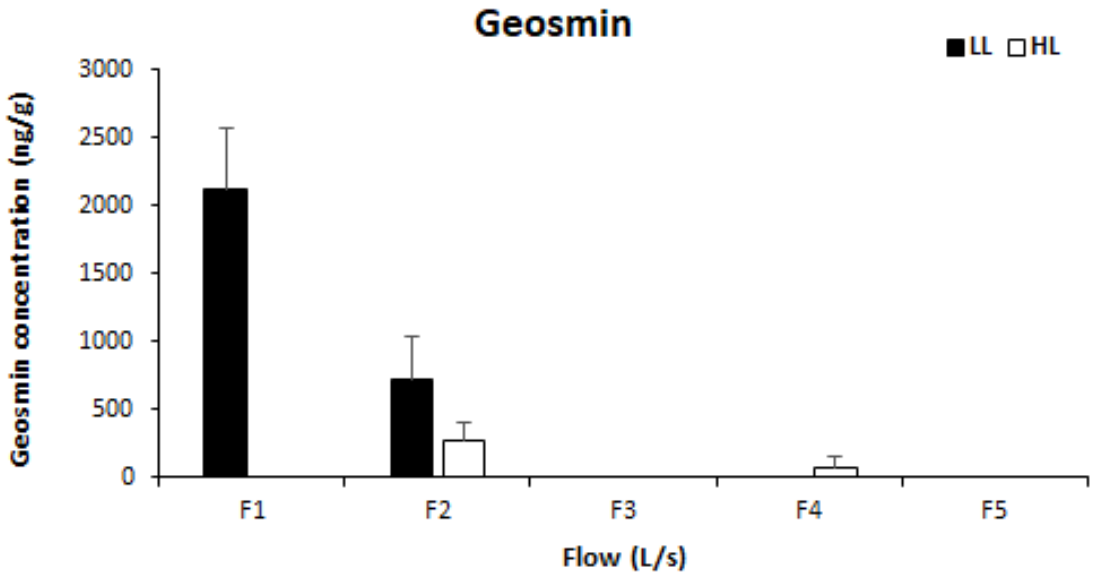

Figure 5.8. Mean values and standard deviation for intracellular geosmin concentration (ng/g) in biofilm of each treatment, from the lowest flow (F1) to the highest (F5), under conditions of natural light (HL) and reduced (LL), at the end of the experiment (t = 41 days).

5.5. Discussion

Light intensity and water flow generated differences in the biofilm structure and functioning. At functional level, low light conditions caused an increase in the photosynthetic capacity (Ymax) of the biofilm, as typically observed in biofilm communities developed under this situation (Corcoll et al., 2012; Villeneuve, Montuelle, and Bouchez, 2009). Riegman et al. (1985) also found out this pattern for the *Oscillatoria agardhii* strain under laboratory conditions. Water flow also affected the photosynthetic capacity of the biofilm community, which was reduced at the lowest flow. This could be explained by the highest presence of *Oscillatoria* in this treatment, since some studies have found that cyanobacteria usually present low photosynthetic values compared with the rest of the algal community (Kirst, Formighieri, and Melis, 2014; Luimstra et al., 2018).

Regarding nutrients uptake, the biofilm developed under LL conditions had a greater ammonium and phosphate uptake capacity, whereas the biofilm developed under HL conditions showed increased nitrate release capacities suggesting greater nitrification activity. This would be in contrast with the inhibitory effect of light on nitrifying organisms reported both in cultures and natural biofilm communities (French et al., 2012; Merbt et al., 2017). However, these studies did not consider the role of flow conditions that could influence the nutrients dynamics by modifying the interactions between dissolved molecules and benthic biota or also generating differences in the diffusion capacity (Battin et al., 2016). Overall, in this study, the ability to consume or release ammonium, nitrate and phosphate is significantly favored at higher flows. Nevertheless, it must be taken into account that it was an approximation considering the nutrients levels measured between the entrance and the outflow of the flumes, and assuming that the nutrients load variation was a consequence of biological activity (both uptake and/or release). Even so, the difference in nutrient uptake or release has been reflected in the DIN:SRP ratio. At the beginning of the flumes, the average DIN:SRP ratio value was 16:1 ± 3:1. However, at the end of the flumes the average was significantly higher in F5 treatments (417:1) than in F1 (11:1). This would be related to the differences in the nutrient uptake and release capacity of the biofilm developed under high water flows, since it has been described that increased flow velocity implicated the increase in the mass transfer between nutrients from water and the biofilm matrix (Battin et al., 2003), while biofilms developed under slow velocities were more reliant on internal resource cycling than those developed under elevated velocities (Battin et al., 2003; Leff et al., 2016). This could be a relevant factor related with geosmin behavior in biofilms as it has

been suggested that lower DIN:SRP ratios can favor the producing organism and its harvesting activity.

At the structural level, Chlorophyll *a* concentration was affected by water flow, with lower Chlorophyll *a* concentration under the most extreme flow rates (F1 and F5). The low Chlorophyll *a* concentration found at the lowest water flow could be explained by the high concentration of geosmin detected in this treatment. In fact, geosmin and Chlorophyll *a* have the same metabolic pathway and it has been described that when cyanobacteria start synthetizing geosmin the production of Chlorophyll *a* decrease or even stops (Cai et al., 2017; Saadoun et al., 2001). Related to the treatment with the highest flow, it is known that during high water velocity, biofilms are sloughed due to high shear stress, drag and abrasion, leading to low biomass (Ponsatí et al., 2016; Wellnitz and Rader, 2007).

Biofilms growing at LL conditions had higher values of AI, suggesting that there was a lower proportion of algal biomass in comparison to the total biomass (Weber, 1973). Higher registered values of AFDM and MI may be linked to the accumulation of accessory pigments and a more aged community, as described by Ceola et al. (2013) and Marcarelli et al. (2009). Light intensity represents an environmentally important factor for cyanobacterial growth (Alghanmi et al., 2018). In the LL treatment, *Oscillatoria* genus was favored within the community, strongly suggesting that low light availability in ecosystems leads to a higher presence of geosmin-producing cyanobacteria. This agrees with what was observed, in laboratory conditions by Sivonen, (1990) and Lee et al. (2017) but contradicts what was observed in the field by Sabater et al. (2003). The study carried out by Sabater et al. (2003) pointed out that full light availability was one of the factors that contributed to generate a favorable environmental scenario for benthic cyanobacteria development at the Llobregat river (Catalonia, NE Spain). However, this and other studies carried out in the same river also suggested a primary role of low water flow and nitrogen to phosphorus ratio in the massive growth of *Oscillatoria* mats (Sabater et al., 2003; Vilalta et al. 2003).

The AFDM, AI and MI were also affected by the different water flows conditions, particularly showing higher values of these parameters under low flow conditions. Ateia et al. (2016) found out that the moderate water flow provided favorable conditions for algal growth and the corresponding biomass accumulation. Nevertheless, the results obtained by Graba et al. (2013) showed that there were no significant differences in AFDM depending on water flow, but this parameter was a selective factor in algal composition. A shift in the algal community composition was also observed in this study, with the proportion of the *Oscillatoria* genus being

much higher under low water flow (F1 and F2). Vilalta (2004) described a cyanobacterial growth favored by slow current velocity areas in a field study performed in a Mediterranean river.

In our study, the highest amount of geosmin in biofilm was detected under low light and low flow conditions, thus confirming the important role of these variables in the production of geosmin by *Oscillatoria* sp. Some studies focused on light effects have found that geosmin produced by *Oscillatoria f. granulata* growing under laboratory conditions increased at lower light (Tsuchiya and Matsumoto (1999). Blevins et al. (1995) and Saadoun et al. (2001) also found that reducing the light intensity resulted in the increased production of geosmin in cultures of *Anabaena* sp. The lowest amount of geosmin found at high light conditions in our study could be attributed to the inhibition of the gas vacuole formation in certain cyanobacteria, as was described under intense light situations by Blevins et al. (1995) and Li et al. (2012). Other studies have evaluated the role of water flow on geosmin concentration in the field. In our study, the higher presence of *Oscillatoria* sp. at the low flow conditions suggest a clear relationship with the geosmin concentration, achieving the highest values under low flow treatments. This result highlights the effect of water flow as a critical factor in the geosmin formation, the maximum geosmin production occurs when water flows is approaching basal flow (Vilalta et al., 2003) specially in Mediterranean areas, where water scarcity is a common situation (Casas-Ruiz et al., 2016; Cid et al., 2017; Karaouzas et al., 2018). It is important to highlight that none of the abovementioned studies has previously tested the independent and combined effect of these two factors on geosmin production under controlled conditions in a mesocosms system receiving water directly from the river. The present study is thus the first one filling the lack of information about the joint effect of light and water flow on geosmin formation in freshwater benthic communities.

According to these results, the interaction of both parameters, water flow and light availability, has an important role in the biofilm geosmin formation, by changing the community composition and thus favoring the intracellular geosmin formation. Freshwater systems affected by low light irradiation and low water flow are of special concern because they are the most susceptible to experience geosmin episodes, having an impact on both odor and taste of surface waters. This will have a negative effect on the customers trust, being an important problem for water utilities in those rivers exploited for drinking water purposes.

Under the most currently accepted climate change predictions, it is expected a reduction in river water flows mainly due to a decrease in rainfall events and an increase in air temperature (IPCC, 2019). Thus, the results obtained in this study strongly suggest a probable increase of geosmin

episodes. The reduction of water flow favors the appearance of cyanobacteria (such as *Oscillatoria* sp.) which may lead to variations in the nutrient uptake capacity of the biofilm increasing the phosphorus concentration in water. In particular, biofilms capture less phosphorus at lower flows because of (i) biological factors, such as a community shift towards one with a lower nutrient uptake capacity or (ii) by physical factors, such as the limitation in nutrients diffusion due to a greater thickness of the biofilm (Battin et al., 2016). Both situations would lead to an optimum scenario for the formation of geosmin by *Oscillatoria* sp.

The results obtained in this study indicated the potential implications for stream ecosystem management to control geosmin appearance. Likewise, they could be used as an early warning system, establishing that in times of drought, which lead to a decrease in water flow, the situation could be optimal for the appearance and development of geosmin producing cyanobacteria on the banks of rivers.

5.6. Conclusions

Overall, this experimental study shows that both light availability and water flow have a clear effect on the biofilm community and thus on the intracellular geosmin formation. Low light and low water flow empower the *Oscillatoria* genus appearance, providing a favorable situation to start producing geosmin. In order to prevent geosmin episodes in those rivers exploited by drinking water purposes, it is important to further control the water nutrient content, and it will be essential to guarantee the environmental flow regimes to prevent the growth and accumulation of geosmin-producing cyanobacteria.

Considering the Ter river scenario, which is affected by a high presence of dams (one every 800 meters), an important factor to take into account in the management of this system, could be to reduce the presence of these dams, totally or partially, to increase the river flow. As far as possible, nutrient entry points to the system should be identified and reduced, avoiding or minimizing eutrophication in rivers thus preventing geosmin episodes.

CHAPTER 6. Driving factors of geosmin appearance in a Mediterranean river basin: the Ter river case

6. Driving factors of geosmin appearance in a Mediterranean river basin: the Ter river case

6.1. Introduction

Rivers are integrative systems of the nature and land uses of its basin, constituting excellent indicators of the quality and state of the environment. In the last decades, due to anthropogenic pressures and climatic change, the water quality of many rivers has gotten worse given rise to different ecological problems like the uncontrolled growth of algal blooms and its consequently alteration of the water properties, such as the water organoleptic characteristics affected by the appearance of geosmin episodes.

In this sense, the chemical composition of river waters can explain different processes occurring at the river basin level and along its flow. In particular, different factors such as weather, lithology and relief of the basin, vegetation, biological processes and human activities along the catchment determine, directly or indirectly, the chemical composition of surface running waters. Of all these factors, climate and geology of the basin could be the natural environmental characteristics that influence the most the structure and functioning of river ecosystems (Toro et al., 2002). In the specific case of areas with a Mediterranean climate, it has been stated that the factors that mainly influence the chemical composition of water are the erosion and dissolution of rocks and soils of the basin together with the existing human activities (Pardo et al., 2002).

As regards human activities, the study of land uses is a key factor in understanding the variation in water quality throughout a basin (Kibuye et al., 2020; Wilson, 2015), in addition, establishing relationships between land uses and water quality can contribute to improve significantly the watershed ecosystem management (Tu, 2011). Many problems related to water quality are generated by an increase in population, urbanization and industrial activities (Ullan et al., 2018). For example, agricultural land use is generally reflected in increased nitrogen and phosphorus concentrations and pesticides release in river water (Woli et al., 2004), whereas industrial and urban land uses are associated with organic pollutants, heavy metals and nutrients. Thus, exploring the relationships between watershed landscape characteristics and water quality, together with season variability of river water quality have considerable importance for watershed management (Ai et al., 2015).

The increase in human activity during the last century has led to changes in the river basins morphology and water quality (Winter et al., 2011). Particularly, the land use of these basins has

been modified shifting from forest-dominated catchments to industrial, livestock and agricultural prevalence, mainly associated with urban expansion and increased human activities. The effects on the water quality induced by the shift of land uses have acted conjointly with the alterations associated with the climate change.

Climatic conditions have changed in recent decades, with a clear decrease in average rainfall, which is much more sporadic and intense, and an increase in the mean temperature (IPCC, 2019). The effects of this climatic changes are of greater importance in rivers affected by situations of water scarcity, like those of the Mediterranean area among others. In these systems, water flow can be extremely reduced during longer periods, thus generating a greater increase of nutrients concentration, among other parameters (e.g. salts, metals, pesticides, etc.), due to the decreased dilution capacity of the system (Karaouzas et a., 2018). As stated in different studies, these conditions can trigger the appearance of algal blooms, with a large number of cases detected worldwide (Vilalta, 2004; Vahtera et al., 2007). These algal blooms can be related to the appearance of undesirable metabolites which can alter the organoleptic water properties, such as Taste and Odor compounds (T&Os), and specifically, geosmin (Watson et al., 2016).

Most of studies on drivers of geosmin appearance in the field have been carried out in reservoirs and lakes (Harris et al., 2016; Ponsatí et al., 2016; Dzialowski et al., 2009). One of the main reported factors promoting geosmin episodes in reservoirs is the excessive nutrient loading, since high nutrient concentrations and low nitrogen to phosphorus ratio (TN:TP) can promote cyanobacteria growth and dominance in freshwater ecosystems (Olsen et al., 2016; Harris et al., 2016). The study carried out by Harris et al. (2016) in 4 reservoirs in USA pointed out that geosmin primarily occurred when the TN:TP ratio was <30:1 (by mass), likely due to higher cyanobacterial biovolumes at lower TN:TP ratios. Similar results were found in the study performed by Vilalta et al. (2004) in the Llobregat river, when geosmin concentration was higher at TN:TP = 10 comparing with TN:TP = 94, when no geosmin was detected. Other factors that have been related with geosmin are light availability and temperature. Depending on the geosmin producers, the value of these factors differed, but in general it has been described that low light availability together with low temperatures favored intracellular geosmin formation (Zhang et al., 2009; Wang and Li, 2015; Alghanmi et al., 2018, Espinosa et al., 2020). Water flow may also have a certain effect on microbial production of geosmin (Espinosa et al., 2020), some studies reported higher concentrations of this metabolite in proximity of dams, where the flow was significantly reduced (Jüttner and Watson, 2007).

Although there are studies on drivers of geosmin in reservoir and lakes, very few have approached this topic in rivers (Vilalta et al., 2004). Geosmin occurrence can be a problem for the companies that exploit rivers to provide drinking water to the surrounding populations, since they do not know under which conditions is produced and thus, they are unable to predict geosmin episodes. Most of these companies cannot incorporate geosmin analytics into their laboratories as geosmin analyses are complex and time-consuming. Moreover, the high analytical costs make difficult for the concerned companies to subcontract the geosmin analysis in external laboratories as a routine. The low capacity to predict geosmin presence in water leads to the reception of consumer complaints and economic losses associated with the decrease in water consumption supplied by the drinking water treatment plants (DWTP). In that sense, there is a growing need to know the drivers associated with the production of geosmin in rivers, helping drinking water treatment companies to be prepared for possible geosmin episodes.

In the Osona region (Catalonia, NE Spain), drinking water treatment companies take water from the upper section of the Ter river to supply to the nearby cities and towns. In recent years, they have suffered several geosmin episodes that have led to customers complaints due to the inability to predict its appearance and to treat it before it reaches consumers houses. This situation has generated the need of a better understanding of the environmental factors associated with geosmin appearance.

6.1. Objective

The main objective of this study was to determine the main triggers of geosmin episodes in a Mediterranean river, subjected to seasonal and annual changes of the weather conditions. To this aim, a 3 years field monitoring (2017, 2018 and 2019) was performed in the upper part of the Ter river basin. In this field study, five sampling sites were evaluated, analyzing both physicochemical and biological parameters. Additionally, a study was carried out during 2017 with the aim of characterizing more precisely the possible anthropogenic pressures related to land uses of the upper part of the Ter river basin and their relationship with water quality. This information could help to explain the reasons why geosmin appears in one sampling site or another.

6.2. Material and methods

6.2.1. Study site

The Ter river is located in the NE of Catalonia (Spain). It is affected by the typical environmental fluctuations of the Mediterranean climate, with higher probability of precipitation during spring and autumn, and dry and warm summers. In the Ter river basin (208 km-long and 3010 km^2 of catchment area), there are anthropogenic activities that drastically affect water flow and quality. The most relevant are the following: (i) small and frequent dams to obtain hydraulic energy, (ii) livestock farming and intensive agriculture, leading to an increase of nutrients concentration, and (iii) a reservoirs system, which supplies energy and raw water for drinking purposes, and affects the river continuum concept differentiating two different areas, upstream and downstream reservoirs system (Céspedes et al., 2008). In this work, the upper part of the Ter river basin (upstream of the reservoirs system) have been studied. The area evaluated included the regions of El Ripollès and Osona, covering a surface of around 2000 km^2. El Ripollès region is at the head of the basin, starting in the Pyrenees, and it is characterized by presenting land uses classified as coniferous forest, natural grasslands, broods-leaved forest and moors and heathlands (CORINE land cover system, 2018). On the other hand, Osona region is affected by strong anthropogenic pressures, being the main land uses of this region related with non-irrigated arable land, industrial and commercial units, and continuous and discontinuous urban fabrics (CORINE land cover system, 2018) (**Figure 6.1.**).

Five sampling sites with different ecological characteristics were identified and choosen to perform a 3-year field study in order to evaluate the optimal conditions in triggering geosmin episodes. The sampling sites choosen were T1, T2, T5, T7 and G1 (**Figure 6.1.**). The upper sampling site located upstream (**T1**, **Figure 6.2.**) was located at the town of Vilallonga de Ter, 10.8 km downstream from the source of the Ter river and was considered as a control or a sampling site with better water quality. T1 is also characterised by a siliceous geological substratum. The next sampling site was located along the Ter river, downstream the municipality of Ripoll (**T2**, **Figure 6.3.**). At this place, the Ter has already received the input of the Freser river and some WWTP effluent. The third sampling site was in the Colonia de Borgonyà area, upstream the town of Torelló (**T5**, **Figure 6.4.)**, at one of the collection points of the drinking water company "Aigües d'Osona", which supplies drinking water to Torelló municipality and surroundings. The last sampling site along the river Ter (**T7**, **Figure 6.5.**) was located in Gurb municipality, 100m upstream to the collection point of "Aigües de Vic", the drinking water company which supplies the city of Vic and surroundings. The sampling site located in the Ges

river (**G1**, **Figure 6.6.**) was located near to its spring (4.3 km from it) and upstream of Sant Pere de Torelló municipality. G1 is considered a control site in a calcareous geological substratum catchment.

To asses the possible anthropogenic factors present in the study area, and their effect on water quality, a parallel study was carried out during 2017. In this study, 13 sampling sites distributes along the upper part of the Ter river basin were evaluated: 8 were located in the Ter river (T1 – T8), 1 was located in the Freser river (F), 2 in the Ges river (G1 and G2), 1 in the Sorreigs stream (S) and 1 in the Gurri river (Gu) (**Figure 6.1.**).

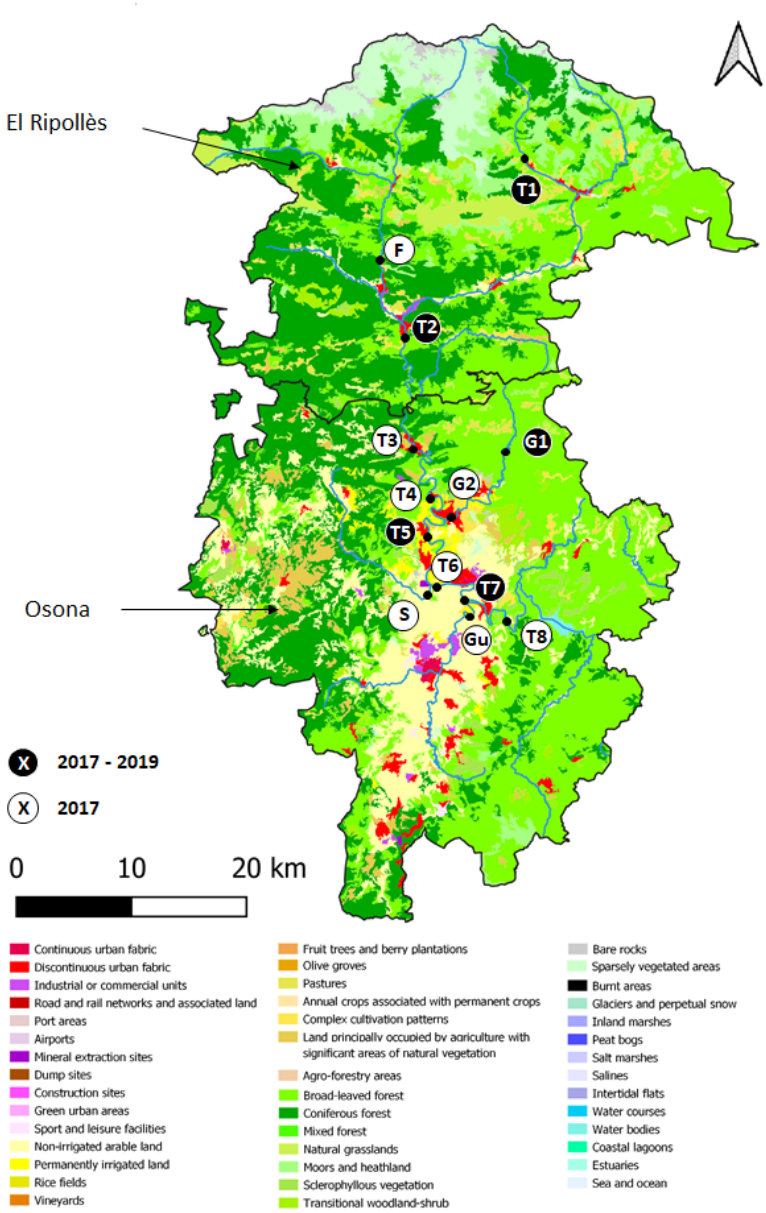

Figure 6.1. Map of land uses catgorized by the CORINE land cover system (2018), of El Ripollès and Osona regions (NE Catalonia, Spain). The white circles referred to the 2017 sampling sites and the black circles referred to the 2017 – 2019 sampling sites.

Figure 6.2. Ter river at Vilallonga de Ter (T1 sampling site) (El Ripollès region) (2019).

Figure 6.3. Ter river downstream Ripoll municipality (T2 sampling site) (El Ripollès region) (2019).

Figure 6.4. Ter river at Colonia de Borgonyà area, upstream Torelló municipality (Osona), and the collection point of "Aigües d'Osona" water drinking company (T5 sampling site) (2019).

Figure 6.5. Ter river at Gurb municipality (Osona), 100m upstream the collection point of "Aigües de Vic" water drinking company (T7 sampling site) (2019).

Figure 6.6. Ges river upstream San Pere de Torelló municipality (G1 sampling site) (2019).

6.2.2. Sampling procedure and physicochemical and biological analysis

Both in the study performed between 2017 – 2019 in five sampling sites, and in the one performed in 2017 in 13 sampling sites, physicochemical and biological parameters were monitored. Nevertheless, some of the parameters evaluated were specific of the study.

In both studies, the following physicochemical parameters were measured *in situ* with specific probes: temperature, dissolved oxygen concentration and oxygen saturation (YSI professional plus, YSI Incorporated, USA), pH (XS pH7+ DHS) and electrical conductivity (XS COND 7+). Water samples were taken and filtered through 0.2 µm nylon membranes filters (Merck Millipore) before the analysis of Soluble Reactive Phosphorus (SRP), NH_4^+, NO_2^- and NO_3^-. 1L water sample was also taken for the analysis of turbidity, suspended solids and organic matter. All samples were stored at -20°C until analysis, which were performed as described in **Chapter 3**. In addition, three cobbles were taken from each sampling site to take biofilm samples for the analysis of Chlorophyll *a* (Chl-*a*) and to obtain the Margalef Index (MI). Biofilm samples were stored at -20°C until analysis which was performed as described in **Chapter 3**.

In the monitoring performed in 2017, chlorides and sulphates concentration in water were also analyzed, while in the sampling done in 2018 and 2019 these analyzes were not made. In the field study performed between 2017 and 2019, a 1L opaque glass bottle was used to collect the

water sample for geosmin quantification, the bottles were stored at 4°C in dark conditions until the analysis, that was performed between 2 – 3 days after collection to avoid degradation and volatilization. Furthermore, in 2019, from each sampling site three cobbles were randomly taken to perform the evaluation of the photosynthetic efficiency and the phototrophic community composition of the biofilm, which was measured *in situ* with an amplitude modulated fluorimetry (Mini-PAM fluorometer Walz, Effeltrich, Germany), and with a BenthoTorch (bbe Moldaenke, Schwentinenta, DK), respectively, as described in **Chapter 3**. After that, each cobble was scrapped in 60 mL of water from the same sampling site to obtain a biofilm suspension. Aliquots of this suspension were used to analyze ash free dry mass (AFDM) and to obtain the Autotrophic Index, being stored frozen (-20°C) until analysis. Aliquots of this suspension were also taken to analyze geosmin in biofilm, but due to the COVID-19 pandemic, only some punctual samples have been analyzed. All the biofilm analysis were performed as described in **Chapter 3**.

During winter (January - March) and spring (April -June) seasons, weekly or bi-weekly sampling campaigns were carried out, whereas from July to November, monthly sampling campaigns were done. The higher sampling intensity during winter and spring was related to the higher probability of geosmin occurrence during these seasons (Vilalta et al., 2004). The total number of sampling days were 53, distributed during the 3 years.

Together with the laboratory analysis, the land uses of the surrounding area affecting the 13 sampling sites evaluated in 2017 were classified and calculated. To obtain this information, spatial analysis was computed using QGIS software as described in the **Chapter 3** of this Thesis.

6.2.3. Data treatment

Before the statistical analysis, the Kolmogorov - Smirnov test was performed to verify that the variables fulfilled the conditions on normal distribution, and if they did not, they were logarithmically transformed. Physicochemical and biological data were analysed using an analysis of variance (ANOVA) using SPSS Statistics software (version 21), being the sampling site, the season, the year and its interaction the factors evaluated. Correlations between geosmin and physicochemical and biological parameters were tested using Pearson's correlation coefficients. This test was also used to evaluate the relationship between land uses and the parameters evaluated in the 2017 study. Statistical significance was set at $p < 0.05$ for all test performed. The distribution of the sampling sites according to the variables was evaluated using a principal component analysis (PCA), performed with RStudio software (version 3.6.0).

6.3. Results

6.3.1. Land uses and its linkage with water quality: one-year field study (2017)

6.3.1.1. Land uses

Different land uses were identified between El Ripollès and Osona regions, mainly related to the economic activities. The composition (%) of land uses types in the 13 study areas are shown in **Figure 6.7**. In this figure, a clear difference can be seen when comparing the header of the river basin located in El Ripollès region and the downstream sections located in Osona region. The highest percentage of forests and scrubs areas was found in El Ripollès area, which is located in the upper part of the basin (T1, T2, T3 and F), with values ranging from 30 to 75%. On the contrary, the sampling sites located in Osona, where higher human activities are carried out, present higher percentages of agriculture (arable land) and industrial/urban/fabric areas. The two sampling sites with higher percentage of arable land are S (62%) followed by Gu (53%), and the areas located downstream (T7 and T8) had a higher percentage of urban fabric and industrial areas (between 25 and 35%). G1 sampling area stands out for being the one with the highest pastures land use value (85%).

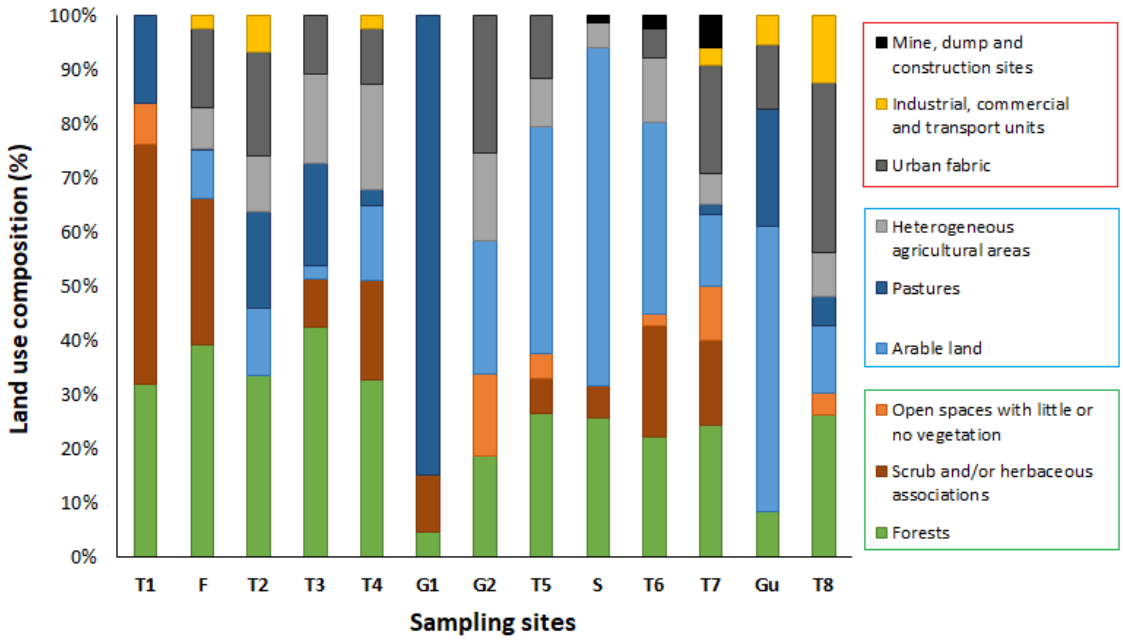

Figure 6.7. Composition (%) of land use types in the 13 different zones in the upper Ter river basin evaluated (NE Catalonia, Spain). In the green box are the land uses from the "Forest and semi-natural areas" (Level 1 CORINE land cover classification), in the blue box are the land uses from the "Agricultural areas" group, and in the red box are the land uses from the "Artificial surfaces" group.

6.4.1.2. Water quality

The sampling sites located in header areas (T1, F, G1 and T2) presented significantly lower values for all physicochemical and biological variables evaluated (ANOVA test) (**Table 6.1.**). Downstream from the headwaters, and associated with the increase in anthropogenic pressures, an increase in the values of the assessed variables was observed. The S and Gu sampling sites stand out above all, with the higher values. The highest differences were found for conductivity (872 ± 148 µS/cm in S and 1421 ± 216 µS/cm in Gu), chlorides (52.8 ± 8.8 mg/L in Sorreigs stream and 216 ± 60 mg/L in Gurri river), sulfates (147 ± 22 mg/L in S and 169 ± 32 I Gu) and all the nitrogenous forms (**Table 6.1.**). The values of chlorophyll *a* and Margalef Index also increase in the sampling sites located downstream. Differences were also observed in the parameters values depending on the season (ANOVA), specifically temperature, electrical conductivity, dissolved oxygen, turbidity, phosphates concentration, sulphates concentration, chlorophyll *a* concentration and Margalef Index ($p < 0.05$). Turbidity, phosphates and sulphates concentration values were higher in spring (Bonferroni test; $p < 0.01$), whereas chlorophyll a and MI values were higher in winter (Bonferroni test; $p < 0.01$).

A principal component analysis (PCA) was carried out with the results obtained in the field study to obtain groups of variables whose dynamics were similar and thus establish an order for the different river sampling sites (**Figure 6.8.**). The first component (45.2% of the variance) is strongly correlated with the conductivity, the concentration of chloride and sulphate, and nitrite and nitrate concentration. The sampling sites mainly differentiated by these variables are the Gurri river (Gu) and the Sorreigs stream (S). Other variables like distance to the mouth and altitude above sea level are negatively correlated to these parameters. The second component (21.5 % of variance) orders the sampling sites according to the longitudinal sequence from the head to the mouth of the river and corresponds with an increase in the nutrients and Chlorophyll *a* concentration. Sampling site T6 is out of place in this natural sequence and it is because it receives the highly polluted inflow of the Sorreigs stream (sampling site S).

Some of the parameters evaluated presented significant correlations with the arable land use category (Pearson's correlation). Specifically, electrical conductivity, chlorides, sulfates, nitrates and phosphates concentration ($p < 0.01$), chlorophyll concentration and organic matter ($p < 0.05$) were positively correlated. These same parameters presented negative correlations with the forest land use (Pearson's correlation). The value of the Pearson's coefficient varied depending on the season, being in the specific case of the phosphorus correlation with arable land, higher in spring ($r = 0.485$). For nitrites, nitrates and ammonium concentration, the coefficient is higher in summer ($r = 0.665$; $r = 0.809$ and $r = 0.462$, respectively).

Table 6.1. Mean values and standard deviation for all the variables evaluated in 2017 (n = 22) in the upper Ter river basin (NE Catalonia, Sapin): altitude (in m), distance to the mouth (in km), pH, electrical conductivity (EC, in µS/cm), temperature (T, in °C), dissolved oxygen (DO, in mg/L), oxygen saturation (Sat, in %), turbidity (Turb.), organic matter (OM), nitrite concentration (in $N\text{-}NO_2^-$ µg/L), nitrate concentration (in $N\text{-}NO_3^-$ mg/L), ammonium concentration (in $N\text{-}NO_4^+$ µg/L), phosphate concentration (in $P\text{-}PO_4^{3-}$ µg/L), chlorides (Cl^-, in mg/L), sulphates (SO_4^{3-}, in mg/L), suspended solids (SS, in mg/L), Chlorophyll a (in µg/cm^2) and Margalef Index (MI), for all the sampling sites: T = Ter river, F = Freser river, G = Ges river, S = Sorreigs stream and Gu = Gurri river.

Sampling Site	Altitude	Distance	pH	EC	Tª	DO	Sat.	Turb.	OM	$N\text{-}NO_2^-$	$N\text{-}NO_3^-$	$N\text{-}NH_4^+$	$P\text{-}PO_4^{3-}$	Cl^-	SO_4^{3-}	SS	Chl-a	MI
T1	1067	10.77	8.1 ± 0.2	131 ± 15	11 ± 4	10.1 ± 1.5	93 ± 8	2.3 ± 1.6	0.1 ± 0.0	2.3 ± 0.4	0.58 ± 0.34	11.9 ± 13.3	24 ± 26	4.3 ± 0.6	24 ± 9	3 ± 5	1.1 ± 0.5	2.3 ± 0.2
F	828	42.25	8.4 ± 0.1	233 ± 65	12 ± 3	10.2 ± 1.6	95 ± 7	2.8 ± 0.3	0.2 ± 0.1	3.0 ± 0.6	0.75 ± 0.35	20.2 ± 4.3	23 ± 15	6.0 ± 1.7	30 ± 15	4 ± 2	0.5 ± 0.2	2.2 ± 0.3
T2	691	18.20	8.5 ± 0.1	271 ± 44	14 ± 5	10.0 ± 1.6	98 ± 10	1.9 ± 0.5	0.2 ± 0.0	11.7 ± 4.3	0.65 ± 0.26	9.6 ± 9.0	31 ± 9	9.3 ± 1.5	34 ± 3	1 ± 1	1.9 ± 1.1	2.3 ± 0.3
T3	587	55.78	8.5 ± 0.1	290 ± 54	14 ± 6	10.8 ± 1.8	104 ± 7	2.5 ± 0.4	0.3 ± 0.0	11.1 ± 1.9	0.71 ± 0.26	16.9 ± 7.0	23 ± 10	11.0 ± 1.0	35 ± 3	17 ± 25	4.2 ± 1.3	2.7 ± 0.2
T4	554	62.78	8.4 ± 0.2	209 ± 65	12 ± 5	11.4 ± 1.6	106 ± 7	6.8 ± 6.1	0.4 ± 0.2	10.7 ± 3.9	0.65 ± 0.45	62.5 ± 53.5	54 ± 34	10.5 ± 2.1	38 ± 7	89 ± 296	5.7 ± 4.8	2.4 ± 0.4
G1	621	4.32	8.7 ± 0.2	328 ± 57	16 ± 7	10.3 ± 1.8	101 ± 11	1.6 ± 2.0	0.3 ± 0.0	7.0 ± 6.1	0.56 ± 0.25	7.8 ± 8.9	37 ± 25	6.8 ± 1.0	27 ± 2	3 ± 5	1.5 ± 0.7	2.4 ± 0.2
G2	520	14.63	8.6 ± 0.3	472 ± 91	15 ± 6	12.5 ± 1.3	126 ± 19	2.6 ± 1.8	0.6 ± 0.1	16.7 ± 9.5	1.49 ± 0.50	53.5 ± 34.8	49 ± 36	12.9 ± 2.8	43 ± 6	1 ± 21	6.7 ± 3.7	2.3 ± 0.3
T5	533	72.80	8.5 ± 0.2	307 ± 70	14 ± 6	11.1 ± 1.9	105 ± 9	6.4 ± 4.5	0.4 ± 0.2	11.0 ± 2.8	0.79 ± 0.36	100 ± 98.3	81 ± 71	10.8 ± 1.7	37 ± 6	80 ± 268	5.5 ± 2.7	2.6 ± 0.2
S	519	9.51	8.5 ± 0.4	872 ± 148	13 ± 5	11.7 ± 2.8	110 ± 24	3.5 ± 4.0	1.2 ± 0.3	71.7 ± 35.3	8.76 ± 1.64	128 ± 31.6	173 ± 184	52.8 ± 8.8	147 ± 22	3 ± 4	4.7 ± 2.7	2.1 ± 0.2
T6	519	77.63	8.4 ± 0.3	366 ± 70	14 ± 6	11.2 ± 1.7	108 ± 10	11.4 ± 4.6	0.6 ± 0.2	22.2 ± 6.7	2.18 ± 0.60	119 ± 99.6	115 ± 89	17.1 ± 1.2	51 ± 10	118 ± 372	5.3 ± 3.6	2.6 ± 0.2
T7	461	84.93	8.3 ± 0.2	321 ± 63	13 ± 6	10.4 ± 2.3	101 ± 12	10.8 ± 5.1	1.2 ± 2.4	16.1 ± 4.8	1.08 ± 0.31	115 ± 89.1	134 ± 76	13.0 ± 3.3	41 ± 6	57 ± 161	5.9 ± 4.7	2.5 ± 0.2
Gu	429	27.97	8.2 ± 0.2	1421 ± 216	16 ± 5	10.0 ± 2.6	98 ± 20	9.8 ± 10.5	2.6 ± 2.4	513 ± 330	8.11 ± 2.42	2528 ± 1504	692 ± 267	216 ± 60	169 ± 32	9 ± 11	6.9 ± 3.5	2.1 ± 0.3
T8	443	87.43	8.2 ± 0.4	395 ± 76	14 ± 6	9.9 ± 2.0	95 ± 11	12.5 ± 6.9	0.7 ± 0.2	36.1 ± 14.5	1.31 ± 0.33	265 ± 154	165 ± 69	20.5 ± 5.2	46 ± 8	87 ± 254	5.0 ± 4.2	2.4 ± 0.3

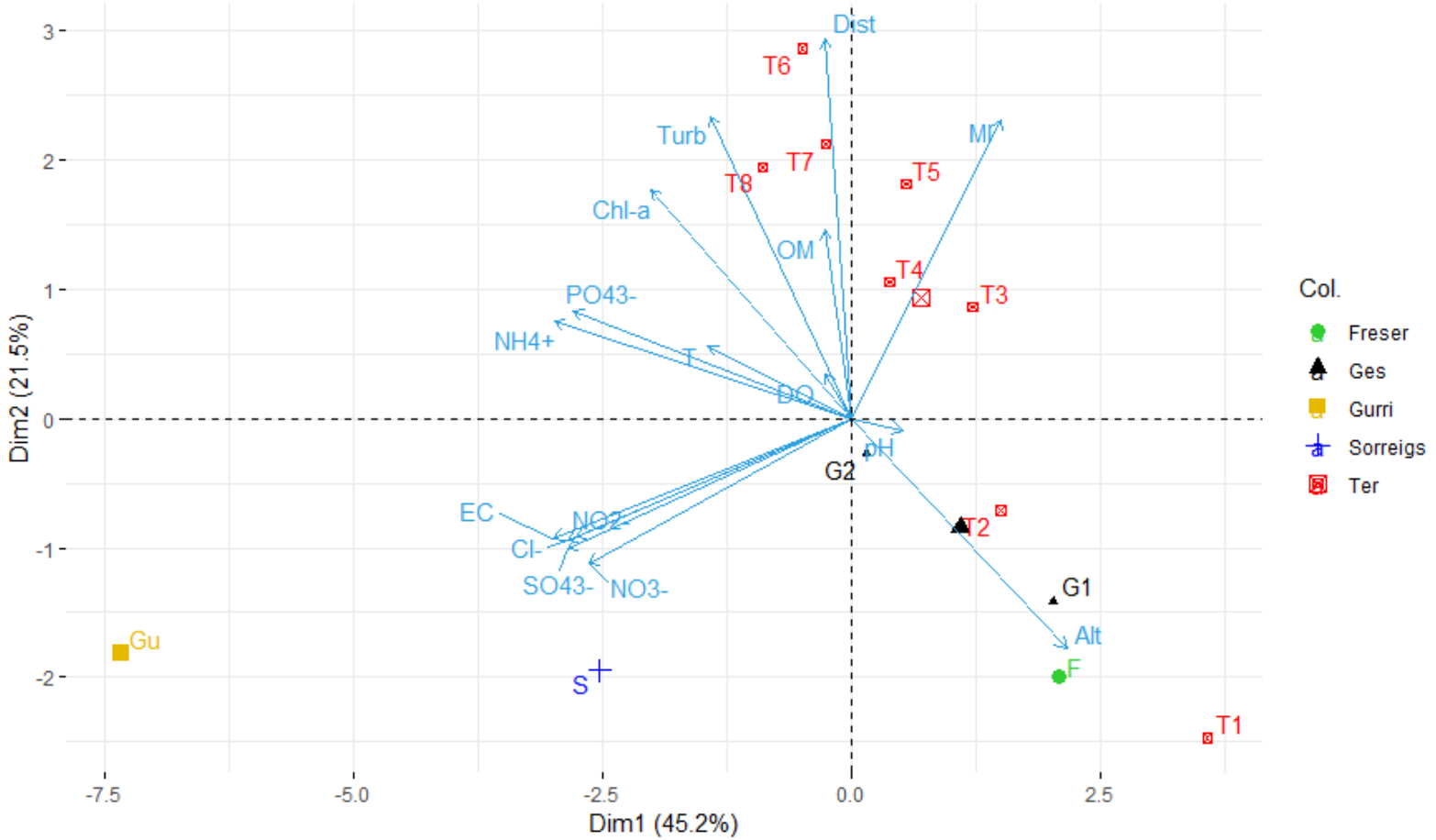

Figure 6.8. Principal Component Analysis showing sampling sites distribution based on the variables evaluated in 2017 in the upper Ter river basin (NE Catalonia, Spain). Axes 1 and 2 combined explain 66.7% of the variance. Sites are differentiated by color: green = Freser river, black = Ges river, yellow = Gurri river, blue = Sorreigs stream and red = Ter river. Variables: pH, Temperature (Temp), electrical conductivity (EC), turbidity, organic matter (OM), dissolved oxygen (DO), nitrite ($N\text{-}NO_2^-$), nitrate ($N\text{-}NO_3^-$), ammonium ($N\text{-}NH_4^+$) and phosphates concentration ($P\text{-}PO_4^{-3}$), chlorides (Cl^-), sulphates (SO_4^{3-}), altitude (Alt) and distance to the mouth (Dist).

6.4.2. Geosmin drivers: three-years field study (2017 – 2019)

6.4.2.1. Geosmin concentration

The presence and concentration of geosmin varied throughout the three years in which the present study was carried out. The highest geosmin concentration was detected in 2019, with a maximum of 249 ± 33 ng/L at sampling site T7 at the end of March (**Figure 6.9.)**. Throughout this year, geosmin was detected at all sampling sites except the one located at the headwaters of the Ter river (T1). In 2017, geosmin was also detected, but in lower concentrations, reaching a maximum geosmin concentration of 52 ng/L at sampling site T5. In 2018, geosmin was not detected at any sampling site. Seasonality also played an important role in geosmin appearance, being during late winter and early spring were the highest values of geosmin were found.

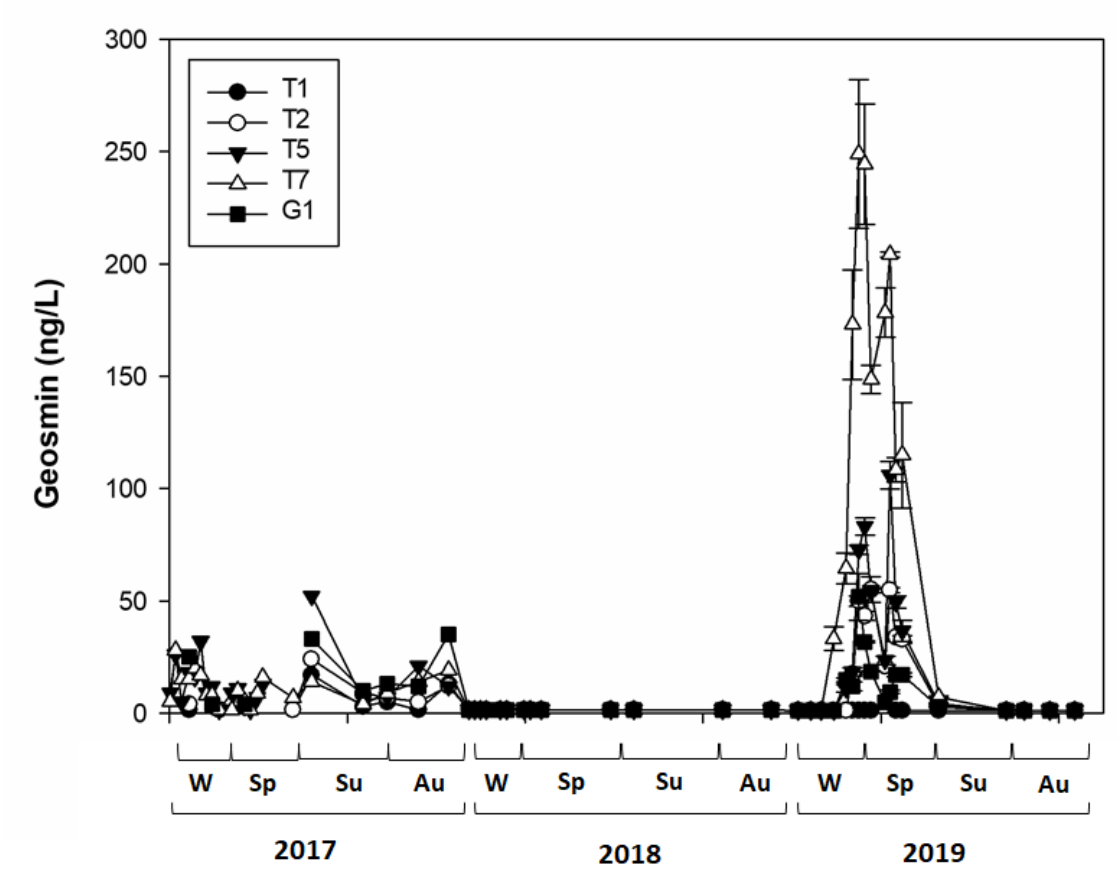

Figure 6.9. Mean value and standard deviation of geosmin concentration in water for the different sampling sites in the upper Ter river basin (NE Catalonia, Spain) (T1 = Ter at Vilallonga de Ter, T2 = Ter at Ripoll, T5 = Ter at Colònia de Borgonyà, T7 = Ter at Gurb and G1 = Ges upstream San Pere de Torelló) for the different sampling days in 2017, 2018 and 2019, being W = winter, Sp = spring, Su = summer and Au = autumn.

Statistically, the geosmin presence in water was significantly affected by the sampling site ($F = 5.697$; $p < 0.001$), the season ($F = 5.673$; $p < 0.001$), the year ($F = 11.302$; $p < 0.001$) and the interactions of the factors ($p < 0.001$ in all the combinations). Sampling site T7 was statistically different from the others (Bonferroni test: $p < 0.001$) being the one with the highest geosmin concentration, and T1 was also statistically different from the rest, in this case for being the one with the lowest values (Bonferroni test: $p < 0.05$). Spring was the season that differs from the rest ($p < 0.001$), being at this season and at T7 sampling site when the highest geosmin concentration was detected in 2019.

Geosmin concentration was positively correlated with pH, temperature, turbidity, nitrites and phosphates concentration(Pearson's correlation, $p < 0.01$ all cases), and negatively correlated with the N:P ratio and the dissolved oxygen (Pearson's correlation, $p < 0.01$ in both cases).

6.4.2.2. Physicochemical parameters

Some of the evaluated physicochemical variables (**Table 6.2.**) changed significantly depending on the sampling site (detailed data by site, season and year in **Annex A**). The lowest values for most of the parameters were found at sampling site T1, mainly highlighting pH, electrical conductivity, temperature and nutrient concentration (ANOVA, $p < 0.05$). The G1 sampling site was the one that presented values more similar to T1 in some of the evaluated parameters, also presenting low values of nutrient concentration, being the sampling site where the lowest phosphorus concentration was detected, 25 ± 22 µgP-PO_4^{3-} comparing with 82 ± 68 µgP-PO_4^{3-} in T7 ($p < 0.01$). Sampling site T7 presented opposite results compared with T1, with very high values especially for the nitrogen forms, whose concentration increases up on average to four times compared to T1.

Seasonality also had an effect in some of the physicochemical parameters evaluated, differentiating electrical conductivity, temperature, dissolved oxygen, phosphates concentration and suspended solids ($p < 0.05$).

During the three years in which this study was carried out, the climatic conditions were very different, particularly regarding precipitation, temperature and water flow (ACA, 2020; Meteocat, 2019). The year 2017 was characterized by higher temperatures and some punctual precipitation, which meant a slight reduction in the water flow of the Ter river (10.9 ± 8.7 m^3/s) compared to the year 2018 (22.7 ± 11.4 m^3/s). The year 2018 had lower water temperature values (6.1 ± 2.5°C) and a greater amount of precipitations (2.03 ± 3.45 L/m^2), which generated an increase in water flow, on average around 5 times greater than in 2019. The year 2019 stood

out for being a very dry year, with a shortage of precipitation (1.32 ± 2.24 L/m^2); combined with higher temperatures (9.9 ± 4.8°C), historical minimums were reached in the water flow values (4.58 ± 3.27 m^3/s).

These different scenarios have also affected the physicochemical parameters evaluated. Specifically, the year 2018 differs from the rest, presenting higher electrical conductivity, dissolved oxygen and N:P values ($p < 0.05$), and a lower concentration of nitrites and phosphates ($p < 0.01$).

A Principal Component Analysis (PCA) was performed with the dataset generated from the average of the three years, to highlight how the sampling sites were distributed according to the different variables (**Figure 6.10.**). This analysis emphasizes that the X axis (explaining the 33.7% of variance) separates the sampling sites in an upstream-downstream gradient, according to water quality, being geosmin and nutrient concentration located in the right area of the figure where the sampling sites located downstream are placed. The Y axis (22.7% of variance) differentiates the sampling sites depending on the season.

Table 6.2. Mean value and standard deviation of the physicochemical variables evaluated for the different sampling sites in the upper Ter river basin (NE Catalonia, Spain) between 2017 and 2019: T1 = Ter at Vilallonga de Ter, T2 = Ter at Ripoll, T3 = Ter at Colònia de Borgonyà, T4 = Ter at Gurb, and G1 = Ges upstream San Pere de Torelló, in winter (W) (n=20), spring (Sp) (n=17), summer (Su) (n=7) and autumn (Au) (n=8).

		pH	EC (µS/cm)	Temp. (ºC)	DO (mg/L)	Sat. (%)	$N\text{-}NH_4^+$ (µg/L)	$N\text{-}NO_2^-$ (µg/L)	$N\text{-}NO_3^-$ (mg/L)	$P\text{-}PO_4^{3-}$ (µg/L)	N:P	SS (mg/L)	Turbidity (NTU)	OM
T1	**W**	7.8 ± 0.6	153 ± 32	4.6 ± 1.3	12.1 ± 1.0	99 ± 16	55 ± 40	2 ± 1	0.37 ± 0.07	66 ± 68	27 ± 19	29 ± 19	13 ± 11	0.395 ± 0.339
	Sp	7.9 ± 0.3	149 ± 37	7.4 ± 1.6	11.6 ± 1.0	105 ± 11	26 ± 13	3 ± 2	0.42 ± 0.06	96 ± 94	19 ± 14	8 ± 4	12 ± 10	0.226 ± 0.348
	Su	8.1 ± 0.4	150 ± 24	12.9 ± 3.0	10.1 ± 1.0	98 ± 10	45 ± 34	9 ± 10	0.30 ± 0.20	36 ± 50	31 ± 20	6 ± 5	10 ± 7	0.297 ± 0.386
	Au	7.8 ± 0.4	148 ± 30	7.0 ± 2.9	11.9 ± 2.0	100 ± 18	21 ± 14	3 ± 5	0.33 ± 0.22	18 ± 10	60 ± 41	13 ± 14	10 ± 7	0.338 ± 0.442
T2	**W**	8.3 ± 0.4	250 ± 46	6.2 ± 2.1	12.7 ± 1.1	106 ± 10	79 ± 35	7 ± 5	0.61 ± 0.16	54 ± 40	42 ± 43	16 ± 11	23 ± 9	0.229 ± 0.261
	Sp	8.3 ± 0.4	291 ± 61	9.5 ± 1.2	11.6 ± 0.7	108 ± 8	54 ± 27	9 ± 8	0.61 ± 0.14	48 ± 25	37 ± 24	23 ± 14	20 ± 8	0.130 ± 0.151
	Su	8.2 ± 0.5	293 ± 67	16.0 ± 3.4	10.2 ± 1.6	104 ± 12	61 ± 33	20 ± 26	0.78 ± 0.54	29 ± 28	74 ± 44	14 ± 13	21 ± 8	0.115 ± 0.091
	Au	8.2 ± 0.5	324 ± 67	7.8 ± 4.4	12.8 ± 1.8	109 ± 13	45 ± 29	14 ± 16	0.48 ± 0.14	34 ± 25	69 ± 55	20 ± 17	22 ± 27	0.282 ± 0.341
T5	**W**	8.4 ± 0.3	343 ± 87	7.5 ± 2.4	12.9 ± 1.1	108 ± 9	80 ± 74	8 ± 5	0.75 ± 0.19	73 ± 57	50 ± 52	27 ± 16	18 ± 13	0.408 ± 0.286
	Sp	8.4 ± 0.1	302 ± 85	12.0 ± 2.5	10.8 ± 1.2	103 ± 10	75 ± 70	10 ± 6	0.67 ± 0.29	73 ± 55	31 ± 18	29 ± 26	19 ± 15	0.327 ± 0.326
	Su	8.5 ± 0.2	338 ± 91	17.2 ± 5.7	11.2 ± 3.1	107 ± 8	78 ± 38	19 ± 23	0.77 ± 0.50	82 ± 100	39 ± 24	19 ± 9	12 ± 5	0.353 ± 0.332
	Au	8.4 ± 0.2	366 ± 76	9.7 ± 5.4	12.7 ± 2.1	111 ± 12	92 ± 119	36 ± 74	0.73 ± 0.45	80 ± 113	71 ± 56	27 ± 21	12 ± 9	0.346 ± 0.352
T7	**W**	8.4 ± 0.3	388 ± 70	7.4 ± 2.4	12.3 ± 0.7	104 ± 8	119 ± 49	14 ± 10	1.48 ± 0.68	87 ± 87	75 ± 61	31 ± 20	21 ± 15	0.349 ± 0.199
	Sp	8.3 ± 0.2	326 ± 75	12.6 ± 3.2	10.4 ± 2.0	101 ± 13	122 ± 90	19 ± 9	1.15 ± 0.42	80 ± 47	54 ± 38	34 ± 29	26 ± 21	0.350 ± 0.301
	Su	8.7 ± 0.5	374 ± 66	21.2 ± 4.3	9.5 ± 1.4	106 ± 12	93 ± 33	26 ± 21	1.23 ± 0.88	102 ± 76	54 ± 53	40 ± 5	18 ± 7	0.187 ± 0.154
	Au	8.4 ± 0.4	405 ± 90	9.7 ± 5.4	11.9 ± 3.0	108 ± 15	75 ± 67	17 ± 9	1.60 ± 0.92	57 ± 47	150 ± 129	19 ± 20	11 ± 9	0.263 ± 0.171
G1	**W**	8.6 ± 0.2	386 ± 67	5.5 ± 3.6	12.3 ± 1.1	99 ± 8	102 ± 70	3 ± 3	0.53 ± 0.29	30 ± 24	104 ± 155	77 ± 103	28 ± 26	0.255 ± 0.189
	Sp	8.7 ± 0.2	377 ± 64	11.4 ± 3.3	11.3 ± 1.3	108 ± 10	45 ± 27	3 ± 2	0.64 ± 0.25	29 ± 24	115 ± 126	67 ± 31	49 ± 32	0.202 ± 0.190
	Su	8.7 ± 0.2	367 ± 104	19.4 ± 7.3	10.0 ± 1.5	108 ± 15	38 ± 34	5 ± 6	0.28 ± 0.17	23 ± 25	51 ± 3	25 ± 21	14 ± 10	0.375 ± 0.275
	Au	8.7 ± 0.2	401 ± 120	7.9 ± 6.2	12.9 ± 1.9	108 ± 12	42 ± 36	2 ± 3	0.40 ± 0.23	12 ± 12	132 ± 106	40 ± 27	22 ± 15	0.249 ± 0.211

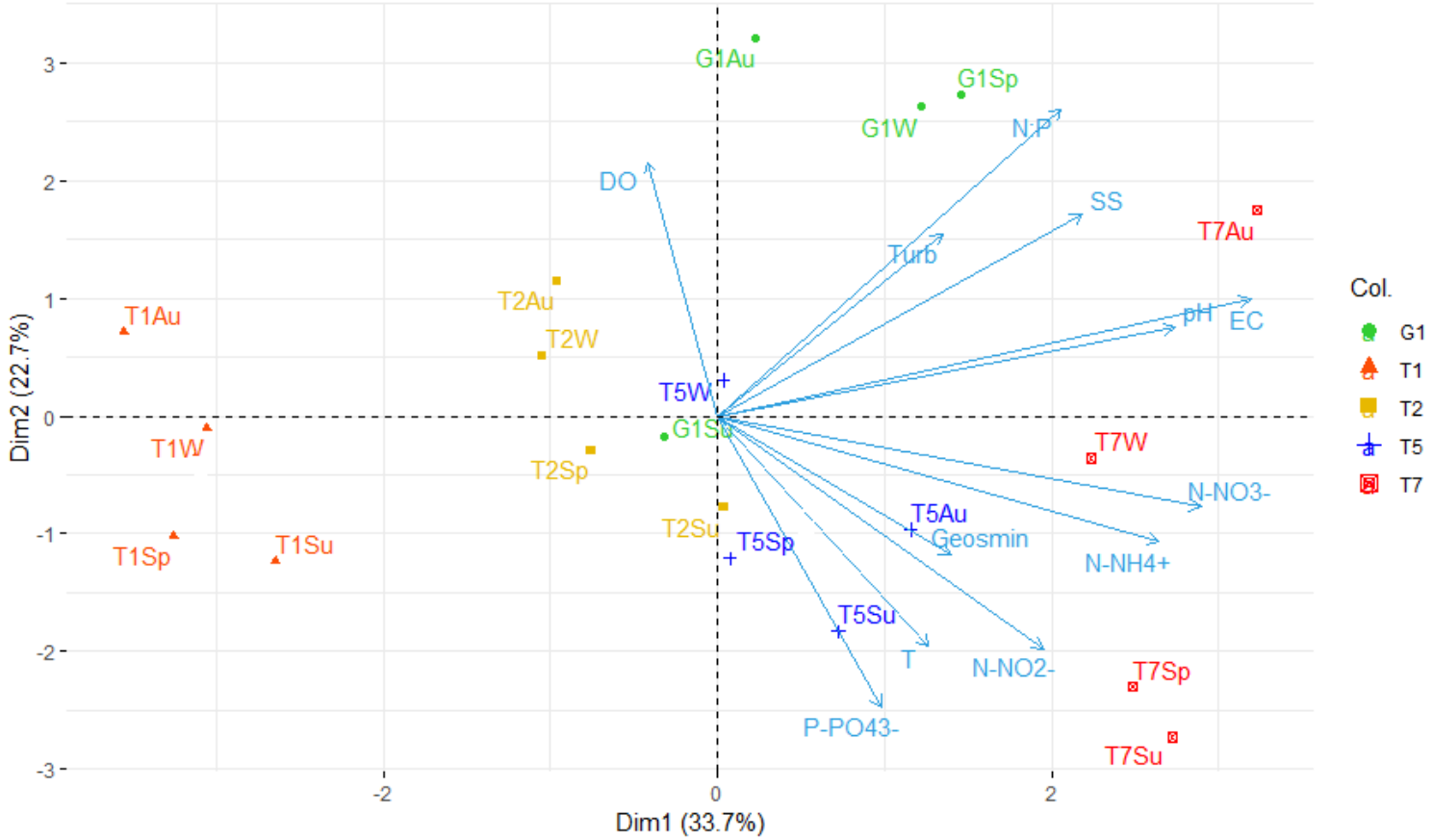

Figure 6.10. Principal Component Analysis showing sampling sites distribution based on the variables evaluated in the upper Ter river basin (NE Catalonia, Spain) between 2017 and 2019. Axes 1 and 2 combined explain 55.9% of the variance. Sites: T1 = Ter at Vilallonga de Ter, T2 = Ter at Ripoll, T3 = Ter at Colònia de Borgonyà, T4 = Ter at Gurb and G1 = Ges upstream San Pere de Torelló, in winter (W), spring (Sp), summer (Su) and autumn (Au). Variables: geosmin in water (Geo), pH, Temperature (Temp), electrical conductivity (EC), dissolved oxygen (DO), turbidity, organic matter (OM), nitrite ($N\text{-}NO_2^-$), nitrate ($N\text{-}NO_3^-$), ammonium ($N\text{-}NH_4^+$) and phosphates concentration ($P\text{-}PO_4^{-3}$) and nitrogen to phosphorus ratio (N:P).

In addition to this evaluation, the moment in which the highest geosmin concentration was detected was investigated in more detail, specifically the T7 sampling site in 2019.

At this sampling site, geosmin concentration was positively correlated with the phosphorus concentration (Pearson's correlation: $r = 0.789$, $p < 0.01$) and negatively correlated with the N:P ratio ($r = -0.868$, $p < 0.01$). Furthermore, geosmin concentration at this sampling site was affected by seasonality, being higher in spring compared with the other seasons. During this season, the N:P ratio was significantly lower (47:1 ± 16:1) compared with the others. On the contrary, autumn was the season showing the highest N:P ratio (221:1 ± 34:1), due to the important decrease of phosphorus concentration (19 ± 11 µg $P\text{-}PO_4^{3-}$ µg/L). In summer, both water temperature (24.4°C) and nitrite concentration (43 ± 26 µg $N\text{-}NO_2^-$/L) increased significantly. This distribution is shown in the PCA (**Figure 6.11.)**, where the X axis (34.9% of the variance) highlighted that the sampling days distribution was driven by five main variables: N:P ratio, nitrate and phosphate concentration, turbidity and geosmin concentration. It was observed that from the second sampling day of winter (W2) the tendency was to move from high N:P ratio values (187:1) towards lower ratios (48:1 in W6). This gradual decrease of N:P ratio was mainly guided by a fall in nitrate concentration (from 2.98 ± 0.02 to 1.26 ± 0.18 mg $N\text{-}NO_3^-$/L) conjointly with a relevant increase of phosphorus concentration (from 32 ± 3.5 to 70 – 100 ± 10.4 µg $P\text{-}PO_4^{3-}$ /L). This change in the N:P ratio seemed to trigger the progressive appearance of geosmin which raised from <2.5 ng/L in W3 to 173 ± 24 ng/L in W6 and reached its maximum in Sp1 (249 ± 33 ng/L).

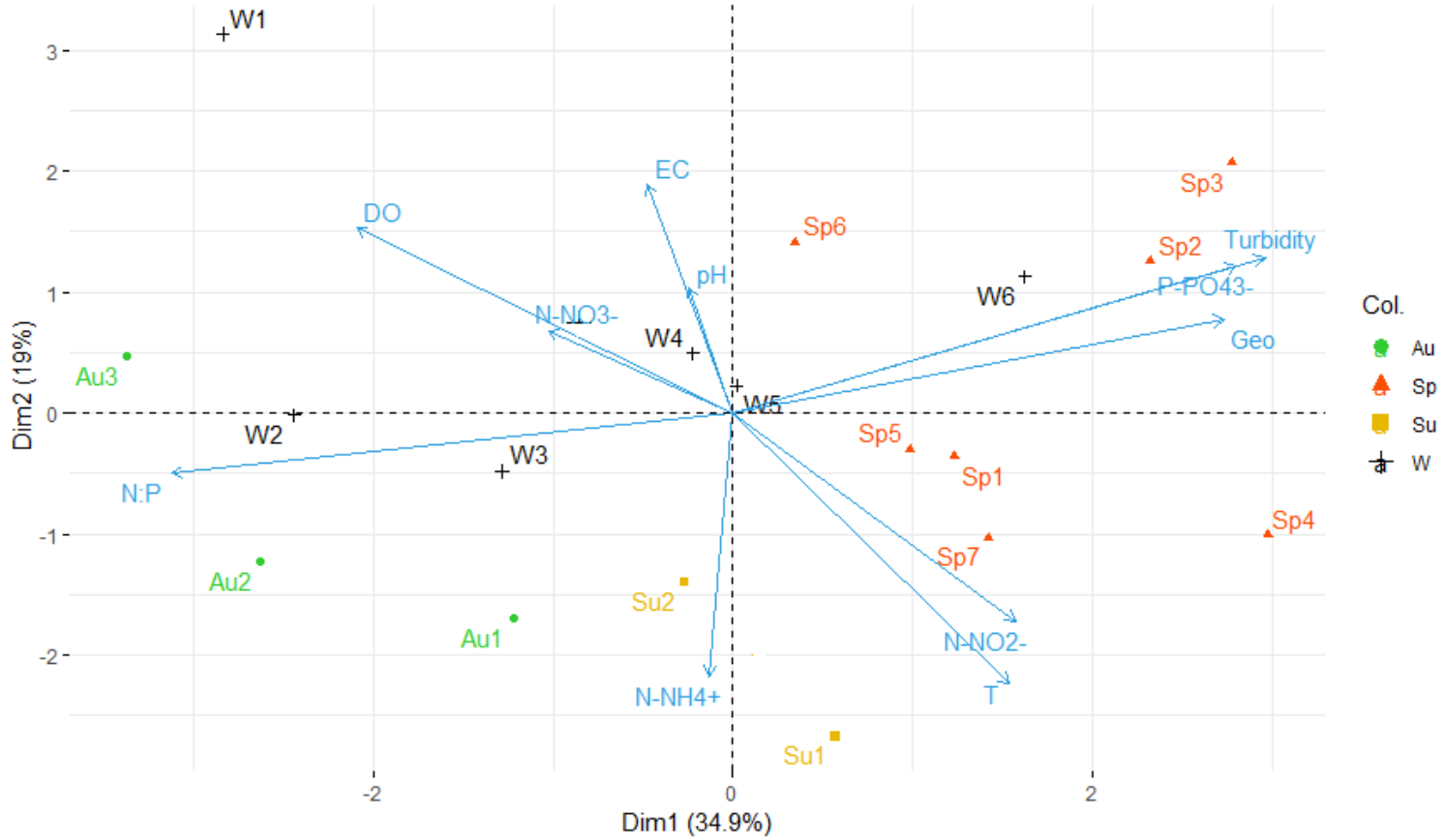

Figure 6.11. Principal Component Analysis showing T7 sampling site distribution based on the variables evaluated in 2019. Axes 1 and 2 combined explain 53.9% of the variance. Seasons are winter (W), spring (Sp), summer (Su) and autumn (Au). Variables: geosmin in water (Geo), pH, Temperature (T), electrical conductivity (EC), dissolved oxygen (DO), turbidity, nitrite ($N\text{-}NO_2^-$), nitrate ($N\text{-}NO_3^-$), ammonium ($N\text{-}NH_4^+$) and phosphate concentration ($P\text{-}PO_4^{-3}$) and nitrogen to phosphorus ratio (N:P).

6.4.2.3. Biological parameters

The biological parameters that were monitored in the three years field study were chlorophyll *a* and Margalef Index (MI). Both parameters presented significant differences depending on the sampling site, with the highest chlorophyll *a* values at sampling site T7 ($p < 0.01$), and the highest MI values at G1 ($p < 0.05$). The season also had an effect on the chlorophyll concentration, higher in winter compared to spring and summer ($p < 0.05$). On the other hand, the MI value was higher in summer compared to spring and autumn ($p < 0.05$). The effect of the year, however, was only reflected in the MI, being less in 2018 compared to the other two years of sampling ($p < 0.01$).

During 2019, additional biological parameters were measured, observing that the values differed depending on the sampling site (**Table 6.4.**), being in most of the cases the G1 significantly different from the others ($p < 0.05$). The sampling site located in the upper part of the Ter river basin (T1) also differed from the rest showing lower values of F_0 (biomass estimation given by the Mini-PAM) (106 ± 46) and cyanobacteria biomass (0.33 ± 0.44 µg Chl*a*/cm^2), whereas the highest chlorophyll *a* values (18.2 ± 17.8 µg/cm^2) were measured at T7 (downstream in the Ter river). Seasonality also affected the biological parameters evaluated. The phototrophic community presented higher biomass values in summer ($p < 0.01$), while the F_0 value was higher in autumn ($p < 0.05$), and chlorophyll *a* concentration, diatoms relative abundance and AFDM had higher values in winter ($p < 0.01$). Statistically, correlations analysis revealed that AFDM was positively correlated with geosmin concentration in water ($r = 0.279$; $p < 0.05$).

Evaluating the sampling site with the highest geosmin concentration (T7), it was found that geosmin concentration in water was negatively correlated with the F_0 (Pearson's correlation: $r = -0.681$, $p < 0.01$), diatoms biomass ($r = -0.661$, $p < 0.01$), Margalef Index ($r = -0.643$, $p < 0.01$) and chlorophyll *a* concentration ($r = -0.533$; $p < 0.05$).

The geosmin concentration in biofilm samples from sampling days with higher cyanobacteria relative abundance in T7 sampling site (12.03.19, 30.04.19 and 24.04.19) were analysed, obtaining the results present in **Table 6.3**.

Table 6.3. Mean value and standard deviation (n = 3) of geosmin concentration in biofilm samples (ng/mg) for three specific sampling days (12.03.19, 30.04.19 and 24.04.19), being LOD the limit of detection for the GC/MC (2.5 ng/L).

Sampling Date	Biofilm geosmin concentration (ng/mg)
12.03.19	0.663 ± 0.110
30.04.19	0.057 ± 0.022
24.04.19	<LOD

Table 6.4. Mean value and standard deviation of the biological variables evaluated for the different sampling sites in the upper Ter river basin (NE Catalonia, Spain) in 2019: T1 = Ter at Vilallonga de Ter, T2 = Ter at Ripoll, T3 = Ter at Colònia de Borgonyà, T4 = Ter at Gurb, and G1 = Ges upstream San Pere de Torelló, in winter (W), spring (Sp), summer (Su) and autumn (Au).

		F_0	Yeff	Cyanobacteria (µg/cm²)	Green Algae (µg/cm²)	Diatoms (µg/cm²)	Cyanobacteria (%)	Green Algae (%)	Diatoms (%)	Chl a (µg/cm²)	MI	AFDM (g/m²)	AI (log)
T1	**W**	113 ± 43	322 ± 92	0.16 ± 0.08	0.02 ± 0.05	3.67 ± 2.80	7.9 ± 7.5	0.0 ± 0.0	89.9 ± 12.0	3.9 ± 3.9	2.0 ± 0.2	44 ± 59	3.8 ± 4.0
	Sp	93 ± 54	350 ± 63	0.18 ± 0.07	0.19 ± 0.14	1.09 ± 0.33	13.3 ± 6.8	0.0 ± 0.0	73.9 ± 12.0	1.0 ± 0.8	1.9 ± 0.1	74 ± 69	4.6 ± 4.9
	Su	89 ± 30	368 ± 132	0.91 ± 1.03	0.00 ± 0.00	0.99 ± 0.39	38.2 ± 25.7	0.0 ± 0.0	61.8 ± 25.7	0.6	2.1	46 ± 61	4.1 ± 4.2
	Au	165	277	0.54 ± 0.61	0.03 ± 0.05	1.82 ± 0.30	19.81 ± 18.82	0.0 ± 0.0	79.3 ± 20.4	3.2 ± 1.8	2.0 ± 0.2	21 ± 18	3.6 ± 3.5
T2	**W**	160 ± 117	489 ± 80	0.45 ± 0.33	0.01 ± 0.03	3.21 ± 2.42	11.4 ± 5.9	0.0 ± 0.0	87.0 ± 3.3	23.9 ± 21.7	2.2 ± 0.1	299 ± 271	3.6 ± 3.6
	Sp	127 ± 58	435 ± 145	0.49 ± 0.27	0.45 ± 0.31	1.49 ± 0.62	19.5 ± 5.9	0.0 ± 0.0	62.2 ± 8.9	2.5 ± 1.6	2.0 ± 0.2	140 ± 111	3.9 ± 3.8
	Su	133 ± 80	452 ± 278	1.02 ± 0.35	0.00 ± 0.00	1.74 ± 0.99	39.5 ± 21.9	0.0 ± 0.0	60.5 ± 21.9	11.1	2.5	17 ± 1	3.0 ± 3.1
	Au	227	630	0.42 ± 0.36	0.00 ± 0.00	2.32 ± 1.43	14.5 ± 5.9	0.0 ± 0.0	85.5 ± 5.9	7.0 ± 8.0	2.3 ± 0.1	48 ± 41	3.1 ± 3.1
T5	**W**	189 ± 64	317 ± 106	0.78 ± 0.48	0.00 ± 0.00	3.59 ± 2.32	18.8 ± 6.2	0.0 ± 0.0	81.2 ± 6.2	18.0 ± 17.3	2.4 ± 0.1	134 ± 133	3.5 ± 2.9
	Sp	149 ± 43	355 ± 134	0.58 ± 0.26	0.03 ± 0.04	1.74 ± 0.53	24.8 ± 6.7	0.0 ± 0.0	74.0 ± 6.4	7.2 ± 3.1	2.3 ± 0.1	196 ± 208	3.7 ± 3.7
	Su	299 ± 108	501 ± 111	1.66 ± 1.12	0.11 ± 0.16	2.38 ± 0.34	37.7 ± 15.2	0.0 ± 0.0	58.8 ± 10.3	8.1	2.3	11.2 ± 1.9	2.2 ± 0.9
	Au	335	530	1.05 ± 0.25	0.00 ± 0.00	2.98 ± 0.71	26.2 ± 4.3	0.0 ± 0.0	73.8 ± 4.3	12.3 ± 2.7	2.3 ± 0.2	81 ± 74	2.9 ± 2.7
T7	**W**	219 ± 115	473 ± 106	0.91 ± 0.63	0.00 ± 0.00	4.19 ± 3.35	21.3 ± 13.7	0.0 ± 0.0	78.7 ± 13.7	31.2 ± 25.4	2.2 ± 0.2	269 ± 288	3.4 ± 3.2
	Sp	160 ± 50	467 ± 118	0.86 ± 0.64	0.02 ± 0.05	1.80 ± 0.41	28.9 ± 11.1	0.0 ± 0.0	70.3 ± 11.6	10.3 ± 6.2	1.8 ± 0.3	140 ± 102	3.4 ± 3.4
	Su	206 ± 0	570 ± 48	1.26 ± 0.31	0.02 ± 0.03	1.83 ± 0.02	40.2 ± 6.2	0.0 ± 0.0	59.0 ± 5.1	11.0	3.0	7	2.4 ± 1.6
	Au	318	499	0.80 ± 0.68	0.00 ± 0.00	5.10 ± 2.41	15.1 ± 14.8	0.0 ± 0.0	84.4 ± 14.8	12.9 ± 4.4	2.4 ± 0.2	48 ± 22	2.5 ± 1.9
G1	**W**	128 ± 38	199 ± 182	0.46 ± 0.30	0.02 ± 0.02	0.45 ± 0.09	46.9 ± 18.1	1.7 ± 2.4	51.4 ± 18.6	0.5	3.1	84.0	4.9
	Sp	148 ± 60	190 ± 142	0.65 ± 0.29	0.01 ± 0.03	1.33 ± 1.10	38.5 ± 12.2	1.2 ± 3.1	60.3 ± 13.3	1.2 ± 0.6	2.9 ± 1.2	119 ± 104	4.7 ± 4.9
	Su	253 ± 78	348 ± 48	0.97 ± 0.18	0.87 ± 1.23	0.99 ± 0.01	37.4 ± 12.4	22.6 ± 32.0	40.0 ± 19.6	6.1	2.4	70 ± 80	3.0 ± 3.0
	Au	331	280	1.03 ± 0.08	0.34 ± 0.33	1.15 ± 0.61	44.8 ± 19.8	12.0 ± 10.6	43.2 ± 13.3	10.5 ± 4.5	2.3 ± 0.1	58 ± 65	3.6 ± 3.6

6.5. Discussion

The study carried out for three years in the upper part of the Ter river basin allowed to highlight how the geosmin concentration is correlated with certain parameters and how its appearance is affected by both weather conditions and water quality.

During the three years in which this study was carried out, the geosmin concentration varied depending on the sampling site, the season and the year (**Figure 6.9**.). The effect of the sampling site was due to the fact that each of the sites evaluated presented different anthropogenic pressures that alter the quality of the waters. While the effect of the season and the year was because the Ter river basin is influenced by the Mediterranean climate, which is characterized by seasonal and interannual variations.

Water flow

Specifically, year 2018 was a very cold year, with an average water temperature of 6.1 ± 2.5°C and a lot of rainfalls and snows (2.03 ± 3.45 L/m^2) which was reflected in an increase in the mean water flow (data from the Water Catalan Agency, 2020). This same year, geosmin was not detected at any of the sampling sites (**Figure 6.9.**) Conversely, 2019 stood out for being a very dry year, with a shortage in precipitation reflected in the average annual value of 1.32 ± 2.24 L/m^2, that together with higher temperature values (9.9 ± 4.8°C) generated historical water flow minimums. In the specific case of the T7 sampling site, the water flow was about five times higher in 2018 than in 2019, going from an average of 22.7 ± 11.4 m^3/s in 2018 to 4.58 ± 3.27 m^3/s in 2019. This sampling site stood out for presenting the highest geosmin concentration at the end of March 2019 with a value of 249 ± 33 ng/L. This value was extremely and historically high, with few moments in which similar values occurred along the Ter river basin (personal communication from the DWTP personnel). Globally, the range of geosmin values reported is very wide, from values of 5 ng/L (Watson and Ridal, 2004) to values of 200 ng/L (Vilalta et al., 2004), with exceptional data such as those of Carcoar Dam (Australia), with 4000 ng/L (Jones and Korth, 1995). This wide range is certainly explained by the differences among the systems evaluated and the geosmin producers involved (Jüttner and Watson, 2007).

The situation observed in 2017 could be considered as intermediate between 2018 (no geosmin) and 2019 (important long episode) since there were punctual significant precipitations, which gave rise to intermediate water flows (10.9 ± 8.7 m^3/s). That year, geosmin was detected at some of the sampling sites (T5 and T7) but showing lower values (maximum 52 ng/L at T5) and shorter duration respect to 2019.

The difference of geosmin concentration depending on the year can be explained by the water flow conditions that can affect the biofilm biomass present in a river, where the main geosmin producers are benthic. In a situation of high water flow, biofilms are sloughed due to high shear stress, drag and abrasion, thus leading to a lower biomass (Wellnitz and Rader, 2007; Ponsatí et al., 2016), whereas moderate to low water flows provided favorable conditions for algal growth and the corresponding biomass accumulation (Ateia et al., 2016; Espinosa et al., 2020). In this study, the highest chlorophyll *a* and AFDM values were obtained in winter 2019, which could be related to the scarcity of rainfall (and the consequent reduced water flow), that prevented biofilm drag and favored biomass accumulation (Marcarelli et al., 2009; Ceola et al., 2013). However, other studies (Graba et al., 2013) showed that there were no significant differences in AFDM depending on the water flow, but this parameter was a selective factor in algal composition. This agrees with the study carried out by Vilalta (2004), which described that slow current velocity areas were favorable for cyanobacterial growth in a field study performed in a Mediterranean river.

Nutrient concentration and N:P ratio

The cyanobacterial growth is also linked to the presence of nutrients, since numerous studies have described that high nutrient concentrations favor the appearance of cyanobacterial blooms (Doods and Smith, 2016; Lee et al., 2017), in many cases related with the geosmin production (Ding et al., 2014). Similar results were observed in this study, where higher nutrient concentration generated a favorable situation for the development of cyanobacterial biomass within biofilm communities during 2019 (0.91 ± 0.58 µg/cm^2 in T7 compared to 0.33 ± 0.44 µg/cm^2 in T1).

The highest nutrient concentration present at T7 sampling site are related to nearby land uses, which in the Osona region are predominantly related to agriculture, urban and industrial development (**Figure 6.7.**). Specifically, the municipalities of Vic, Torelló, Manlleu and Gurb have a high concentration of arable land with a total amount of 6,300 ha (35% of the total area), moreover, the biggest cities (high population and industries) are also located in this municipalities. These conditions generated both point-source (urban and industry) and non-point source (agriculture) pollution. The main WWTPs in the area treat around 40,000 m^3/d and the treated effluent has a total average concentration of N and P of 8.1 mg/L and 0.85 mg/L respectively, which means a daily emission to the surrounding water bodies of 324 kg N/d and 34 kg P/d (Osona WWTP data). Non-point source pollution is mainly related to agriculture and use of fertilizers that can be estimated taking into account the soil N application and the total amount of usable agricultural area; assuming a N application of 170 kg N/ha (from organic

sources) a total amount of 1,000 tons of N per year are spread to arable land. Egas et al. (2019) estimated that approximately 30% of nitrogen applied to soil is leached to water bodies which in that case is equivalent to an average leaching of 800 kg N/day. Other studies have described the influence of land use in nutrient and sediment concentration in rivers, like the one developed by Ongley et al. (2010) which reported that the agriculture contributes >50% of the total load, and the fraction of this total load is highly dependent on the proportion of agriculture in the watershed (Shi et al., 2017).

Agricultural activities are linked to climatic conditions, with spring being the season that, due to a greater number of rains and higher temperatures, favors better growth and development of crops. This makes agricultural land uses have a greater impact on water quality in winter and spring, when planting occurs and crops are fertilized, generating higher values of ammonium and phosphates concentration in T7 sampling site during spring (**Table 6.1., Table A.1.**). Moreover, in these seasons large amount of rainfall could cause the fertilizer used in the crops to overflow into the river leaches, thereby leading to the deterioration of river water quality.

This seasonal change in the nutrient concentration gives rise to differences in the N:P ratio, which also has an important effect in the cyanobacteria development and in triggering geosmin episodes. A study done by Jankowiak et al. (2019) described that phosphorus availability excess may stimulate the magnitude of cyanobacteria blooms, and Vilalta et al. (2003), in a study performed in the Llobregat river (NE Spain), pointed out that unbalanced proportion between nitrogen and phosphorus had an effect on benthic geosmin production. A similar result has been obtained in this study, since geosmin concentration was positively correlated with the phosphorus concentration ($p < 0.001$) and negatively with the N:P ratio ($p < 0.001$). The effect was clearly observed at T7 in 2019, the sampling site with higher nutrient concentration where in late winter-early spring there was a pronounced decrease of the N:P ratio value (**Figure 6.11.**), associated with an important episode of geosmin. The interaction between N:P ratio and nutrient concentration, seems to be an important driver favoring the production and release of this metabolite from benthic cyanobacteria in Ter River.

This can be corroborated from the results obtained at the sampling sites located upstream, in El Ripollès region. These sites (T1, T2, F and G) showed lower nutrient concentrations that were significantly correlated with a higher percentage of forest (between 31.2 and 42.5%) and pastures (up to 84.9% at the Ges River head). The lower nutrient concentration is attributed mainly to the lack of potential point (industrial) and non-point (agriculture) source pollution but also to the fact that forests and pastures are environments that can contribute to reduce surface

erosion and soil sediment run-off, which are among the main diffuse sources of phosphorus to freshwater rivers. This fact can be clearly observed in the Ges river (G1), which is the site with the highest percentage of pastures and the lowest phosphorus concentration (25 ± 22 µg $P\text{-}PO_4^{3-}$). Sampling site located upstream (T1) stands out because, despite having the lowest concentration values of nitrogenous forms, its concentration of phosphorus in winter and spring was high. This can be related to anthropogenic activities since during these seasons there is an increase in the population of the Pyrenees' villages, mainly consequence of snow tourism which provoke a reduction in the performance of the unique Wastewater Treatment Plant (WWTP) in the area, located in Vilallonga de Ter. This WWTP was designed to treat a water inflow of 300 m^3 per day, corresponding to an equivalent population around 1200. In winter and spring, the increased population, consequence of tourism, means that, at specific times, the water flow to be treated is much higher than 400 m^3 per day, provoking a significant WWTP performance reduction (data from the Water Catalan Agency, 2020). The WWTP has a biological treatment with only nitrogen removal, thus may be a possible explanation of the lower N:P ratios observed during winter and spring (**Table 6.2., Table A.1.),** however, the basal concentration of nutrients at T1 was still low and no episodes of geosmin were observed at this sampling site, highlighting the importance of the interaction between N:P ratio and nutrient concentration in triggering geosmin episodes.

Chlorophyll a

In the study conducted on the Ter river, the chlorophyll *a* concentration increases throughout the basin independently from the season, from values of 2.6 ± 2.9 µg/cm^2 in T1 to average values of 18.2 ± 17.8 µg/cm^2 in T7. This increase in the chlorophyll a concentration can be associated with a greater nutrient concentration present in the water, which favor the development of algal biomass and a great production of chlorophyll a (Urrea-Clos et al., 2014). If the T7 sampling site in 2019 is evaluated in detail, it was observed that in late winter – spring, when the geosmin peak occurred, the chlorophyll *a* values were lower (10.3 ± 6.2 µg/cm^2) than the rest of the seasons (26.0 ± 21.3 µg/cm^2) (**Table 6.2., Table A.1.),** founding a significant negative correlation between geosmin and chlorophyll *a* (Pearson correlation, $p < 0.05$). This could be because geosmin and chlorophyll *a* have the same metabolic pathway, and it has been described that when cyanobacteria start to synthesize geosmin, the chlorophyll *a* production decreases or even stops (Cai et al., 2017; Espinosa et al., 2020). Other studies have shown that under elevated nitrate concentrations, a greater amount of chlorophyll *a* is synthesized, with a correspondent decrease of geosmin synthesis (Saadoun et al., 2001). This partially agrees with our results, since under elevated nitrogen conditions we found the highest chlorophyll *a* concentration, but also

the highest geosmin production. This can indicate that a nitrogen threshold exists and its needed and that, when it co-occurs with a high phosphorus concentration, give rise to the optimal condition for geosmin production. This would evidence again the importance of the interaction between nutrient concentration and N:P ratio, and the fundamental role of the phosphorus concentration in the geosmin production.

Cyanobacteria relative abundance

In this field study no significant correlations were found between geosmin and cyanobacteria abundance, this is somehow surprising as these microorganisms are described as the main geosmin producers in freshwater ecosystems, but can be explained since the presence of geosmin in water implies that the cyanobacteria in the biofilm die or cease to be attached to the substrate. This is due to the life cycle of cyanobacteria, specifically with the optimal geosmin production (growth phase) and release time (biomass decomposition and/or cell lysis), since it has been described that many cyanobacteria species can produce geosmin although they may not actively release it until cell lysis occur (Kim et al., 2018). Furthermore, the relative amounts of intra and extracellular portions of geosmin may also vary considerably with cell age, environmental conditions and among different species (Alghanmi et al., 2018).

However, trends have been observed, such as the one shown in **Figure 6.12.** This figure represents geosmin concentration at T7 sampling site, throughout the year 2019, together with the cyanobacteria relative abundance, the N:P ratio and temperature. This figure shows a notable increase in the cyanobacteria presence in the first months of the year, reaching almost 50% of the biofilm community at the beginning on March, and decreasing markedly 15 days later, which coincides with the geosmin peak. A similar behavior was observed at the end of April. Nevertheless, this trend only occurs in winter and spring. In summer, the cyanobacteria presence was also high but there was no geosmin, indicating that the factors that trigger its production are not stable throughout the year and that a set of specific conditions have to co-occur for the geosmin production by benthic cyanobacteria to be triggered. Some of the factors that differs between these two moments were the N:P ratio and the temperature, which presented significantly lower values in winter - spring than in summer (**Figure 6.12.**). The study performed by Alghanmi et al. (2018) pointed out that many cyanobacteria growth better under 25°C conditions, but this does not imply a higher geosmin production. In fact, some studies have found higher geosmin concentration and production yield at 10°C compared with higher temperatures (25 and 35°C) (Wang and Li, 2015), indicating that lower temperatures could stimulate geosmin production and favor the accumulation of geosmin in cells whereas higher temperatures would stimulate intracellular geosmin release into the medium (Zhang et al.,

2009). This would agree with the results obtained in the study carried out in the Ter river, when a higher concentration of intracellular geosmin was observed at temperatures close to 10°C (0.66 ± 0.11 ng/mg), whereas at higher temperatures (20 - 25°C) was not detected (**Table 6.3.**). Moreover, considering that low light conditions have been described to favor intracellular geosmin production in river biofilms (Espinosa et al., 2020), the increased light availability occurring in summer may be an additional limiting factor for microbial geosmin production in Ter river. This would be reflected in T1 sampling site, where temperatures in summer resemble those of T7 sampling site in late winter – early spring, but the higher light incidence prevents gaseous vacuoles formation and geosmin production. In fact, in the study performed by Alghanmi et al. (2018), was shown that at temperatures of 25°C, higher light intensity hinders the production of geosmin by cyanobacteria, and Oh et al. (2017) showed that *Anabaena* could growth well at temperatures <20°C, but was sensitive to high light intensities.

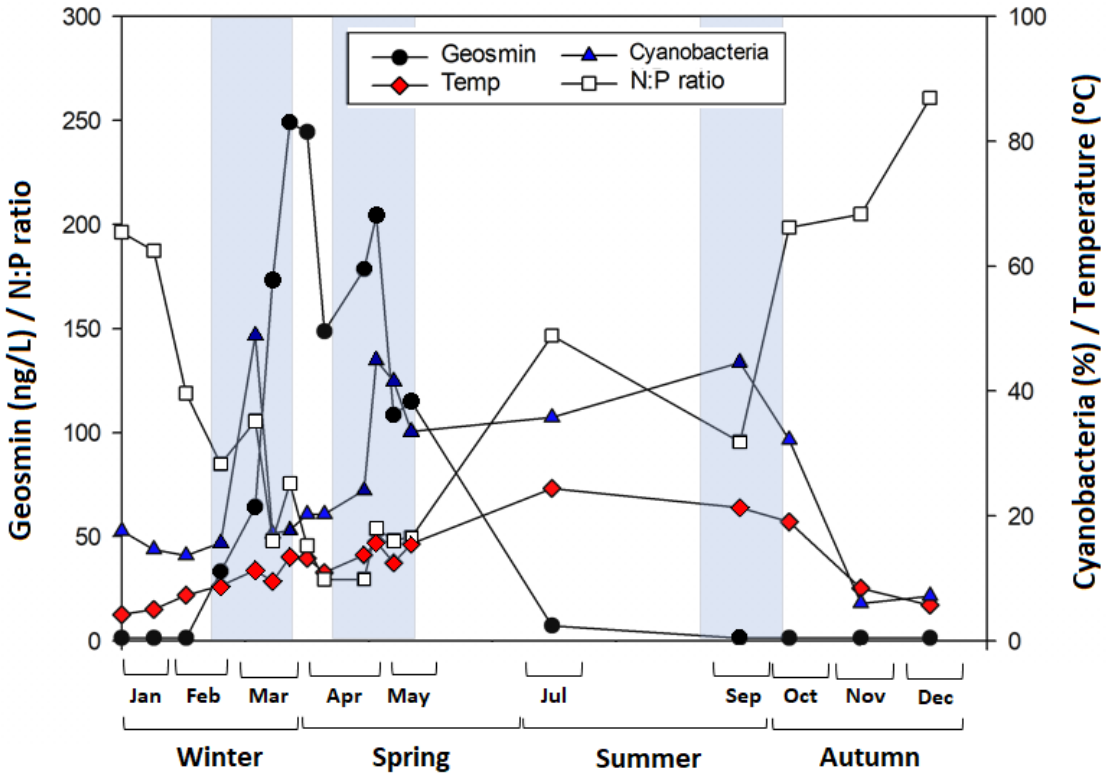

Figure 6.12. Mean value and standard deviation of geosmin concentration (ng/L), N:P ratio (mol/mol), cyanobacteria relative abundance (%) and temperature (°C) in T7 sampling site for the different sampling days in 2019, being Jan = January, Feb = February, Mar = March, Apr = April, May = May, Jul = July, Sep = September, Oct = October, Nov = November and Dec = December. The blue boxes indicate the time when cyanobacteria relative abundance in the biofilm was high.

6.6. Conclusions

Overall, this field study showed that both climate change and anthropogenic factors are potential drivers of geosmin episodes in Mediterranean rivers.

River stretches which land uses of the surrounding areas favor high nutrient concentrations, , are more susceptible to be affected by geosmin episodes. For example, agricultural watersheds, are used to experience an increase of phosphorous concentration associated with planting and fertilization periods that may generate an N:P ratio decrease especially during late winter – early spring. This situation would favor cyanobacteria development especially in areas near the riverbanks, where the water flow is lower, and the light availability is reduced because of the riparian forest buffering effect. Under these conditions, cyanobacterial cells would start to produce geosmin, that would be released into the water between 7 and 15 days after the cyanobacteria peak in biofilms.

However, climatic conditions may also play an important role, since low water flow associated with a reduction of the average precipitations and mild temperatures, seem to be conditions favoring cyanobacterial development and geosmin production under the nutrient conditions mentioned above.

These results could help drinking water treatment companies in the forecasting and management of geosmin episodes, being able to understand under which ecological conditions, the water they supply could present geosmin.

CHAPTER 7. Predicting geosmin episodes in a Mediterranean river using a 3-year dataset

7. Predicting geosmin episodes in a Mediterranean river using a 3-year dataset

7.1. Introduction

As described throughout this Thesis, in the Ter river (NE Catalonia, Spain), which waters are used for drinking water supply purposes, several geosmin episodes were documented during the last years. With all the work presented in the previous chapters, the triggers of geosmin production have been understood, but to apply it to reality, all this knowledge must be translated into a predictive model.

Due to the problems associated with the alteration of the water organoleptic characteristics that cyanobacteria blooms cause, several studies have been carried out whose objective was to generate predictive models of these blooms formation and their secondary metabolite production. Most studies have used linear models to predict cyanobacteria and their secondary metabolites (Beaulieu et al., 2014; Dzialowski et al., 2009), others have used nonlinear modelling techniques, including neural networks (Millie et al., 2014; Parinet et al., 2013), partial least squares and random forest (Harris and Graham, 2017; Jacoby et al., 2015). However, all these models were carried out with databases from lakes or reservoirs, being none of them focused on geosmin episodes occurring in rivers. Rivers are different freshwater systems than lakes and reservoirs and, in this case, the geosmin producers are different. Therefore, the weight of the involved variables in the triggering of the geosmin episodes may differ in rivers compared with other freshwater ecosystems.

7.2. Objectives

The objective of this study was to assure a real application of the results obtained in this Thesis in order that they could be useful for the Drinking Water Treatment Plants having problems with geosmin episodes. In this sense, the aim has been to generate two types of predictive models: a) one that indicates the presence or absence of geosmin, and b) one that allows the determination of geosmin concentration in rivers. To achieve this objective, the 3-year database (2017 – 2019) generated monitoring physicochemical and biological parameters in five sampling sites located in the upper Ter river basin has been used (**Chapter 6**).

7.3. Sampling procedure and physicochemical and biological analysis

The Ter and the Ges rivers (left tributary of the Ter) have been studied to obtain a dataset that allows to generate the geosmin predictive models. A total of 5 sampling sites were selected in the upper part of the Ter river basin, 4 of them located along the Ter river and 1 in the Ges river (**Figure 7.1.**). These sampling sites were chosen for presenting different ecological water quality, as described in **Chapter 6**.

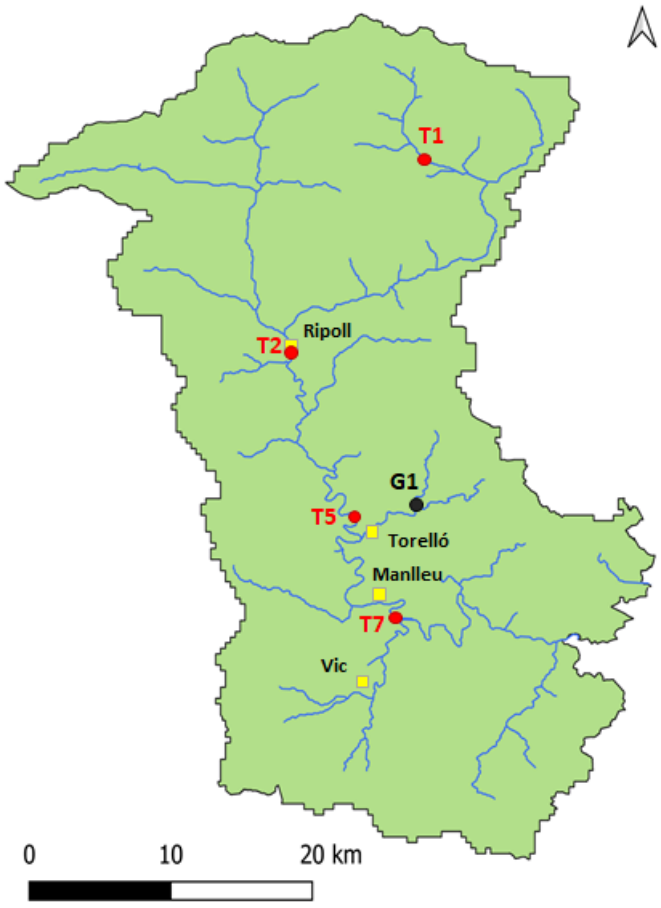

Figure 7.1. Map of the upper Ter river basin (El Ripollès and Osona region, NE Catalonia, Spain) with the sampling sites evaluated in the Ter river (red dots) and Ges river (black dot), and the main municipalities (yellow square).

To summarize, geosmin, physicochemical parameters and chlorophyll *a* were monitored for three years (2017 – 2019). During winter and spring (January – June), weekly or bi-weekly sampling campaigns were carried out, whereas from July to November, monthly sampling campaign were done. The higher sampling intensity during winter and spring is related to the higher probability of geosmin occurrence during these seasons (Vilalta et al., 2004).

The pH, temperature, dissolved oxygen and saturation, and electrical conductivity were measured *in situ*, while water samples for Soluble Reactive Phosphorus (SRP), NH_4^+, NO_2^- and NO_3^-, turbidity, suspended solids, organic matter and geosmin were taken and analyze as described in **Chapter 3**. Biofilm samples for the chlorophyll *a* analyses were also taken.

7.4. Methodology used for model development

The development of the geosmin predictive models have been done with the collaboration of the Computer Science Department of the Verona University. Before starting to develop the models, a database treatment was carried out. Any potential explanatory variable with >10% of the observations missing was removed for further analysis (Harris and Graham, 2017), leaving 13 potential explanatory variables: pH, temperature, electrical conductivity, dissolved oxygen, oxygen saturation, turbidity, organic matter, chlorophyll *a*, nitrites, nitrates, ammonium and phosphates concentration and the N:P ratio. If the value of any of these variables was missing one day on a sampling site, the whole data for that day and sampling site was removed. Thus, a database with 115 data inputs was used to develop the models. Finally, for modeling, the geosmin concentration was transformed to a logarithmic scale, to fulfil the conditions on normal distribution and homogeneity of variance.

With this database six different model approaches were performed, including linear and non-linear regression models (**Table 7.1.**). All the models were obtained using the programming software Phyton 3.8.2.

Table 7.1. List of compared modeling approaches and their abbreviation.

Model	Abbreviation
Logistic regression	LoR
Linear regression	LiR
Least Absolute Shrinkage and Selection Operator regression	LASSO
Artificial Neural Network model	MANN
Principal Component Analysis model	MPCA
Linear Discriminant Analysis model	MLDA

The logistic regression (LoR) is a type of regression analysis used to predict the outcome of a categorical variable, in our study the presence (1) or absence (0) of geosmin, depending on the independent or predictor variables. A linear regression (LiR) is a linear approximation that is used to establish the relationship between a response or dependent variable, which in this specific study case is the geosmin concentration, and one or more independent or explanatory variables. The Least Absolute Shrinkage and Selection Operator (LASSO) regression is a

regression analysis method that chooses a set of variables and regularizes them with the aim of increasing the precision of the statistical model generated and the results interpretation. To achieve these objectives, LASSO is based on forcing the sum of the absolute value of the regression coefficients less than a set value. This forces the coefficients that have a lower weight in the model to be switched to zero, resulting in a simpler model that does not include all variables.

The Artificial Neural Network (ANN) consists of a set of units, called artificial neurons, connected to each other to transmit signals. The ANN has the ability to detect all possible interactions between predictors. The relationship between input and output variables can be established without assumptions about mathematical representation of the phenomena to be modelled (Zhang et al., 2004). Information admitted in the input layer (turbidity, phosphate concentration…) is processed by the hidden and the output layers by way connections between elements characterized by numerical weights. The importance (number of elements) of the input and output layers is determined respectively by the number of predictors and predicted variables of the problem, while the required number of hidden layers and their importance is generally determined through testing (Parinet et al., 2013). Different architectures are obtained depending on the topology, structure or connection pattern of the neural network. The first architecture performed (20x30x30x1) was like the one represented in the **Figure 7.2.,** which, when making all possible combinations, obtains an amount of 18,000 coefficients.

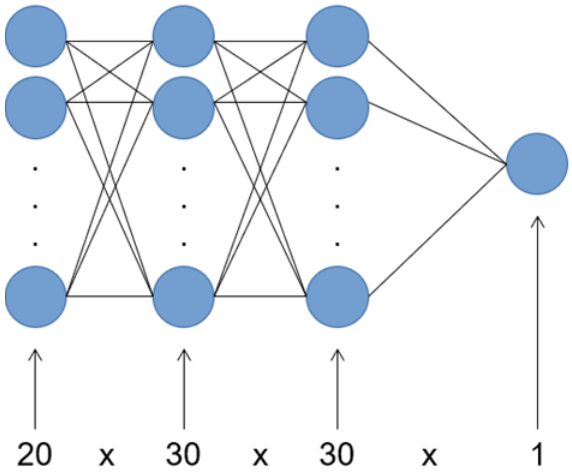

Figure 7.2. Graphical representation of the Artificial Neural Network.

To perform this model, the Huber loss function was chosen. In statistics, this loss function is used in robust regression, being less sensitive to outliers in data than the squared error loss. A loss function is a function that maps an event or values of one or more variables onto a real number intuitively representing some “cost” associated with the event. In statistics, is typically used for

parameter estimation, and the event in question is some function of the difference between the estimated and the true values for an instance data.

In addition to the architecture presented above, eight more architectures were evaluated, to see if the performance could be improved. The architecture types tested were the following:

- Architecture A: 3x1
- Architecture B: 20X1
- Architecture C: 10x10x1
- Architecture D: 10x30x1
- Architecture E: 30x10x1
- Architecture F: 60x40x20x1
- Architecture G: 20x40x60x1
- Architecture H: 20x40x20x1

In these approximations, the function of the layers was the Rectified Liner Unit (ReLU) activation function. This is the most used activation function, and it is used in neural networks to obtain results with less error than the ones generated with other activations functions, like the logistic sigmoid (Eckle and Schmidt-Hieber, 2019). For each architecture, cross validation was performed to choose the best batch size or number of training examples utilized in one iteration. Each cross validation for each batch size was done 5 times, then performances were averaged.

In addition, a PCA was used to pre-process the data given to the ANN models generating a new model with the two principal components selected (MPCA). A Linear Discriminant Analysis (LDA) was also performed to the data given by the ANN models. With the LDA, a new dimension was found where the data was well divided based on the classes presented in the dataset. It was used in order to introduce the concept of "critical level of geosmin", meaning that geosmin above the threshold was labeled as 1, and as 0 the ones below the threshold.

To obtain all these models, the database was randomly split into a database to generate the model (training database) and a database to validate it (test database). This split was done 10 times, and the results represented in this Chapter (**Section 7.5.**) are the average of the results obtained. All the models present information about the train score and the test score (R^2). The term R^2 or coefficient of multiple determination, is the percentage of variation of the response variable that explains its relationship with one or more predictor variables. This value can increase by including more variables in the model, making one think that the model is better, for this reason it must be adjusted by the number of predictors in the model (Sokal and Rohlf, 1995). The more this value approaches 1, the greater the model's ability to predict the presence and concentration of geosmin.

Except for the Logistic regression (LoR), the Root-Mean Square Error (RMSE) was performed on the test data set. The RMSE is a measure of accuracy, to compare forecasting errors of different

models for a particular dataset, and it is scale dependent. RMSE is always non-negative and a value of 0 would indicate a perfect fit to the data, thus a lower RMSE is better than a higher one.

To calculate the number of false positive and negative cases given by the models, the number of predicted observations that were above (false positives) or below (false negatives) one was calculated based on the real value, with one being the threshold value (in logarithmic scale) of the geosmin concentration detected by humans. The percentage of cases was calculated based on the total number of observations (n = 115).

The robustness of the database in terms of amount of observations (n = 115) is comparable to that of other authors, which in similar studies carried out with geosmin in lake and reservoir data, the models generated presented a number of observations ranged from 57 to 185 (Dzialowski et al., 2009; Parinet et al., 2013, Harris and Graham, 2017).

7.5. Results

7.5.1. Environmental variables and geosmin concentration

The evaluated sampling sites showed differences depending on the physicochemical and biological parameters, which were influenced by the nearby land uses (more information in **Chapter 6**). Sampling sites located upstream of the Ter river basin, with higher percentage of forests and pastures (T1 and G1), presented low nutrient concentrations, and low temperature and conductivity values. The sampling site located in Ripoll municipality (T2) showed an increase on the values of the analysed parameters comparing to T1, due to the greater presence of urban area. The sampling sites T5 and T7 stood out for their higher values of nutrients associated with the largest presence of agricultural and industrial areas.

As a result of the interannual variation associated with the Mediterranean climate, differences between years were observed as regard precipitation, water flow and temperature values, all of them associated with the climatic conditions. The year 2017 was characterized by higher temperatures and some punctual precipitation, which meant a slight reduction in the water flow of the Ter river compared to the year 2018. The year 2018 had lower water temperature values and a greater number of precipitations, which generated an increase in water flow. The year 2019 stood out for being a very dry year, with a shortage of precipitation; combined with higher temperature, historical minimums were reached in the water flow values. These different scenarios, together with the specific conditions of each sampling site described in **Chapter 6**, have led to differences in the geosmin concentration obtained for each year.

The highest geosmin concentration in water was detected in 2019, with a maximum of 249 ± 33 ng/L at sampling site T7 (**Figure 7.3.**). In 2017, geosmin was also detected, but in lower concentrations, reaching a maximum geosmin concentration of 52 ng/L at sampling site T5. In 2018, geosmin was not detected at any sampling site. Seasonality also played an important role in geosmin appearance, being during winter and spring were the highest values of geosmin were found. Geosmin concentration was positively correlated with pH, temperature, nitrites and phosphates concentration, and turbidity, and negatively correlated with the N:P ratio and the dissolved oxygen.

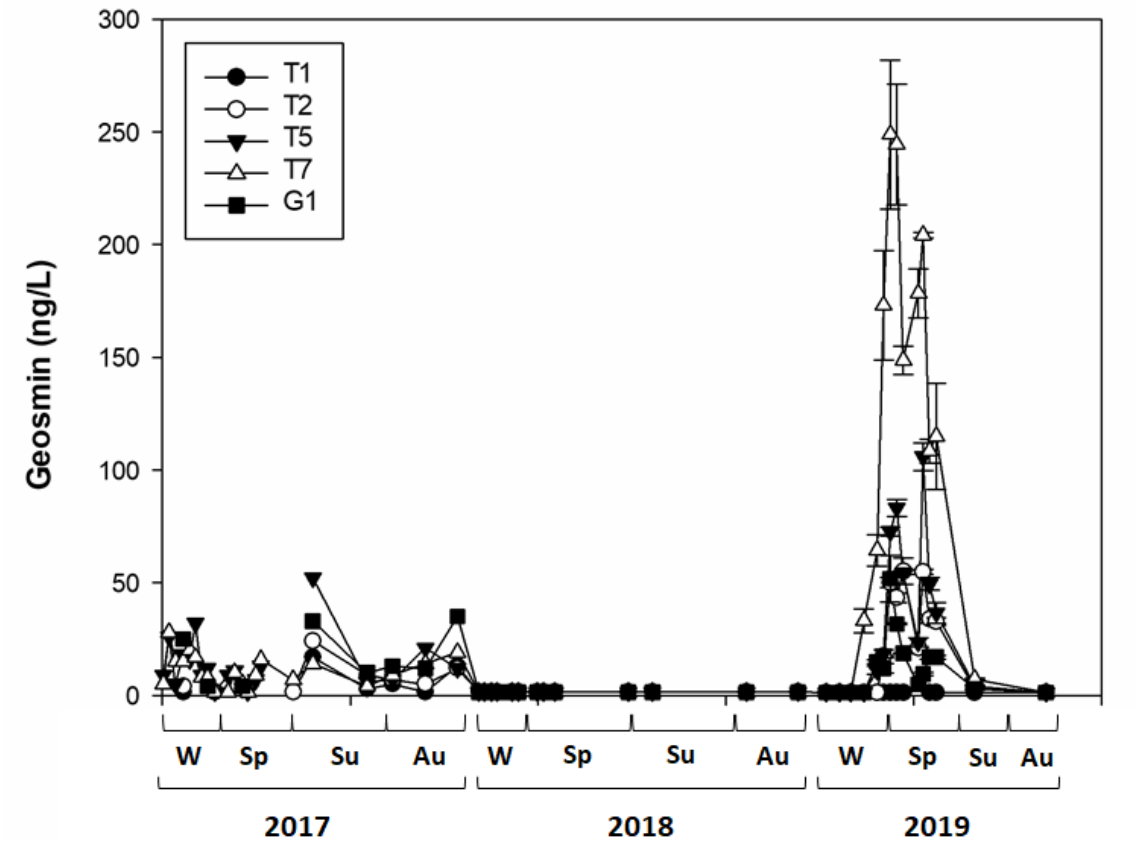

Figure 7.3. Mean and standard deviation values of geosmin concentration in water for the sampling sites evaluated in 2017, 2018 and 2019: T1 = Ter at Vilallonga de Ter, T2 = Ter at Ripoll, T5 = Ter at Colònia de Borgonyà, T7 = Ter at Gurb and G1 = Ges upstream San Pere de Torelló, W = winter, Sp = spring, Su = summer and Au = autumn.

7.5.2. Geosmin models

7.5.2.1. Statistical coefficients and parameters

The linear models (LoR, LiR and LASSO) give information about the selected parameters and the value of the coefficients obtained. The coefficient indicates the weight of the variable within the model. The higher the coefficient, the greater its weight. The positive or negative sign indicates the correlation between the variable and the geosmin concentration and if the value is 0 it means that the model decided not to include this variable. To summarize, these results have been represented in the **Table 7.2.** The performance of the tested models is summarized in the **Table 7.3.,** which gives information about the RMSE value, the train and the test score (r^2).

Table 7.2. Variables chosen by the model (LoR, LiR and LASSO) and its corresponding coefficient.

	Coefficients		
Variable	**LoR**	**LiR**	**LASSO**
pH	0.893	0.084	0.256
EC	0.247	0.120	0.001
Temperature	0.007	0.030	0.016
DO	0	-0.037	-0
Oxygen Saturation	0.128	0.027	0
Turbidity	1.167	0.287	0.018
OM	-0.247	-0.073	-0.166
Chl *a*	-0.215	-0.103	-0.009
Nitrites	0.625	0.257	19.418
Nitrates	0	-0.029	-0
Ammonium	-0.064	-0.003	-0
Phosphate	0.440	0.095	1.333
DIN:SRP	-0.992	-0.168	-0.002

Table 7.3. Performance of the tested models.

Model	RMSE	R^2 Train	R^2 Test	False positive (%)	False negative (%)	Accuracy (%)	Number of variables
LoR		0.870	0.827				11
LiR	0.490 ± 0.132	0.634	0.465	8.39	7.83	83.78	13
LASSO	0.489 ± 0.124	0.612	0.379	12.17	6.09	81.74	9
MANN	0.497 ± 0.138	0.755	0.504	12.17	6.08	81.75	13
MPCA	0.426 ± 0.098	0.659	0.598	11.30	7.83	80.87	13
MLDA	0.416 ± 0.105	0.648	0.596	6.09	6.96	86.96	13

7.5.2.2. Logistic regression

In this study case, to obtain the highest values of train and test score, the model includes eleven latent vectors out of 13 (**Table7.2.**).

The train score obtained in this approach was 0.870 and the test score was 0.827. The results of this model are represented in the **Figure 7.4**., where the blue dots are the real geosmin values (0-1) and the yellow dots are the geosmin values predicted by the model.

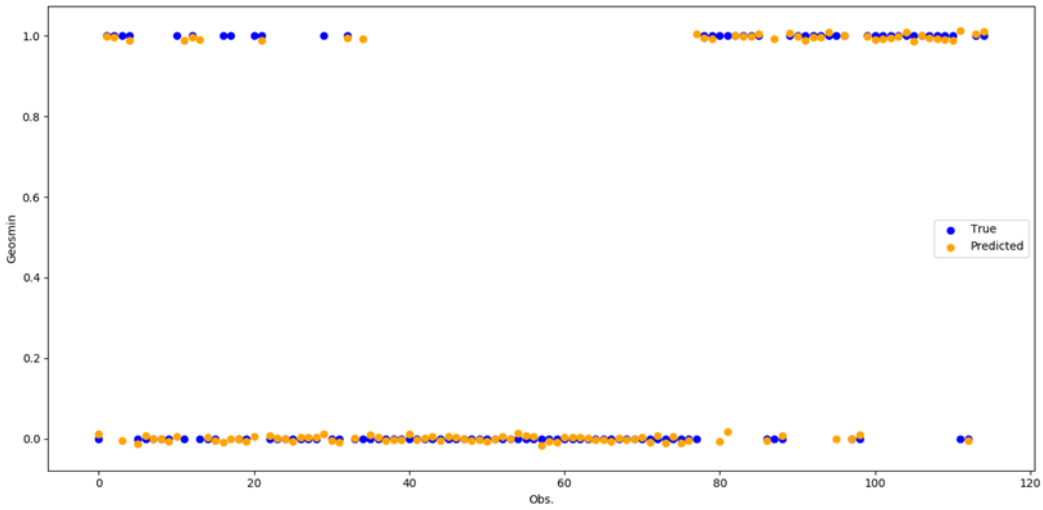

Figure 7.4. Graphical representation of the Logistic regression model results. In blue, the real values of geosmin, and in yellow, the predicted ones.

7.5.2.3. Linear regression

In this approach, all variables were included in the model, and the results of the coefficients obtained are shown in the **Table7.2.** In this model, the train score value was 0.634 and the test score was 0.465, and the RMSE value was 0.490 ± 0.132 (**Table 7.3.**). The results obtained are represented in the **Figure 7.5.A**.

A linear regression was made between the real values and the predicted ones, which are shown in **Figure 7.5.B**. With this model, 7.8% of the cases are false positive and 8.4% are false negative, thus, the model correctly predicts the presence or absence of geosmin in 83.8% of cases.

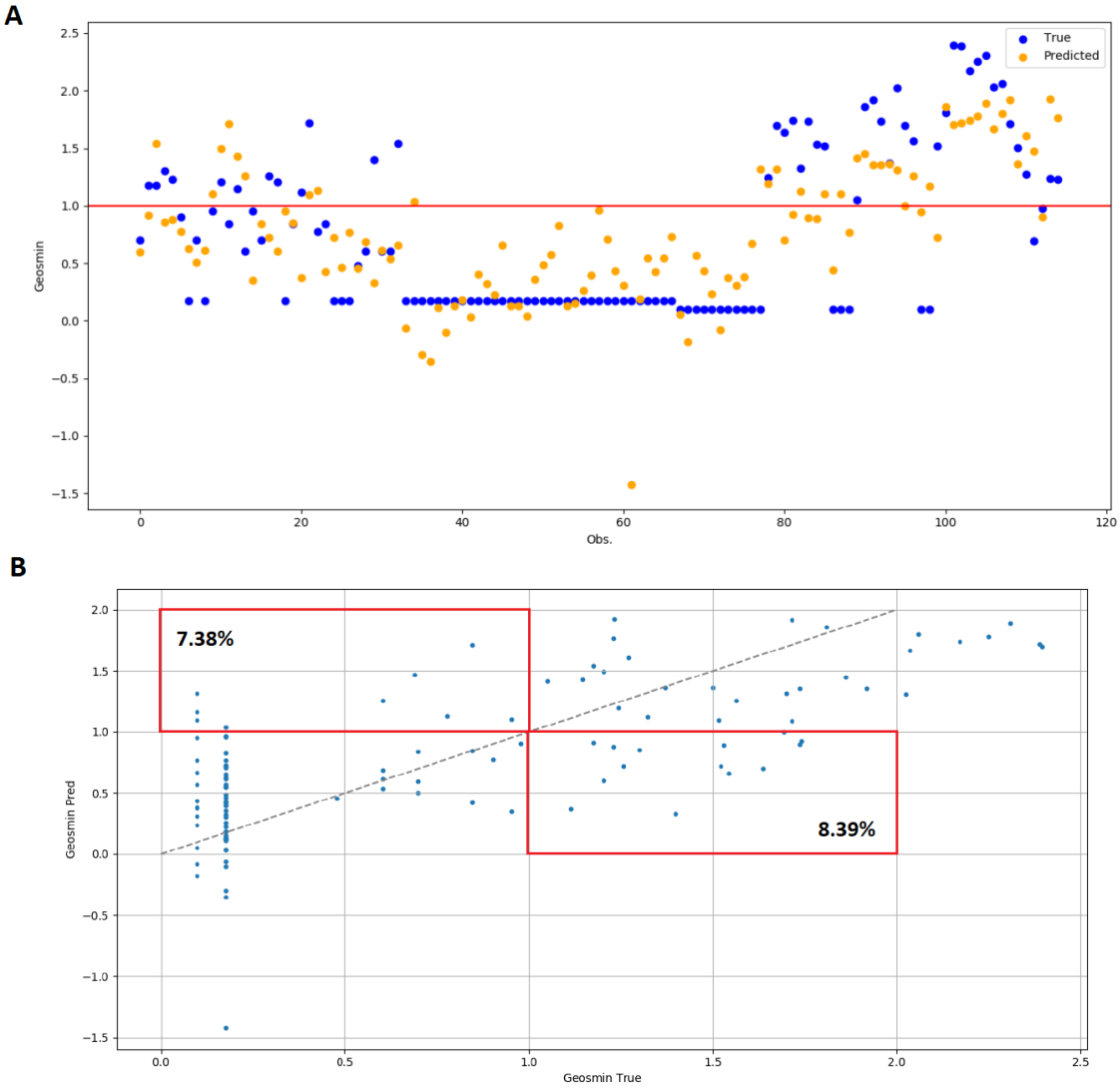

Figure 7.5. A. Graphical representation of the results from the linear regression model (LiR). The blue dots are the real values of geosmin, and the yellow dots are the predicted ones. The red line represents the detection limit of geosmin by humans (10 ng/L). Being on a logarithmic scale, it was located at the value of 1. **B.** Linear regression between real and predicted geosmin concentration values for the linear regression model (LiR). The red box frames the false positives and false negatives of the model.

7.5.2.4. Least Absolute Shrinkage and Selection Operator regression

In this study case, the model chose 9 out of 13 variables to have the highest value of train and test score, being the value of train score of 0.612 and the value of test score of 0.379. The RMSE value generated was 0.489 ± 0.124, a bit lower than the LiR model. The variables chosen by the model are shown in the **Table 7.2.**, and the results obtained in **Figure 7.6.A**. Carrying out a linear regression between the real values and the predicted ones, it was observed that 6.1% of the

cases were false positive and 12.2% of the cases were false negative (**Figure 7.6.B.**). The model correctly predicts the presence - absence of geosmin in 81.7% of cases.

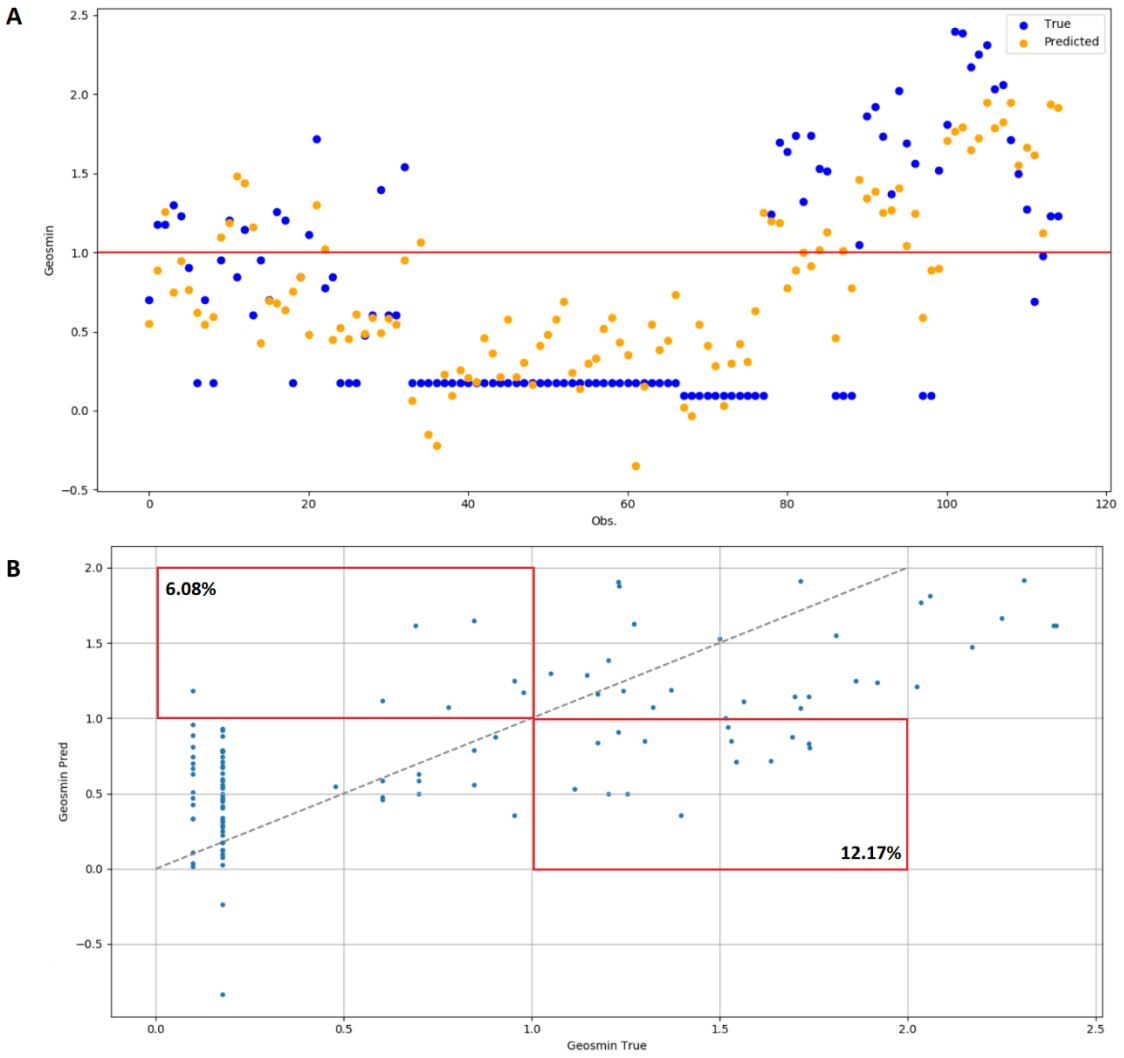

Figure 7.6. A. Graphical representation of the results from the LASSO regression model. The blue dots are the real values of geosmin, and the yellow dots are the predicted ones. The red line represents the detection limit of geosmin by humans (10 ng/L). Being on a logarithmic scale, it was located at the value of 1. **B.** Linear regression between real and predicted geosmin concentration values for the LASSO regression model. The red box frames the false positives and false negatives of the model.

7.5.2.5. Artificial Neural Network

The first architecture performed (20x30x30x1) was like the one represented in the **Figure 7.2.,** which, when making all possible combinations, obtains an amount of 18,000 coefficients.

With this model, the highest values obtained from all the possibilities evaluated were 0.755 for the train score and 0.504 for the test score, and the RMSE value was 0.497 ± 0.138 (**Table 7.3.**). The results are represented in **Figure 7.7.A**. The ANN model had the same number of false negatives and false positives than the previous model (LASSO regression) (**Figure 7.7.B.**), but with this model the ability to predict better higher geosmin concentration values increased.

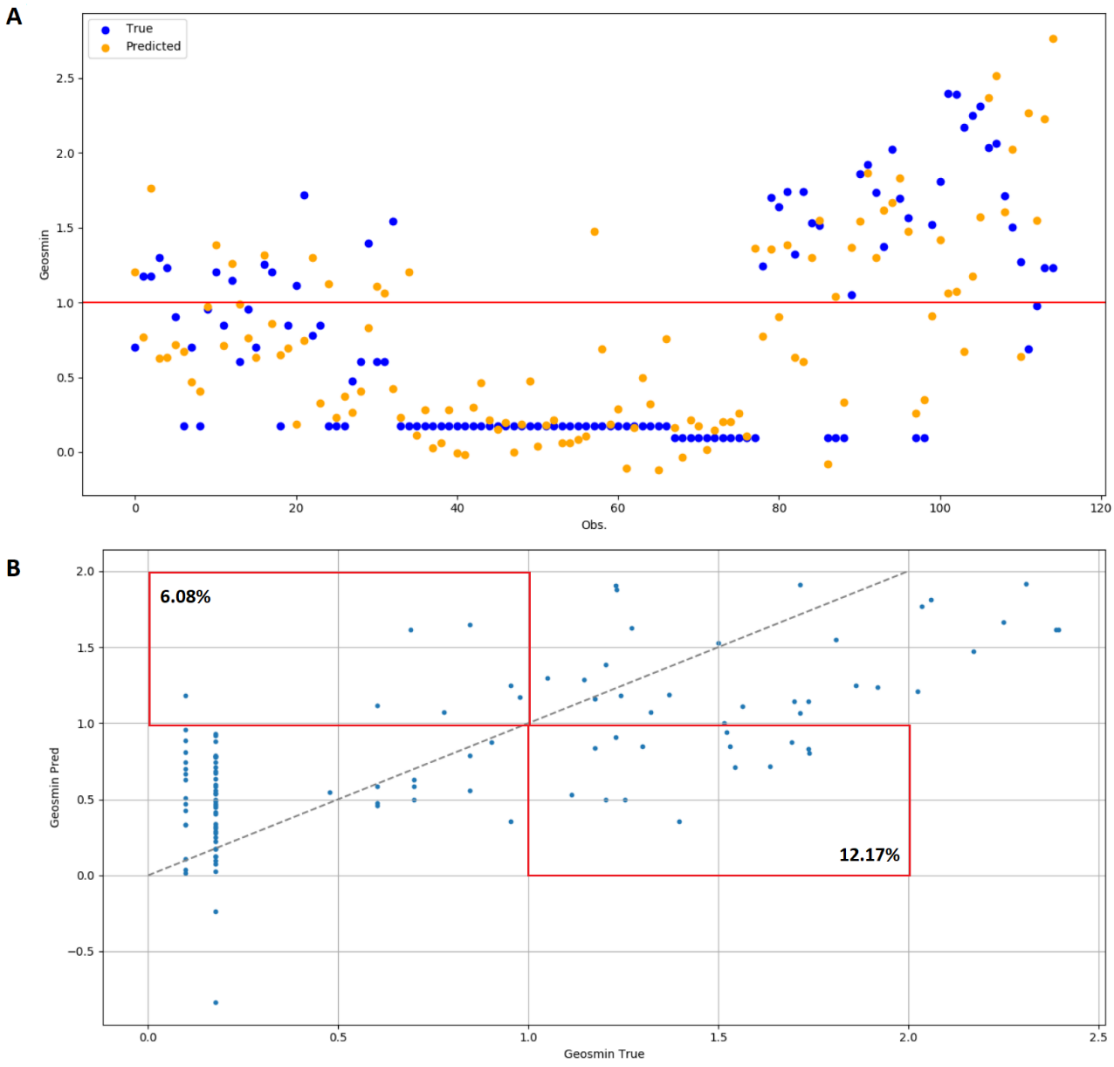

Figure 7.7. A. Graphical representation of the results from the Artificial Neural Network 20x30x30x1. The blue dots are the real values of geosmin, and the yellow dots are the predicted ones. The red line represents the detection limit of geosmin by humans (10 ng/L). Being on a logarithmic scale, it was located at the value of 1. **B.** Linear regression between real and predicted geosmin concentration values for the Artificial Neural Network 20x30x30x1. The red box frames the false positives and false negatives of the model.

In addition, a PCA was used to preprocess the data given by the ANN models. The best model was obtained with the architecture E (30x10x1) improving the RMSE value, which went down from 0.497 ± 0.138 to 0.426 ± 0.098, with the dimensionality reduced to just 2 components (**Figure 7.8.A.**). The train score of this model was 0.659 and the test score was 0.598 (**Table 7.3.**). Carrying out a linear regression between the real values and the predicted ones, it was observed that 7.8% of the cases were false positive and 11.3% of the cases were false negative (**Figure 7.8.B.**). The model correctly predicts the presence - absence of geosmin in 80.9% of cases.

With the LDA, a new dimension was found where the data was well divided based on the classes presented in the dataset, having a total of three considered dimensions. With this approximation, and with the architecture C (10x10x1), the performance further improves (RMSE = 0.416 ± 0.105) (**Figure 7.7.B.**).The train score of this model was 0.648 and the test score was 0.596. In addition to decreasing the RMSE value, it improves the geosmin prediction at high concentrations. Carrying out a linear regression between the real values and the predicted ones, it was observed that 6.9% of the cases were false positive and 6.1% of the cases were false negative (**Figure 7.9.B.**). The model correctly predicts the presence - absence of geosmin in 87% of cases.

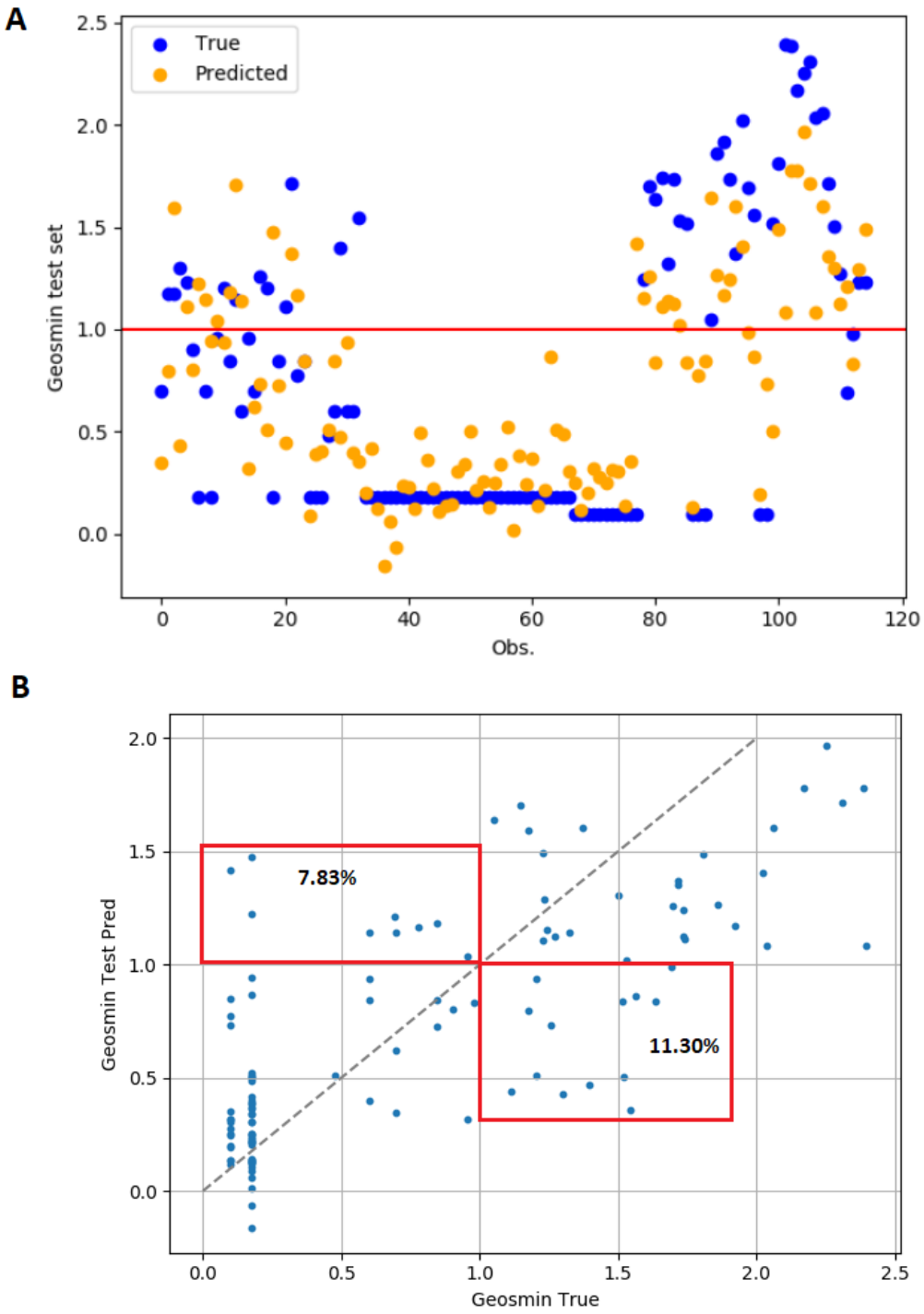

Figure 7.8. A. Graphical representation of the results from the Artificial Neural Network PCA (Architecture E: 30x10x1). The blue dots are the real values of geosmin, and the yellow dots are the predicted ones. The red line represents the detection limit of geosmin by humans (10 ng/L). Being on a logarithmic scale, it was located at the value of 1. **B.** Linear regression between real and predicted geosmin concentration values for the Artificial Neural Network PCA (Architecture E: 30x10x1). The red box frames the false positives and false negatives of the model.

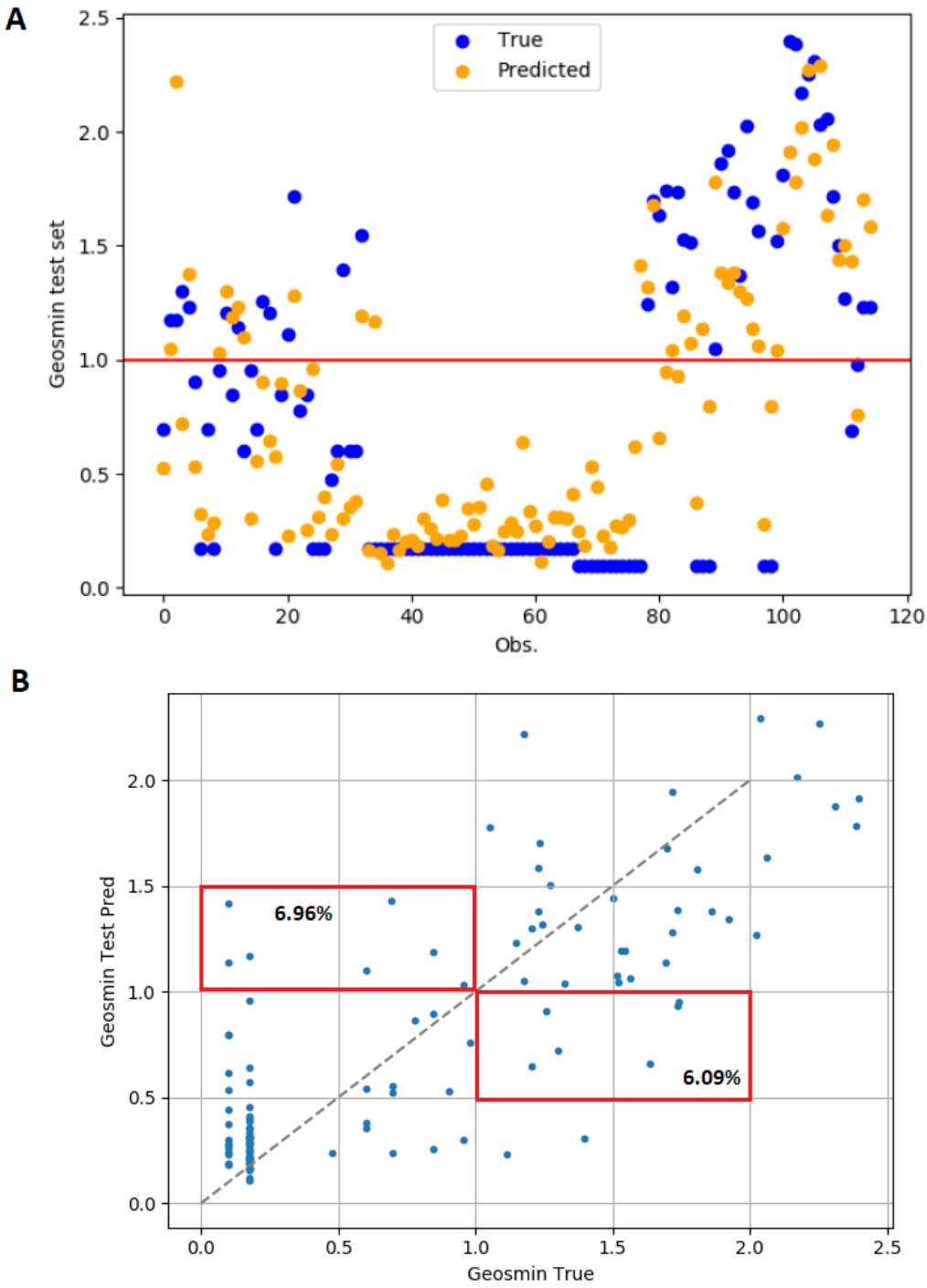

Figure 7.9. A. Graphical representation of the results from the Artificial Neural Network PCA (Architecture C: 10x10x1). The blue dots are the real values of geosmin, and the yellow dots are the predicted ones. The red line represents the detection limit of geosmin by humans (10 ng/L). Being on a logarithmic scale, it was located at the value of 1. **B.** Linear regression between real and predicted geosmin concentration values for the Artificial Neural Network PCA (Architecture C: 10x10x1). The red box frames the false positives and false negatives of the model.

7.6. Discussion

Thanks to the different evaluated approaches, it has been possible to obtain information on the involved variables in the geosmin appearance in the Ter river, as well as obtain capable models of determining the presence/absence of geosmin and its concentration in the water.

7.6.1. Discussion of the selected variables related with geosmin appearance

Most of the evaluated variables have been included in the models (**Table 7.2.**), and those that have been discarded are highly correlated with included variables (i.e. nitrites and nitrates, nitrates and N:P ratio, conductivity and oxygen). The difference in the approximations is based in the value of the coefficients of the variables, which indicate the weight they have within the model, the higher the coefficient the greater its role.

The variables with the greatest coefficients in the LoR model have been turbidity and the N:P ratio (**Table 7.2.**), the N:P ratio chosen in a negative way. These same variables are also the ones that have the most weight in the LiR model, along with the nitrite concentration. The LASSO approach, however, does not include them, choosing nitrite and phosphorus concentration first.

Based on these results, and as seen in the previous chapters (**Chapter 4** and **Chapter 6**), the nutrients concentration together with the N:P ratio are the determining factors in triggering geosmin episodes, and its monitoring is essential in the geosmin prediction. Similar results were found in other studies carried out with the aim of predicting geosmin concentration, which had also observed that low TN:TP ratio was predictive of the presence of geosmin and microcystins in reservoirs (Jacoby et al., 2015; Dzialowski et al., 2009). Although it has not been evaluated in this Thesis, spring phosphorus loads has been described as important explanatory variable for predicting cyanobacterial blooms (Bertani et al., 2016; Millie et al., 2014), whose presence has been widely related with the geosmin appearance (Watson et al., 2016).

Turbidity also seems to be a strong predictor variable of geosmin concentration (**Table7.2.**). This could have different explanations: the first one is that turbidity reduce the light incidence, factor that promote geosmin-cyanobacteria producers' development (**Chapter 5**). Another one is that when the geosmin-cyanobacteria producers are detached from the cobble, in addition to releasing the intracellular geosmin, it also releases different material, which can generate an increase in the turbidity value (i.e. solids trapped within thick biofilms in slow flow waters). Also, there are studies that have correlated a higher phosphorus concentration with a higher turbidity value (Schilling et al., 2017), which also occurs in this study (**Chapter 6**). This variable has been described as a predictive parameter in other studies, like the one performed by Harris and

Graham (2017) which recognized that maxima geosmin concentrations in Cheney reservoir was depended on turbidity and silica. Christensen et al. (2006) also found that turbidity and specific conductivity explained 71% of the geosmin appearance and Stone et al. (2013) was able to explain (only in a 21%) the variation in geosmin concentration with a linear model based on the turbidity and pH.

Chlorophyll *a* concentration has only played an important role in the LiR model, and its contribution has been negative (**Table 7.2.**). The inclusion of this parameter can be explained from what was observed in the experiments and in the field monitoring performed in this Thesis (**Chapter 4**, **Chapter 5** and **Chapter 6**), which is that it was negatively correlated with geosmin by decreasing its production when cyanobacteria begin to produce geosmin (Cai et al., 2017). However, it must be borne in mind that not all chlorophyll *a* concentration is produced only by the cyanobacteria present in the biofilm, existing more organisms that can influenced in this value. Although this parameter is included by the models evaluated, it is difficult to monitor by the drinking water treatment plants, so that in future models its inclusion would have to be reconsidered. Furthermore, the correlations found between chlorophyll and geosmin sometimes differs, since certain authors note correlations sometime positives and sometimes negative (Dzialowski et al., 2009; Saadoun et al., 2001). This could be due to the period chosen to carry out the study, the results of which could have been affected depending on whether the conditions were optimal for algal bloom. Another possibility is that the chlorophyll evaluated in this study comes from the biofilm, which may imply a temporality problem associated with geosmin beginning to develop first in the biofilm and then being released into the water, with a temporary mismatch between the factors involved in its production and release, and on the other hand, the geosmin is washed away, probably appearing further downstream of its production, generating in this case a spatial mismatch.

7.6.2. Discussion of model performance

One of the main problems when obtaining a good model has been the difficulty of predicting correctly the highest geosmin concentrations in the Ter river. One reason for the underestimation of high concentration by the models developed could be that geosmin exhibited substantial intra- and inter-annual variation (**Figure 7.3.**), which caused that model techniques (except MANN and MLDA) to underestimate the highest concentrations observed in the dataset.

Each of the evaluated models presents a series of advantages and disadvantages. The LoR model present a high test score value (r^2 = 0.827), and also reduces the number of variables to 11.

However, it only indicates the presence/absence of geosmin, which may be useful to the drinking water treatment plants as a first approximation but is inconsistent in determining the magnitude of the geosmin episode that may occur.

The LiR model is capable of predicting the presence/absence of geosmin in 83.8% of cases, however its ability to predict the exact geosmin concentration is low, presenting an r^2 score value of 0.465 (**Table 7.3.**). In comparison, the LASSO model reduces the variables to be analyzed by 4, including only 9 (**Table 7.2.**). But a disadvantage in its application is that its ability to determine the exact concentration of geosmin is less than the LiR model (r^2 score = 0.379, RMSE = 0.489 ± 0.124), and two of the variables it excludes (ammonium and nitrates) are necessary for the calculation of the N:P ratio, so it really only reduces the analysis of two variables, not being the best option for the management companies.

All approaches with ANN increase the value of test scores (**Table 7.3.**), highlighting the MPCA and MLDA models, with values of r^2 score of 0.598 and 0.596, respectively. These approximations also decrease the RMSE value significantly, up to 0.426 ± 0.098 for MPCA and 0.416 ± 0.105 for MLDA. Furthermore, the MLDA model can predict the presence/absence of geosmin in almost 87% of cases and achieves a good accuracy at high geosmin concentrations (**Figure 7.7.B.**). As a disadvantage of these models is that the 13 evaluated variables are included.

The comparison of the different models allows to conclude that the best model obtained that the drinking water treatment companies could implement in their facilities would be the MLDA, since it is the one that best predicts the presence/absence of geosmin as well as the exact concentration.

From these results, future objectives emerge, such as evaluating for example, the possibility of including other variables that have been seen to have a notable influence in the geosmin appearance, such as the water flow value, or generating new variables such as the change in temperature or N:P ratio between sampling days, instead of considering the absolute value. Likewise, trying to reduce the number of variables chosen by the models while maintaining predictive capacity, which would be an economic benefit for the drinking water treatment companies in the protocol for monitoring the appearance of geosmin.

Finally, an important point to keep in mind is that predictive models are based on recognizing processes based on patterns; however, because of climate change, these processes are and will continue to be altered. It has been described that climate change will generate more extreme events, resulting in increasing environmental variability. Therefore, the patterns affected by

climate change cause the predictive capacity of existing models to be altered and they will require continuous updating.

7.6.3. Monitoring recommendations for drinking water treatment plants

From the results generated, it has been seen that with a little more information about some key parameters, it can be easy to predict the appearance of geosmin, by simply introducing small changes in the water quality monitoring strategy carried out by Drinking Water Treatment Plants.

Currently, the drinking water treatment plants follow the regulations established in the R.D. 140/2003, modified by R.D. 902/2018, which establish the sanitary criteria for the water quality of human consumption. Clean and safe water for human consumption means that the water does not contain any type of microorganisms, parasite or substance, in an amount or concentration that may be a risk for human health. In case of geosmin, because it is a non-toxic substance, is not a parameter of mandatory analysis and monitoring for drinking water treatment plants.

To ensure that the water they are supplying meets the established requirements, the drinking water treatment plants have to carry out control analyzes. In this case, the protocol established includes the analysis of odor, taste, turbidity, color, conductivity, pH, ammonium, *E. coli* and coliform bacteria. The samples to be analyzed have to be taken at the collection point, the DWTP exit, each delivery point between the different managers and in the distribution network. The minimum sampling frequency depends on the volume of water distributed or produced each day in a supply area (e.g. >10000 m^3 means a monthly control analysis).

Considering the results obtained in the modelling process, it could be stated that if drinking water treatment plants are suffering geosmin episodes and they want to use the MLDA model developed, it would be recommended that they follow the following monitoring protocol:

a. Include the analysis of nitrites, nitrates and phosphorous concentration, organic matter, temperature, dissolved oxygen and percentage of saturation of the water samples from the collection point.
b. Include the analyses of chlorophyll *a* from a biofilm sample taken in a possible sampling site close to the water collection point.
c. Based on the results, carry out the N:P ratio calculation, where N is the sum of all the nitrogenous forms (N-ammonium, N-nitrites, N-nitrates), and both this value and the phosphorus concentration are transformed into moles.

d. Seeing the seasonal geosmin episodes, increase the number of analytics of water samples at the collection point between the months of January to June, starting with an analysis every 15 days and increasing the frequency depending on being in a situation where:
    a. The weather conditions are favorable for the development of cyanobacteria, such as a shortage of rainfall associated with a notable decrease in water flow.
    b. There is a progressive decrease between sampling days in the N:P ratio (more than 50%), guided by an increase in phosphorus concentration and a decrease in nitrate concentration.
    c. There is a progressive increase in the nitrite and turbidity values.

The implementation of this model would be very useful for companies responsible for the distribution of drinking water, since they could anticipate the geosmin presence in water and prevent it from reaching consumers' taps, without this entailing a high economic cost.

7.7. Conclusions

With the database generated by monitoring five sampling sites in the upper part of the Ter river basin for three years, it has been possible to develop a series of predictive models for the geosmin appearance. Between the evaluated models, the one with the highest predictive capacity was the MLDA, with a success rate of 87% and a RMSE value of 0.416 ± 0.105. Furthermore, this model is capable of predicting unusual high geosmin concentrations.

The implementation of this model in the drinking water treatment companies would represent a great advance in the prediction of geosmin episodes, without significant changes in their laboratory routines and significantly reducing the users complains and the possible economic losses associated with the decrease in drinking water quality. Since when carrying out the proposed monitoring, they will be prepared and will be able to apply the corresponding treatment on time, thus preventing water containing geosmin from leaving the treatment plant.

Despite the highly relevant results obtained in this study, a future step of validating the model has to be considered, with new data from the Ter river basin, even evaluating whether to include data from other basins.

CHAPTER 8. General discussion

8. General discussion

The different experimental approaches carried out in this Thesis have made possible to elucidate the main factors involved in triggering geosmin episodes by benthic producers in rivers. Thus, providing useful information for the water utilities and filling the gap leaved by other studies in the topic, which were focused in reservoirs and lakes or carried out with single species cultures under controlled laboratory conditions.

The main drivers of geosmin production identified in this Thesis have been: N:P ratio, nutrient concentration, water flow, light availability, turbidity and temperature. All of them have favored benthic cyanobacteria development, specifically of the *Oscillatoria* sp. genus.

Biofilm community composition

In freshwater ecosystems, cyanobacteria are considered the main geosmin producers (Olsen et al., 2016), and the most commonly genus present are *Oscillatoria* sp., *Anabaena* sp., *Lynghya* sp., and *Symploca* sp. (Smith et al., 2009). In both studies carried out in microcosms (aquariums) (**Chapter 4**) and in mesocosms (experimental rivers) (**Chapter 5**), it was identified that the cyanobacterium *Oscillatoria* sp. was the main geosmin producer present in the biofilm. At the end of the experiment carried out in the microcosms (t=21d), *Oscillatoria* sp. present a 45% of the total biofilm biovolume in the low N:P ratio – high nutrients treatment, while at the end of the experiment carried out in the experimental rivers was around 21% of the community in the biofilm developed under low water flow – low light availability, being in both cases its presence much higher than in the other treatments. In both situations the biofilm samples presented geosmin, 2.0 ± 0.7 ng/mg in the microcosms experiment and 2.1 ± 0.5 ng/mg in the mesocosms experiment.

In the study developed in the Ter river (**Chapter 6**) it was not possible to carry out the biofilm community composition identification at genus level, although at the time of the greatest geosmin episode it was possible to identify *in situ* the *Oscillatoria* sp. flocs. However, the main algal groups were identified: cyanobacteria, green algae and diatoms. The results obtained, highlights that the sampling site characterized by suffering a greater number of geosmin episodes (T7) was the one with the highest cyanobacteria presence compared to the sampling site in which no geosmin was detected (T1) (0.91 ± 0.58 µg/cm^2 in T7 compared to 0.33 ± 0.44 µg/cm^2 in T1). However, being a field study, it was more difficult to find significant correlations between geosmin and cyanobacteria abundance, since the presence of geosmin in water implies that the cyanobacteria in the biofilm die or cease to be attached to the substrate. This is due to the life cycle of cyanobacteria, specifically with the optimal geosmin production (growth phase)

and release time (biomass decomposition and/or cell lysis), since it has been described that many cyanobacteria species can produce geosmin although they may not actively release it until cell lysis occur (Kim et al., 2018). This fact could be corroborated in the experiment carried out in aquariums, where the cyanobacteria abundance decreased on the last day (t=21d) compared to the previous sampling day (t=16d), from 1.63 ± 0.36 µg chl*a*/cm^2 to 0.87 ± 0.38 µg chl*a*/cm^2, arguably because of cells degradation, and at this moment, there was an increase in the concentration of geosmin in water reaching 136 ± 6 ng/L. The time lag between a greater cyanobacteria presence and a notable increase in geosmin in water was one week (in aquariums) and 15 days in the field. These results agree with other studies which showed that, depending on the cyanobacterial strain, the growth phase can last between 8 and 24 days (Kruskopf & Du Plessis, 2006; Jindal et al., 2011).

Nutrient concentration and N:P ratio

Several studies performed in reservoirs and lakes have reported that cyanobacterial presence and growth is linked to the nutrient concentration, being greater their appearance under high nutrient conditions (Doods and Smith, 2016; Lee et al., 2017). The increase in the appearance of cyanobacteria is, in many cases, related with the geosmin production (Ding et al., 2014). Similar results were observed in the experiments performed throughout this Thesis, where higher nutrient concentration generated a favorable situation for the development of cyanobacterial biomass both in the experiment carried out in the microcosms (**Chapter 4**) and in the field (**Chapter 6**). In the experiment carried out in the microcosms, cyanobacteria biomass was higher (1.95 ± 0.36 µg/cm^2) under conditions of 682 ± 49 µg P-PO_4^{3-} and 1.17 ± 0.11 mg N-NO_3^- and in the field study, higher nutrient concentrations generated a favorable situation for the development of cyanobacteria biomass (0.91 ± 0.58 µg/cm^2). The average nutrient conditions (3 years) at sampling site T7, the one located downstream, was 82 ± 68 µg P-PO_4^{3-} and 1.36 ± 0.68 mg N-NO_3^-, whose high variation was related to the differences in the nutrients values generated by seasonality (**Chapter 6**), that also affected the N:P ratio value.

Although there are discrepancies in this regard, various studies have indicated that low N:P ratios can promote geosmin production (Vilalta et al., 2004). The study carried out in microcosms could determine that lower N:P ratios favored the production and release of geosmin by the cyanobacteria present, specifically the *Oscillatoria* sp. Furthermore, this study pointed out that the key situation driving geosmin production is the interaction of both factors. That is, the optimal conditions for geosmin production are higher nutrient concentration along with a lower N:P ratio. In the field study, this was clearly observed when comparing sampling sites T1 and T7. T1 was the sampling site located upstream, with the lower values of nutrient,

but with sporadic episodes of higher phosphorus concentration related to the poor performance of the WWTP in the area when they have an increase in the tourism, which generated lower N:P ratios (39:1 ± 27:1). However, no geosmin episodes were observed at this sampling site, corroborating *in situ*, that the interaction of both factors is needed for the development of this metabolite. Conversely, the T7 sampling site was located further downstream in the basin, undergoing greater anthropogenic pressure resulting in higher nutrient concentrations. At this sampling site, when there was an increase in the phosphorous concentration associated with agricultural land uses, the sowing of which occurs mainly in spring, a clear decrease in the N:P ratio value was observed. In the year 2019, a pronounced decrease in the N:P value gave rise to a very significant geosmin episode in T7, which reached values of almost 250 ng/L.

Even though the conditions in T7 didn't reach the lowest N:P ratio evaluated in the aquariums experiment, there was a decrease in the N:P ratio value between winter and spring in 2019 of almost 65%. This decrease in percentage was close to the one evaluated in the microcosms, that decrease between the colonization period and the treatment period (in the low ratio treatment) a 75%. Slightly lower N:P ratio decrease was observed in T5 (52 ± 4.2% N:P ratio decrease). While in the rest of the sampling sites, the N:P ratios remained fairly stable or even increased, with punctual moments in which there was a N:P decrease of around 20% (17% in T2, 20% in T1 and 24% in G1). With this data, it seems evident that reductions in N:P ratio higher than 50% can lead to the generation and release of geosmin into the water.

Water flow

Physicochemical and biological parameters can be affected by both land use and climatic conditions, thus having an effect on geosmin episodes. During the three years in which the field sampling was carried out, the climatic conditions were very varied, which has allowed identifying factors that favor the presence of geosmin in waters, since the geosmin concentration differed remarkably depending on the season and the year (**Chapter 6**).

Various studies have indicated that cyanobacteria develop better in calm waters, such as lakes and reservoirs, or in rivers, in areas close to dams or on riverbanks (Jüttner and Watson, 2007; Vilalta et al., 2004). The effect of the water flow was clearly observed when comparing the years 2018 and 2019, which were very different from each other. Being 2018 a very rainy year, with very cold average temperatures that gave rise to high water flows, while 2019 stood out for being a very dry year, with the absence of precipitation and high average temperatures, all this giving rise to historical minimum water flows. Under high nutrient concentrations and minimum water flows (T7 sampling site in 2019), cyanobacteria development was favored and a major

geosmin episode was triggered, reaching exceptionally high concentrations. Under the same conditions of high nutrient concentrations but with a higher water flow (T7 sampling site in 2018), no geosmin was detected. This makes clear the importance of the water flow factor in triggering geosmin production.

These results are completely in line with what was found in the mesocosms experiment (**Chapter 5**), where under low water flow and light availability, freshwater biofilms started to produce geosmin. This can be explained since water flow conditions can affect the biofilm biomass presence, being the biofilm growth favored under conditions of low – moderate water flow (Ateia et al., 2016). In a situation of high waterflow, biofilms are sloughed due to high shear stress, drag and abrasion, thus leading to a low biomass (Wellnitz and Rader, 2007; Ponsatí et al., 2016), as could be shown in the mesocosms experiment. Punctual precipitations can also generate this slough, altering the cyanobacteria life cycle and thus geosmin episodes, as happened in the field in 2017. This year there were geosmin episodes at some of the sampling sites (T5 and T7) but with lower values and shorter durations, since the conditions were favorable for cyanobacteria development, but the punctual rainfalls dragged the biofilm and it had to start developing from scratch.

Light availability

In the experiment carried out with the mesocosms was possible to observe that low water flows favored cyanobacteria development, but the interaction between low water flow and low light availability was the optimal condition for the geosmin production by these cyanobacteria (**Chapter 5**). Several studies pointed out that light affects the production of some volatile organic compounds (VOCs) and the growth of algal species (Lee et al., 2017; Alghanmi et al., 2018), being a key factor for geosmin production (Wang and Li, 2015). Indeed, it has been shown that high light availability can inhibit the formation of gaseous vacuoles in certain cyanobacteria (Li et al., 2012), which explain the low geosmin concentration found under natural light conditions compared with reduced light availability treatments evaluated in the mesocosms experiment. In the field campaign (**Chapter 6**), the effect of light availability could also be observed (although it could not be quantified), when it was detected, during the highest geosmin episode, a greater presence of *Oscillatoria* sp. close to the riverbank, where the waterflow was lower and the riparian forest buffered light incidence (personal observation). In addition to these local level differences, light availability varies throughout the year. In winter, values are around 75 µmol photons/m^2·s, in spring the PAR irradiance can increase up to 275 µmol photons/m^2·s, reaching the maximum in summer, with values over 500 µmol photons/m^2·s (Ruiz-González et al., 2012).

Therefore, seasonality plays an important role in the development of cyanobacteria, being winter and spring the most favorable seasons for its growth due to the lower light incidence.

Turbidity

In addition to the riparian forest, a factor that can affect the light incidence is the water turbidity, since high turbidity values could decrease the light availability favoring cyanobacteria development.

From the models generated (**Chapter 7**), turbidity seems to be a strong predictor variable of geosmin concentration, which could be for different reasons. The first one is the one mentioned above, the correlation existing between geosmin and turbidity is due to the consequence this last has on light availability and cyanobacteria development. Another possibility is the relationship also existing between turbidity and phosphorus, which has been described as a key factor triggering geosmin episodes, situation that happen in this study (**Chapter 6**) and that have been described in other studies (Schilling et al., 2017). This relationship may be due to the fact that much of the phosphorus that reaches the waters comes from the use of fertilizers in the cultivation fields. But before sowing, the land is plowed, which leads to the generation of particulate matter, which can be carried into the waters along with phosphorus, leading to an increase in the turbidity of the waters. The last possible explanation is that, when the geosmin-cyanobacteria producers are detached from the cobble, in addition to releasing the intracellular geosmin, it also releases different material (i.e. solids trapped within thick biofilm in slow flow waters), which can generate an increase in the turbidity value.

Temperature

This parameter has been chosen by the evaluated models, being positive correlated with geosmin (**Chapter 7**), however, the weight it presents was very low in all of them. This may be because the temperature factor has an effect on the geosmin formation only in a specific temperature range.

In the field study performed, the temperature value varied depending on the sampling site, seasonality and year. The sampling sites located upstream presented colder mean values (7.4 ± 3.6°C in T1) compared to those located downstream, whose mean temperature was higher (11.8 ± 5.2°C in T7) and where higher geosmin concentrations have been detected. However, in this sampling site (T7), geosmin was detected mainly at the end of winter – early spring when the temperatures were 10.3 ± 5.5°C for winter and 11.2 ± 5.5°C for spring, not finding geosmin in summer, even when the cyanobacteria relative abundance was also high and the average temperature increased until 21.2 ± 4.3°C. This may indicate that high temperatures can inhibit

the formation of this metabolite, agreeing with the study performed by Wang and Li (2015) which found that the maximal geosmin concentration and production were yield at 10°C compared with higher temperatures (25 and 35°C). Furthermore, the same average temperature (10 ± 3°C) was measured in the mesocosms experiment (**Chapter 4**), while in the microcosms experiment was fixed at 14°C (**Chapter 5**) indicating that slightly higher temperature remains optimal for geosmin formation.

Co-occurring events triggering geosmin episodes

From the different experimental approaches carried out throughout this Thesis, it was observed that it is a set of factors that, when co-occurring at a certain moment, give rise to the formation and subsequent release of geosmin in rivers.

Higher nutrient concentrations favor the cyanobacteria development in freshwater systems, being in the specific case of the Ter river the benthic cyanobacterium *Oscillatoria* sp. the one mainly related with geosmin episodes. Furthermore, this cyanobacterium growth is improved by low water flow, which can be generated by a punctual scarcity of rainfall, or more constantly in areas of stagnant water, such as areas close to dams or in the riverbanks. In addition, a higher light availability inhibits the formation of gas vacuoles, so that cyanobacteria are favored to develop under the shade of the riparian forest, in winter and spring, when the incidence of sunlight is lower. Temperature is added to these factors. Although there are studies that indicate that cyanobacteria are favored to grow at temperatures of 25°C, geosmin production is linked to lower temperatures, close to 10°C.

In a scenario such as the one defined, when is observed a significant decrease (> 50%) in the value of the N:P ratio, guided by an increase in the phosphorus concentration coming mainly from the adjacent farmland, the optimal conditions for these cyanobacteria to start producing geosmin co-occur. In addition, along with this phosphorous particulate matter is entrained, which increases the turbidity of the water, decreasing the availability of light, which favors even more the development of these cyanobacteria.

When all these factors co-occur, optimal conditions that trigger the production and release of geosmin are obtained, as occurred in 2019, which led to one of the largest geosmin episodes in the Ter river.

Chlorophyll a

Although it is not a trigger for geosmin formation, in all the studies carried out in this Thesis, the chlorophyll *a* concentration has proved to be a parameter intrinsically related to geosmin concentration. In the study performed in microcosms (**Chapter 4**) a negative correlation was

found between geosmin and chlorophyll *a* concentration in biofilm. This was observed at the end of the experiment, when the highest chlorophyll *a* concentration (18.3 ± 0.09 µg/cm^2) was measured in the treatment in which there was no geosmin production. In the mesocosms experiment (**Chapter 5**), it was observed that those treatments with extreme water flows, both the minimum and the maximum, presented a chlorophyll *a* concentration lower than the rest (both with values around 5 ± 1 µg/cm^2). In the treatment with the lowest water flow, the low chlorophyll *a* could be explained because the biofilms were sloughed due to high shear stress, drag and abrasion, leading to low biomass, as have been described in other studies (Wellnitz and Rader, 2007; Ponsatí et al., 2016). In the treatment with the lowest water flow, the low chlorophyll *a* concentration could be explained by the high geosmin concentration detected in biofilm in this treatment (2.12 ± 0.46 ng/mg). A similar pattern could be observed in the study conducted on the Ter river (**Chapter 6**). In this study, the chlorophyll a concentration increases throughout the basin, from values of 2.6 ± 2.9 µg/cm^2 in T1 to average values of 18.2 ± 17.8 µg/cm^2 in T7. This increase in the chlorophyll a concentration can be associated with a greater nutrient concentration present in the water, which favor the development of algal biomass and a great production of chlorophyll a (Urrea-Clos et al., 2014). But if the T7 sampling site in 2019 is evaluated in detail, it was observed that in late winter – spring, when the geosmin peak occurred, the chlorophyll a values were lower (10.3 ± 6.2 µg/cm^2) than the rest of the seasons (26.0 ± 21.3 µg/cm^2), founding a significant negative correlation between geosmin and chlorophyll. The reason behind this opposite behavior between chlorophyll *a* and geosmin found in all the experiments performed may be due to the fact that geosmin and chlorophyll *a* have the same metabolic pathway, and it has been described that when cyanobacteria start to synthesize geosmin, the chlorophyll a production decreases or even stops (Cai et al., 2017).

Therefore, monitoring the chlorophyll *a* concentration present in the biofilm may be indicative of the presence or absence of geosmin, provided that the conditions described in the previous section are met. The importance of this factor is reflected in the models generated, always being included negatively and with more or less weight depending on the model evaluated (**Chapter 7**).

Implementation of results in drinking water treatment plants

The results obtained in this Thesis have allowed, on the one hand, to identify the factors associated with the geosmin appearance in the waters of a Mediterranean river and how these have to interact to trigger the geosmin formation and, on the other, to generate a database robust enough to generate predictive models that can be implemented in drinking water treatment plants (DWTP).

By simply introducing small changes in the water quality monitoring strategy that the DWTP currently are carrying out it can be easy to predict the appearance of geosmin in the waters they supply. The main recommendations are:

- Include the analysis of nitrites, nitrates and phosphorous concentration, organic matter, temperature, dissolved oxygen and percentage of saturation of the water samples from the collection point.
- Carry out the DIN:SRP ratio calculation.
- Include the analyses of chlorophyll *a* from a biofilm sample taken in a possible sampling site close to the water collection point.
- Seeing the seasonal geosmin episodes, increase the number of analytics of water samples at the collection point between the months of January to June, starting with an analysis every 15 days and increasing the frequency if:
    - The weather conditions are favorable for the development of cyanobacteria, such as a shortage of rainfall associated with a notable decrease in water flow.
    - There is a progressive decrease between sampling days in the N:P ratio (more than 50%), guided by an increase in phosphorus concentration and a decrease in nitrate concentration.
    - There is a progressive increase in the nitrite and turbidity values.

With this information, the DWTP will be able to implement the LDA model developed in **Chapter 7**, and they could anticipate the geosmin presence in water and prevent it from reaching consumers' taps, without this entailing a high economic cost.

Future perspectives

The studies carried out and presented throughout this Thesis have established a good starting point for understanding the triggers of geosmin episodes in river systems from benthic producers. However, there are still questions that have remained unresolved.

A good point to evaluate is the effect generated by other trophic compartments in the development of the biofilm and in the production and subsequent release of geosmin into the water. For example, the presence of macroinvertebrates could alter the accumulation of geosmin. It can be hypothesized that a situation that favored a high percentage of grazers, which feed on biofilm, debris and submerged plants, would break the tendency of geosmin accumulation in the biofilm and release into the water that has been seen in experiments. Likewise, increasing the trophic level, the inclusion of fish in the study can be a very interesting factor since, on the one hand, they alter the presence of macroinvertebrates, and on the other,

they are organisms that can accumulate geosmin in their tissues, which means a problem for the aquaculture sector since fish with a high geosmin concentration have an unpleasant taste.

Finally, it should be noted that the models proposed in this Thesis have to pass a validation process. This means increasing the database with new samplings which could include other sampling sites in the Ter river basin with different ecological conditions, and also sampling sites located in different basins.

CHAPTER 9. General conclusions

9. General conclusions

This Thesis has reflected the study carried out during three years with the final aim of investigating the parameters associated with the production and release of geosmin, specifically from benthic communities in river ecosystems, and thus generate useful information that allows Drinking Water Treatment Plants to predict geosmin episodes. To achieve this objective, a multi-scale approach study has been carried out, starting from very controlled conditions (microcosm) to field studies. With the data generated in the field monitoring, a predictive model of the geosmin appearance has been developed.

The main conclusions derived from this Thesis are presented below.

- The N:P ratio and its interaction with the nutrient's concentration are key factors triggering geosmin episodes. In situations where there is a high concentration of nutrients, an imbalance in the N:P ratio generated by a higher phosphorus concentration favors the development and growth of cyanobacteria such as *Oscillatoria* sp. which, under these conditions, begin to produce geosmin.
- The N:P ratio does not only have an effect as an absolute value, but a reduction between 50 – 75% of this N:P ratio, guided by a specific increase in phosphorus concentration and a decrease in nitrate concentration, is a key factor in triggering the geosmin production.
- The interaction between water flow and light availability also have an important effect in the geosmin appearance. Low water flow conditions together with low light availability (80% light reduction) favor the development of cyanobacteria, specifically *Oscillatoria* sp., and the geosmin production by them.
- The effect of all these parameters can be affected by weather conditions, since the number of precipitations and their intensity, together with the ambient temperature, can alter the average water flow determining whether or not episodes of geosmin may occur.
- Although it is not a trigger, it has been observed that the chlorophyll *a* concentration present in the biofilm may be indicative of the geosmin appearance, since it presents a negative correlation with this metabolite.
- With the information obtained, it has been seen that from the cyanobacteria begin to produce geosmin until they are released, 15 days pass. So, when the conditions are favorable for the cyanobacteria development, including the analysis of geosmin in biofilm can be very useful, considering that once detected in the biofilm it will take 15 days to detect geosmin in water.

- The physicochemical variables studied better explain the geosmin presence in water, while the biological variables are more related to the concentration of geosmin in biofilm. Specifically, cyanobacteria biomass has been positively correlated with the geosmin concentration present in the biofilm. Therefore, a useful tool for water utilities may be to include cyanobacteria or *Oscillatoria* sp. presence monitoring in their routine.
- With the information obtained in the study carried out in the field, it has been possible to develop different approaches to obtain a geosmin predictive model. The best developed model has been the *Linear Discriminant Analysis* (MLDA), capable to predict the exact geosmin concentration with a test r^2 = 0.596, and correctly predicting the geosmin presence – absence in 87% of cases. This result is of great importance since it is the first developed model to predict geosmin in rivers.
- In order to carry out this model implementation and solve the problems caused by the presence of geosmin, a change in the monitoring strategy must be carried out. The sampling at the catchment point of the drinking water treatment plants must be increased and it has to include the analysis of the nitrites, nitrates and phosphorous concentration in the water, water temperature, dissolved oxygen and organic matter. The monitoring of the chlorophyll concentration present in the biofilm must also be included. These variables are easy to monitor and analyze by the water treatment plants laboratories, and do not represent such a high economic cost as the analysis of geosmin concentration per se.
- The parameters that have been identified as triggers of geosmin episodes are greatly affected by land uses and weather. This implies that areas that currently do not present the favorable conditions, due to changes in land uses associated with urban and industrial growth and changes in climatic conditions associated with global change, could become susceptible to geosmin episodes in the future. Therefore, the information generated in this Thesis can serve as a tool to identify future geosmin situations in situations that casuistry does not currently exist.

As future work to point out is that the predictive model developed in this Thesis, which has been generated with a 3-year database, would need to be validated using new data in the coming years before being applied in the reality by Drinking Water Treatment plants.

References

Acuña, V., & Tockner, K. (2010). The effects of alterations in temperature and flow regime on organic carbon dynamics in Mediterranean river networks. *Global Change Biology*, *16*(9), 2638–2650.

Afed Ullah, K., Jiang, J., & Wang, P. (2018). Land use impacts on surface water quality by statistical approaches. *Global Journal of Environmental Science and Management*, *4*(2), 231-250.

Aguilera Becker, R. (2015). Effects of land uses and climate variability on the water quality of Mediterranean rivers: towards a regional vision of global change.

Ai, L., Shi, Z. H., Yin, W., & Huang, X. (2015). Spatial and seasonal patterns in stream water contamination across mountainous watersheds: Linkage with landscape characteristics. *Journal of Hydrology*, *523*, 398-408.

Alghanmi, H. A., Alkam, F. M., & Al-Taee, M. M. (2018). Effect of light and temperature on new cyanobacteria producers for geosmin and 2-methylisoborneol. *Journal of Applied Phycology*, *30*(1), 319–328.

Allan, J. D., & Castillo, M. M. (2007). *Stream ecology: structure and function of running waters*. Springer Science & Business Media.

Argudo, M., Gich, F., Bonet, B., Espinosa, C., Gutiérrez, M., & Guasch, H. (2020). Responses of resident (DNA) and active (RNA) microbial communities in fluvial biofilms under different polluted scenarios. *Chemosphere*, *242*, 125108.

Artigas, J., Romaní, A. M., & Sabater, S. (2008). Relating nutrient molar ratios of microbial attached communities to organic matter utilization in a forested stream. *Fundamental and Applied Limnology/Archiv für Hydrobiologie*, *173*(3), 255-264.

Artigas, J., García-Berthou, E., Bauer, D. E., Castro, M. I., Cochero, J., Colautti, D. C., ... & Giorgi, A. (2013). Global pressures, specific responses: effects of nutrient enrichment in streams from different biomes. *Environmental Research Letters*, *8*(1), 014002.

Artigas, J., Romaní, A. M., & Sabater, S. (2015). Nutrient and enzymatic adaptations of stream biofilms to changes in nitrogen and phosphorus supply. *Aquatic Microbial Ecology*, *75*(2), 91-102.

Ateia, M., Nasr, M., Ikeda, A., Okada, H., Fujii, M., Natsuike, M., & Yoshimura, C. (2016). Nonlinear relationship of near-bed velocity and growth of riverbed periphyton. *Water (Switzerland)*, *8*(10), 1–12.

Bai, M., Yu, Y., Cheng, J., Ji, Z., & Li, J. (2019). OH degraded 2-Methylisoborneol during the removal of algae-laden water in a drinking water treatment system: Comparison with ClO2. *Chemosphere*, *236*, 124342.

Bangash, R. F., Passuello, A., Sanchez-Canales, M., Terrado, M., López, A., Elorza, F. J., … Schuhmacher, M. (2013). Ecosystem services in Mediterranean river basin: Climate change impact on water provisioning and erosion control. *Science of the Total Environment*, *458–460*, 246–255.

Barral-Fraga, L., Martiñá-Prieto, D., Barral, M. T., Morin, S., & Guasch, H. (2018). Mutual interaction between arsenic and biofilm in a mining impacted river. *Science of the Total Environment*, *636*, 985-998.

Battin, T. J., Kaplan, L. A., Newbold, J. D., & Hansen, C. M. (2003). Contributions of microbial biofilms to ecosystem processes in stream mesocosms. *Nature*, *426*(6965), 439-442.

Battin, T. J., Besemer, K., Bengtsson, M. M., Romani, A. M., & Packmann, A. I. (2016). The ecology and biogeochemistry of stream biofilms. *Nature Reviews Microbiology*, *14*(4), 251.

Beaulieu, M., Pick, F., Palmer, M., Watson, S., Winter, J., Zurawell, R., & Gregory-Eaves, I. (2014). Comparing predictive cyanobacterial models from temperate regions. *Canadian Journal of Fisheries and Aquatic Sciences*, *71*(12), 1830-1839.

Becher, P. G., Verschut, V., Bibb, M. J., Bush, M. J., Molnár, B. P., Barane, E., ... & Buttner, M. J. (2020). Developmentally regulated volatiles geosmin and 2-methylisoborneol attract a soil arthropod to Streptomyces bacteria promoting spore dispersal. *Nature Microbiology*, 1-9.

Bechtold, H. A., Marcarelli, A. M., Baxter, C. V., & Inouye, R. S. (2012). Effects of N, P, and organic carbon on stream biofilm nutrient limitation and uptake in a semi-arid watershed. *Limnology and Oceanography*, *57*(5), 1544-1554.

Bertani, I., Obenour, D. R., Steger, C. E., Stow, C. A., Gronewold, A. D., & Scavia, D. (2016). Probabilistically assessing the role of nutrient loading in harmful algal bloom formation in western Lake Erie. *Journal of Great Lakes Research*, *42*(6), 1184-1192.

Birgand, F., Skaggs, R. W., Chescheir, G. M., & Gilliam, J. W. (2007). Nitrogen removal in streams of agricultural catchments—a literature review. *Critical Reviews in Environmental Science and Technology*, *37*(5), 381-487.

Blevins, W. T., Schrader, K. K., & Saadoun, I. (1995). Comparative physiology of geosmin production by Streptomyces halstedii and Anabaena sp. *Water Science and Technology*, *31*(11), 127.

Bonnineau, C., Guasch, H., Proia, L., Ricart, M., Geiszinger, A., Romaní, A. M., & Sabater, S. (2010). Fluvial biofilms: a pertinent tool to assess β-blockers toxicity. *Aquatic Toxicology*, *96*(3), 225-233.

Bowes, M. J., Ings, N. L., McCall, S. J., Warwick, A., Barrett, C., Wickham, H. D., ... & Lehmann, K. (2012). Nutrient and light limitation of periphyton in the River Thames: implications for catchment management. *Science of the Total Environment*, *434*, 201-212.

Cai, T., Park, S. Y., & Li, Y. (2013). Nutrient recovery from wastewater streams by microalgae: status and prospects. *Renewable and Sustainable Energy Reviews*, *19*, 360-369.

Cai, F., Yu, G., Zhang, K., Chen, Y., Li, Q., Yang, Y., … Li, R. (2017). Geosmin production and polyphasic characterization of *Oscillatoria limosa Agardh ex Gomon*t isolated from the open canal of a large drinking water system in Tianjin City, China. *Harmful Algae*, *69*, 28–37.

Cane, D. E., He, X., Kobayashi, S., Ōmura, S., & Ikeda, H. (2006). Geosmin biosynthesis in Streptomyces avermitilis. Molecular cloning, expression, and mechanistic study of the germacradienol/geosmin synthase. *The Journal of antibiotics*, *59*(8), 471-479.

Casas-Ruiz, J. P., Tittel, J., von Schiller, D., Catalán, N., Obrador, B., Gómez-Gener, L., ... & Marcé, R. (2016). Drought-induced discontinuities in the source and degradation of dissolved organic matter in a Mediterranean river. *Biogeochemistry*, *127*(1), 125-139.

Castellini, A., Franco, G. & Rodegher, M. (2009). Tutorial: Linear Regression Plugin for MetaPlab.

Ceola, S., Hödl, I., Adlboller, M., Singer, G., Bertuzzo, E., Mari, L., … Rinaldo, A. (2013). Hydrologic Variability Affects Invertebrate Grazing on Phototrophic Biofilms in Stream Microcosms. *PLoS ONE*, *8*(4).

Céspedes, R., Lacorte, S., Ginebreda, A., & Barceló, D. (2008). Occurrence and fate of alkylphenols and alkylphenol ethoxylates in sewage treatment plants and impact on receiving waters along the Ter River (Catalonia, NE Spain). *Environmental Pollution*, *153*(2), 384–392.

Christensen, V. G., Graham, J. L., Milligan, C. R., Pope, L. M., & Ziegler, A. C. (2006). *Water quality and relation to taste-and-odor compounds in the North Fork Ninnescah River and Cheney Reservoir, south-central Kansas, 1997-2003*. U. S. Geological Survey.

Chróst, R. J., & Krambeck, H. J. (1986). Fluorescence correction for measurements of enzyme activity in natural waters using methylumbelliferyl-substrates. *Archiv für Hydrobiologie*, *106*(1), 79-90.

Cid, N., Bonada, N., Carlson, S. M., Grantham, T. E., Gasith, A., & Resh, V. H. (2017). High variability is a defining component of Mediterranean-climate rivers and their biota. *Water*, *9*(1), 52.

Clements, W. H., & Newman, M. C. (2003). *Community ecotoxicology*. John Wiley & Sons.

Corcoll, N., Bonet, B., Leira, M., Montuelle, B., Tlili, A., & Guasch, H. (2012). Light History Influences the Response of Fluvial Biofilms to Zn Exposure. *Journal of Phycology*, *48*(6), 1411–1423.

Dal Sasso, S. F., Sole, A., Mirauda, D., Volpe Plantamura, A., & Masi, V. (2015). Riverbed dynamic evolution following landslide dam: a case study. *Journal of Applied Water Engineering and Research*, *3*(2), 67–79.

De Fraiture, C., Giordano, M., & Liao, Y. (2008). Biofuels and implications for agricultural water use: blue impacts of green energy. *Water policy*, *10*(S1), 67-81.

de Sanidad, G. (1980). Real Decreto 140/2003, de 7 de febrero, por el que se establecen los criterios sanitarios de la calidad del agua de consumo humano.

Dickschat, J. S., Bode, H. B., Mahmud, T., Müller, R., & Schulz, S. (2005). A novel type of geosmin biosynthesis in myxobacteria. *The Journal of organic chemistry*, *70*(13), 5174-5182.

Ding, Z., Peng, S., Jin, Y., Xuan, Z., Chen, X., & Yin, L. (2014). Geographical and seasonal patterns of geosmin and 2-methylisoborneol in environmental water in Jiangsu Province of China. *Journal of Analytical Methods in Chemistry*, 2014.

Dodds, W. K., Smith, V. H., & Lohman, K. (2002). Nitrogen and phosphorus relationships to benthic algal biomass in temperate streams. *Canadian Journal of Fisheries and Aquatic Sciences*, *59*(5), 865-874.

Dodds, W. K. (2003). The role of periphyton in phosphorus retention in shallow freshwater aquatic systems. *Journal of Phycology*, *39*(5), 840-849.

Dodds, W. K., & Smith, V. H. (2016). Nitrogen, phosphorus, and eutrophication in streams. *Inland Waters,* 6(2), 155-164.

Dzialowski, A. R., Smith, V. H., Huggins, D. G., deNoyelles, F., Lim, N. C., Baker, D. S., & Beury, J. H. (2009). Development of predictive models for geosmin-related taste and odor in Kansas, USA, drinking water reservoirs. *water research*, *43*(11), 2829-2840.

Echenique-Subiabre, I., Dalle, C., Duval, C., Heath, M. W., Couté, A., Wood, S. A., ... & Quiblier, C. (2016). Application of a spectrofluorimetric tool (bbe BenthoTorch) for monitoring potentially toxic benthic cyanobacteria in rivers. *Water research*, *101*, 341-350.

Eckle, K., & Schmidt-Hieber, J. (2019). A comparison of deep networks with ReLU activation function and linear spline-type methods. *Neural Networks*, *110*, 232-242.

Egas, D., Vasilaki, V., Katsou, E., Stanchev, P., Ponsá, S., & Colon, J. (2019). Implementation of the Product Environmental Footprint Category Rules for dairy products: An approach to assess nitrogen emissions in a mass balanced dairy farm system. *Journal of cleaner production*, *215*, 1149-1159.

Elosegi, A., & Sabater, S. (2013). Effects of hydromorphological impacts on river ecosystem functioning: a review and suggestions for assessing ecological impacts. *Hydrobiologia*, *712*(1), 129-143.

Espinosa, C., Abril, M., Guasch, H., Pou, N., Proia, L., Ricart, M., Ordeix, M. & Llenas, L. (2020). Water flow and light availability influence on intracellular geosmin production in river biofilms. *Front. Microbiol.* 10.3002.

Fai, P. B., Grant, A., & Reid, B. (2007). Chlorophyll a fluorescence as a biomarker for rapid toxicity assessment. *Environmental Toxicology and Chemistry: An International Journal*, *26*(7), 1520-1531.

Farinelli, A., Zanotto, E., & Pagello, E. (2017). Advanced approaches for multi-robot coordination in logistic scenarios. *Robotics and Autonomous Systems*, *90*, 34-44.

Feio, M. J., Ferreira, J., Buffagni, A., Erba, S., Dörflinger, G., Ferréol, M., ... & Urbanič, G. (2014). Comparability of ecological quality boundaries in the Mediterranean basin using freshwater benthic invertebrates. Statistical options and implications. *Science of the Total Environment*, *476*, 777-784.

Felisberto, S. A., Leandrini, J. A., & Rodrigues, L. (2011). Effects of nutrients enrichment on algal communities: an experimental in mesocosms approach. *Acta Limnologica Brasiliensia*, 23(2), 128-137.

First, P. J. (2019). Global Warming of 1.5 C An IPCC Special Report on the Impacts of Global Warming of 1.5 C Above Pre-Industrial Levels and Related Global Greenhouse Gas Emission Pathways, in the Context of Strengthening the Global Response to the Threat of Climate Change. *Sustainable Development, and Efforts to Eradicate Poverty. https://www. ipcc. ch/sr15/. Accessed*, *1*.

French, E., Kozlowski, J. A., Mukherjee, M., Bullerjahn, G., & Bollmann, A. (2012). Ecophysiological characterization of ammonia-oxidizing archaea and bacteria from freshwater. *Appl. Environ. Microbiol.*, *78*(16), 5773-5780.

Geider, R. J., & La Roche, J. (2002). Redfield revisited: variability of C [ratio] N [ratio] P in marine microalgae and its biochemical basis. *European Journal of Phycology*, *37*(1), 1-17.

Giglio, S., Jiang, J., Saint, C.P., Cane, D.E., & Monis, P.T. (2008). Isolation and characterization of the gene associated with geosmin production in cyanobacteria. *Environmental Science & Technology*, 42(21), 8027-8032.

Graba, M., Sauvage, S., Moulin, F. Y., Urrea, G., Sabater, S., & Sanchez-Pérez, J. M. (2013). Interaction between local hydrodynamics and algal community in epilithic biofilm. *Water research*, *47*(7), 2153-2163.

Graham, A. A., McCaughan, D. J., & McKee, F. S. (1988). Measurement of surface area of stones. Hydrobiologia, 157(1), 85-87.

Grizzetti, B., Bouraoui, F., Billen, G., van Grinsven, H., Cardoso, A. C., Thieu, V., ... & Johnes, P. (2011). Nitrogen as a threat to European water quality.

Grossart, H. P., Tang, K. W., Kiørboe, T., & Ploug, H. (2007). Comparison of cell-specific activity between free-living and attached bacteria using isolates and natural assemblages. *FEMS microbiology letters*, *266*(2), 194-200.

Guasch, H., Lehmann, V., Van Beusekom, B., Sabater, S., & Admiraal, W. (2007). Influence of phosphate on the response of periphyton to atrazine exposure. *Archives of environmental contamination and toxicology*, *52*(1), 32-37.

Guasch, H., Leira, M., Montuelle, B., Geiszinger, A., Roulier, J. L., Tornés, E., & Serra, A. (2009). Use of multivariate analyses to investigate the contribution of metal pollution to diatom species composition: search for the most appropriate cases and explanatory variables. *Hydrobiologia*, *627*(1), 143-158.

Guo, W., Ngo, H. H., & Li, J. (2012). A mini-review on membrane fouling. *Bioresource technology*, *122*, 27-34.

Harris, T. D., & Graham, J. L. (2017). Predicting cyanobacterial abundance, microcystin, and geosmin in a eutrophic drinking-water reservoir using a 14-year dataset. *Lake and reservoir management*, *33*(1), 32-48.

Harris T, Smith V, Graham J, Van de Waal D, Tedesco L, Clercin N. (2016). Combined effects of nitrogen to phosphorus and nitrate to ammonia ratios on cyanobacterial metabolite concentrations in eutrophic Midwestern USA reservoirs. *Inland Waters*. 6:199–210.

Hill, W. R., Fanta, S. E., & Roberts, B. J. (2009). Quantifying phosphorus and light effects in stream algae. *Limnology and oceanography*, *54*(1), 368-380.

Hillebrand, H., Dürselen, C. D., Kirschtel, D., Pollingher, U., & Zohary, T. (1999). Biovolume calculation for pelagic and benthic microalgae. *Journal of phycology*, *35*(2), 403-424.

Ho, L., Dreyfus, J., Boyer, J., Lowe, T., Bustamante, H., Duker, P., Meli, T., Newcombe, G. (2012) Fate of cyanobacteria and their metabolites during water treatment sludge management processes. *Sci Total Environ* 424:232–238.

Jacoby, J., Burghdoff, M., Williams, G., Read, L., & Hardy, F. J. (2015). Dominant factors associated with microcystins in nine midlatitude, maritime lakes. *Inland Waters*, *5*(2), 187-202.

Jankowiak, J., Hattenrath-Lehmann, T., Kramer, B. J., Ladds, M., & Gobler, C. J. (2019). Deciphering the effects of nitrogen, phosphorus, and temperature on cyanobacterial

bloom intensification, diversity, and toxicity in western Lake Erie. *Limnology and Oceanography*, 64(3), 1347-1370.

Jeffrey, S.W. & Humphrey, G.F. (1975). New spectrophotometric equations for determining chlorophylls a, b, c_1 and c_2 in higher plants, algae and natural phytoplankton. *Biochemical Physiology Pflanzen*, 167, 191 - 194.

Jiang, J., & Cane, D. E. (2008). Geosmin biosynthesis. Mechanism of the fragmentation–rearrangement in the conversion of germacradienol to geosmin. *Journal of the American Chemical Society*, *130*(2), 428-429.

Jindal, N., Singh, D. P., & Khattar, J. I. S. (2011). Kinetics and physico-chemical characterization of exopolysaccharides produced by the cyanobacterium *Oscillatoria formosa*. *World Journal of Microbiology and Biotechnology*, 27(9), 2139-2146.

Jones, G. J., & Korth, W. (1995). In situ production of volatile odour compounds by river and reservoir phytoplankton populations in Australia. *Water Science and Technology*, *31*(11), 145-151.

Jordà-Capdevila, D., Rodríguez-Labajos, B., & Bardina, M. (2016). A five-step assessment of river ecosystem services to inform conflictive water-flows management–the Ter River case. *VertigO-la revue électronique en sciences de l'environnement*, (Hors-série 25).

Jørgensen, N. O., Podduturi, R., & Burford, M. A. (2016). Relations between abundance of potential geosmin-and 2-MIB-producing organisms and concentrations of these compounds in water from three Australian reservoirs. *Journal of Water Supply: Research and Technology-Aqua*, *65*(6), 504-513.

Jüttner, F., & Watson, S. B. (2007). Biochemical and Ecological Control of Geosmin and 2-Methylisoborneol in Source Waters*. Applied and Environmental Microbiology, 73*(14), 4395–4406.

Karaouzas, I., Theodoropoulos, C., Vardakas, L., Kalogianni, E., & Th. Skoulikidis, N. (2018). A review of the effects of pollution and water scarcity on the stream biota of an intermittent Mediterranean basin. *River Research and Applications*, *34*(4), 291–299.

Karatan, E., & Watnick, P. (2009). Signals, regulatory networks, and materials that build and break bacterial biofilms. *Microbiol. Mol. Biol. Rev.*, *73*(2), 310-347.

Kibuye, F. A., Gall, H. E., Veith, T. L., Elkin, K. R., Elliott, H. A., Harper, J. P., & Watson, J. E. (2020). Influence of hydrologic and anthropogenic drivers on emerging organic contaminants in drinking water sources in the Susquehanna River Basin. *Chemosphere*, *245*, 125583.

Kim, K., Park, C., Yoon, Y., & Hwang, S. J. (2018). Harmful Cyanobacterial Material Production in the North Han River (South Korea): Genetic Potential and Temperature-Dependent Properties. *International journal of environmental research and public health*, 15(3), 444.

Kirst, H., Formighieri, C., & Melis, A. (2014). Maximizing photosynthetic efficiency and culture productivity in cyanobacteria upon minimizing the phycobilisome light-harvesting antenna size. *Biochimica et Biophysica Acta (BBA)-Bioenergetics*, *1837*(10), 1653-1664.

Klausen, C., Nicolaisen, M. H., Strobel, B. W., Warnecke, F., Nielsen, J. L., & Jørgensen, N. O. (2005). Abundance of actinobacteria and production of geosmin and 2-methylisoborneol in Danish streams and fish ponds. *FEMS microbiology ecology*, *52*(2), 265-278.

Krammer, K., Lange-Bertalot, H., 1991-1997. Bacillariophyceae. Süsswasserflora von Mitteleuropa, Vol. 2. Fischer, Stuttgart.

Kruskopf, M., & Du Plessis, S. (2006). Growth and filament length of the bloom forming *Oscillatoria simplicissima* (Oscillatoriales, Cyanophyta) in varying N and P concentrations. *Hydrobiologia*, 556(1), 357-362.

Kurz, M. J., Drummond, J. D., Martí, E., Zarnetske, J. P., Lee-Cullin, J., Klaar, M. J., ... & Datry, T. (2017). Impacts of water level on metabolism and transient storage in vegetated lowland rivers: Insights from a mesocosm study. *Journal of Geophysical Research: Biogeosciences*, *122*(3), 628-644.

Lange-Bertalot, H., 2001. Diatoms of Europe. Navicula sensu strictu, 10 genera separated from Navicula sensu lato, Frustulia, 2. Gantner Verlag, Ruggell.

Lee, J., Rai, P. K., Jeon, Y. J., Kim, K. H., & Kwon, E. E. (2017). The role of algae and cyanobacteria in the production and release of odorants in water. *Environmental Pollution*, *227*, 252–262.

Leff, L., Van Gray, J. B., Martí, E., Merbt, S. N., & Romaní, A. M. (2016). Aquatic biofilms and biogeochemical processes. *Aquatic biofilms: Ecology, water quality and wastewater treatment*, 89-108.

Li, Z., House, J., Burch, M. D., Hobson, P., Yang, M., & An, W. (2012). Earthy odor compounds production and loss in three cyanobacterial cultures. *Water Research*, *46*(16), 5165–5173.

Li, J., Hansson, L. A., & Persson, K. M. (2018). Nutrient control to prevent the occurrence of cyanobacterial blooms in a eutrophic lake in Southern Sweden, used for drinking water supply. *Water*, *10*(7), 919.

Lindholm-Lehto, P.C. & Vielma, J. (2018). Controlling of geosmin and 2-methylisoborneol induced off-flavours in recirculating aquaculture system farmed fish – A review. *Aquaculture Research,* 50(1), 9 – 28.

Ludwig, F., Medger, A., Börnick, H., Opitz, M., Lang, K., Göttfert, M., & Röske, I. (2007). Identification and expression analyses of putative sesquiterpene synthase genes in Phormidium sp. and prevalence of geoA-like genes in a drinking water reservoir. *Appl. Environ. Microbiol.*, *73*(21), 6988-6993.

Luimstra, V. M., Schuurmans, J. M., Verschoor, A. M., Hellingwerf, K. J., Huisman, J., & Matthijs, H. C. P. (2018). Blue light reduces photosynthetic efficiency of cyanobacteria through an imbalance between photosystems I and II. *Photosynthesis Research*, *138*(2), 177–189.

Lurling, M., Mello, M. M., van Oosterhout, F., De Senerpont Domis, L. N., & Marinho, M. M. (2018). Response of natural cyanobacteria and algae assemblages to a nutrient pulse and elevated temperature. *Frontiers in microbiology*, 9, 1851.

Marcarelli, A. M., Bechtold, H. A., Rugenski, A. T., & Inouye, R. S. (2009). Nutrient limitation of biofilm biomass and metabolism in the Upper Snake River basin, southeast Idaho, USA. *Hydrobiologia*, *620*(1), 63–76.

Margalef, R. (1960). Recientes progresos en el estudio de las comunidades vegetales por medio de la extracción de pigmentos.

McClellan, K., Altenburger, R., & Schmitt-Jansen, M. (2008). Pollution-induced community tolerance as a measure of species interaction in toxicity assessment. *Journal of Applied Ecology*, *45*(5), 1514-1522.

Merbt, S. N., Bernal, S., Proia, L., Martí, E., & Casamayor, E. O. (2017). Photoinhibition on natural ammonia oxidizers biofilm populations and implications for nitrogen uptake in stream biofilms. *Limnology and Oceanography*, *62*(1), 364-375.

Nikolcheva, L. G., & Bärlocher, F. (2004). Taxon-specific fungal primers reveal unexpectedly high diversity during leaf decomposition in a stream. *Mycological Progress*, *3*(1), 41-49.

de Catalunya, G. (2018). Servei Meteorològic de Catalunya. *Anuari de dades meteorològiques 2009*.

Millie, D. F., Weckman, G. R., Fahnenstiel, G. L., Carrick, H. J., Ardjmand, E., Young, W. A., ... & Shuchman, R. A. (2014). Using artificial intelligence for CyanoHAB niche modeling: discovery and visualization of Microcystis–environmental associations within western Lake Erie. *Canadian Journal of Fisheries and Aquatic Sciences*, *71*(11), 1642-1654.

Montuelle, B., Dorigo, U., Bérard, A., Volat, B., Bouchez, A., Tlili, A., ... & Pesce, S. (2010). The periphyton as a multimetric bioindicator for assessing the impact of land use on rivers: an overview of the Ardières-Morcille experimental watershed (France). In *Global Change and River Ecosystems—Implications for Structure, Function and Ecosystem Services* (pp. 123-141). Springer, Dordrecht.

Mora-Gómez, J., Freixa, A., Perujo, N., & Barral-Fraga, L. (2016). Limits of the biofilm concept and types of aquatic biofilms. *Aquatic Biofilms. Ecology, Water Quality and Wastewater Treatment*, 229.

Murphy, J. A. M. E. S., & Riley, J. P. (1962). A modified single solution method for the determination of phosphate in natural waters. *Analytica chimica acta*, *27*, 31-36.

Oh, H. S., Lee, C. S., Srivastava, A., Oh, H. M., & Ahn, C. Y. (2017). Effects of environmental factors on cyanobacterial production of odorous compounds: geosmin and 2-methylisoborneol. *Journal of microbiology and biotechnology*, *27*(7), 1316-1323.

Olsen, B. K., Chislock, M. F., & Wilson, A. E. (2016). Eutrophication mediates a common off-flavor compound, 2-methylisoborneol, in a drinking water reservoir. *Water Research*, *92*, 228–234.

Ongley, E. D., Xiaolan, Z., & Tao, Y. (2010). Current status of agricultural and rural non-point source pollution assessment in China. *Environmental Pollution*, *158*(5), 1159-1168.

Pagliai, M., Vignozzi, N., & Pellegrini, S. (2004). Soil structure and the effect of management practices. *Soil and Tillage Research*, *79*(2), 131-143.

Pardo, I., Álvarez, M., Casas, J., Moreno, J. L., Vivas, S., Bonada, N., ... & Robles, S. (2002). El hábitat de los ríos mediterráneos. Diseño de un índice de diversidad de hábitat. *Limnetica*, *21*(3-4), 115-133.

Parinet, J., Rodriguez, M. J., & Sérodes, J. (2010). Influence of water quality on the presence of off-flavour compounds (geosmin and 2-methylisoborneol). *Water Research*, *44*(20), 5847–5856.

Parinet, J., Rodriguez, M. J., & Sérodes, J. B. (2013). Modelling geosmin concentrations in three sources of raw water in Quebec, Canada. *Environmental monitoring and assessment*, *185*(1), 95-111.

Ponsatí, L., Corcoll, N., Petrović, M., Picó, Y., Ginebreda, A., Tornés, E., … Sabater, S. (2016). Multiple-stressor effects on river biofilms under different hydrological conditions. *Freshwater Biology*, *61*(12), 2102–2115.

Price, K. J., & Carrick, H. J. (2016). Effects of experimental nutrient loading on phosphorus uptake by biofilms: evidence for nutrient saturation in mid-Atlantic streams. *Freshwater Science*, *35*(2), 503-517.

Proia, L., Vilches, C., Boninneau, C., Kantiani, L., Farré, M., Romaní, A. M., … Guasch, H. (2013). Drought episode modulates the response of river biofilms to triclosan. *Aquatic Toxicology*, *127*, 36–45.

Proia, L., Romaní, A., & Sabater, S. (2017). Biofilm phosphorus uptake capacity as a tool for the assessment of pollutant effects in river ecosystems. *Ecotoxicology*, *26*(2), 271-282.

Pu, C., Liu, H., Ding, G., Sun, Y., Yu, X., Chen, J., ... & Gong, X. (2018). Impact of direct application of biogas slurry and residue in fields: in situ analysis of antibiotic resistance genes from pig manure to fields. *Journal of hazardous materials*, *344*, 441-449.

Rand, M. C., Greenberg, A. E., and Taras, M. J. (1976). Standard Methods for the Examination of Water and Wastewater. Washington, DC: American Public Health Association.

Reardon, J., Foreman, J. A., & Searcy, R. L. (1966). New reactants for the colorimetric determination of ammonia. *Clinica Chimica Acta*, *14*, 403-405.

Redfield, A. C. (1963). The influence of organisms on the composition of seawater. *The sea*, *2*, 26-77.

Ricart Viladomat, M. (2011). *Effects of priority and emerging pollutants on river biofilms*. Universitat de Girona.

Ricart, M., Barceló, D., Geiszinger, A., Guasch, H., de Alda, M. L., Romaní, A. M., ... & Sabater, S. (2009). Effects of low concentrations of the phenylurea herbicide diuron on biofilm algae and bacteria. *Chemosphere*, *76*(10), 1392-1401.

Riegman, R., Rutgers, M., & Mur, R. R. (1985). Effects of photoperiodicity and light irradiance on phosphate-limited *Oscillatoria agardhii* in chemostat cultures. *Archives of microbiology*, *142*(1), 66-71.

Romaní, A. M. (2010). Freshwater biofilms. *Biofouling. Wiley-Blackwell, Oxford*, 137-153.

Romaní, A. M., & Marxsen, J. (2002). Extracellular enzymatic activities in epilithic biofilms of the Breitenbach: microhabitat differences. *Archiv für Hydrobiologie*, *155*(4), 541-555.

Romaní, A. M., Giorgi, A., Acuna, V., & Sabater, S. (2004). The influence of substratum type and nutrient supply on biofilm organic matter utilization in streams. *Limnology and Oceanography*, *49*(5), 1713-1721.

Romero, F., Sabater, S., Font, C., Balcázar, J. L., & Acuña, V. (2019). Desiccation events change the microbial response to gradients of wastewater effluent pollution. *Water research*, *151*, 371-380.

Rubio-Gracia, F., García-Berthou, E., Zamora, L., Martí, E., Almeida, D., Espinosa, C., … Flecker, A. S. (2017). Combined effects of hydrologic alteration and cyprinid fish in mediating biogeochemical processes in a Mediterranean stream. *Science of The Total Environment*, *601–602*, 1217–1225.

Ruiz-Gonzalez, C., Lefort, T., Galí, M., Montserrat Sala, M., Sommaruga, R., Simo, R., & Gasol, J. M. (2012). Seasonal patterns in the sunlight sensitivity of bacterioplankton from Mediterranean surface coastal waters. *FEMS microbiology ecology*, *79*(3), 661-674.

Saadoun, I. M. K., Schrader, K. K., & Blevins, W. T. (2001). Environmental and nutritional factors affecting geosmin synthesis by Anabaena sp. *Water Research*, *35*(5), 1209–1218.

Sabater, S., Guasch i Padró, H., Martí, E., Armengol Bachero, J., Vila, M., & Sabater, F. (1992). The Ter, a Mediterranean river system in Spain. *© Limnética, 1992, vol. 8, núm. 1, p. 141-149*.

Sabater, S., Vilalta, E., Gaudes, A., Guasch, H., Munoz, I., & Romani, A. (2003). Ecological implications of mass growth of benthic cyanobacteria in rivers. *Aquatic Microbial Ecology*, *32*(2), 175-184.

Sabater, S., Guasch, H., Ricart, M., Romaní, A., Vidal, G., Klünder, C., & Schmitt-Jansen, M. (2007). Monitoring the effect of chemicals on biological communities. The biofilm as an interface. Analytical and bioanalytical chemistry, 387(4), 1425-1434.

Sabater, S., Artigas, J., Corcoll, N., Proia, L., Timoner, X., & Tornés, E. (2016). Ecophysiology of river algae. In *River Algae* (pp. 197-217). Springer, Cham.

Schilling, K. E., Kim, S. W., & Jones, C. S. (2017). Use of water quality surrogates to estimate total phosphorus concentrations in Iowa rivers. Journal of Hydrology: Regional Studies, 12, 111-121.

Serra, A., Guasch, H., Admiraal, W., Van der Geest, H. G., & Van Beusekom, S. A. M. (2010). Influence of phosphorus on copper sensitivity of fluvial periphyton: the role of chemical, physiological and community-related factors. *Ecotoxicology*, *19*(4), 770-780.

Sharma, N. K., Choudhary, K. K., Bajpai, R., & Rai, A. K. (2011). Freshwater cyanobacterial (blue-green algae) blooms: Causes, consequences and control. *Impact, Monitoring and Management of Environmental Pollution*, 73-95.

Shi, P., Zhang, Y., Li, Z., Li, P., & Xu, G. (2017). Influence of land use and land cover patterns on seasonal water quality at multi-spatial scales. *Catena*, *151*, 182-190.

Sivonen, K. (1990). Effects of light, temperature, nitrate, orthophosphate, and bacteria on growth of and hepatotoxin production by *Oscillatoria agardhii* strains. *Appl. Environ. Microbiol.*, *56*(9), 2658-2666.

Smith, V. H., DeNoyelles, F., Pan, S., Sieber-Denlinger, J., Randtke, S. J., Strasser, V. A., … Blain, G. T. (2009). Managing Taste and Odor Problems in a Eutrophic Drinking Water Reservoir. *Lake and Reservoir Management*, *18*(4), 319–323.

Sokal, R. R., & Rohlf, F. J. (1995). Biometry: The Principles and Practice of Statistics in Biological Research. 3d Edition. WH Freeman Company. *San Francisco, CA, USA*.

Spiteller, D., Jux, A., Piel, J., & Boland, W. (2002). Feeding of [5, 5-2H2]-1-desoxy-D-xylulose and [4, 4, 6, 6, 6-2H5]-mevalolactone to a geosmin-producing Streptomyces sp. and Fossombronia pusilla. *Phytochemistry*, *61*(7), 827-834.

Srinivasan, R. & Sorial, G. Treatment of taste and odor causing compounds 2-methylisoborneol and geosmin in drinking water: A critical review. *Journal of Environmental Sciences,* 23(1), 1 – 13.

Stevenson, R. J., Bothwell, M. L., Lowe, R. L., & Thorp, J. H. (1996). *Algal ecology: Freshwater benthic ecosystem*. Academic press.

Stone, M. L., Graham, J. L., & Gatotho, J. W. (2013). *Model documentation for relations between continuous real-time and discrete water-quality constituents in Cheney Reservoir near Cheney, Kansas, 2001--2009* (No. 2013-1123). US Geological Survey.

Stroom, J. M., & Kardinaal, W. E. A. (2016). How to combat cyanobacterial blooms: strategy toward preventive lake restoration and reactive control measures. *Aquatic Ecology*, *50*(3), 541-576.

Suurnäkki, S., Gomez-Saez, G. V., Rantala-Ylinen, A., Jokela, J., Fewer, D. P., & Sivonen, K. (2015). Identification of geosmin and 2-methylisoborneol in cyanobacteria and molecular detection methods for the producers of these compounds. *Water Research*, *68*(Viikinkaari 9), 56–66.

Tang, E. P. Y., Tremblay, R., & Vincent, W. F. (1997). Cyanobacterial dominance of polar freshwater ecosystems: Are high-latitude mat-formers adapted to low temperature? *Journal of Phycology*, *33*(2), 171–181.

Tlili, A., Dorigo, U., Montuelle, B., Margoum, C., Carluer, N., Gouy, V., ... & Bérard, A. (2008). Responses of chronically contaminated biofilms to short pulses of diuron: an experimental study simulating flooding events in a small river. *Aquatic Toxicology*, *87*(4), 252-263.

Toro, M., Robles, S., Avilés, J., Nuño, C., Vivas, S., Bonada, N., ... & Jáimez-Cuéllar, P. (2002). Calidad de las aguas de los ríos mediterráneos del proyecto GUADALMED. Características físico-químicas. *Limnetica*, *21*(3-4), 63-75.

Tsuchiya, Y., & Matsumoto, A. (1999). Characterization of *Oscillatoria f. granulata* producing 2-methylisoborneol and geosmin. *Water science and technology*, *40*(6), 245-250.

Tu, J. (2011). Spatial and temporal relationships between water quality and land use in northern Georgia, USA. *Journal of Integrative Environmental Sciences*, *8*(3), 151-170.

Tung, S. C., Lin, T. F., Yang, F. C., & Liu, C. L. (2008). Seasonal change and correlation with environmental parameters for 2-MIB in Feng-Shen Reservoir, Taiwan. *Environmental Monitoring and Assessment*, *145*(1–3), 407–416.

Urrea-Clos, G., García-Berthou, E., & Sabater, S. (2014). Factors explaining the patterns of benthic chlorophyll-a distribution in a large agricultural Iberian watershed (Guadiana river). *Ecological indicators*, *36*, 463-469.

Vadeboncoeur, Y., & Steinman, A. D. (2002). Periphyton function in lake ecosystems. *The Scientific World Journal*, *2*, 1449-1468.

Vahtera, E., Conley, D. J., Gustafsson, B. G., Kuosa, H., Pitkänen, H., Savchuk, O. P., ... & Wulff, F. (2007). Internal ecosystem feedbacks enhance nitrogen-fixing cyanobacteria blooms and complicate management in the Baltic Sea. *Ambio*, 186-194.

Van Meter, K. J., Basu, N. B., Veenstra, J. J., & Burras, C. L. (2016). The nitrogen legacy: emerging evidence of nitrogen accumulation in anthropogenic landscapes. *Environmental Research Letters*, *11*(3), 035014.

Vilalta, E., Guasch, H., Muñoz, I., Navarro, E., Romaní, A. M., Valero, F., … Sabater, S. (2003). Ecological factors that co-occur with geosmin production by benthic cyanobacteria. The case of the Llobregat River. *Algological Studies*, *109*(1), 579–592.

Vilalta, E. (2004). *Structure and function in fluvial biofilms: implications in river DOC dynamics and nuisance metabolite production* (Doctoral dissertation, Ph. D. Thesis dissertation, University of Barcelona, Barcelona, Spain).

Villeneuve, A., Montuelle, B., & Bouchez, A. (2010). Influence of slight differences in environmental conditions (light, hydrodynamics) on the structure and function of periphyton. *Aquatic Sciences*, *72*(1), 33-44.

Von Schiller, D., Martí, E., Riera, J. L., Ribot, M., Argerich, A., Fonolla, P., & Sabater, F. (2008). Inter-annual, annual, and seasonal variation of P and N retention in a perennial and an intermittent stream. *Ecosystems*, *11*(5), 670-687.

Wingender, J., & Flemming, H. C. (2011). Biofilms in drinking water and their role as reservoir for pathogens. *International journal of hygiene and environmental health*, *214*(6), 417-423.

Wollheim, W. M. (2016). From headwaters to rivers to river networks: Scaling in stream ecology. In *Stream ecosystems in a changing environment* (pp. 349-388). Academic Press.

Wang, Z., & Li, R. (2015). Effects of light and temperature on the odor production of 2-methylisoborneol-producing Pseudanabaena sp. and geosmin-producing Anabaena ucrainica (cyanobacteria). *Biochemical Systematics and Ecology*, *58*(7), 219–226.

Watson, S. B., & Ridal, J. (2004). Periphyton: a primary source of widespread and severe taste and odour. *Water Science and Technology*, *49*(9), 33-39.

Watson, S. B., Monis, P., Baker, P., & Giglio, S. (2016). Biochemistry and genetics of taste- and odor-producing cyanobacteria. *Harmful Algae*, *54*, 112–127.

Weber, C. I. (Ed.). (1980). *Biological field and laboratory methods for measuring the quality of surface waters and effluents* (Vol. 73, No. 1). National Environmental Research Center, Office of Research and Development, US Environmental Protection Agency.

Weigelhofer, G., Hein, T., & Bondar-Kunze, E. (2018). Phosphorus and nitrogen dynamics in riverine systems: Human impacts and management options. *Riverine Ecosystem Management*, *187*.

Wellnitz, T., & Rader, R. B. (2003). Mechanisms influencing community composition and succession in mountain stream periphyton: interactions between scouring history,

grazing, and irradiance. *Journal of the North American Benthological Society*, *22*(4), 528-541.

Wilson, C. O. (2015). Land use/land cover water quality nexus: quantifying anthropogenic influences on surface water quality. *Environmental monitoring and assessment*, *187*(7), 424.

Winter, J. G., Desellas, A. M., Fletcher, R., Heintsch, L., Morley, A., Nakamoto, L., & Utsumi, K. (2011). Algal blooms in Ontario, Canada: Increases in reports since 1994. *Lake and Reservoir Management*, *27*(2), 105–112.

Woli, K. P., Nagumo, T., Kuramochi, K., & Hatano, R. (2004). Evaluating river water quality through land use analysis and N budget approaches in livestock farming areas. *Science of the Total Environment*, *329*(1-3), 61-74.

Xu, H., Paerl, H. W., Qin, B., Zhu, G., Hall, N. S., & Wu, Y. (2015). Determining critical nutrient thresholds needed to control harmful cyanobacterial blooms in eutrophic Lake Taihu, China. *Environmental science & technology*, *49*(2), 1051-1059.

Ylla, I., Borrego, C., Romaní, A. M., & Sabater, S. (2009). Availability of glucose and light modulates the structure and function of a microbial biofilm. *FEMS microbiology ecology*, 69(1), 27-42.

Zarnetske, P. L., Skelly, D. K., & Urban, M. C. (2012). Biotic multipliers of climate change. *Science*, *336*(6088), 1516-1518.

Zhang, Q. J., Cudrak, A. A., Shariff, R., & Stanley, S. J. (2004). Implementing artificial neural network models for real-time water colour forecasting in a water treatment plant. *Journal of Environmental Engineering and Science*, *3*(S1), S15-S23.

Zhang, T., Li, L., Song, L., & Chen, W. (2009). Effects of temperature and light on the growth and geosmin production of Lyngbya kuetzingii (Cyanophyta). *Journal of applied phycology*, *21*(3), 279-285.

Annex A

Table A.1. Mean value and standard deviation of the physicochemical variables evaluated (pH, electrical conductivity (EC, in µS/cm), temperature (T, in °C), dissolved oxygen (DO, in mg/L), oxygen saturation (Sat, in %), ammonium concentration (in $N\text{-}NO_4^+$ µg/L), nitrite concentration (in $N\text{-}NO_2^-$ µg/L), nitrate concentration (in $N\text{-}NO_3^-$ mg/L), phosphate concentration (in $P\text{-}PO_4^{3-}$ µg/L), N:P ratio, suspended solids (SS, in mg/L), turbidity (Turb.) and organic matter (OM),) for the different sampling sites: T1 = Ter at Vilallonga de Ter, T2 = Ter at Ripoll, T5 = Ter at Colònia de Borgonyà, T7 = Ter at Gurb, and G1 = Ges upstream San Pere de Torelló, in winter (W), spring (Sp), summer (Su) and autumn (Au), in 2017, 2018 and 2019.

Table A.1. Mean value and standard deviation of the physicochemical variables evaluated.

2017		pH	EC (µS/cm)	Temp. (ºC)	DO (mg/L)	Sat. (%)	N-NH_4^+ (µg/L)	N-NO_2^- (µg/L)	N-NO_3^- (mg/L)	P-PO_4^{3-} (µg/L)	N:P	SS (mg/L)	Turbidity (NTU)	OM
T1	**W**	7.7 ± 0.1	156 ± 17	5.8 ± 0.7	11.6 ± 1.1	94 ± 7	3 ± 1	9 ± 2	0.39 ± 0.05	24 ± 31	4 ± 8	1 ± 5	2 ± 7	0.158 ± 0.061
	Sp	8.2 ± 0.3	122 ± 24	7.9 ± 1.3	12.6 ± 1.9	107 ± 15	31 ± 19	9 ± 3	0.39 ± 0.23	87 ± 53	11 ± 15	1 ± 9	1 ± 4	0.135 ± 0.115
	Su	8.1 ± 0.2	134 ± 13	15.2 ± 2.3	9.0 ± 0.3	90 ± 3	44 ± 56	6 ± 4	0.25 ± 0.07	52 ± 81	26 ± 28	8 ± 7	6 ± 6	0.018 ± 0.011
	Au	8.2 ± 0.6	139 ± 9	6.3 ± 3.1	10.8 ± 3.9	83 ± 22	9 ± 5	3 ± 0	0.29 ± 0.20	12 ± 16	88 ± 12	7 ± 17	2 ± 3	0.017 ± 0.095
T2	**W**	8.7 ± 0.2	295 ± 31	7.9 ± 1.1	11.7 ± 0.7	102 ± 9	0 ± 1	13 ± 1	0.869	39 ± 15	50 ± 15	0 ± 1	1 ± 2	0.237 ± 0.093
	Sp	8.6 ± 0.1	246 ± 37	9.4 ± 2.2	12.5 ± 1.9	114 ± 17	11 ± 7	16 ± 5	0.718	77 ± 21	21 ± 9	2.4 ± 2	2 ± 3	0.249 ± 0.209
	Su	8.5 ± 0.2	264 ± 30	19.0 ± 2.0	8.7 ± 0.7	94 ± 10	8 ± 4	6 ± 1	0.38 ± 0.49	42 ± 58	20 ± 7	30 ± 21	23 ± 4	0.047 ± 0.022
	Au	8.5 ± 0.0	318 ± 45	6.6 ± 5.5	11.9 ± 1.9	96 ± 4	21 ± 15	12 ± 11	0.36 ± 0.02	48 ± 33	30 ± 28	13 ± 15	4 ± 2	0.028 ± 0.015
T3	**W**	8.5 ± 0.3	305 ± 49	8.5 ± 1.5	12.8 ± 0.4	110 ± 5	81 ± 116	6 ± 5	0.68 ± 0.09	136 ± 44	14 ± 5	4 ± 2	5 ± 2	0.373 ± 0.042
	Sp	8.4 ± 0.1	273 ± 86	12.6 ± 2.8	11.0 ± 1.3	104 ± 6	85 ± 100	9 ± 5	0.75 ± 0.35	96 ± 74	31 ± 21	8 ± 6	8 ± 7	0.460 ± 0.321
	Su	8.5 ± 0.3	291 ± 21	22.5 ± 4.2	9.2 ± 0.5	106 ± 14	72 ± 54	11 ± 4	0.79 ± 0.13	175 ± 153	18 ± 16	16 ± 13	11 ± 4	0.067 ± 0.018
	Au	8.4 ± 0.3	373 ± 58	9.9 ± 6.9	11.6 ± 2.0	102 ± 9	126 ± 198	8 ± 1	0.43 ± 0.08	172 ± 155	13 ± 9	26 ± 33	10 ± 9	0.041 ± 0.004
T4	**W**	8.3 ± 0.1	357 ± 43	8.4 ± 1.5	12.0 ± 0.4	103 ± 5	85 ± 34	16 ± 5	1.07 ± 0.22	168 ± 121	24 ± 19	9 ± 5	9 ± 3	0.517 ± 0.039
	Sp	8.2 ± 0.2	284 ± 77	13.1 ± 3.3	9.8 ± 2.6	98 ± 11	137 ± 116	17 ± 5	1.01 ± 0.33	95 ± 51	39 ± 27	15 ± 9	12 ± 6	0.580 ± 0.270
	Su	8.3 ± 0.3	329 ± 3	23.5 ± 3.7	8.5 ± 1.2	100 ± 17	83 ± 45	13 ± 6	0.64 ± 0.10	131 ± 16	13 ± 3	40 ± 5	22 ± 1	0.075 ± 0.021
	Au	8.4 ± 0.5	370 ± 26	8.4 ± 5.7	10.6 ± 2.9	103 ± 17	22 ± 32	13 ± 2	0.83 ± 0.32	113 ± 3	17 ± 6	5 ± 1	17 ± 11	0.068 ± 0.015
G1	**W**	8.8 ± 0.3	401 ± 27	7.1 ± 1.3	12.7 ± 0.8	101 ± 6	4 ± 2	2.1 ± 0.8	0.95 ± 0.31	48 ± 9	44 ± 9	11 ± 2	1 ± 2	0.337 ± 0.132
	Sp	8.7 ± 0.1	374 ± 32	11.6 ± 2.4	11.7 ± 2.1	107 ± 11	5 ± 1	2.1 ± 1.3	0.53 ± 0.14	68 ± 15	17 ± 5	1 ± 3	1 ± 1	0.344 ± 0.209
	Su	8.7 ± 0.2	285 ± 18	19 ± 9	9.0 ± 1.7	93 ± 9	8.5 ± 0.7	0 ± 0	0.16 ± 0.12	34 ± 48	8 ± 9	21 ± 29	18 ± 12	0.185 ± 0.128
	Au	8.8 ± 0.1	342 ± 87	6.2 ± 8.3	12.3 ± 1.2	101 ± 15	13 ± 16	0.6 ± 0.8	0.19 ± 0.12	19 ± 18	30 ± 23	29 ± 40	15 ± 21	0.067 ± 0.001

2018		pH	EC (µS/cm)	Temp. (ºC)	DO (mg/L)	Sat. (%)	$N\text{-}NH_4^+$ (µg/L)	$N\text{-}NO_2^-$ (µg/L)	$N\text{-}NO_3^-$ (mg/L)	$P\text{-}PO_4^{3-}$ (µg/L)	N:P	SS (mg/L)	Turbidity (NTU)	OM
T1	W	7.7 ± 0.8	176 ± 9	4.2 ± 0.5	11.6 ± 0.6	89 ± 5	80 ± 5	0.5 ± 0.0	0.34 ± 0.06	34 ± 11	28 ± 9	10 ± 8	20 ± 14	0.671 ± 0.298
	Sp	7.8 ± 0.3	188 ± 11	6.7 ± 0.9	11.2 ± 0.8	107 ± 15	39 ± 7	1.1 ± 0.3	0.36 ± 0.06	30 ± 5		57 ± 3	25 ± 8	1.04 ± 0.45
	Su	8.0 ± 0.1	176 ± 7	9.8 ± 2.1	11.4 ± 0.2	116 ± 4	30,000	0.3 ± 0.2	0.15 ± 0.02	19 ± 2	19 ± 2	5 ± 0	19 ± 5	0.740 ± 0.106
	Au	7.9 ± 0.6	177 ± 9	6.8 ± 3.1	13.5 ± 3.9	109 ± 22	18	0.7 ± 0.3	0.15 ± 0.20	27 ± 16	10 ± 12	22 ± 18	14 ± 3	0.820 ± 0.095
T2	W	7.9 ± 0.5	223 ± 11	5.5 ± 0.8	12.1 ± 0.6	97 ± 6	102 ± 21	1.3 ± 1.8	0.67 ± 0.09	33 ± 22	63 ± 68	9 ± 5	22 ± 6	0.514 ± 0.211
	Sp	7.6 ± 0.4	299 ± 3	8.1 ± 0.4	11.6 ± 0.5	113 ± 1	37 ± 16	1.1 ± 0.2	0.71 ± 0.32	8.6 ± 10	81 ± 1	9 ± 5	21 ± 8	0.389 ± 0.001
	Su	7.5 ± 0.0	386 ± 16	12.6 ± 2.5	11.8 ± 1.3	113 ± 6	88 ± 14	1.4 ± 0.2	1.41 ± 0.11	19 ± 5.7	118 ± 4	6 ± 1	19 ± 14	0.183 ± 0.076
	Au	8.0 ± 1.0	392 ± 28	7.7 ± 3.2	15.0 ± 0.7	127 ± 4	93	5.7 ± 6.8	0.55 ± 0.09	42 ± 15	58 ± 31	28 ± 22	30 ± 32	0.536 ± 0.299
T3	W	8.4 ± 0.3	395 ± 63	6.2 ± 1.2	13.0 ± 1.5	105 ± 13	96 ± 49	5.6 ± 3.7	0.86 ± 0.27	31 ± 17	88 ± 66	29 ± 9	17 ± 8	0.725 ± 0.114
	Sp	8.5 ± 0.0	398 ± 15	8.5 ± 0.8	11.4 ± 0.6	108 ± 1	55 ± 33	1.5 ± 1.7	0.80 ± 0.01	43 ± 17	51 ± 24	49 ± 60	10 ± 1	0.721 ± 0.170
	Su	8.5 ± 0.3	453 ± 31	14.4 ± 2.2	11.1 ± 0.3	111 ± 6	41	8.6 ± 2.8	0.35 ± 0.12	27 ± 5.6	33 ± 15	21 ± 12	14 ± 6	0.640 ± 0.047
	Au	8.5 ± 0.4	432 ± 35	8.4 ± 3.7	14.8 ± 3.0	125 ± 8	47	14 ± 14	0.74 ± 0.27	31 ± 27	75 ± 44	27 ± 12	14 ± 9	0.651 ± 0.008
T4	W	8.4 ± 0.2	439 ± 66	5.8 ± 1.2	12.3 ± 0.8	98 ± 6	162 ± 44	1.8 ± 0.9	1.27 ± 0.62	51 ± 29	78 ± 56	31 ± 12	16 ± 8	0.435 ± 0.087
	Sp	8.5	348 ± 2	7.2 ± 0.3	11.4 ± 0.1	98 ± 5	53 ± 58	5.7 ± 2.2	0.89 ± 0.49	24 ± 12	139 ± 14	15 ± 11	8 ± 1	0.374 ± 0.070
	Su	9.2 ± 0.4	465 ± 47	16.1 ± 2.1	11.2 ± 0.4	112 ± 6	86 ± 11	29 ± 27	1.61 ± 1.72	126 ± 143	48 ± 34	43	12 ± 8	0.355 ± 0.016
	Au	8.5 ± 0.6	519 ± 32	9.9 ± 5.0	13.4 ± 5.4	111 ± 29	40 ± 11	18 ± 14	2.56 ± 0.66	28 ± 14	243 ± 168	232 ± 283	5 ± 0	0.360 ± 0.038
G1	W	8.6 ± 0.3	404 ± 53	4.2 ± 2.9	13.4 ± 0.9	94 ± 5	150 ± 73	2.8 ± 4.3	0.49 ± 0.35	23 ± 15	140 ± 212	122 ± 132	12 ± 10	0.408 ± 0.108
	Sp	8.4 ± 0.1	441 ± 14	7.4 ± 0.2	11.5 ± 0.8	112 ± 6	64 ± 47	0.7 ± 0.0	1.08 ± 0.00	21 ± 14	156 ± 100	48 ± 3	5 ± 0	0.497 ± 0.226
	Su	8.6 ± 0.1	510 ± 45	13.8 ± 2.3	11.6 ± 0.4	118 ± 5	37	3.0 ± 1.2	0.39 ± 0.04	13 ± 5	73 ± 25	32	8 ± 3	0.659 ± 0.008
	Au	8.8 ± 0.3	537 ± 65	8.9 ± 5.8	14.7 ± 3.0	120 ± 4	29	0.4 ± 0.3	0.69 ± 0.12	7.3 ± 4.2	241 ± 97	51 ± 11	29 ± 7	0.432 ± 0.005

2019		pH	EC (µS/cm)	Temp. (ºC)	DO (mg/L)	Sat. (%)	$N\text{-}NH_4^+$ (µg/L)	$N\text{-}NO_2^-$ (µg/L)	$N\text{-}NO_3^-$ (mg/L)	$P\text{-}PO_4^{3-}$ (µg/L)	N:P	SS (mg/L)	Turbidity (NTU)	OM
T1	W	7.9 ± 0.3	128 ± 32	4.8 ± 1.7	12.7 ± 1.2	110 ± 17	43 ± 15	2 ± 1	0.41 ± 0.06	70 ± 62	30 ± 27	54 ± 25	8 ± 1	0.157 ± 0.124
	Sp	7.9 ± 0.3	131 ± 30	7.8 ± 2.0	11.6 ± 1.2	103 ± 10	22 ± 14	1 ± 2	0.45 ± 0.06	56 ± 31	24 ± 14	10 ± 3	7 ± 1	0.020 ± 0.009
	Su	8.8	129	13.6	10.5	101	54 ± 33	20 ±7	0.50 ± 0.25	29 ± 20	48 ± 16	21 ± 11	5 ± 1	0.056 ± 0.011
	Au	7.5 ± 0.1	138 ± 37	7.9 ± 3.5	11.9 ± 0.6	112 ± 14	34 ± 11	5 ± 7	0.48 ± 0.17	16 ± 56	78 ± 18	69 ± 19	6 ± 2	0.159 ± 0.078
T2	W	8.5 ± 0.3	261 ± 55	6.3 ± 2.8	13.3 ± 1.2	113 ± 7	76 ± 21	9 ± 2	0.53 ± 0.14	70 ± 47	27 ± 14	24 ± 8	27 ± 3	0.038 ± 0.004
	Sp	8.4 ± 0.2	281 ± 76	10.0 ± 1.1	11.5 ± 0.8	106 ± 9	65 ± 22	10 ± 8	0.56 ± 0.07	56 ± 15	27 ± 7	30 ± 11	22 ± 6	0.039 ± 0.008
	Su	8.6	246	15.8	10.7	108	61 ± 1	47 ± 21	0.56 ± 0.10	27 ± 6	57 ± 18	23 ± 6	21 ± 3	0.041 ± 0.012
	Au	8.1 ± 0.2	285 ± 82	9.1 ± 5.3	12.3 ± 1.2	109 ± 0	46 ± 16	20 ± 23	0.55 ± 0.18	16 ± 10	115 ± 63	65 ± 28	16 ± 4	0.052 ± 0.020
T3	W	8.4 ± 0.3	328 ± 121	7.9 ± 3.5	12.7 ± 1.2	112 ± 7	63 ± 18	12 ± 3	0.71 ± 0.11	49 ± 33	48 ± 32	40 ± 90	32 ± 10	0.072 ± 0.014
	Sp	8.4 ± 0.2	308 ± 78	12.2 ± 1.6	10.5 ± 1.3	100 ± 13	69 ± 30	13 ± 6	0.53 ± 0.21	55 ± 8	25 ± 10	47 ± 8	35 ± 7	0.062 ± 0.003
	Su	8.5	277	20.1	9.7	107	103 ± 8	39 ± 37	1.16 ± 0.74	45 ± 28	66 ± 3	39 ± 9	22 ± 11	0.065 ± 0.013
	Au	8.3 ± 0.2	315 ± 89	10.4 ± 6.6	12.3 ± 1.2	111 ± 4	72 ± 11	16 ± 12	1.02 ± 0.64	20 ± 12	127 ± 12	137 ± 93	26 ± 12	0.095 ± 0.028
T4	W	8.6 ± 0.5	363 ± 72	8.1 ± 3.4	12.7 ± 0.9	112 ± 7	114 ± 36	24 ± 7	2.35 ± 0.49	48 ± 19	116 ± 71	51 ± 12	39 ± 19	0.079 ± 0.020
	Sp	8.4 ± 0.2	368 ± 59	13.6 ± 1.7	9.6 ± 1.6	103 ± 16	124 ± 58	25 ± 10	1.38 ± 0.44	79 ± 39	47 ± 16	58 ± 26	47 ± 17	0.080 ± 0.017
	Su	8.8	345	24.4	9.1	110	114 ± 32	43 ± 26	1.73 ± 1.17	33 ± 13	121 ± 36	56 ± 10	24 ± 8	0.057 ± 0.011
	Au	8.3 ± 0.1	363 ± 98	11.0 ± 7.0	12.3 ± 1.9	111 ± 2	151 ± 23	18 ± 10	1.73 ± 0.90	19 ± 11	221 ± 34	92 ± 37	39 ± 9	0.102 ± 0.028
G1	W	8.6 ± 0.2	364 ± 85	6.9 ± 4.4	12.1 ± 1.6	104 ± 8	69 ± 15	3 ± 1	0.50 ± 0.13	36 ± 32	73 ± 63	36 ± 35	52 ± 22	0.063 ± 0.023
	Sp	8.8 ± 0.2	358 ± 66	12.5 ± 3.0	11.1 ± 1.5	107 ± 12	45 ± 18	3 ± 3	0.52 ± 0.12	25 ± 24	118 ± 141	81 ± 18	68 ± 6	0.097 ± 0.017
	Su	9.1	373	26.8	9.4	117	68 ± 33	13 ± 0	0.33 ± 0.25	21 ± 16	50 ± 16	59 ± 20	44 ± 13	0.079 ± 0.003
	Au	8.5 ± 0.1	369 ± 124	8.8 ± 6.6	12.4 ± 1.7	108 ± 2	75 ± 25	5 ± 3	0.42 ± 0.09	9 ± 8	160 ± 72	78 ± 17	59 ± 14	0.063 ± 0.034